

THE UNIVERSITY OF NOTTINGHAM

School of Chemical, Environmental and Mining Engineering

THE INTEGRATION OF CFD AND VR METHODS TO ASSIST  
AUXILIARY VENTILATION PRACTICE

BY  
STEPHEN A SILVESTER  
BENG

Thesis submitted to The University of Nottingham for the degree of  
Doctor of Philosophy, October 2002

# TABLE OF CONTENTS

ABSTRACT.....	VII
LIST OF FIGURES.....	VIII
TERMINOLOGY.....	XIV
ABBREVIATIONS.....	XVI
ACKNOWLEDGEMENTS.....	XVII

## CHAPTER 1 INTRODUCTION

1.1 INTRODUCTION.....	1
1.2 PROBLEM DEFINITION.....	3
1.3 AIMS AND OBJECTIVES OF THE RESEARCH PROJECT .....	4
1.4 RESEARCH METHODOLOGY ADOPTED .....	5
1.5 THESIS OUTLINE.....	7

## CHAPTER 2 MINING ENVIRONMENTAL

2.1 INTRODUCTION.....	11
2.2 CURRENT AND HISTORICAL MINING METHODS.....	11
2.3 MINE ATMOSPHERE.....	13
2.3.1 Gases.....	13
2.3.1.1 Methane Detection .....	17
2.3.2 Dust and Particulates.....	17
2.3.2.1 Particulate Concentration Measurement .....	19
2.3.3 Exposure Limits .....	19
2.3.4 Ignition.....	19
2.3.5 Heat and Humidity.....	20
2.4 MINE VENTILATION: EQUIPMENT AND METHODS.....	21
2.4.1 Main systems.....	21
2.4.2 Booster Systems.....	22
2.4.3 Auxiliary systems.....	23
2.4.4 Fan Types.....	26
2.4.5 Losses.....	28
2.5 ANALYTICAL AND COMPUTATIONAL METHODS.....	29
2.5.1 Fundamental Laws.....	29
2.5.1.1 Ideal Gas Laws.....	29
2.5.1.2 Bernoullis Law .....	30
2.5.1.3 Kirchoffs Laws.....	30
2.5.1.4 Atkinsons Equation.....	31
2.5.2 General Flow Characteristics .....	31
2.5.2.1 Laminar Flow & Reynolds Number.....	31
2.5.2.2 Turbulence.....	32
2.5.3 Fan Characteristics.....	33
2.5.4 Network Analysis.....	34
2.5.4.1 The Hardy Cross Iterative Method.....	35
2.6 SUMMARY.....	36

## CHAPTER 3 COMPUTATIONAL FLUID DYNAMICS

3.1 INTRODUCTION.....	37
3.2 METHODOLOGY.....	39
3.3 PREPROCESSING.....	40
3.3.1 Meshing.....	42
3.4 SOLVING.....	44
3.4.1 The Finite Element Method.....	44
3.4.2 The Finite Difference Method.....	45
3.4.3 The Finite Volume Method.....	45
3.5 POSTPROCESSING.....	46
3.6 GOVERNING EQUATIONS.....	47
3.6.1 The Continuity Equation.....	48
3.6.2 The Momentum Equation.....	48
3.6.3 The Energy Equation.....	50
3.7 TURBULENCE MODELLING.....	50
3.7.1 Transition.....	51
3.7.2 Turbulence models.....	52
3.8 CONTRIBUTIONS TO SUB SURFACE VENTILATION MODELLING...54	
3.8.1 Validation Studies.....	54
3.8.1.1 Experimental Validation Studies.....	55
3.8.2 Modelling of Gas Dispersion and Methane Levels.....	60
3.8.3 Modelling of Sub Surface Fires.....	63
3.8.4 Evaluation of Alternative Ventilation Configurations.....	64
3.8.5 Discussion.....	68
3.9 SUMMARY.....	69

## CHAPTER 4 VISUALISATION

4.1 INTRODUCTION.....	71
4.2 HISTORY.....	73
4.3 DATA SOURCES & FORMATS.....	74
4.3.1 Medical Scanning.....	74
4.3.2 Computational Simulation Sources.....	75
4.4 PRE-PROCESSING.....	76
4.4.1 Point Location.....	77
4.4.2 Interpolative Methods.....	81
4.4.2.1 Hill Climbing.....	81
4.4.2.2 Spatial Interpolation.....	82
4.5 DATA OPTIMISATION.....	83
4.5.1 Simplification.....	83
4.5.2 Feature Extraction.....	87
4.6 FLOW VISUALISATION METHODS.....	88
4.6.1 Glyph Based Visualisation.....	88
4.6.1.2 Vectors.....	89
4.6.1.3 Particle Tracing.....	92
4.6.1.3.1 Variable Time Stepping.....	96
4.6.1.3.2 Streamlines, Ribbons & Tubes.....	97
4.6.1.4 Contours.....	99
4.6.1.5 Isosurfaces.....	101

4.6.1.5.1 Volume Rendering.....	104
4.7 SUMMARY.....	105

## **CHAPTER 5 VIRTUAL REALITY & COMPUTER GRAPHICS**

5.1 INTRODUCTION.....	107
5.2 HISTORY OF THE IMMERSIVE ENVIRONMENT.....	108
5.3 THE HUMAN INTERFACE.....	110
5.3.1 Colour & Computer Graphics.....	110
5.3.2 Current Visual Technology.....	112
5.3.3 Haptic & Audio Feedback.....	114
5.4 3D ENVIRONMENT BUILDING.....	114
5.4.1 Concept of Primitives, The Top-Down Approach.....	115
5.4.2 WireFrames, Faces & Volumes.....	116
5.4.3 Object Optimisation.....	117
5.4.4 Realism; Textures & Surface Maps.....	119
5.4.5 Light Sources & Shading.....	120
5.5 3D FORMATS AND STANDARDS.....	122
5.5.1 Virtual Reality Modelling Language (VRML).....	122
5.5.2 CAD Based Formats; IGES and DXF.....	125
5.5.3 Direct X™.....	126
5.6 APPLIED VIRTUAL REALITY.....	126
5.6.1 Education & Industrial Training.....	127
5.6.2 Scientific Data & Information Visualisation.....	130
5.6.3 Discussion.....	133
5.7 EVALUATION OF VR.....	135
5.8 SUMMARY.....	139

## **CHAPTER 6 INITIAL SPECIFICATION AND EVALUATION STUDIES OF CFD/VR INTEGRATION**

6.1 INTRODUCTION.....	141
6.2 SUMMARY OF LITERATURE REVIEW .....	141
6.3 THE TECHNICAL SPECIFICATION OF THE REAL WORLD MODELS .....	142
6.4 EVALUATION OF SUPPORTING SOFTWARE.....	147
6.4.1 Introduction to World Building using SAFE-VR™.....	148
6.4.2 VRML.....	149
6.4.3 Discussion.....	150
6.5 PRELIMINARY MODEL STUDIES.....	152
6.6 CONSTRUCTION OF PRELIMINARY PROTOTYPE.....	152
6.6.1 Introduction.....	152
6.6.2 CFD Prototype Test Model.....	153
6.6.3 Construction of SAFEVR™ Simulation.....	155
6.7 EVALUATION OF PRELIMINARY PROTOTYPE.....	156
6.7.1 Results.....	156
6.7.2 Assessment of Computational Efficiency.....	157
6.7.3 Visualisation Effectiveness.....	158
6.7.4 Discussion.....	159



6.8 CONCLUSIONS.....	160
6.9 SUMMARY.....	161

## **CHAPTER 7 DESIGN & EVALUATION OF VISUALISATION INTERFACE**

7.1 INTRODUCTION.....	163
7.2 SUMMARY OF THE AIRFLOW & POLLUTANT DISPERSION FEATURES .....	164
7.3 THE SPECIFICATION & DESIGN OF THE NUMERICAL ALGORITHMS GOVERNING THE VISUALISATION INTERFACE .....	166
7.3.1 The Variable Type.....	168
7.3.2 Sample Data Points.....	168
7.3.3 Interpolation Scheme.....	170
7.3.4 Time Stepping Parameters.....	170
7.4 VISUALISATION CALIBRATION & RESIDUAL ERROR ANALYSIS....	171
7.4.1 Identification of Reference Data.....	172
7.4.2 Scalar Data.....	173
7.4.2.1 The Performance of the HC & VSI Interpolation Scheme..	174
7.4.2.2 Discussion of Results.....	176
7.4.3 Particle Trace Generation.....	179
7.4.3.1 Introduction.....	179
7.4.3.2 HC Stream Divergence using Fixed Global time step change .....	180
7.4.3.3 VSI Stream Divergence using Fixed Global Time Step change.....	182
7.4.3.4 Vector Residuals from VSI & HC scheme at Fixed Global time steps.....	183
7.4.3.5 Variable Time Step HC Streamline Divergence According to Error Tolerance change.....	185
7.4.3.6 Variable Time Step VSI Streamline Divergence According to Error Tolerance change.....	186
7.4.3.7 Variable Time Step HC & VSI Comparison.....	189
7.4.3.8 Combined Residual Analysis Compared to optimum theoretical method.....	189
7.4.4 Conclusions.....	191
7.5 GRAPHICAL REPRESENTATIONS OF NUMERICAL DATA.....	192
7.5.1 Methane.....	192
7.5.1.1 Node Point Plots.....	193
7.5.1.2 Uniform Distribution.....	196
7.5.1.3 Random Distribution.....	198
7.5.1.4 2D Contouring.....	199
7.5.1.5 Generation of 3D Isosurfaces.....	201
7.5.2 Airflow.....	204
7.5.2.1 Animation of Ventilated Airflows.....	204
7.5.2.2 Stream Line Generation.....	208
7.6 FINAL DEFINITION OF INTERFACE CAPABILITIES.....	210
7.7 SUMMARY.....	211

## **CHAPTER 8 APPLICATION DESIGN & DEVELOPMENT**

8.1 INTRODUCTION.....	213
8.2 OUTLINE OF THE DEVELOPMENT PROCESS .....	214
8.3 CFD DATA LIBRARY SPECIFICATION.....	215
8.3.1 Data Library Map.....	215
8.3.2 CFD Model Parameters.....	216
8.3.3 Classification of Variables.....	217
8.4 IDENTIFICATION & CLASSIFICATION OF POTENTIAL HAZARDS.....	218
8.5 PHASE ONE SIMULATION CONSTRUCTION.....	219
8.5.1 World Building.....	219
8.5.2 Animation Map.....	221
8.5.3 The Post Processing of the CFD Simulation Data .....	223
8.5.3.1 Selection of Visualisation Graphical Form.....	223
8.5.3.2 Visualisation Parameters.....	224
8.5.4 Interactive Expert Control System (IECS) Design.....	225
8.5.4.1 Specifications.....	225
8.5.4.2 IECS Decision Making Process Map .....	226
8.5.4.3 User Control Methodology.....	230
8.5.5 Application Screen Shots.....	231
8.5.6 Preliminary Assessment of the Application .....	236
8.5.7 Developments.....	237
8.5.8 Discussion & Conclusions.....	237
8.6 PHASE TWO SIMULATION CONSTRUCTION.....	238
8.6.1 Introduction.....	238
8.6.2 Additional Specifications & Proposed Enhancements.....	239
8.6.2.1 Data Library Map.....	240
8.6.2.2 Use of HTML Media for Online Assistance.....	241
8.6.2.3 Hazard Identification.....	242
8.6.2.4 Extension to Initial CFD data Library.....	243
8.6.2.5 The Development of the Final Application Hazard Map ..	244
8.6.3 The Creation of the Additional CFD Simulation Models .....	248
8.6.3.1 Parameters.....	248
8.6.3.2 Application of CFD to Extended Scenarios .....	249
8.6.3.3 Classification of Additional Models.....	254
8.6.4 IECS Map.....	256
8.6.5 Application Screen Shots.....	257
8.7 APPLICATION ASSESSMENTS.....	262
8.7.1 Extent of Hardware Capabilities.....	262
8.7.2 Performance of Scientific Data Visualisations.....	263
8.7.3 Comparison of Application with Project Objective.....	264
8.7.4 Conclusions.....	265
8.8 SUMMARY.....	266

## CHAPTER 9 CONCLUSIONS & FUTURE WORK

9.1 SUMMARY OF THESIS INVESTIGATIONS .....	268
9.2 ORIGINAL CONTRIBUTIONS TO KNOWLEDGE.....	270
9.3 FURTHER WORK .....	271

REFERENCES.....	273
APPENDICES.....	288
APPENDIX I  Runge-Kutta 2 <sup>nd</sup> and 4 <sup>th</sup> Order.....	288
APPENDIX II VRML '97 Nodes.....	289
APPENDIX III Model Textures.....	290
APPENDIX IV CFD Results Data .....	291

## **ABSTRACT**

The current trend towards the adoption of retreat longwall mining methods and the associated rapid development of the access drivages has exacerbated the environmental conditions experienced within these workings. The combined use of roof bolt and continuous miner systems has improved the face advance rate within rapid development drivages. In order to maintain adequate dust and gas control it is essential that the auxiliary ventilation and monitoring systems are correctly installed and maintained

The causes of many potential environmental hazards experienced within auxiliary ventilated rapid development drivages, are often attributed to a failure by the workforce and supervisory officials to maintain the correct installation, maintenance and operational standards of the ventilation and mining systems. The potential ventilation hazards encountered may include: the failure to deliver the required fresh air quantity and velocity to rapidly dilute and disperse methane gas liberated in the vicinity of the cutting face, or the failure to maintain sufficient exhaust air quantity in the vicinity of the cut to adequately capture dust produced on cutting and loading of the extracted mineral.

Results of recent research studies have demonstrated that validated Computational Fluid Dynamics (CFD) simulation models can adequately replicate examples of good and bad ventilation. CFD models may be constructed and solved to examine the relative ventilation benefits produced by alternative mining and auxiliary ventilation configurations. These models enable the practitioner to predict and visualise the velocity, pressure and contaminant fields within an auxiliary ventilated drive. This research project has developed a prototype educational aid, which animates and visualises these airflow and pollutant dispersion patterns within a Virtual Reality (VR) model. By introducing a pollutant such as methane into the CFD models, the VR simulation highlights regions of potential methane concentration build-up to the trainee. The application also allows the user to select/investigate the environmental consequences of enacting a number of remedial actions.

## LIST OF FIGURES

FIGURE 2.1 EARLY COAL EXTRACTION METHODS, BELL PIT (LEFT) AND DRIFT MINE (RIGHT) .....	12
FIGURE 2.2 GAS DISTRIBUTION AT SEA LEVEL .....	13
FIGURE 2.3 THE COWARD DIAGRAM .....	15
FIGURE 2.4 METHANE GAS LAYERING EFFECT AND CAUSES .....	16
FIGURE 2.5 MINE VENTILATION SYSTEM USING SURFACE EXHAUST FANS (MCPHERSON 1992).....	22
FIGURE 2.6 FORCING AUXILIARY VENTILATION .....	24
FIGURE 2.7 AXIAL FAN, PRINCIPLE OF OPERATION .....	26
FIGURE 2.8 TYPICAL JET FAN ASSEMBLY.....	27
FIGURE 2.9 GENERAL FORM AND APPLICATION OF BERNOULLI'S LAW	
30	
FIGURE 2.10 LAMINAR FLOW.....	31
FIGURE 2.11 TURBULENT FLOW .....	32
FIGURE 2.12 RADIAL FAN OUTLET VELOCITY DIAGRAM .....	33
FIGURE 2.13. PRACTICAL HEAD CURVE FOR BACKWARD CURVED RADIAL FAN .....	33
FIGURE 2.14 HEAD CHARACTERISTICS FOR SERIAL (LEFT) AND PARALLEL (RIGHT) FAN COMBINATIONS.....	34
FIGURE 3.1 OPTIMISING CAD GENERATED GEOMETRY FOR CFD ANALYSIS.....	40
FIGURE 3.2 DEFINITION OF FLUID DOMAIN.....	41
FIGURE 3.3 EXAMPLES OF CFD BOUNDARY CONDITIONS.....	41
FIGURE 3.4 COMMONLY USED CFD MESH CELL TYPES.....	43
FIGURE 3.5 STRUCTURED QUAD BASED MESH (LEFT), UNSTRUCTURED TET BASED MESH (RIGHT).....	43
FIGURE 3.6 EXAMPLES OF CFD POST PROCESSING IMAGERY .....	46
FIGURE 3.7 THE UNIT VOLUME REPRESENTATION.....	47
FIGURE 3.8 TURBULENT VELOCITY FLUCTUATIONS.....	51
FIGURE 3.9 1/10 <sup>TH</sup> SCALE MODEL EXPERIMENT (MOLONEY 1997).....	55
FIGURE 3.10 SUPERIMPOSED EXPERIMENTAL & CFD DATA (MOLONEY 1997).....	57
FIGURE 3.11 WISTOW COLLIERY CASE STUDY MODEL (MOLONEY 1997).....	58
FIGURE 3.12 DIMENSIONLESS W MEASURED VELOCITY PLOT AGAINST CFD PREDICTIONS (MOLONEY 1997).....	58
FIGURE 3.13 CHARACTERISTIC FLOW REGIME PLANE FROM CFD PREDICTIONS (MOLONEY 1997).....	59
FIGURE 3.14 WOODBURN'S EXPERIMENTAL TUNNEL FIRE MODEL (WOODBURN AND BRITTER 1996).....	63
FIGURE 3.15 QUALITATIVE VENTILATION FLOW COMPARISONS (HARGREAVES ET AL 2000).....	65
FIGURE 3.16 QUANTITATIVE EVALUATIONS OF VENTILATION FLOW USING POINT SAMPLES (HARGREAVES ET AL 2000).....	66
FIGURE 3.17 HARGREAVES CM REPRESENTATION (HARGREAVES ET AL 2000).....	66

FIGURE 3.18 CUT CYCLE MODELLED BY HARGREAVES (HARGREAVES ET AL 2000).....	67
FIGURE 4.1 TETRAHEDREAL CELL PHYSICAL AND NATURAL CO-ORDINATE NUMBERING.....	78
FIGURE 4.2 CELL SEARCH CONDITIONS.....	80
FIGURE 4.3 DEPICTION OF HILL CLIMBING APPROXIMATION.....	81
FIGURE 4.4 SINGLE TETRAHEDRAL CELL NODE NUMBERING SCHEME ..	82
FIGURE 4.5 OCTREE BASED DATA REDUCTION PROCEDURE (KUHNER ET AL 2001).....	85
FIGURE 4.6 OCTREE BASED REDUCTION CRITEREA.....	86
FIGURE 4.7 EXAMPLE OF TREE BASED REDUCTION APPLIED TO A 2D REGULAR MESH.....	86
FIGURE 4.8 CONTEMPORARY VECTOR GLYPHS USED FOR FLUID FLOW VISUALISATION.....	90
FIGURE 4.9 VECTORS ON A 2D PLANE.....	91
FIGURE 4.10 VECTORS PLOTTED ACCORDING TO MESH INTERSECTIONS IN 2D .....	91
FIGURE 4.11 COMBINING 2D VECTOR SAMPLING PLANES IN A 3D DOMAIN.....	92
FIGURE 4.12 TIME STEPPED PARTICLE TRACING.....	93
FIGURE 4.13 PARTICLE STEERING ERROR.....	94
FIGURE 4.14 ADAPTIVE TIME STEPPING USING STEP-DOUBLING.....	97
FIGURE 4.15 TWO-STREAMLINE TRIANGULATION ERROR.....	98
FIGURE 4.16 TYPICAL 2D PLANE SCALAR CONTOUR VISUALISATIONS.....	99
FIGURE 4.17 LINEAR BASED 2D CONTOURING METHODOLOGY.....	100
FIGURE 4.18 SINGLE CELL CASE, NODES DEFINED AS ABOVE OR BELOW THRESHOLD.....	102
FIGURE 4.19 TRIANGULATION CASES FROM LORENSON'S CASE TABLE (LORENSON AND CLINE 1987).....	103
FIGURE 5.1 HUMAN SENSITIVITY TO LIGHT SPECTRUM COLOURS.....	111
FIGURE 5.2 RGB COLOUR CONTROL.....	112
FIGURE 5.3 PRIMARY PRIMITIVE ENTITIES USED IN CONVENTIONAL 3D MODELLING.....	115
FIGURE 5.4 PRIMITIVE WIREFRAME REPRESENTATION OF A BOX.....	116
FIGURE 5.5 APPROXIMATED CURVE USING LINE SEGMENTS ON A CYLINDER.....	117
FIGURE 5.6 EXAMPLE OF POLYGONAL MESH SIMPLIFICATION (LUEBKE 2001).....	119
FIGURE 5.7 BITMAPS USED FOR TEXTURE MAPPING.....	120
FIGURE 5.8 POINT LIGHT (LEFT), SUNLIGHT (CENTRE) AND SPOT LIGHT (RIGHT) SOURCES.....	121
FIGURE 5.9 EXAMPLES OF FLAT (LEFT) & SMOOTH (RIGHT) SHADING.....	121
FIGURE 5.10 VRML '97 TEXT FORMAT FOR PRIMITIVE BOX OBJECT....	123
FIGURE 5.11 THE 'VIRTUAL UNIVERSITY' (JIN AND WEN 2001).....	124
FIGURE 5.12 SCHULTZ'S VIRTUAL ENVIRONMENT FOR FEA DATA ANALYSIS (SCHULTZ ET AL 1998).....	131

FIGURE 5.13 TASK COMPLETION TIMES BASED ON ALTERNATIVE VR FORMATS (BOUD ET AL 1999).....	136
FIGURE 5.14 COMPARISONS OF ALTERNATIVE LEARNING TECHNIQUES (WITTENBURG 1995).....	137
FIGURE 6.1 PROJECT OBJECTIVE IN CONTEXT OF KEY TECHNOLOGICAL APPLICATIONS.....	142
FIGURE 6.2 COMPONENTS OF PROPOSED INTEGRATED VR ENVIRONMENT.....	147
FIGURE 6.3 OPERATORS USED FOR INTERACTIVE CONTROL WITHIN SAFEVR.....	148
FIGURE 6.4 EXAMPLE OF IMPLEMENTATION OF SAFEVR OPERATOR LANGUAGE.....	149
FIGURE 6.5 CFD MODEL GEOMETRY USED FOR EVALUATION.....	154
FIGURE 6.6 LONGITUDINAL VECTOR PLOT.....	156
FIGURE 6.7 3D COMBINATION VECTOR PLOT.....	157
FIGURE 6.8 ISOSURFACE GAS DISPERSION PLOT.....	157
FIGURE 7.1 NUMERICAL SIDE OF INTERFACE FLOW DIAGRAM.....	167
FIGURE 7.2 SPECIFICATION OF VARIABLE TYPE SUB FLOW DIAGRAM.....	167
FIGURE 7.3 SPECIFICATION OF SAMPLING POINTS SUB FLOW DIAGRAM.....	168
FIGURE 7.4 SPECIFICATION OF INTERPOLATIVE SCHEME SUB FLOW DIAGRAM.....	170
FIGURE 7.5 SPECIFICATION OF TIME STEPPING PARAMETERS SUB FLOW DIAGRAM.....	171
FIGURE 7.6 SAMPLING GRID TAKEN FROM CFX5.....	173
FIGURE 7.7 GRAPH DEPICTING LINEAR RESIDUALS BETWEEN HC AND VSI INTERPOLATION.....	174
FIGURE 7.8 GRAPH DEPICTING LINEAR RESIDUALS PERCENTAGE ERROR BETWEEN HC AND VSI.....	175
FIGURE 7.9 RESIDUALS PLOTTED IN WIREFRAME MODEL CONTEXT...	175
FIGURE 7.10 RESIDUAL PLOTTED AS PERCENTAGE ERROR IN WIREFRAME CONTEXT.....	176
FIGURE 7.11 SPHERE GLYPH VISUALISATION DEMONSTRATING IMPERCEPTIBLE ERROR.....	178
FIGURE 7.12 GRAPH DEPICTING STREAM DIVERGENCE FOR HC FIXED TIME STEP SCHEME.....	181
FIGURE 7.13 HC FIXED TIME STEP STREAM DIVERGENCE VISUALISATION.....	181
FIGURE 7.14 GRAPH DEPICTING STREAM DIVERGENCE FOR VSI FIXED TIME STEP SCHEME.....	182
FIGURE 7.15 VSI FIXED TIME STEP STREAM DIVERGENCE VISUALISATION.....	183
FIGURE 7.16 HC & VSI FIXED SCHEME RESIDUAL DIVERGENCE GRAPH.....	184
FIGURE 7.17 HC AND VSI 30FPS STREAM DIVERGENCE VISUALISATION.....	185

FIGURE 7.18 HC SCHEME VARIABLE TIME STEP STREAM DIVERGENCE VISUALISATION.....	186
FIGURE 7.19 VSI VARIABLE TIME STEP STREAMLINE DIVERGENCE....	187
FIGURE 7.20 VSI SCHEME VARIABLE TIME STEP STREAM DIVERGENCE VISUALISATION.....	187
FIGURE 7.21 FRAME RATES PRODUCED BY STEP DOUBLING SCHEME ACROSS TRACE LIFE.....	188
FIGURE 7.22 HC AND VSI STREAMLINE VISUALISATION USING ERROR TOLERANCE OF 0.0125M.....	189
FIGURE 7.23 OVERALL STREAM DIVERGENCE RESIDUAL GRAPH.....	190
FIGURE 7.24 OVERALL STREAMLINE DIVERGENCE VISUALISATION..	190
FIGURE 7.25 CM21 DATA SET VRML REPRESENTATION.....	192
FIGURE 7.26 NODE DEPENDENT SCATTERED POINT GAS DISPERSION PLOT (1%).....	194
FIGURE 7.27 NODE DEPENDENT SCALED SCATTERED POINT GAS DISPERSION PLOT (1%).....	194
FIGURE 7.28 NODE DEPENDENT COLOUR GRADED SCATTERED POINT GAS DISPERSION PLOT (1%).....	195
FIGURE 7.29 NODE DEPENDENT REDUCED COLOUR GRADED SCATTERED POINT GAS DISPERSION PLOT (1%).....	195
FIGURE 7.30 REGULAR SAMPLED SCATTERED POINT GAS DISPERSION PLOT (1%).....	197
FIGURE 7.31 DENSE RANDOM POINT GAS DISPERSION PLOT (1%).....	198
FIGURE 7.32 LOW DENSITY RANDOM POINT GAS DISPERSION PLOT (1%).....	199
FIGURE 7.33 2D CONTOURING SCHEME USING VRML.....	200
FIGURE 7.34 EXAMPLES OF CONTOURS PRODUCED USING VRML DISPLAYED WITH GRID DETAIL.....	200
FIGURE 7.35 MC GENERATED ISOSURFACE USING COARSE 0.25M SPACING.....	202
FIGURE 7.36 MC GENERATED ISOSURFACE USING 0.125M SPACING...	202
FIGURE 7.37 MC GENERATED ISOSURFACE USING FINE 0.0625M SPACING.....	203
FIGURE 7.38 SEED POINT PLANES USED FOR PARTICLE STREAM ANIMATION.....	205
FIGURE 7.39 SINGLE (ABOVE) AND PULSED (BELOW) DUCT PARTICLE ANIMATIONS.....	206
FIGURE 7.40 FACE SEEDED PARTICLE ANIMATIONS AT FOUR TIME INTERVALS.....	207
FIGURE 7.41 SIDE VIEW DUCT SEEDED EXTRUDED STREAMLINES.....	209
FIGURE 7.42 PLAN VIEW DUCT SEEDED EXTRUDED STREAMLINES....	209
FIGURE 7.43 INTERNAL VIEW (1) DUCT SEEDED EXTRUDED STREAMLINES.....	209
FIGURE 7.44 INTERNAL VIEW (2) DUCT SEEDED EXTRUDED STREAMLINES.....	210
FIGURE 7.45 STREAM LINE EXTRUSION FACE CONSTRUCTION PROCESS.....	210
FIGURE 7.46 FINAL DEFINITION OF INTERFACE CAPABILITIES AND GRAPHICAL OUTPUT.....	211



FIGURE 8.1 OUTLINE DEVELOPMENT PROCEDURE FLOW DIAGRAM...	214
FIGURE 8.2 OPERATOR SIDE CFD DATA MODEL REPRESENTATION (HARGREAVES ET AL 2000).....	215
FIGURE 8.3 BUTTOCK SIDE CFD DATA MODEL REPRESENTATION (HARGREAVES ET AL 2000).....	216
FIGURE 8.4 CFD DATA LIBRARY MAP.....	217
FIGURE 8.5 CONSTITUENT 3D MODEL PARTS.....	220
FIGURE 8.6 CFD GEOMETRY (LEFT) AND DETAILED 3D REPRESENTATION (RIGHT).....	221
FIGURE 8.7 CM ANIMATION DETAIL AND FRAMES.....	222
FIGURE 8.8 DRIVAGE ANIMATION DETAIL AND FRAMES.....	224
FIGURE 8.9 IECS DESIGN OUTLINE.....	226
FIGURE 8.10 USER REQUEST CONTROL PATHS.....	227
FIGURE 8.11 PHYSICAL WORLD UPDATE PATHS.....	228
FIGURE 8.12 VISUALISATION UPDATE PATHS.....	229
FIGURE 8.13 USER CONTROL PANEL USED IN VE.....	231
FIGURE 8.14 STARTUP SCREEN DETAILING VR DRIVAGE AT INITIAL CUT STAGE.....	232
FIGURE 8.15 CUT 1, BOOM RAISED, FACE PARTICLE FLOW AND METHANE CONCENTRATION.....	232
FIGURE 8.16 CUT 2, BOOM LOWERED, FACE PARTICLE FLOW AND METHANE VISUALISATION.....	233
FIGURE 8.17 CUT 4, BOOM LOWERED, DUCT PARTICLE FLOW AND METHANE VISUALISATION.....	233
FIGURE 8.18 CUT 6, BOOM LOWERED, DUCT AIRFLOW DETAIL.....	234
FIGURE 8.19 CUT 6, BOOM LOWERED, FACE PARTICLE FLOW DETAIL.....	234
FIGURE 8.20 CUT 6, BOOM LOWERED, METHANE DETAIL.....	235
FIGURE 8.21 CUT 6, BOOM LOWERED, SCRUBBER ACTIVATED, METHANE DETAIL.....	235
FIGURE 8.22 CFD DATA LIBRARY DATA SETS INCLUDED IN SECOND PHASE.....	241
FIGURE 9.23 FINAL APPLICATION DATA LIBRARY MAP.....	245
FIGURE 8.24 SHORT DUCT CFD MODEL.....	249
FIGURE 8.25 REDUCED FLOWRATE CFD MODEL.....	249
FIGURE 8.26 OFF-CENTRE DUCT INSTALLATION CFD MODEL.....	250
FIGURE 8.27 EXTENDED DUCT CFD MODEL (OPERATOR SIDE).....	250
FIGURE 8.28 EXTENDED DUCT CFD MODEL (BUTTOCK SIDE).....	250
FIGURE 8.29 OVERLAP CFD MODEL, BOOM RAISED.....	251
FIGURE 8.30 OVERLAP CFD MODEL, BOOM LOWERED.....	251
FIGURE 8.31 SCENARIO 18, CM GHOST WITH DUCT AIRFLOW VISUALISATION ACTIVE.....	252
FIGURE 8.32 SCENARIO 11, LEVEL 3 HTML DOCUMENTATION .....	253
FIGURE 8.33 SCENARIO 5, CM GHOST WITH METHANE AND FACE VENTILATION VISUALISATIONS.....	253
FIGURE 8.34 SCENARIO 3, LEVEL 2 HTML DOCUMENTATION (GENERAL HELP) ACTIVE.....	254
FIGURE 8.35 SCENARIO 4, LEVEL 3 HTML DOCUMENTATION, METHANE AND FACE AIRFLOW VISUALISATION.....	254
FIGURE 8.36 SCENARIO 18, LEVEL 3 HTML DOCUMENTATION, DUCT AIRFLOW VISUALISATION.....	255

FIGURE 8.37 SCENARIO 12, FACE AIRFLOW VISUALISATION.....	255
FIGURE 8.38 MINER REVERSING INTO BUTTOCK SIDE CUT POSITION..	256
FIGURE 8.39 SCENARIO 18, METHANE GAS DISPERSION.....	256

## TERMINOLOGY

**Air Way:** An underground tunnel or passage along which air passes through

**Auxiliary Fan:** Fan used within the mine, usually in working faces to assist ventilation provided by the main surface fans. Used in conjunction with ducting to direct airflow at face.

**Belt:** Long belt system used to convey large quantities of coal from the face to along the roadway.

**Black Damp:** High concentration of carbon dioxide, low oxygen.

**Booster Fan:** An additional fan used to increase delivery of air flow and pressure.

**Canvas Door:** Doorway used to block or direct airflow

**Carbon Dioxide:** Gas present in 'normal' atmosphere, exhaled, also produced via combustion of carbon based matter

**Carbon Monoxide:** Highly toxic gas formed via incomplete carbon based combustion processes.

**Colliery:** Alternative term for coal mine

**Computational Fluid Dynamics:** Process of seeking a flow solution by using computers to solve the navier stokes equations

**Continuous Miner:** Large mechanised coal extracting machine, works directly on the cutting face using a large rotating cutting boom.

**Davy Lamp:** Early safety lamp, prevents ignition of methane through a safety gauze

**DirectX™:** Microsoft 3D software environment

**Element:** A single part of a meshed flow domain, and element in 3D takes the form of a geometric shape, typically a tetrahedron or cube, where nodes are positioned at its endpoints

**Extraction:** Process of removal of coal or other mined ores from ground

**Face:** (1) Immediate region of coal extraction (2) small facet of a geometric object, 3d Objects are constructed of a number of faces

**Fault:** A discontinuity in a coal seam or strata

**Feeder:** Term used to describe gas liberation from rock, associated with a hissing noise, sometimes called a 'blower'

**Fire Damp:** Potentially explosive mixture primarily of methane and air

**Fissure:** Small continuous crack in rock

**Fossil Fuel:** A product of the decomposition of carbon based matter over millions of years, coal, oil and gas are all fossil fuels

**Gallery:** Underground horizontal roadway

**Gob:** Waste material

**Heading:** A roadway which is under development

**Hydrogen Sulphide:** Gas associated with 'stink damp' owing to its unpleasant aroma.

**Hygrometer:** Instrument used to measure relative humidity

**Isosurface:** The three-dimensional variant of a contour, the surface acts as the boundary between specified values within a dataset

**Main Fan:** Surface fan providing sub surface ventilation usually by blowing

**Manometer:** Instrument for pressure measurement

**Mesh:** A computational grid dividing a predefined flow domain into smaller elements

**Methane:** Potentially explosive gas, fire damp

**Methane Drainage:** Process used to extract methane from coal in controlled manner, sometimes used as useful energy source.

**Natural Ventilation:** Ventilation via non forced means

**Nitrogen:** Gas occupying 79% of the breathable atmosphere

**Outbye:** Opposite direction to face, back to pit shaft

**Outburst:** Sudden, violent explosion of pressurised gas from a face cut

**Oxygen:** Life supporting gas occupying around 20% of breathable atmosphere

**Pillar:** Pillar of unexcavated coal used as a roof support

**Pit:** Alternative term for coal mine

**Pneumoconiosis:** Lung disease resulting from dust inhalation

**Respirable Dust:** Coal dust particles Sub 10 microns

**Return:** Road way which air passes through after the cut face

**Return Air:** Air that has already passed through the working

**Rock Dust:** Fine stone dust spread on roadways as a thermal inhibitor to prevent coal dust explosions.

**Roof Bolt:** Steel rod secured into a hole in the roof, used alongside wire mesh for roof support

**Roof Support:** General term for equipment/objects used to hold up roofs, rods, mesh, pillars etc.

**Roof Bolter:** Machine used to fix rods into roof

**Safety Lamp:** (Davy Lamp) Specially designed flame lamp isolating flame from external gases via a gauze.

**Self Rescuer:** Term for small canister worn on miners belt containing respirator.

**Shaft:** Vertical connecting passage between surface and workings

**Shift:** Any single working length of time, usually 8 hours.

**Shuttle Car:** Machine used to transfer coal from working face to conveyor.

**Stink Damp:** Hydrogen Sulphide, identified by foul odour.

**Stone Dust:** See 'Rock Dust'

**Stopping:** Brick or plaster wall used to seal off old workings for the purpose of redirecting airflow.

**Streamline:** Path taken by a massless particle released into a fluid flow domain recorded over time

**Sump:** Low point in mine, used to collect drainage water.

**Tip:** Mine waste material heaped at the surface.

**Trailing Cable:** Heavy duty cable used to provide electrical power to sub surface equipment.

**Undercut:** A cut below the coal face.

**Upcast Shaft:** Shaft through which air is exhausted to the surface.

**Vector:** Icon usually in the form of an arrow shape defining direction and scalar quantity of velocity in terms of scale and/or colour

**Ventilation:** General term for supply of clean air to workings and exhausting of contaminants.

**Virtual Reality:** Interactive computational representation of a real world scenario

**Viscosity:** Fluid dynamics term, property of a fluid that resists flow.

**White Damp:** Carbon Monoxide rich gas mixture.

## **ABBREVIATIONS**

**AR** Augmented Reality  
**CFD** Computational Fluid Dynamics  
**CG** Computer Graphics  
**CM** Continuous Miner  
**DEEE** Diesel Engine Exhaust Emissions  
**DPM** Diesel Particulate Matter  
**FPS** Frames Per Second  
**HC** Hill Climbing  
**HMD** Head Mounted Display  
**HTML** Hyper Text Markup Language  
**IECS** Interactive Expert Control System  
**IGES** Initial Graphics Exchange Specification  
**MC** Marching Cubes  
**MR** Mixed Reality  
**PPM** Parts Per Million  
**VR** Virtual Reality  
**VRML** Virtual Reality Modelling Language  
**VSI** Volume Space Interpolation

## **ACKNOWLEDGEMENTS**

The author wishes to thank the following persons for their assistance and support over the duration of this research project and write up period.

- Dr Ian Lowndes for his supervision and advice throughout the project.
- Dr Dave Hargreaves & Dr Damian Schofield for technical assistance concerning the CFD and VR studies respectively.
- UK Coal Ltd. for assistance and consultation.
- My office colleagues for wise words and encouragement.
- Ruth for tolerance and eternal optimism.
- My family for further necessary tolerance and eternal optimism.
- Lorenzo for numerous adventures over the years and the Italian research perspective.

# **CHAPTER 1**

## **INTRODUCTION**

### **1.1 Introduction**

The current trend towards the use of increased mechanisation and environmental monitoring technology has greatly increased the productivity of modern coal mines. In particular, the adoption of retreat continuous longwall mining methods and their associated rapid development drivages has greatly enhanced the mineral output from UK coal mining operations. However, these improvements in productivity and efficiency have been accompanied by an increase in the pollutant burden placed upon the mine ventilation and cooling systems. This has demanded improvements to the design, maintenance and operation of these control systems to effect satisfactory environmental conditions within these high production workings.

Despite the introduction of increased extraction and mineral transport systems the mining process today is still dependent on the presence of manual workers to supervise, operate and maintain the equipment installed within the production and development workings. The provision and maintenance of a safe working environment is therefore of paramount importance, to both protect the workforce to and minimise disruption to production process.

The maintenance of the environmental safety within mines accommodates a greater range of hazards than most other heavy industrial working environments, where the chief risks of a physical nature, including the operation equipment etc.

Within longwall coalfaces and rapid development drivages a range of pollutants, including gases, dusts and heat and humidity are emitted during the mineral extraction and transport processes. The primary means of control

of these emissions is the design and operation of safe and reliable ventilation systems, in order to deliver air at the correct quality and quantity to rapidly dilute and remove these pollutants. The level of the pollutant loads within the ventilating air must be constantly or routinely monitored, to ensure that the concentration levels of gas or particulate contaminants are maintained below prescribed threshold levels.

To ensure the maintenance of adequate dust and gas control within rapid development drivages, it is essential that the auxiliary ventilation and monitoring systems are correctly installed, operated and maintained. This requires an understanding and appreciation of the effects that any alteration to the ventilation control parameters may produce, and in particular highlight the creation of potentially hazardous situations. In addition, it is important to demonstrate the impact all factors, such as the incorrect installation or maintenance of equipment, may have on the atmosphere within a mine working.

The primary objective of the research project is the development of a prototype software based educational tool, suitable for training of ventilation supervisory officials and heading teams. The construction of the training package will enable the visualisation of the consequences of potentially hazardous events associated with the ventilation of rapid development drivages. The project will involve the structured integration of the results of the solution to Computational Fluid Dynamics (CFD) models within a Virtual Reality (VR) world environment. The use of this tool would allow trainees to gain a greater appreciation of the reasoning behind current regulations and operational good practice procedures, which govern the correct installation and operation of the mining and auxiliary ventilation systems.

Previous research studies have identified that human factors are responsible for increasing risk in these environments as a result of limitations of perception, (Walsha et al 1998 and Squelch 1998). The current research project seeks to address this concern, by providing a training platform



increasing the perception of the trainee and allowing a safe exposure to hazardous situations not obtainable through traditional training techniques.

A parallel aim of the project was to perform a feasibility study to evaluate the integration of two technologies, CFD and VR, which have been the subject of many independent research studies in recent times. The key objective of this study was to identify the advantages that may be gained by the novel development of a combined application of these two separate technologies. The results produced by the project have provided a benchmark, by which to evaluate the capability of current desktop-computing platforms to deliver an authentic educational environment based on VR technology. The future development of improved computational hardware and graphical processor capacity will allow the further objectives, principles and methodologies outlined in this thesis to be realised.

## **1.2 Problem Definition**

Recent research has indicated that incidents related to environmental control in rapid development workings are related to human factors associated with the installation, operation and maintenance of auxiliary ventilation systems, (Squelch 1998). It has been indicated that traditional training techniques, which rely upon traditional instruction methods, do not transfer well to the working environment. It is therefore essential that improved training methods be constructed to ensure that workers are truly aware of the environmental effects they may be produced by unscheduled or unplanned change of the operation of the mining or ventilation system.

The working environment, within a rapid development drivage, is influenced by a large number of variables. Should these parameters be changed singly or cumulatively, they may produce significant changes to the ventilation characteristics required to maintain a safe atmosphere in terms of gaseous and particulate contaminant general body concentrations. The quality of the atmosphere the workers are exposed to is dependent on the rate at which

pollutants are introduced, and the ventilation flow rate delivered. The rate a pollutant rate is introduced is dictated by a combination of factors including, the geology and the rate of mineral production.

For a given geology and mining system, the auxiliary ventilation system will be designed to deliver the required fresh air quantity and distribution to adequately dilute the methane gas liberated and to provide effective control of dust. An optimised auxiliary ventilation system will be designed to have capacity to accommodate minor fluctuations in pollutant emission. For such a system it is commonplace for workers to become complacent and to develop routine incorrect operational standards that may seemingly have no detrimental effect. The ventilation system and the workforce may then not be able to cope with less common, sudden increases in pollutant levels, which may lead to potentially fatal consequences. The key factor is that the work force needs to develop a true appreciation of the direct environmental impact of their actions. The problem this project seeks to address is the development of a tool to enhance the educational experience of the workforce with regard to good ventilation practice and environmental hazard assessment.

### **1.3 Aims and Objectives of the Research Project**

The global objective of the project was the development of a software application to enhance the training needs of both the supervisory officials and miner workers, within a modern rapid development drive. Several methods and technologies were available concerning the acquisition of scientific data, the formatting and display medium. This application would achieve this target via the utilisation of scientific data to communicate important information regarding the state of the working atmosphere in relation to the workers actions. This scientific data originated from the application of CFD to a generalised rapid development drive providing data capable of describing all characteristics of the atmosphere relevant to maintaining a safe working environment. The scientific data was then processed employing conventional visualisation and feature extraction

techniques to produce a series of flow visualisations. These visualisations were then placed in context via means of a Virtual Environment whereby trainees could experience an "action consequence" relationship in universal terms easily understood and transferred to the working environment. The project therefore contains a series of local objectives concerning, data acquisition, data post processing, visualisation and consolidation within a virtual environment. These stages are outlined in a structured way in the following section.

## **1.4 Research Methodology Adopted**

To achieve the project objectives the following individual tasks were executed:

- A summary review of the published research literature related to the subsurface environmental control, and in particular:
  - A review of current ventilation methods employed in the rapid development drive environment
  - The application of Computational Fluid Dynamics (CFD) to the solution of mine ventilation problems.
  - The use of numerical methods for the visualisation and interpretation of 3D volume data sets such as those produced through CFD simulations.
  - The use of virtual reality methods for training and information display in hazardous environments.
- The identification of a suitable software application on which to build and link the integration of the CFD simulation model data and the Virtual Reality (VR) world environments
- A familiarisation with programming languages specific to virtual worlds and others deemed necessary.

- The development and consolidation of interface methods between the data protocols of the Virtual Reality (VR) environment and the Computational Fluid Dynamic (CFD) simulations.
- The testing and appraisal of proposed CFD/VR interface methods described above.
- The identification of a specific range of mining/ventilation scenarios that may create a ventilation hazard. The cause and effect of these occurrences should be detailed. In addition, the range of corrective means and procedures that may be employed to recover such a hazardous situation should be identified
- The development of CFD models to covering the range of ventilation hazards identified that may be created and the consequences of initiating corrective measures and/or evacuation procedures.
- The development of VR representations and simulations of the animated airflow, gas and dust dispersion patterns and hazard levels predicted by the validated CFD models utilising the interfacing methods identified and tested. These models will visualise the environmental consequences of the occurrence of such hazards and of initiating corrective measures.
- The development of a tutorial and training interface to allow the trainee to observe the consequences of the occurrence of the various hazards, to review the causes and the range of correct and incorrect remedial and evacuation options.

## 1.5 Thesis Outline

During the course of the research project a comprehensive series of literature reviews were conducted to provide both background to support and a foundation on which to build the resultant training application. Consequently, Chapters 2 to 6 all include a brief summary of the major conclusions drawn from the research investigations identified by these literature surveys.

Chapter 2 presents a brief historical overview of the development of UK coal mining methods to the present day, and highlights the various mine environmental hazards encountered and the development of the various ventilation, engineering and management methods to control these hazards. The source of each pollutant is detailed and the potential effects to human health and safety and mineral production summarised.

The topic of subsurface mine environmental engineering spans a wide range of subjects relevant to the whole extraction process, this review provides a general background to the ventilation solutions employed and in particular focuses on the ventilation requirements of the auxiliary ventilation systems employed in rapid development drivages.

To understand ventilation flow characteristics it is necessary to apply some fundamental principles of fluid flow to the analysis of common ventilation flows. Chapter 3 presents an overview of those of fluid mechanics principles that are applicable to the study and solution of sub surface ventilation problems, and provides a background to the basic principles upon which the conventional theories are based.

Since mine ventilation systems form a basic airflow circuit, the transient and steady flow behaviour experienced by such systems may be described in terms of the governing laws of fluid flow. The complexity of the model chosen to describe a particular flow phenomenon depends on a number of

factors, which include the level of detail required. For example, if an assessment of the pressure drop experienced along a length of ventilation ducting is required, a one-dimensional mathematical model may be employed to produce a satisfactory estimate. However, if it is required to understand the mixing of a gas emission in the vicinity of the face of a mechanized heading a more three-dimensional solution of the governing fluid equations as afforded by CFD may be required.

Chapter 4 provides an overview of CFD, which is subsequently employed to model the ventilation flows and pollutant dispersion experienced within auxiliary ventilated rapid development drivages. The process referred to as CFD contains a number of sub processes, pre-processing, solving and post processing. This chapter provides a summary of each process highlighting the major contribution to the analysis as a whole. A review of the current state of research activity into the application of CFD methods to subsurface ventilation and associated areas is also provided.

Chapter 5 outlines the development of algorithmic tools with which to visualise large and complex data sets, such as produced by the CFD simulation of ventilation flows within rapid development drivages. With the continuing expansion and development of computational analysis methods the resulting data sets have increased in size and type to such an extent that the range of numerical methods that may be applied to their interpretation has become an active research discipline in its own right. This chapter therefore focuses upon areas such as feature extraction, data optimisation, interpolation techniques and graphical data representation, all of which play a part in the visualisation of ventilation data.

Chapter 6 presents an overview of the development and application of *Virtual Reality* (VR) tools within which to view visualisations of complex CFD ventilation and gas pollutant dispersion data. This chapter summarises the technology and construction methods necessary to build a virtual environment, and provides an evaluation of current applications and summarises key VR related research issues.

Chapter 7 overviews the research work conducted to determine the hardware and software specifications required to construct interactive VR world representations of a conventional rapid development drivage within which to view the ventilation and pollutant dispersion data predicted by CFD simulation models.

The focus of the work reported in this Chapter is the critical evaluation of the integration of CFD visualisations and VR worlds and interactive control systems using existing methods only previously applied for independent applications of CFD and VR. The strengths and weaknesses of these methods and applications are highlighted through a simple case study using a representative CFD data set.

Chapter 8 summarises the results of the research work conducted to develop a single interface with which to import and process raw CFD simulation data and produce a series of flow visualisations suitable for display and interpretation within an immersive VR environment.

The methods adopted were built on the foundation of the various numerical techniques introduced in Chapter 5. The appropriate numerical processing algorithms were identified and then applied to the CFD simulation data. The comparative performance of a number of alternative methods employing a single reference data set was conducted to identifying the best numerical method in terms of accuracy and computational economics.

The chapter concludes with the definition of the final specification of the performance capabilities required of the developed CFD/VR interface program and of the evaluation criteria to judge the levels of scientific and perception accuracy.

Chapter 9 reviews the results of the research work undertaken to undertake the design and development of the final integrated CFD and VR prototype training application. The process of the specification, design and

construction of this application, is built on the foundation of both the results of the evaluation studies presented in Chapter 7 and the components of the interface programme identified in Chapter 8.

The Chapter details the two development phases used to construct the VR application. The first phase of development includes an evaluation of the application and a number of conclusions are drawn, upon which the second phase of the application development was built.

The operation of the prototype training application is illustrated using an extensive range of computer screen shots. The Chapter concludes with a section that discusses the performance of the application with respect to the original requirements and the specifications detailed in Chapter 7.

Chapter 10 summarises the key conclusions drawn during the project and includes a summary of potential future development work.



## CHAPTER 2

### THE MINING ENVIRONMENT

#### 2.1 Introduction

This Chapter presents a brief historical overview of the development of UK coal mining methods to the present day, and highlights the various mine environmental hazards encountered and the development of the ventilation, engineering and management methods to control these hazards. The source of each pollutant is detailed and the potential effects to human health and safety and mineral production summarised. This review provides a general background to the ventilation solutions employed and in particular focuses on the ventilation requirements of the auxiliary ventilation systems employed in rapid development drivages together with details of those methods of analysis employed by the mining community to gain a greater understanding of the prevailing ventilation characteristics.

#### 2.2 Current and Historical Mining Methods

The extraction and utilisation of ore and other deposits from surface and deep mines is perhaps one of the oldest industries practised across the world. Originally mining concentrated primarily on the extraction of metal bearing ore for use in the manufacture of weapons and tools. It was not until the early middle ages that coal became an acceptable fuel source, although the use of the technology available at the time limited these excavations to near surface. These type of excavations were referred to as *Bell Pits* owing to the familiar shape. Right up until the 18<sup>th</sup> Century other near surface methods were employed such as the excavation of coal seams visible at the edge of hillsides, these were referred to as *Drift Mines*. These early methods used little or no methods of roof support or ventilation. The fact that many became unsafe and collapsed probably reduced the requirement for any kind of mechanised ventilation. The 18<sup>th</sup> century saw the introduction and use of

the more modern room and pillar method which used unexcavated coal pillars to form the roof support. Figure 2.1 illustrates typical bell pit and drift mine examples.

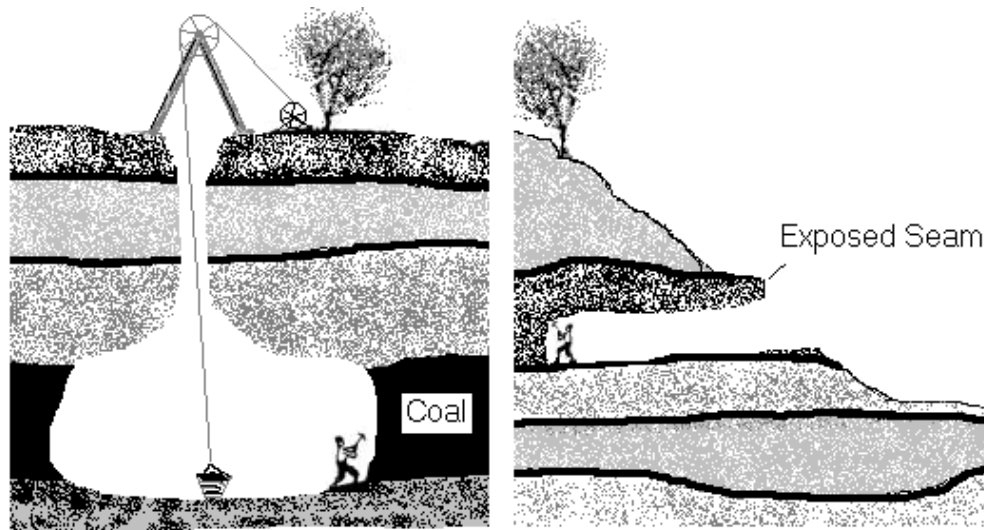


Figure 2.1 Early coal extraction methods, bell pit (left) and drift mine (right)

The development of roof supports, which allowed the excavations to move further away from the surface connections and to move to greater depth necessitated the development of thermal and mechanical ventilation methods to supplement the use of natural ventilation currents. Safety in these early mines had not been given much attention but following the recommendations made by a number of government colliery accident inquiries a series of legislation governing the health and safety within UK mine workings was formulated. Today, industrial safety related regulations are based upon the modern Health and Safety Act of 1974 upon which are based the monitoring and mining technology and operational procedures existing today.

Contemporary coal mining methods in the UK have developed in response to increased competition, increased health and safety legislation and the availability of heavy industrial equipment such as the continuous miner. The typical production rate of a contemporary drivage may now exceed 100m/week in order for that mine to remain a viable operation, typical development rates fall in the 75-150m range depending on local conditions

and requirements. Other similar mechanised methods, such as the mono and twin boomed road header systems are also employed throughout the world. The progress of a cut into the coal seam is limited by the requirement to periodically set roof support and to maintain the advance rate and integrity of the associated auxiliary ventilation systems. As the continuous miner progresses the face cut, the cut mineral is loaded onto a shuttle car. Once the miner has advanced the face by a stipulated distance the miner is backed out of the cut to allow the performance of roof bolting operations to provide roof support, the miner may then continue the procedure. The roof bolting operation employs mesh and steel or composite bolts into the roof and walls to provide support. Within UK deep coal mine operations a continuous miner may typically be allowed to advance a cut a distance of up to 5m before roof supports are required to be set. Although where local rock conditions allow progress beyond 5m, known as an *extended cut* is possible.

## 2.3 Mine atmosphere

### 2.3.1 Gases

The ideal surface composition of atmospheric air at sea level consists of a number of primary gases, oxygen, nitrogen, carbon dioxide and argon at normal average concentrations given in figure 2.2. below

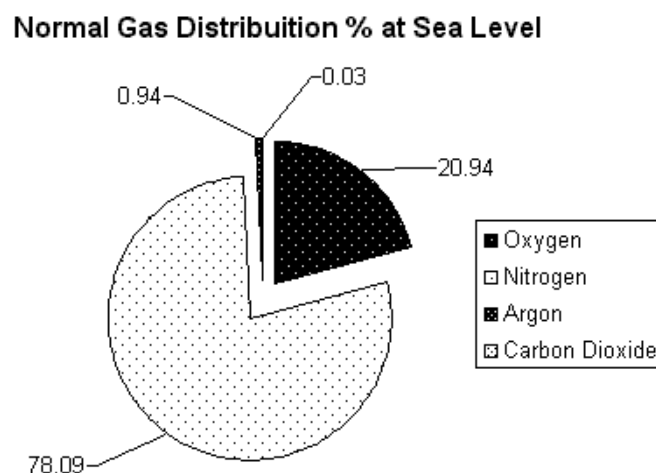


Figure 2.2 Gas distribution at sea level

The range of gases that may be emitted into the atmosphere of an underground mine may be classified as being: irritants, asphyxiants, carcinogens, allergens poisonous, flammable and/or explosive. The range of gases, dust and heat and humidity liberated underground is dependent upon a number of factors including the geology and the mining method employed. During coal mining gases are primarily released from the strata, explosives and diesel powered mining equipment. In an enclosed environment such as a mine the introduction of pollutant gases may either consume or displace oxygen. If the oxygen level is depleted below a given level this may cause asphyxiation. To avoid the onset of these deleterious physiological effects UK Mining Health and Safety regulations stipulates a minimum oxygen level of 19.5% by volume in the ventilation air. The most commonly found gases present within deep UK coalmines are, oxygen, nitrogen, carbon monoxide/dioxide and methane. Methane is primarily emitted from the coal seams and bed separation cavities, its properties are detailed as follows:

- |                                 |                           |
|---------------------------------|---------------------------|
| • Chemical Formula              | CH <sub>4</sub>           |
| • Identifiable Characteristics  | No odour/taste/visibility |
| • Source                        | Decayed carbon matter     |
| • Explosive Range (air mixture) | 5 - 15%                   |
| • Specific Gravity              | 0.555                     |

Other gases present in deep mines at lesser quantities include hydrogen sulphide produced by the dissolution of sulphur in water, and poor ventilation, nitrogen dioxide (a product of diesel combustion exhaust gas) and sulphur dioxide (produced by the chemical or physical combustion of sulphide ores). All of these gases are considered to be deleterious to human health and they may all be considered in varying degrees to be destructive to life.

Methane is often released as a constituent of a cocktail of gases referred to as *firedamp*. The formation of this cocktail of gases is principally a by-product during the formation of coal and is thus is liberated as part of the coal

extraction process. The chief constituent methane is contained within the coal, adsorbed on the surface coal structure and absorbed within the open pores. Non-porous inter coal measure rocks often cap and prevent the release of these gases prior to mining. The methane gas may often be stored under great pressure, which may be released by a number of mechanisms either in a controlled or highly uncontrolled manner leading to *outbursts*.

The principal danger firedamp presents to coal mine workers is associated with its explosive properties. The inflammable content of firedamp almost entirely consists of methane. Methane in air is explosive in the range of 5-15% . Gas mixed within this range is inflammable, at levels nearer 5% the mixture will burn locally around the ignition source, at levels at around 9.5% the mixture is at its most explosive, higher or lower concentrations reduce the explosivity of the mixture. These levels can change in relation to the composition of the surrounding atmosphere, for example, lower levels of oxygen will lower the upper limit of inflammability. Figure. 2.3 illustrates the *Coward diagram* developed by Coward (1929) detailing the flammability and explosivity ranges of methane in air (McPherson 1992)

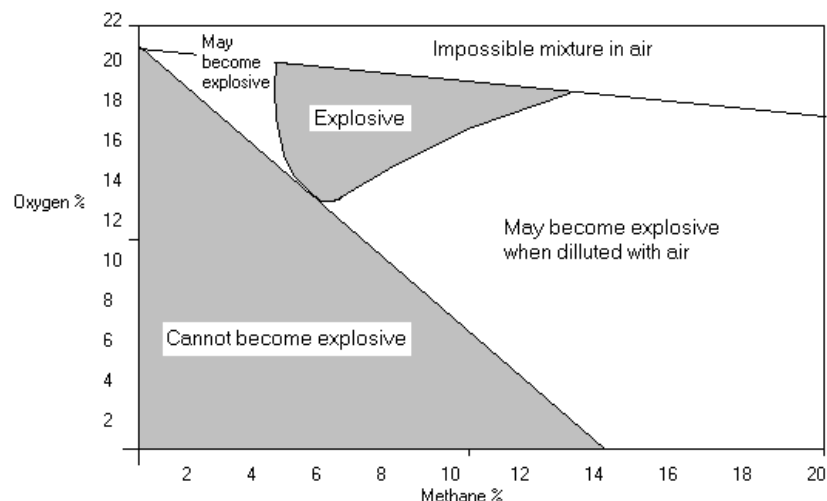
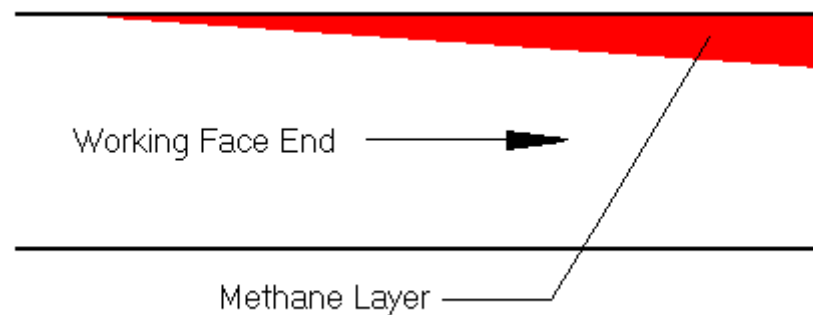


Figure 2.3 The Coward Diagram

The properties of methane also present a unique problem when dealing with the presence of firedamp. As methane, possesses a low specific gravity (0.555) it is lighter than air, and therefore if it is not rapidly mixed on

emission it may become buoyant and collect in roof cavities. This phenomenon is referred to as *gas layering*. This characteristic is dependent on the capabilities of the ventilation system in use and the rate at which the firedamp is emitted from the face. Lower rates tend to be easily diffused into the surrounding atmosphere whilst higher rates, requiring more time to diffuse present an opportunity for the fire damp to collect in roof recesses creating the potential for an explosive mixture to develop. This occurrence is of particular concern in development drivages of both level and inclined form. Figure 2.4 illustrates the mechanism by which methane can concentrate in these type of workings.



#### Principle Parameters Governing Layering Effect

1. Velocity of ventilation airflow
2. Rate of gas emissions
3. Drivage dimensions (width)
4. Inclination of airway
5. Relative densities of air and gas
6. Roof roughness above gas layer

Figure 2.4 Methane gas layering effect and causes

The layering effect has a number of factors directly influencing its severity (Bakke and Leach 1962) also detailed in figure 2.4. Where ventilation flow descends into the drivage layering takes a slightly different form owing to viscous effects at the leading edge of the layer resulting in eddies or backflow. The danger represented here is that of evacuated methane recirculated back creating possible explosive mixtures.

### **2.3.1.1 Methane Detection**

In the UK the maximum methane concentration permitted within a powered return roadway is 1.25% , in Germany 1.0% whilst in France levels up to 2.0% are permissible (Noack 1996). Methane detection can be accomplished in a number of ways. The most basic method, and the oldest, utilises the properties of methane by burning it in air. This method originated from the use of the flame safety lamp. The flame produced by a methane air mixture varies according to the precise mixture weighting thus allowing an interpretation of the local concentration

The more prevalent form of methane detection device is known as the *filament or pelistor methanometer*, which has been found to be more reliable and repeatable than its predecessor. The filament methanometer works again by causing gases to burn in air. The heat of combustion raises the temperature of the electrical filament resulting in a change in resistance that can be calibrated against known concentrations.

Chemical methods of gas detection are also utilised, the most common being the *colourimetric stain tube*. The stain tube is essentially a vacuum sealed glass tube containing indicators that change colour in reaction to the presence of certain gases.

### **2.3.2 Dust and Particulates**

Aside from gaseous pollutants the other major pollutant to the mine atmosphere is the presence of airborne particulate matter, primarily consisting of mineral dusts. Dusts may further classified as being, toxic, carcinogenic, fibrogenic, explosive or nuisance. Coal dust and quartzite dusts are the principal cause of concern with UK coalmines. Sub micron particulates may remain in suspension causing the greatest risk of both explosion and respirable illness. Inhalation of particulate matter is directly related to its size, particulates sub 10µm are considered to be respirable, the lower the size the further the penetration down the respiratory tract. The

risks presented by coal dust are therefore twofold, firstly there is a risk of respiratory illness brought on by prolonged exposure to coal dust. This usually takes the form of lung pneumoconiosis, in terms of industrial respiratory illnesses this is the most widespread (Chiyotani et al 1998). The second risk is associated with the explosivity of airborne dust.

Dust suppression and ignition inhibition techniques have been developed to prevent or reduce the severity of potential dust explosions. Conventional mines make extensive use of rock dust to inhibit dust explosions. Factors that have acted to reduce the potential of dust explosions include the increased use of permissible electrical equipment, safe explosives and effective ventilation (Sapko et al 2000). Experiments concerned with measuring the explosivity of certain mixtures of coal dust and gases continue today, (Cashdollar 1996 and Sapko 2000), utilising specially designed explosion chambers where accurate measurements can be made. The 1975 UK Coalmines (respirable dust) regulations provide legal limits for the exposure of workers to coal dust. (amended 1978 Coal Mines (Respirable Dust ) Regulations).

Diesel particulate matter or DPM presents a significant hazard to mine workers as these are considered as carcinogenic. The international agency for research on cancer defines diesel exhaust as a group 2A carcinogen (IARC, 1989) 'probably carcinogenic to humans'. Diesel engine exhaust emissions (DEEE) comprise a complex mix of gases, vapours, liquid aerosols and particulate matter. The volume of carbon particles or soot usually lies in the 60-80% range depending on use and engine type. The sub micron size of these particulates makes them almost completely respirable and as such a hazard to health. The status of this complex mixture is covered to varying degrees in a number of regulations (Groves and Cain 2000). The general provisions of the control of substances hazardous to health (COSHH HSE 1999a) require that exposure to DEEE be prevented or, where not practicable, reasonably controlled.



### 2.3.2.1 Particulate Concentration Measurement

Instrumentation is primarily designed to indicate concentrations of respirable dust, up to 10µm. As with gas measurement, principles vary, however, in recent times the use of personal samplers has increased (Gadomski et al 1985), these instruments utilise the principle of *gravimetric methods*. The gravimetric dust sampler is advantageous for environmental monitoring as it can be used to provide a continuous reading. When worn as part of a personal sampling device on miners, it can provide an individual history proving useful when correlating working habits with dust exposure. Airflow is directed through a chamber where larger particles are expelled. Smaller particles (<5µm) can then be collected on a filter, the concentration is obtained by the additional weight of the filter over the sampling period.

### 2.3.3 Exposure limits

To quantify the exposure of workers to pollutants, *threshold limit values*, TLVs, are defined for each class and type of pollutant. The TLV defines the upper exposure limit of a particular airborne pollutants that workers may be exposed to over a given time period with no ill effects. TLVs are defined according to the findings of current occupational medical research and are therefore subject to change. There are three classifications of TLVs (McPherson 1992), Time Weighted Average (TWA), Short-Term Exposure Limit (STEL) and the Ceiling Limit.

### 2.3.4 Ignition

There are a number of mechanisms by which an ignition source can come into being in the mining environment. In contemporary mining there is considerable use of mechanised and electrical equipment. Modern subsurface mining utilises intrinsically safe electrical equipment whereby sources of potential ignition such as heat or sparking are isolated from the environment. However, ignition can still occur where equipment is not used

or maintained properly. To minimise the risk of frictional sparking, cutting picks are usually fitted with pick back flushing water sprays that help to entrain air around the cut to disperse liberated methane and to quench potential sparks. Increased direct ventilation delivered to the cut may also be used to dilute and disperse methane quickly as it is liberated, however this may cause other problems concerned with the dispersion of excessive dust from the vicinity of the cut.

### **2.3.5 Heat and Humidity**

The major source of heat transfer within UK coalmines is attributable to the strata due to the geothermal gradient. Within the UK coalfields the geothermal gradient is typically 5 °C /100 metres, with many of the coalmines operating at depths in excess of 900 metres the strata temperature may be between 40-45 °C. Mathematically heat flow, or flux from the strata can be defined as being proportional to the cross sectional area of flow, the temperature difference between fixed points and the inverse distance between fixed points. The principle mathematical expression of this relationship, with the addition of a constant of conductivity, is known as 'Fourier's law' and forms the basis of heat conductivity analysis. A full derivation of the equations relating to radial heat flow through rock strata and applied solutions utilised in mine network analysis programs is provided in (McPherson 1992).

With the high degree of mechanisation present within UK coal mines, machine heat is the second predominant source of heat transfer. Within a typical longwall coal district between 1.5-2.0 MW of electrical power may be installed, and within a rapid development drivage between 750 –1000 kW of electrical power may be installed. What fraction of the installed power that is not used to overcome gravity during the cutting or transport process is conveyed in the form of heat to the ventilating air stream.

Measuring temperature in an environment where humidity is a factor is divided into two types of reading, that of *wet* and *dry* bulb temperatures. These readings are normally taken from a combined wet and dry bulb measurement device that contains two balanced thermometers. One thermometer, the dry bulb, is exposed to the prevailing air stream giving an indication of the ordinary temperature of the surrounding air. The other thermometer, the wet bulb, provides a second lower reading, depressed due to the evaporation of water from the saturated muslin jacket covering the bulb of the thermometer. The wet bulb is therefore a critical indication of the ability of the prevailing atmospheric conditions to remove heat from personnel by the evaporation of sweat from the skin surface.

## **2.4 Mine Ventilation; Equipment and Methods**

The primary objective of a mine ventilation system is the provision of an acceptable working atmosphere through the supply of fresh air and the dilution and removal of pollutants within the boundaries of regulated limits. In addition to gas dilution and removal, a mechanical ventilation system is responsible for the maintenance of a satisfactory climate and dust control.

There are two types of ventilation that can be considered independently (Star Wu and Topuz 1998). *Natural ventilation* is where the flow of air is governed purely as a resultant of temperatures, pressures and elevation and forms a natural ventilation circuit. The second type of ventilation is termed *mechanical ventilation* where fans and ducting are utilised to direct airflow in a controlled manner to specific locations within the mine as well as providing general atmospheric control.

### **2.4.1 Main Ventilation Systems**

The *main ventilation system* of a subsurface mine is responsible for the delivery and distribution of the fresh air around the main mine ventilation network. This is principally achieved by the correct choice of the number,

type and location of main surface or near surface fans. The main fans will provide ventilation to the subsurface mine by either exhausting the polluted air out of the mine or by forcing fresh clean air into the mine. In the ventilation of many large and extensive mining operations a combined force/exhaust (push/pull) main fan ventilation combination is employed. McPherson (McPherson, 1992) proposes four main factors to be considered in the choice between the force/exhaust configurations. These are gas control, transportation, maintenance and performance (efficiency).

UK deep coalmines currently employ exhaust main mine ventilation systems, as these systems afford a fail-safe in the control of waste gas emissions on the loss of the main fan power. Figure 2.5 illustrates a simplified mine ventilation network detailing main surface fans, booster fans, the major intake and return roadways, regulators, stoppings and other ventilation control devices.

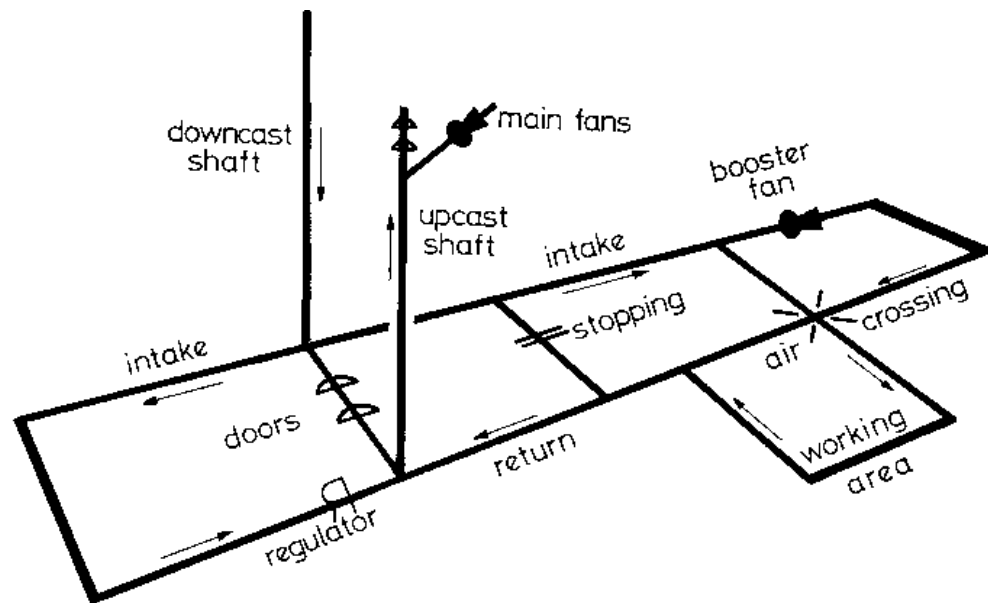


Figure 2.5 Mine ventilation system using surface exhaust fans (McPherson 1992)

#### 2.4.2 Booster Fan Systems

In circumstances where a mine network may extend to a greater depth or lateral extent to exploit additional reserves, the main fans may not be able to

produce the pressures required to distribute the required fresh air. A common solution is to install additional subsurface booster fans to assist in the distribution of the fresh air by providing the pressure required to overcome the additional resistance afforded by the extended circuit. *Booster fans* provide a high outlet velocity creating an excess of momentum that exerts a forward force on the normal airflow. Booster fans form part of the main ventilation system

### **2.4.3 Auxiliary Ventilation Systems**

Where a development working extends beyond 5 metres from a main trunk airway UK mining law requires the use of a mechanical auxiliary ventilation system. Auxiliary ventilation is required to provide a fresh air supply to the face of the heading to effect a continuous dilution and removal of pollutants from the cutting face. During the development of the roadway the face of the heading will move further way from the trunk fresh airway, consequently an auxiliary ventilation is utilised to maintain optimum ventilation in these areas.

There are two major types of auxiliary ventilation system, namely the line brattice, and ducted fan systems. The line brattice system functions by the installation of curtains within the drivage that divide the flow into fresh air in, polluted air out. This method of auxiliary ventilation is primarily employed within room and pillar environments in the US and Australia where the room and pillar method is viable owing to the greater strengths of coal and consequent reduced pillar size.

The line and brattice system, although simple, has a number of disadvantages inherent in its design. The system depends upon a large number of stoppings to be constructed which in turn creates an increased potential for leakage, this in turn limits the length of heading for which line and brattice can be employed with any useful effect (McPherson 1992). The opportunity for leakage is exacerbated by the high resistance of these systems, leading to greater leakage losses than would otherwise be incurred

where line and brattice were not employed. UK regulations prohibit the use of line and brattice auxiliary ventilation for headings on the basis of these disadvantages although room and pillar environments are cited as an exception (Moloney 1997).

Ducted auxiliary ventilation systems have a number of key advantages over the line brattice system.

- Controlled, directional ventilation at working face
- Introduce no additional leakage to the main ventilation network
- Introduce no additional resistance to the main ventilation network
- Can be used in long headings (30+m) beyond useful limits of line and brattice.

The ducted auxiliary ventilation systems require the installation and maintenance of an electrical supply, environmental monitoring, and the ventilation fans and duct systems. The auxiliary ventilation system needs to be advanced with the cut to maintain effective environmental control in the vicinity of the face. Careful and routine maintenance must be practised to maintain the integrity of the system, including the detection and repair to the joints or damage to the ducting, and the routine maintenance of the fan and monitoring systems. Auxiliary ducted fan systems may be installed in a number of configurations each of which has its own merits.

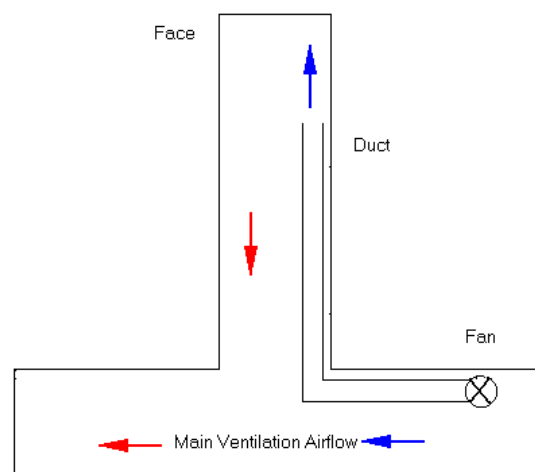


Figure 2.6 Forcing auxiliary ventilation

There are two primary forms of ducted auxiliary ventilation, namely the primary *force* and primary *exhaust* systems. Figure 2.6 illustrates a typical primary force layout.

These systems employ one or more fans outbye of the face located normally in the main trunk roadway and, if necessary in long headings, further fans may be located at intervals along the duct. In UK deep coal mines the duct is normally positioned eccentrically alongside a wall of the drivage. The simple *force* system propels the air from the end of the ducting in the form of a jet, towards the face causing a *scouring* motion across the face, which in the process rapidly dilutes and disperses any methane and dust liberated. However, the polluted airflow returning from the vicinity of the face does flow past any workers present in the drivage, thus exposing them to all airborne pollutants picked up along the way. The other problem with forcing systems is that they do not provide any means by which to control dust.

The simple *exhaust* auxiliary ventilation system provides an efficient means of dust capture. With this system the fresh air is drawn along the length of the drivage from the trunk fresh air roadway towards the face of the heading. Any dust liberated in the vicinity of the cut at the face is drawn towards the inlet to the exhaust duct and thus away from the work force. As the return air is contained within the exhaust duct it may be passed through a dry or wet filter to remove the entrained dust before the air is discharged into the main trunk airway. The disadvantage with simple exhaust systems is the reduced ability to *scour* the face with sufficient air velocity to rapidly dilute and disperse any methane liberated at the face.

Where there are both gas and dust liberation, hybrid systems may be employed that incorporate the best features of both the simple force and exhaust auxiliary ventilation systems. These configurations are known as *overlap* systems. There are two types, a primary force with secondary exhaust overlap system and primary exhaust with secondary force overlap system. The former is the most commonly employed in UK deep coal mines mechanised rapid development drivages. One prominent characteristic of

overlap systems is the reduction in general airflow in the region of overlap between the forcing and exhausting duct. This leads to a degree of controlled recirculation in this region and hence the requirement that the length of overlap should be minimised. Recirculation can be defined as the movement of air past a single point more than once and is prohibited under UK coal mine regulations.

#### 2.4.4 Fan Types

In purely mechanical terms there are two distinct types of fan utilised in mine ventilation each relying on different mechanical modes of operation. These are *centrifugal* and *axial* flow fans. Both of these devices can be termed as *rotodynamic* machines and are associated with high flow rates and low pressures. The other branch of mechanical pumping concerns *positive displacement machines* that offer the reverse, low flow rates and high pressures. The former is ideal for ventilation whilst the latter is used mainly in the pumping of hydraulic systems.

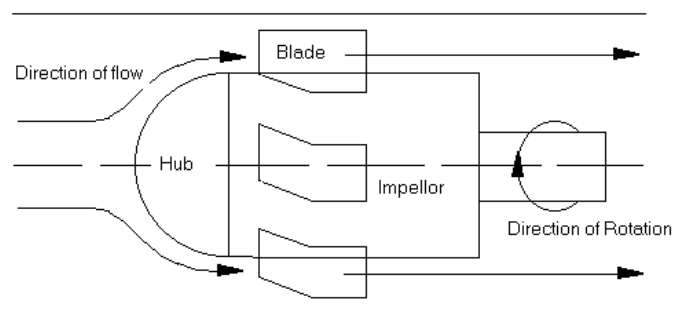


Figure 2.7 Axial fan, principle of operation

Axial flow fans are the preferred fan type for subsurface use although they are also suitable for surface systems. The principle of operation concerns the intake of airflow along a path parallel to the axis of rotation (see figure 2.7). The air then passes through the rotor blades mounted on the rotating shaft. The blades of an axial fan can be adjusted to provide different characteristics, sometimes while the fan is in use for greater flexibility. The in line design of the axial fan allows it to be installed with ease into



ventilation ducting systems in series or in parallel. A sub set of the axial fan is known as the *bifurcated fan* where the in line motor is isolated from the airflow by a streamlined casing. This is important when used in an exhaust system owing to the presence of contaminated air, the casing serves to isolate the motor from any pollutants.

In addition to the traditional fan types described here there has been some research into the utilisation of ductless jet fans. A jet fan (figure 2.8) is essentially an unducted axial freestanding fan employed for general mining or tunnelling ventilation purposes.

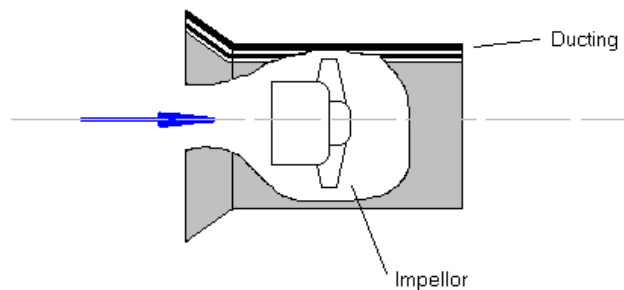


Figure 2.8 Typical jet fan assembly

Currently they have found use in South African mines for the purposes of ventilating short ends. To enhance air penetration distances a discharge device is fitted (Meetz and Meyer 1993). The jet fan produces a high velocity jet of air which due to the *coanda effect* (Konduri et al 1997), clings to the adjacent wall prior to dispersing over the face. The advantage of jet fans over ducted systems primarily concerns the removal of all the problems associated with ducting, such as the obvious obstruction to free passage of large vehicles and maintenance issues. Research into jet fan dynamics is limited at this time compared to the more traditional ducted systems (Mutama 1996). However work has been undertaken with a view to comparing these systems, Thimons et al (1986) demonstrated the ability of a jet fan to provide effective clearance for diesel exhaust and methane gases whilst ducted systems offered greater abilities in clearance of methane layering.

The arrangement of auxiliary fans, whether centrifugal or axial, within the ductline can vary dependant upon the local requirements. For typical applications, a single inline axial or centrifugal fan can provide sufficient flow to the face. For cases where the length of the heading leads to a single fan being unable to provide the required face airflow, a number of identical fans may be staged in series along the length of duct. Where a single fan is unable to provide sufficient airflow to the face of the heading for a given length of duct, a number of fans arranged in parallel may be able to achieve the required volume.

#### **2.4.5 Losses**

Losses in ventilated subsurface mines essentially refer to all factors within a ventilation network that result in a loss of useful energy and resultant pressure drop. An ideal flow circuit would offer no resistance to flow and no resultant losses, in practice this is impossible, the circuit has a global loss comprised of a series of small local losses. The *mine resistance* is the term associated with this global loss. The *mine losses* can broadly be classified into two groups, the *leakage* and the *resistance*.

The leakage of air from force ducting is almost inevitable, it can be minimised only through proper installation, maintenance and operation. The manner in which ducting is joined, often by loose coupling, contributes towards the general leakage. This can become more significant the longer the duct (Calizaya and Mousset-Jones 1997). The tearing of flatlay duct is unfortunately commonplace due to the flexibility of the ducting material and relative ease at which damage can be inflicted. It is easy for this damage to go unnoticed as it tends to be small and localised, however cumulative leakage can become significant.

Stoppings, seals and airlocks all contribute towards leakage in varying degrees. Again this is generally not of design but as a result of incorrect installation or operative procedures. Any non geographical barrier is a potential leakage path.

Airway resistance is probably the greatest source of global resistance within a subsurface ventilation environment. It is quantifiable through use of standardised frictional coefficients obtained for airway geometries and wall material types. Another primary source of resistance is termed *shock loss*, which is associated with the expenditure of energy required for a fluid to suddenly change direction. In modern, well developed mines the presence of sharp bends, junctions, obstructions and geometric changes are inevitable and the disruption to flow caused by each contributes an individual resistance to the overall effect. Generally speaking anything which produces air turbulence generates a shock loss.

## 2.5 Analytical and Computational Methods

### 2.5.1 Fundamental Laws

Fluid dynamics, whilst being a broad subject, is based upon a small number of fundamental laws, which need to be defined. These laws may be modified to suit individual applications or where appropriate used in their original form. The laws discussed in this section are those most relevant to the study of the movement of air and gases in confined flow circuits.

#### 2.5.1.1 Ideal Gas Laws

*Boyle's law*, defines the relationship between the pressure and volume of an ideal gas. The law dictates that the product of the volume of a gas and the pressure at the same moment in time is constant equation 2.1. In terms of a real gas the law is only an approximation, albeit a very good one, suitable for most practical applications. An extension to Boyle's law is defined in *Charles' Law* whereby for a given mass at constant pressure, the volume is directly proportional to the temperature.

$$P \propto 1/V \quad (2.1)$$

$$V \propto T \quad (2.2)$$

Both Boyles and Charles laws can be combined mathematically to produce what is referred to as '*the general equation of state for an ideal gas*'.

### 2.5.1.2 Bernoulli's Law

Bernoulli's equation is of fundamental importance to the engineering analysis of a confined flow system since it expresses a relationship between the fundamental variables of height (h), velocity (v) and pressure (P). The general form and application is shown in figure 2.9. In principle, the equation is an expression of a *conservation* concept, where energy due to elevation, pressure or velocity is maintained across a flow domain.

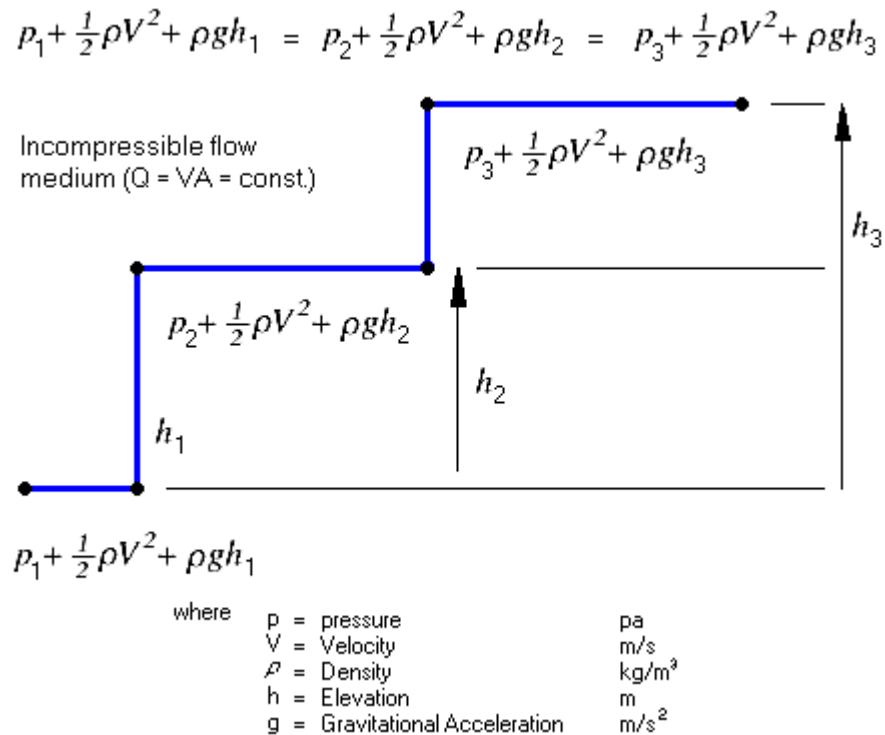


Figure 2.9 General form and application of Bernoulli's law

### 2.5.1.3 Kirchoff's Laws

To characterise the flows within a fluid circuit it is necessary to express relationships that govern the distribution of flow and energy within the various components within the network. These relationships are expressed in terms of *Kirchoff's laws*.

The flow circuits Kirchoff was interested in were of the electrical type where the flow medium would be considered as the current (I). The laws are completely transferable to flow circuits with a fluid medium subject to familiar assumptions. Kirchoff's first law states that the mass flow rate at the inlet to a junction must equal the mass flow rates at the outlet(s) of that junction. This law is a restatement of the basic law of mass flow conservation. Kirchoff's second law, in its original form stated that the algebraic sum of all potential differences in an electrical circuit must equal zero.

#### 2.5.1.4 Atkinson's Equation

Atkinson's equation is analogous to Ohm's law regarding the flow of electrical current through circuits. Potential difference (V) is replaced by barometric pressure (P). In the same way that electrical current (I) flows through a circuit path airflows through the mine network branches (Q). Finally, resistance (R) impedes flow in the same manner. Atkinson's expression uses the square of flow (Q) since the cross sectional area is taken into account, this is irrelevant in terms of electrical circuitry. It is commonly expressed as the 'square law of mine ventilation'.

### 2.5.2 General Flow Characteristics

#### 2.5.2.1 Laminar Flow & Reynolds Number

Another common assumption used within the analysis of fluid flow is that of steady flow characteristics, or *laminar flow*. Laminar flow is what is perceived as a controlled predictable flow characterised by relatively slow moving motion occupying single streamlines with no interference, figure 2.10.

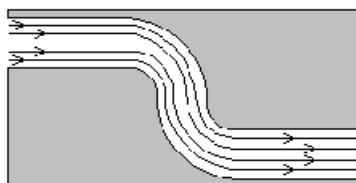


Figure 2.10 Laminar flow

Laminar flow in a fluid system can be predicted by using the *Reynold's equation* to determine a *Reynolds number*. The Reynolds number, proposed by Osbourne Reynolds in the 1880's, provides a dimensionless value determined as a function of fluid density, dynamic viscosity, velocity and a characteristic length, equation 2.3. This number expresses the ratio of the inertial to viscous forces of the flow. The value of this number is used to indicate the type of flow regime experienced within a particular flow. Laminar flow corresponds to a low Reynolds number up to a maximum of about 2000. Viscous forces are considered to be dominant when this ratio is below this value. The term D represents a characteristic length, in tunnel ventilation analysis, usually taken as the mean airway diameter.

$$\text{Reynolds No. } Re = \frac{\rho v D}{\mu} \quad (2.3)$$

### 2.5.2.2 Turbulence

The other characteristic flow is perceived as chaotic and unpredictable and is associated with fast moving low viscous flows, it is referred to as *turbulent flow* (figure 2.11).

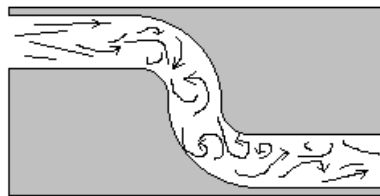


Figure 2.11 Turbulent flow

It follows from the previous section that a Reynolds number above 2000 will indicate the onset of a turbulent flow. Transition from laminar to turbulent is not instantaneous but occurs over a range approximately from 2000-3000 between which elements of both laminar and turbulent flow are evident. This is known as the *transitional period* of flow and is characterised by both examples of laminar and turbulent flow in varying degrees. Airflow within subsurface ventilation systems is primarily turbulent in nature, however with laminar flow may occur where local conditions permit.

### 2.5.3 Fan Characteristics

The operational characteristics of a given fan can be defined through the use of *velocity diagrams* and fan *characteristic curves*. Figure 2.12 illustrates a typical outlet velocity diagram for a backward curved radial fan. By the application of the Euler head rise equation to these velocity diagrams an ideal head (theoretical) can be calculated for the fan. Practical modifications to the ideal characteristic head take into account friction, proportional to the square of the flow rate and shock, whereby the fluid must change direction at flow rates above or below the fans *design point*.

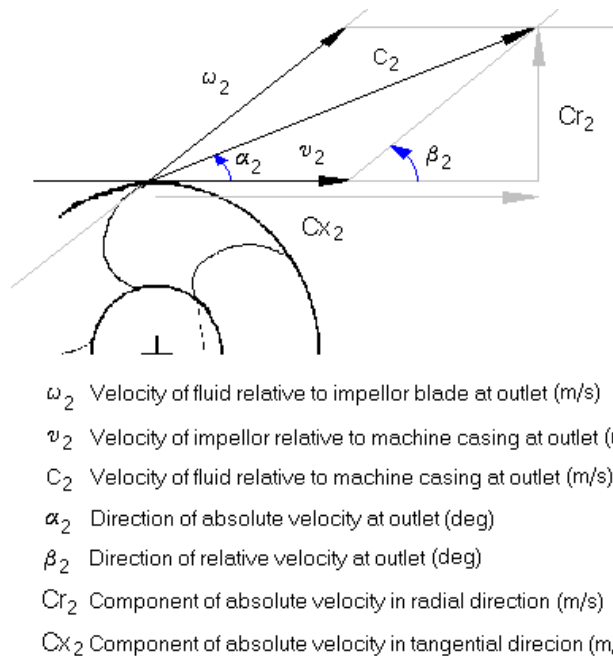


Figure 2.12 Radial fan outlet velocity diagram

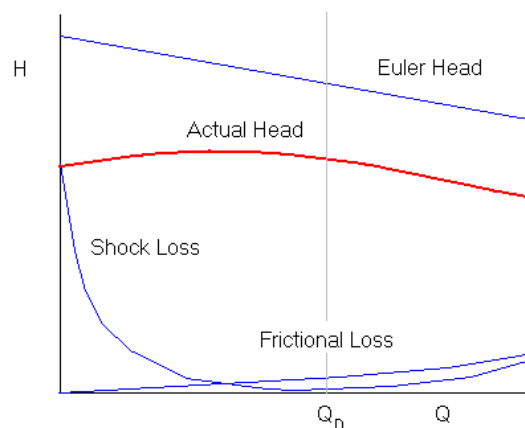


Figure 2.13. Practical head curve for backward curved radial fan

Figure 2.13 illustrates a typical characteristic curve taking these practical considerations into account.

The treatment of axial fans is essentially no different to the radial fan although the resultant characteristics are different. Axial fans are particularly prone to a condition known as *stall*. This condition occurs as a result of the boundary layer over the upper surface of the aerofoil blade becoming detached from the surface causing a loss of lift and propagation of turbulent vortices. This characteristic is a function of airflow and angle of attack.

It is common practice in mine ventilation systems for multiple fans to be installed such that a combined effect can be exploited thus extending the range of the ventilation system utilising existing fans. In general, fans installed in series will provide an increased head for a specific flow and parallel installations will extend the flow range for a specific head (figure 2.14).

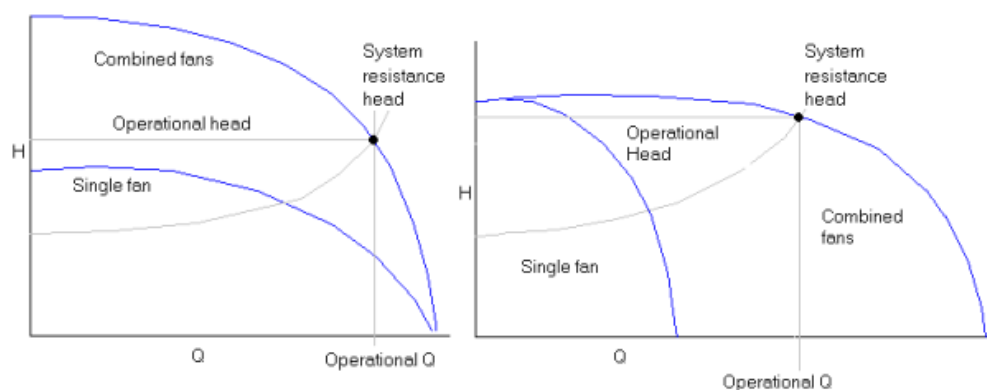


Figure 2.14 Head characteristics for serial (left) and parallel (right) fan combinations

#### 2.5.4 Network Analysis

Ventilation network analysis is primarily concerned with defining a number of unknown quantities through the application of established circuit based equations and relationships such as the *Kirchoff* and *Atkinson* laws to the known variables of the mine network. Known resistances of branches within networks will enable a quantitative analysis leading to the specification of airflows through those passages and consequent requirements of fan



systems. Known specifications of airflow variables will enable the consequent design of the network to accommodate these quantities. Early models utilised electrical circuitry to simulate the relationships expressed through Kirchoff and Atkinson using variable rheostats to adjust resistance. With the adoption of digital technology in the 1960's the computer now provides the foundation upon which all network analysis methods are based.

#### **2.5.4.1 The Hardy Cross Iterative Method**

The Hardy Cross iterative method is commonly applied to the analysis of the kind of large complex mine networks present within the mining industry in modern times. The method is based upon some underlying principles, which are listed below:

- For any given arrangement of mine network components (resistances/fans etc) there is one possible air mass flow distribution throughout that network.
- Regardless of the complexity, the network can be broken down into a series of 'nodes', these nodes are connected via roadways or 'paths' and can have any number of connections.
- The method is iterative and therefore the solution is dependent upon the accuracy of the required initial estimate of the variables at each of the nodes and the overall complexity of the network.

At each of the nodes the estimated pressure ( $P$ ) is applied. The unknown flow ( $Q$ ) through each node is given an error, the addition of which to the assumed value of  $Q$  gives the correct value. The error of  $Q$  at each node is then successively reduced through the iterative procedure until the entire network balances according to Kirchoff's laws.

## 2.6 Summary

This Chapter has briefly outlined the development of modern UK coal mining methods and ventilation systems. The background theory behind the emission and control and measurement of the various gaseous, dust and heat and humidity pollutant hazards associated with the underground environment has been described.

The role of the design of a safe, reliable and efficient mine ventilation systems to control of these pollutant hazards has been highlighted. In particular, this chapter has discussed the general characteristics and requirements of a modern main ventilation system and its auxiliary sub systems. The components of a main ventilation system, including the main and booster fans, stoppings etc., have been introduced. Particular attention has been paid to the subject of the design and operation of auxiliary ventilation systems. Individual configurations have been discussed and their comparative merits highlighted.

In summary, the subsurface mine environment is historically a dangerous working environment in terms of worker fatalities and injuries per head of the workforce. Technology has provided further safeguards to protect the workforce. However, there are many ways in which miners can be exposed to risk by their own actions, or as a result of others. This chapter has defined the hazardous mining environment in terms of cause, effect, remedial action and consequences.

## CHAPTER 3

### COMPUTATIONAL FLUID DYNAMICS

#### 3.1 Introduction

This Chapter provides an overview of *Computational Fluid Dynamics* (CFD), which is subsequently employed to model the ventilation flows and pollutant dispersion experienced within auxiliary ventilated rapid development drivages. Versteeg et al (1995) defines CFD as the analysis of systems involving fluid flow, heat transfer and associated phenomena such as chemical reactions, by means of computer based simulation. The fundamental principles behind the process have been well established in the field of fluid dynamics analysis and numerical methods for many years. However, the development of the computational power necessary to deliver solutions to complex flow problems has only relatively recently given the process of CFD a wider audience outside specialist industry and academic research. The process of CFD modelling is, at the foundation level, a general purpose tool suitable for a wide variety of flow related applications. CFD has seen widespread use in the following areas of engineering analysis;

- Aircraft aerodynamics
- Aerofoil design
- Marine hydrodynamics
- Chemical engineering, pipeflow, mixing & reactions
- Polymer & plastics extrusion processes
- Weather pattern analysis
- Heat exchanger design
- Turbomachinery
- Building services engineering
- Subsurface ventilation
- Environmental engineering, sewerage & effluent control
- Biomechanical engineering

As the engineering and wider scientific community increasingly accepts CFD as a valid and powerful analytical tool for fluid flows, the number of applications and tailor made CFD solutions increases.

Initially developed as an academic research tool, CFD has now been developed into a sophisticated commercial engineering software application. Modern software development companies such as Fluent, Cham and AEA Technology have all produced marketable CFD codes based upon familiar windows based systems, which has helped to open up a new user based market. The great complexity and consequent development required to go into a marketable CFD code means that at the current time the CFD market is dominated by only perhaps 3-4 CFD software packages.

CFD is primarily used during the design and product development stage of a project whereby the specification of a product has a primary relationship to a fluid flow caused by or inflicted upon that product. Much of the success of CFD as an analytical design tool can be assigned to a few basic but significant advantages over experimental methods.

- Control
  - A successful experiment requires absolute control over all variables or at least minimisation of uncontrolled variables. CFD enables precise specification of the entire experimental environment within the computer simulation thus eradicating this uncertainty commonplace in experimental methods.
- Cost
  - Product development is subject to fierce competition; any reduction in costs therefore translates to an overall saving. Experimental rigs require large amounts of man power, logistics and maintenance all of which is minimised with a CFD based process

- Repeatability
  - A design process is often iterative in nature, small problems are gradually ‘ironed’ out, improvements gradually brought in, and the process is often an evolution. This type of process requires a constant testing environment such that all designs are subject to the same conditions thus enabling accurate parametric studies and evaluations to take place.
- Safety
  - Particularly in areas such as aircraft design and turbomachinery where product failure could have potentially life threatening results the use of CFD enables designs to be tested under hazardous conditions normally considered too risky for full experimental testing.

The complexity of the project that can successfully be solved by CFD modelling is constrained by the limits of the processing hardware available. However, as computing power is currently increasing exponentially, new and more advanced applications appear on a regular basis. With respect to mining, CFD has seen increasing use in the design and optimisation of both network layout and fan design. Although CFD has yet to succeed as an all inclusive source of mine ventilation data the promise it has shown in partial network analysis points to an increasingly important role in this complex area of flow analysis. (Hargreaves and Lowndes 2001)

### **3.2 Methodology**

The development and solution of a representative CFD model is a multi-stage process. The process is based upon the definition and discretisation of the flow domain, and the construction and solution of complex numerical equations representing the flow within the domain subject to specified boundary conditions. The resultant steady state or time dependent solutions may be graphically viewed as a series of 2 and 3 dimensional, vector, streamline or contour plots.. These stages of model development and

solution are universally classified under the following headings which the analysis undertakes in order;

- Pre-Processing
- Solving
- Post-Processing

Each of the three sub processes listed above is required to solve a particular problem and as such are often developed independently. Major steps forward in CFD are usually a result of gradual development of all of these areas rather than one owing to the interdependent relationship between them.

### 3.3 Pre-Processing

Pre-processing can be thought of as being analogous to setting up of experimental equipment. The job of the pre-processor is to define the physical environment and the fluid medium under analysis. Geometry creation within modern CFD applications bears considerable resemblance to conventional *Computer Aided Design* (CAD) packages. The geometry can be imported from pre-built models or constructed from scratch using a combination of points, lines and surfaces that together form a volume. The creation of geometry in a CFD application differs slightly from its CAD counterpart in that connections between points, lines and surfaces must be computationally absolute, often CAD packages produce visual connections only hence if geometry is imported some degree of ‘clean up’ is required (figure 3.1).

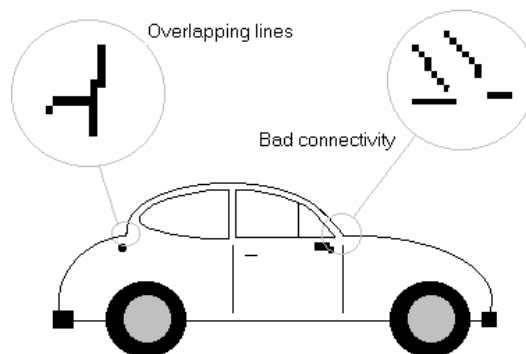


Figure 3.1 Optimising CAD generated geometry for CFD analysis

Surplus environmental geometry plays no role in the analysis, as the CFD code concerns itself only with factors that influence the fluid flow (figure 3.2).

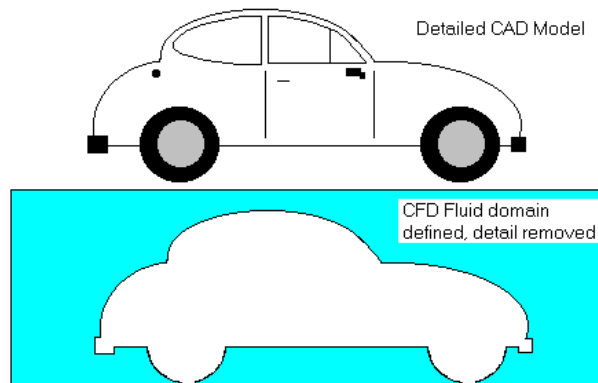


Figure 3.2 Definition of fluid domain

Any external influence on the fluid can be referred to as a ‘boundary condition’, an example would be a no slip condition imposed on the fluid by the presence of a fixed wall or a velocity imposed by a moving part (figure 3.3). Every physical surface represented in the computational model will have at least one boundary condition associated with it detailing one or all of velocity, pressure and temperature for a basic CFD analysis. Fluid boundaries such as inlets, outlets and openings are all subject to boundary conditions. It is normal for at least one fluid boundary to be subject to a known boundary condition, the others may be set to ‘free’ boundaries meaning that the fluid conditions at those points will be resolved

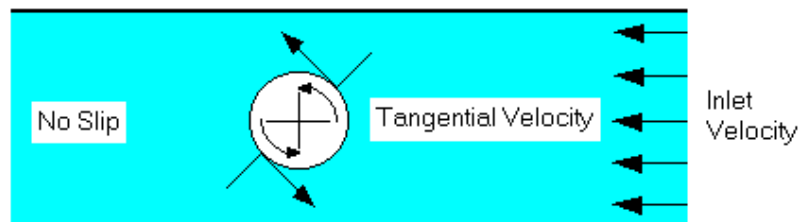


Figure 3.3 Examples of CFD boundary conditions

### 3.3.1 Meshing

Once the flow domain is defined, the free flow volume is sub divided into ‘cells’, the total number of cells join together to form the flow domain that together create a large interconnected net. This net, whether in 2D or 3D, is referred to as the *mesh*. The points of interconnection of the edges of each mesh are termed the nodes. The fluid flow equations are subsequently numerically solved at each of these nodes within the flow domain. The construction of the mesh plays a significant role in the ultimate accuracy of the CFD solution. Since the solution is only provided at this finite number of nodes on the mesh it is important that the distances between the nodes are sufficiently small to capture all the relevant detail and characteristics of the flow in that area.

Ideally, to prevent any inaccuracies arising from inter node distance, the mesh density would simply be set as high as possible. Unfortunately the greater the number of cells in the mesh the greater the demands on the computational hardware. Mesh refinement is therefore an art of balancing accuracy against practicality.

To identify the optimum size of mesh, it is normal procedure for a CFD engineer to produce a number of model solutions at steadily increasing mesh densities. Once the numerical difference between the two consecutive model solutions is, to a given criteria, negligible, the solutions to the model can then be considered ‘mesh independent’. This defines the optimum mesh density.

The process of meshing a flow domain during the pre-processing stage has a number of options associated with it. The primary options concern the type of mesh, this can be structured or unstructured. Structured meshing utilises regular shape cells whilst unstructured meshing makes use of triangular based cells (figure 3.4).



The key advantage of unstructured meshing over structured is the ability to represent complex irregular geometries due to the inherent flexibility of the triangular geometry. An example of unstructured and structured meshing is illustrated in figure 3.5 detailing a familiar 2D aerofoil domain meshed with triangular and quad based cells.

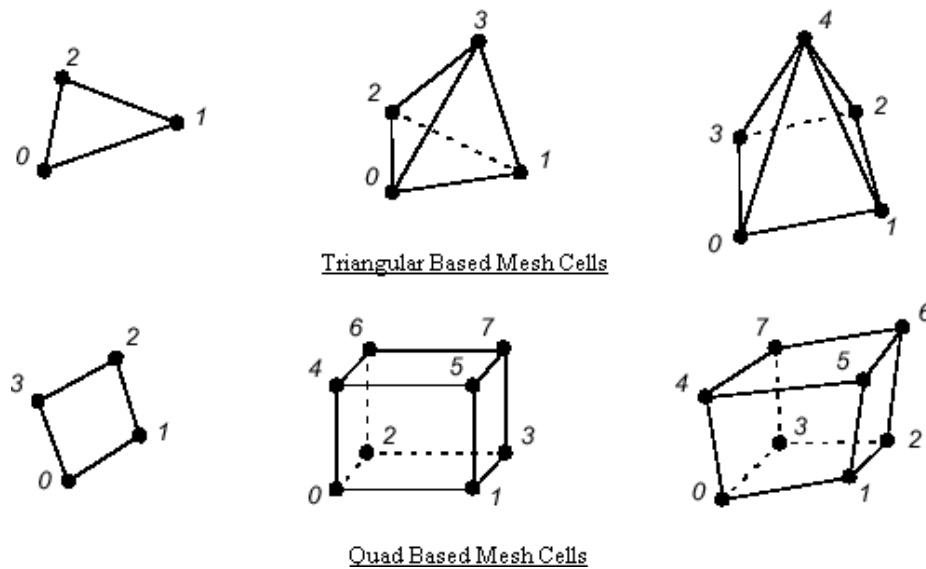


Figure 3.4 Commonly used CFD mesh cell types

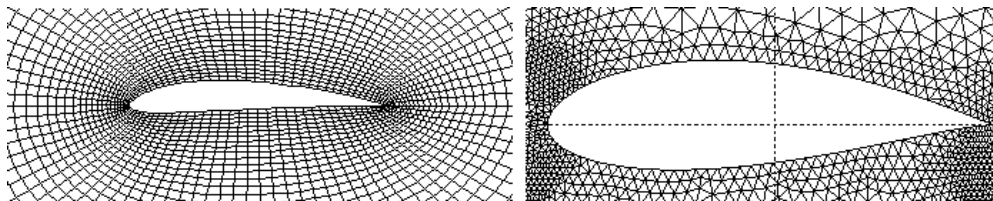


Figure 3.5 Structured quad based mesh (left), Unstructured Tet based mesh (right)

Complex geometries do sometimes present problems concerning mesh quality giving rise to small numbers of poorly defined cells where the meshing algorithm fails to fit the domain. The number of nodes within each cell varies according to the cell type. Meshing of the flow domain usually entails the definition of the required number of cell divisions on the domain edges such that a surface mesh can be constructed using automated meshing algorithms. The volume mesh can then be created on the basis of the surface mesh.

With the geometry, boundary conditions and meshing complete all that remains within the pre-processing section is the definition of fluid properties and the selection of any appropriate solution procedures if options are available. Applications vary from one to the other but common options include the definition of the iterative solution method used to find a solution to the flow equations and various other numerical options such as the convergence criteria. The most common convergence criteria is the definition of the error between two successive iterations of the solution, known as the residual value. Once the residual value is less than a given value the solution method is terminated.

### **3.4 Solving**

Once the model has been defined at the completion of the pre-processing stage, the solution of the flow equations for the specified conditions, may be initiated. This is referred to as the process of ‘solving’. According to Versteeg (1995) there are three basic numerical steps towards attaining a converged solution to the flow problem;

- Approximation of unknown variables by simple functions.
- Discretisation by substitution of the approximations into governing flow equations.
- Solution of algebraic equations.

There are three widely used methods for the process of approximation and discretisation, these are the finite element method, the finite difference method and the finite volume method.

#### **3.4.1 The Finite Element Method**

The finite element method was originally developed for the solution of solid stress analysis problems but has found success in the transfer to fluid flow problems. Local variations of the unknown flow variables are approximated

with linear or quadratic functions; these functions are then substituted into the governing equations resulting in a residual where the exact solution is not obtained. To minimise the residual, a process of multiplication by weighting factors and integration is undertaken resulting in a set of algebraic equations representing the unknown coefficients in the original approximations.

### **3.4.2 The Finite Difference Method**

Finite difference methods employ a number of samples taken at points on a grid, these sample are used to describe the unknowns of the flow problem. Finite difference approximations of derivatives in terms of the point samples at each of the grid points are generated. The finite differences are then used to replace the derivatives appearing in the governing equations leaving an algebraic expression for the unknowns at each grid point.

### **3.4.3 The Finite Volume Method**

The finite volume method, which is increasingly the most popular amongst contemporary applications, evolved from the finite difference formulation. The first step of the finite volume method is the integration of the governing flow equations for all finite control volumes within the flow domain. The integral equations must then be converted into algebraic expressions. This is achieved by substituting finite difference approximations into the governing equations. Finally, the algebraic expression must be solved for. The solution, or near solution, is normally found using one or a combination of iterative methods depending upon the type of problem and degree of numerical accuracy desired.

The finite volume method is favoured amongst engineers largely owing to its intuitive use of the control volume approach giving a clear expression of conservation of fluid properties across a finite volume or cell.

### 3.5 Post Processing

Post-processing represents the final stage in the CFD analysis method. Despite the fact that much of the hard work in terms of finding a solution has been completed at the solution stage the vast amounts of data produced and the nature and structure of this data requires an expert application to filter, format and deliver meaningful graphical representations of the various flow phenomena. The accuracy of the interpretation of the results is vital if the effort put into pre-processing and solving is to be justified. It is often the case that the CFD engineer may only be interested in a small part of the flow domain, for efficiency it is therefore important that the post-processor is able to filter out redundant data. In general, post-processors have the task of effecting appropriate data filtering and display, usually in the form of familiar icons such as vectors or contours. The power of graphical workstations is such that large data sets can be explored using graphical methods quickly and easily. Some examples of common flow plots are illustrated in figure 3.6 depicting familiar flow situations.

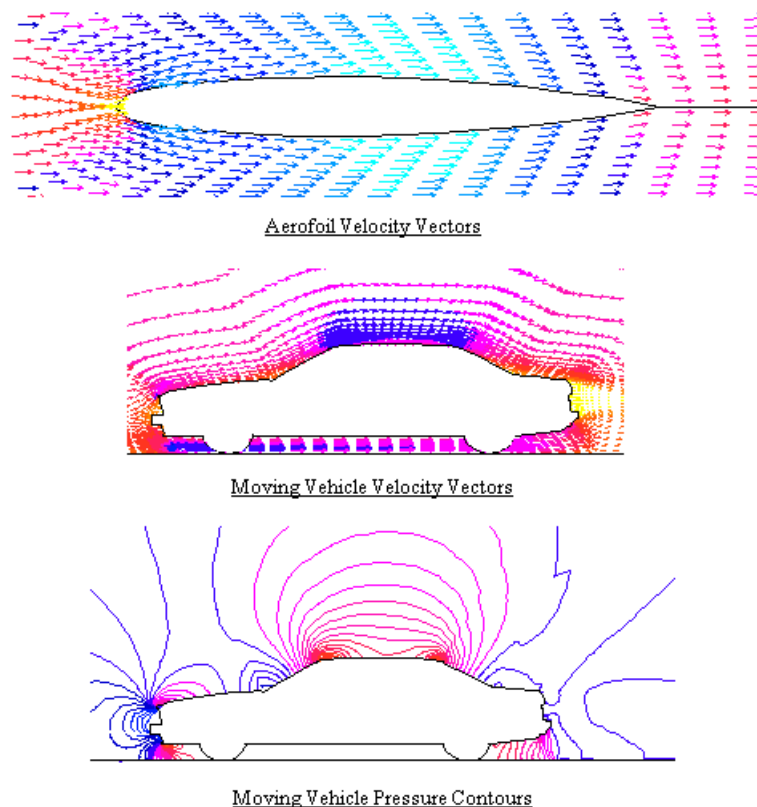


Figure 3.6 Examples of CFD post processing imagery

The major achievement of the modern post-processor is the ability to communicate a representation of a complex flow data set in a form recognisable to the non-expert user. This ability has seen CFD take a place in many unfamiliar environments such as business presentations and the media owing to its familiarity with a wider audience.

Post-processing is however by no means simplistic, the underlying algorithms and methods represent a highly active research area covering complex numerical techniques. These technical issues will be discussed in depth in the following chapter.

### 3.6 Governing Equations

For the purposes of a general understanding of the CFD process a number fundamental laws must be applied and resulting equations derived that govern fluid flow. There are three core equations common to all CFD analyses based upon the following laws of conservations;

- Conservation of mass
- Conservation of momentum
- Conservation of energy

A derivation can be applied to each of these laws first simplifying the flow problem to a simple unit volume as depicted in figure 3.7.

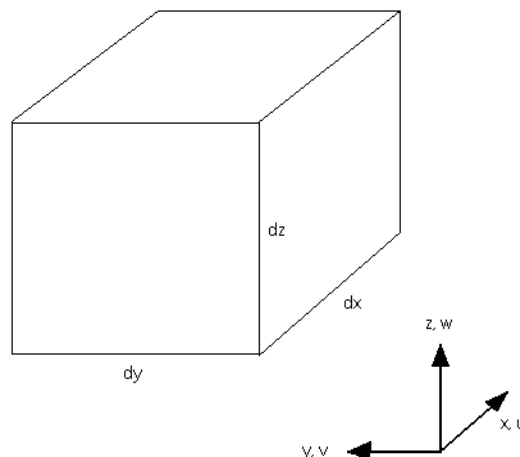


Figure 3.7 The unit volume representation

### 3.6.1 The Continuity Equation

The fluid volume illustrated in figure 3.7 can be considered such that the constituent lengths are small enough such that linear functions may approximate changes across the faces.

Fluid mass can enter via any face and leave via any face thus the mass accumulation within the element is the difference between that entering and that leaving. If a single face is considered the rate of mass entering that face is a product of the face area, the velocity and the fluid density. The mass leaving the volume is again a result of this product but velocity and density may be subject to change.

$$\frac{\Delta \rho}{\Delta t} + \frac{\Delta(\rho u)}{\Delta x} + \frac{\Delta(\rho v)}{\Delta y} + \frac{\Delta(\rho w)}{\Delta z} = 0 \quad (3.1)$$

The above equation is a representation of the general continuity equation whereby the term on the left represents the change in density over time and the remaining terms together represent the net flow of mass out of the element across its boundaries referred to as the *convective* term. For incompressibility the density term can be discarded leaving equation 3.2.

$$\frac{\partial u}{\partial x} + \frac{\partial v}{\partial y} + \frac{\partial w}{\partial z} = 0 \text{ (incompressible fluid)} \quad (3.2)$$

In the case where flow can be considered steady resulting in zero time derivatives the equation becomes;

$$\frac{\partial(\rho u)}{\partial x} + \frac{\partial(\rho v)}{\partial y} + \frac{\partial(\rho w)}{\partial z} = 0 \quad (3.3)$$

### 3.6.2 The Momentum Equation

The *momentum* equation, or the *Navier Stokes* equations, concerns the expression of Newton's second law, the rate of change of momentum equals

the sum of all forces acting on a fluid particle. Considering the unit volume approach it is clear that the rate of change of momentum must equal the net momentum flux into the unit volume plus all external forces acting upon it. The derivation can be split between the expression of momentum change and the expression of external forces. The sum of all external forces acting upon the fluid volume can be given by equation (3.4).

$$\left( \rho \frac{\partial u}{\partial t} + \rho u \frac{\partial u}{\partial x} + \rho v \frac{\partial u}{\partial y} + \rho w \frac{\partial u}{\partial z} \right) \Delta x \Delta y \Delta z = \sum F_x \quad (3.4)$$

The derivation of the forces concerns two types of force, body forces and surface forces. Body forces are exerted upon the entire control volume, the most common referred body force is that resulting from gravitational acceleration. Other body forces such as electromagnetic effects can be considered for specific cases, this represents an advanced application in terms of a CFD analysis and is not relevant for the applications covered within this thesis. Surface forces act upon one surface of the control volume at any given time, common sources are pressure and viscous stresses. Surface stress is directional and acts outwards relative to the control volume surface.

The majority of fluids can be considered as having constant viscosity in relation to shear stress, these are referred to as *Newtonian fluids*, air for example can be considered as a low viscosity Newtonian fluid. Fluids such as industrial inks, non-drip paint and butter are all high viscosity *Non-Newtonian* fluids where the viscosity is a function of applied shear stress.

By substitution of these stresses into the momentum equation the Navier Stokes equation in three dimensions is derived for the x component.

$$\rho \left( \frac{\partial u}{\partial t} + u \frac{\partial u}{\partial x} + v \frac{\partial u}{\partial y} + w \frac{\partial u}{\partial z} \right) = \rho g_x - \frac{\partial p}{\partial x} + \mu \left( \frac{\partial^2 u}{\partial x^2} + \frac{\partial^2 u}{\partial y^2} + \frac{\partial^2 u}{\partial z^2} \right) \quad (3.5)$$

### 3.6.3 The Energy Equation

The *energy equation* is the final of the governing equations required for a fundamental mathematical expression of fluid flow. In cases where the fluid flow can be considered to be incompressible, or the temperature changes are insignificant or the process is isothermal, the energy equation can be omitted from the analysis. In these cases the analysis need only to define fluid velocity and pressure using the continuity equation and two or three momentum equations for a 2D or 3D analysis respectively. Where compressibility and/or temperature are an issue, the energy equation must be used to provide an expression for these additional variables. The underlying principle of the derivation of the energy equation is the relationship between work and energy, and the fact that work can be expressed as the product of velocity and force.

$$\begin{aligned}
 & \frac{\partial}{\partial t} \left[ \rho \left( e + \frac{1}{2} v^2 \right) \right] + \frac{\partial}{\partial x} \left[ \rho u \left( e + \frac{1}{2} v^2 \right) \right] + \frac{\partial}{\partial y} \left[ \rho v \left( e + \frac{1}{2} v^2 \right) \right] + \frac{\partial}{\partial z} \left[ \rho w \left( e + \frac{1}{2} v^2 \right) \right] = \\
 & \quad k \left( \frac{\partial^2 T}{\partial x^2} + \frac{\partial^2 T}{\partial y^2} + \frac{\partial^2 T}{\partial z^2} \right) - \left( u \frac{\partial p}{\partial x} + v \frac{\partial p}{\partial y} + w \frac{\partial p}{\partial z} \right) \\
 & + \mu \left[ u \frac{\partial^2 u}{\partial x^2} + \frac{\partial}{\partial x} \left( v \frac{\partial v}{\partial x} + w \frac{\partial w}{\partial x} \right) + v \frac{\partial^2 u}{\partial y^2} + \frac{\partial}{\partial y} \left( u \frac{\partial u}{\partial y} + w \frac{\partial w}{\partial y} \right) + w \frac{\partial^2 u}{\partial z^2} + \frac{\partial}{\partial z} \left( u \frac{\partial u}{\partial z} + v \frac{\partial v}{\partial z} \right) \right] \\
 & + 2\mu \left[ \left( \frac{\partial u}{\partial x} \right)^2 + \frac{\partial u}{\partial y} \frac{\partial v}{\partial x} + \left( \frac{\partial v}{\partial y} \right)^2 + \frac{\partial v}{\partial z} \frac{\partial w}{\partial y} + \left( \frac{\partial w}{\partial z} \right)^2 + \frac{\partial w}{\partial x} \frac{\partial u}{\partial z} \right] + \rho u g_x + \rho v g_y + \rho w g_z
 \end{aligned} \tag{3.6}$$

This equation demonstrates that the change in fluid energy within a control volume is equal to the rate of work done by surface forces plus the rate of heat transferred into the control volume and is fundamental to most CFD fluid flow analysis where compressibility or temperature fluctuations form part of the analysis. A full derivation can be found in Versteeg (1995).

### 3.7 Turbulence Modelling

The modelling of turbulent flows is of particular importance in the analysis of underground ventilation systems where the flow is by nature almost entirely within the turbulent region (McPherson 1992). In situations where flow primarily occupies Reynolds numbers above the laminar/turbulent



transition (2500-3000), specialised numerical models are required in order to approximate for the turbulent fluctuations in flow. Turbulent flow is essentially a chaotic series of fluctuations around a mean variable value. For example, if a mean velocity  $V$  is considered, a representation of turbulence at a point in the turbulent flow domain would take the form illustrated in figure 3.8. Turbulent flow acts in three dimensions and exhibits high levels of circular flow known as *turbulent eddies*. Under these conditions fluid mixing is inevitable leading to high coefficients of diffusion for mass, momentum and heat.

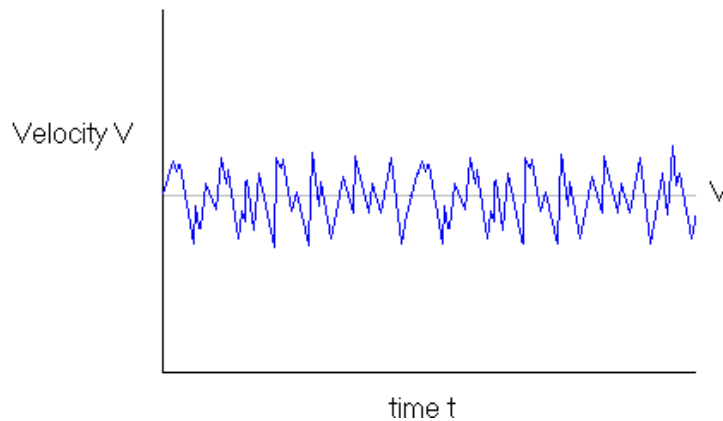


Figure 3.8 Turbulent velocity fluctuations

The turbulent eddies themselves can be classified into *large eddies* and *small eddies*. The distinction is that for large eddies the order of the characteristic length ( $D$ ) and velocity ( $V$ ) scales is the same as that for the flow domain leading to characteristic high Reynolds numbers where viscous effects are negligible and the eddies are dominated by inertia effects. Small eddies conversely are dominated by viscous effects, the work done against these effects leads to the generation of heat which accounts for the energy loss associated with turbulent flow. In addition, large eddies can be considered directional, or anisotropic owing to their interaction with the mean flow regime while small eddies are conversely non-directional, or isotropic.

### 3.7.1 Transition

It is important to note that in any flow domain where both laminar and turbulent activity exists there must exist a transition region. Most CFD codes

do not provide any accommodation for transition modelling providing a straight choice between laminar and turbulent flow models (Versteeg 1995). The justification for this stems from the fact that transition regions often only comprise a small percentage of the total flow domain and are often not of interest, thus the error associated with this neglected region is small.

### 3.7.2 Turbulence Models

The inclusion of turbulent flow in a CFD analysis introduces a number of new terms into the general momentum equations. To accommodate for time averaged fluctuations in flow velocity three additional normal stresses and three additional shear stresses must be incorporated into the time averaged momentum equations. These additional stresses are known as the *Reynolds stresses*, (Versteeg 1995). The task of the turbulence model is to provide a suitable prediction of these additional stresses such that an overall solution to the flow domain can be found. There are four classical turbulence models which have found success in commercial CFD codes, they are all approximations by nature and therefore are suitable for differing applications dependent on the associated assumption inherent in each model. These are;

- Zero equation model (*mixing length* model).
  - Economic use of computational resources
  - Well established
  - Incapable of describing separation and recirculation
- Two equation model (*k-ε* model)
  - Most widely validated turbulence model
  - Wide industrial application
  - More computationally intensive than mixing length
  - Poor performance in rotational flow and unconfined flow
- Reynolds stress equation model (RSM)
  - Highly accurate calculation of mean flow properties
  - Accepted as most general turbulence model
  - Extremely computationally intensive

- Similar difficulties as k-e model for rotational and unconfined flow
- Less validation
- Algebraic stress model
  - Relatively economic use of computational resources
  - Combines generality of RSM model with efficiency of k-e model but less validation than mixing length/k e models.

These four models are by no means the only models for turbulence available, they are however currently the most economic in computational terms and certainly, as a result of their widespread use, the most thoroughly validated. Authors such as Chen and Xu (1998) and Lam and Bremhosrt (1981) have both investigated advanced k-e models evaluating possible modifications to the basic k-e model to accommodate for near wall turbulence where limitations have been exposed.

In terms of commercially available CFD codes the mixing length and k-e models represent the general standard for general purpose turbulence modelling. Both of these models use a presumed analogy between viscous stress and the Reynolds stress on the averaged flow. A key distinction between the two is that the mixing length model uses an algebraic expression for the dynamic turbulent viscosity in terms of position in order to describe the stresses whilst the k-e model accommodates for the transportation of turbulent properties via diffusion and the mean flow regime. In general the k-e model represents a more general but more computationally intensive method whereby  $k$ , the turbulent kinetic energy and  $e$ , the rate of dissipation of turbulent kinetic energy are described via two respective transport equations. A thorough derivation of the constituent equations describing these models is given in (Versteeg 1995).

### 3.8 Contributions to Sub Surface Ventilation Modelling

The use of CFD as a means of analysing and predicting sub surface ventilation characteristics in complex mine networks is currently a relatively new approach seeing a steady increase over the last fifteen years. Despite the ongoing advances in computational power, CFD is still currently unable to provide an economic analysis of an entire mine network. CFD has however been utilised to a great extent to model local airflow conditions such as fan characteristics, duct flow and face ventilation. The following sections will therefore summarise in detail those major contributions to the field of the application of CFD to sub surface ventilation analysis.

#### 3.8.1 Validation Studies

The term *validation* is of great importance within the field of CFD analysis since it is this process that provides the engineer with the degree of confidence necessary for the application of the results to design. Aeschliman et al (1995) goes further in defining *Verification, Calibration and Validation* (VCV) as the proper terminology for the process of increasing the accuracy and reliability of CFD solutions. The term *certification* has also been introduced and defined by Mehta (1988) as the 'entire process of establishing the credibility of a code'. Aeschliman (1995) has also defined *calibration* loosely as 'a codes ability to reproduce valid data over a specified range of parameters without necessarily assessing the overall correctness of the physical models employed'. Although many terms are employed describing various aspects of the whole process of improving the accuracy of CFD solutions it is satisfactory for the purposes of this thesis to refer to the whole process as *validation* since there is no official definition.

Validation may be defined as the process of correlating a CFD models parameters with data from non-computational sources such as scale experiment with the aim to ensure that the results obtained from the CFD model match those from experiment as closely as possible. It is generally

accepted that a well-validated CFD model should have undergone correlation with another data source, specifically an experimental data source as opposed to another computational source (Bradley 1988). The contrary view point supported by Aeschliman proposes that contemporary CFD models can be reliably validated through the use of exact analytical solutions to flow problems or by comparison with previously experimentally validated models thus using secondary experimental correlation. Since validation is an expensive task, the argument for the latter method continues to receive some support though the debate is sure to continue for many years to come. Currently therefore, experimental validation is the only universally accepted method of proving a satisfactory level of confidence in ones CFD results.

### 3.8.1.1 Experimental Validation Studies

Work conducted by Moloney (1997) concerned a full evaluation of the application of a commercial CFD code, Fluent™, to the problem of predicting airflows in auxiliary ventilated headings. The validation utilised experimental data obtained from a 1/10<sup>th</sup> scale model using *Laser Doppler Anemometry* (LDA) as a means of obtaining flow velocity in addition to traditional visualisation methods such as illuminated smoke tracers. Figure 3.9 illustrates Moloney's 1/10<sup>th</sup> scale experimental set up.

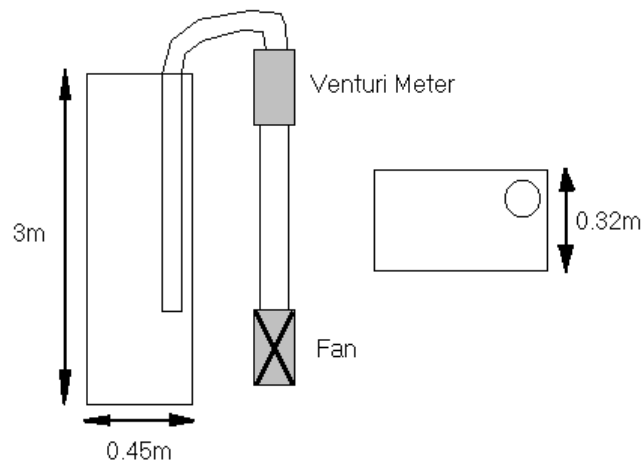


Figure 3.9 1/10<sup>th</sup> scale model experiment (Moloney 1997)

LDA uses the interference pattern generated when two laser beams are crossed. Tracer particles passing through this intersection scatter light at a frequency directly related to the particle velocity thus a visualisation can be constructed (Durst et al 1981). Employing smoke tracers as a means of visualising airflow works particularly well in flows where the bulk motion is two dimensional and where there is little or no recirculation. The method is therefore ideal for the wind tunnel experiments often used to evaluate the performance of vehicular aerodynamics. For the complex recirculating three-dimensional flows encountered within sub surface dead end ventilation, visualisations quickly become confused owing to uncontrollable mixing. Moloney utilised laser sheet illumination methods to overcome the common difficulty with complex three-dimensional flow of isolating areas of interest through the smoke cloud. By using laser sheet illumination Moloney produced a series of 2D sheets providing precise planes of view that served as ideal comparisons to the CFD data in addition to the particle LDA plots obtained from the experiment.

The CFD model constructed for this validation was a full three dimensional model utilising Fluent™ 4.3 and 4.4 representing a tunnel drivage 4.5m wide by 3.5m high with a forcing duct placed 10m from the face supplying  $6\text{m}^3/\text{s}$  of fresh air. For the purposes of validation a mesh sensitivity analysis was conducted using four cell counts of 14, 37, 63 and 82,000 in addition to two turbulence models, the k-e, RSM and the modified k-e *renormalisation group theory* model (RNG).

Moloney found that for the CFD model grid sizes of 63 and 82,000 achieved mesh independence referencing the tunnel fire models of Chasse (1993) who used similar grid sizes. This investigation also found that in the initial studies the RSM turbulence model produced more consistent predictions for grids of smaller densities.

A further series of CFD models utilising the k-e RNG turbulence model demonstrated a qualitative comparison with data obtained by (Lowndes et al 1994) from full-scale gallery measurements. These models used a forcing duct set back distance of 5m, 15m and 25m. Figure 3.10 illustrates two results planes reported by Moloney detailing CFD predictions superimposed onto tracer experimental data.

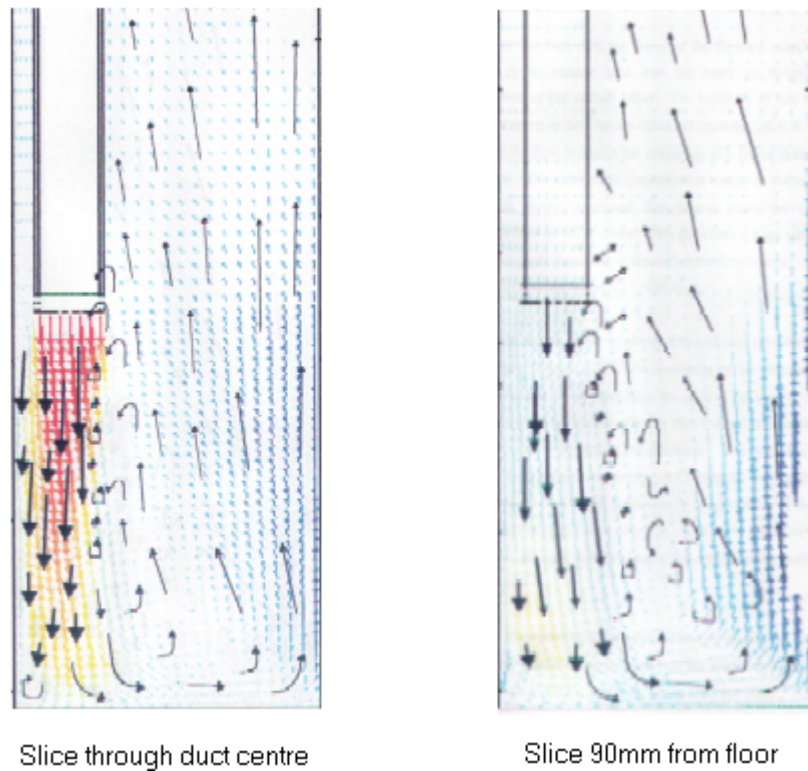


Figure 3.10 Superimposed experimental & CFD data (Moloney 1997)

It was reported that significant characteristics such as entrainment adjacent to the forcing jet and behind the duct outlet were confirmed in addition to the excessive turbulence caused in the case of placing the duct 5m from the face. It was also reported that the k-e RNG turbulence model gave the best forecast for 5 and 10m duct configurations.

By performing a comparison of the experimental smoke pattern and LDA studies Moloney concluded that:

*'the CFD predictions obtained from the model generally agree with the flow patterns attained from the flow visualisation study'*

A further case study was included in this study, based in a gallery in Wistow colliery in North Yorkshire. The CFD model constructed used a simple geometric representation of the continuous miner and the conveyor (Figure 3.11).

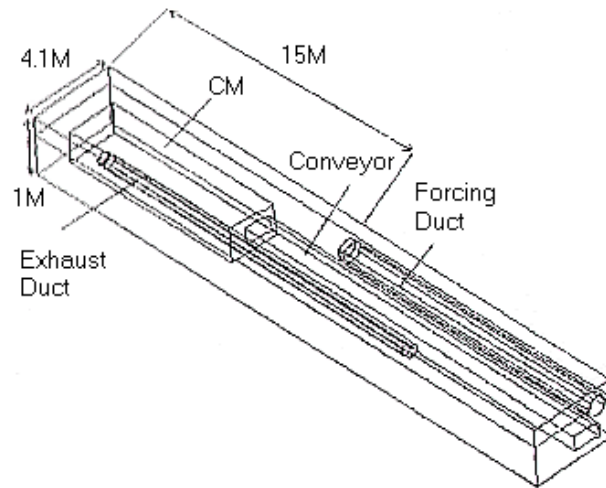


Figure 3.11 Wistow colliery case study model (Moloney 1997)

This model included a representation of a conventional auxiliary force-exhaust overlap system with the exhausting duct taking a 56% volume of air delivered through the forcing duct stated as  $2.5\text{m}^3/\text{s}$ . The 900mm diameter forcing duct was placed 15m from the face end while the 600mm diameter exhausting duct was placed 3m from the face end. The solution was processed using the k-e RNG turbulence model. The results produced by the CFD simulation model were compared with the point anemometer

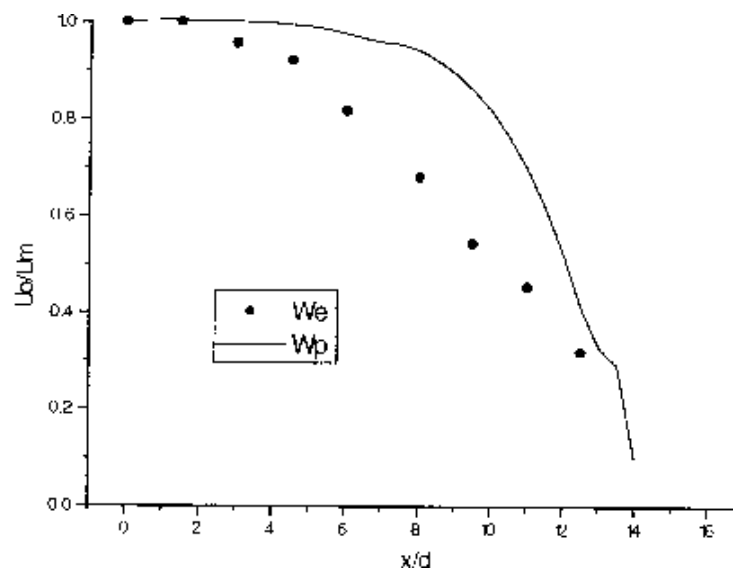


Figure 3.12 Dimensionless W measured velocity plot against CFD predictions (Moloney 1997)



measurements and smoke tubes or suspended ribbons results obtained during a ventilation survey of the given gallery. A degree of under prediction of the flow was evident with regard to the dispersion of the jet (Figure 3.12) although the characteristic flow regime (figure 3.13) was found to represent known flow characteristics reasonably well.

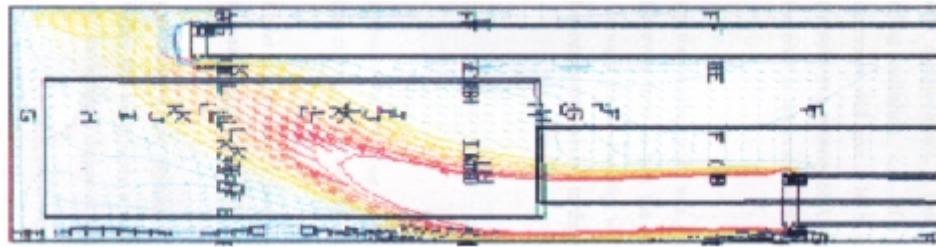


Figure 3.13 Characteristic flow regime plane from CFD predictions (Moloney 1997)

Moloney concluded broad support to the application of CFD to the solution of sub surface ventilation systems; however, he raised several points that addressed the potential limitations of the application of CFD to investigate such systems. In particular, Moloney identified the difficulties of making accurate and comprehensive ventilation surveys within a production environment. The use of this data he suggested may produce a possible source of uncertainty in the validation of the computational models. In addition, the CFD models produce a steady state solution that may not be representative of the many transient influences that exist in a busy working environment. It was proposed, in conclusion, that the CFD models validated within the study were sufficiently accurate that they may be used to assess the characteristics of alternative ventilation configurations prior to the initiation of full scale testing.

Further work conducted by Uchino and Inoue (1997) demonstrated a validation of a CFD code using a full size mine gallery in addition to scale experiment. The specification followed a 2.8m by 2.4m cross section comprising a delivery rate of  $1\text{m}^3/\text{s}$ . The conclusions drawn pointed to a satisfactory performance of the CFD code in general flow characteristic and gas diffusion terms with a tendency to a poorer performance with regard to exhaust flows.

Konduri et al (1997) described a series of experiments conducted to evaluate the performance of jet fans for ventilating blind headings in underground mines. Field measurements and laboratory experimental readings were used to provide velocity point samples in the heading and characteristic flow patterns via the release of a tracer gas (CO<sub>2</sub>). A 2D CFD representation was constructed using Fluent™ software comprising a cell count of 50,000 that was compared qualitatively to the experimental and field ventilation survey measurements. Flow patterns, streamlines, and forcing duct jet penetration were reported to be very similar to those observed during the experiments.

### **3.8.2 Modelling of Gas Dispersion and Methane Levels**

The use of CFD modelling methods for the prediction of gas dispersion in contained environments has a broad engineering application base where human risk is a factor. Gaining an advance understanding of the dispersion characteristics of a flammable or toxic gas release in a contained environment such as a building, tunnel, subway or mine is an essential part of the risk assessment process.

Gilham et al (2000) used the commercial code, STAR-CD™, to predict CO<sub>2</sub> levels within a cubic volume of air using a 300 second transient analysis with 1 second time steps using the k-e turbulence model. The principal objective of the study was to provide an evaluation of the application of CFD to this class of problem. From an analysis of the performance of the models it was concluded that the CFD model generally produced a good qualitative and quantitative agreement with experimental studies.

Hargreaves and Lowndes (2000) conducted a series of CFD studies to investigate the use of alternative auxiliary ventilation systems to ventilate the cutting face of a rapid development drive, excavated by a continuous miner system. The efficiency of each ventilation configuration was assessed by performing a comparative analysis of the dilution characteristics obtained from a uniform fixed rate emission of methane across the face of the drive. The CFD models were constructed using AEA technologies CFX v5™

computational code, and incorporated a full 3D representation of the *Continuous Miner* (CM) machine and ancillary equipment, the various auxiliary ventilation configurations including a CM mounted exhaust scrubber duct system. The standard k-e turbulence flow model was employed. For these initial studies the relative density of methane was neglected, and thus the study provided a qualitative interpretation of the dispersion characteristics driven by the dominant mixing characteristics and turbulence produced predominantly by the force duct ventilation jet.

In the model developed by Hargreaves and Lowndes (2000) it was assumed that the methane was uniformly released across the cutting face. Various experimental and computational studies have been conducted to describe the rate of methane dilution in mathematical terms such that an expression could easily be imported into a CFD simulation. Campbell and Dupree (1987) proposed an empirically derived model termed the *Methane Dilution Capacity* index (MD) (equation 3.7), and later Van Zyl (1999) proposed the more complex *Face Ventilation Effectiveness* measure (FVE).

$$MD = \frac{FL}{(C_{max} - CI)}$$

(3.7)

Where

MD = Methane dilution capacity  
 FL = Peak methane face liberation rate  
 C<sub>max</sub> = Max methane concentration detected  
 CI = Intake duct concentration

Both of these models work upon the basis of integrating the measurement of point gas samples taken across a given flow section, whereas CFD works upon the principle of prediction at a finite number of points (or infinite number through interpolation). Hargreaves et al (1998) proposed a solution to this problem by the introduction of a method based upon the mean concentration measured or predicted within the ventilated volume 5m closest to the face. Hargreaves expressed this through the ratio equation 3.8. It was found that the ratio proposed by Hargreaves confirmed the findings of

previous work conducted by Shuttleworth (1963) concerned with evaluating the influence of duct to face distance on methane emissions measured within the region of the face.

$$\frac{C_{\text{mean}}}{C_b} = \frac{q_s}{Q_d}$$

Where

(3.8)

$C_{\text{mean}}$  = Mean concentration

$C_b$  = Theoretical well mixed concentration

$q_s$  = Face methane flow rate

$Q_d$  = Duct volume flow rate

Ren et al (1997), reported the results of a computational study of the application of CFD to simulate methane flow through permeable strata around longwall coal faces. The authors initially used the Fluent™ computational code, to construct a 2D simulation prior to the construction of a full 3D model of a 200m \* 250m \* 80m mining block containing a longwall production face. The block contained an additional methane bearing seam located 80m above the current working seam. The CFD model solutions provided good agreement with field measurements demonstrated the characteristics flow of methane migration around the longwall district. However, it was concluded that validation of the solutions of the CFD models was required using field data.

In addition to the emission and dispersion characteristics of methane gas within a heading, the study of the potential ignition of such mixtures has also received some attention from the CFD modelling community. Jazbek (2000) used CFX v4™ for the purposes of modelling a lean methane air mixture combustion process using a reduced kinetic mechanism in a 2D domain using the k-e turbulence model. Whilst the application concerned the design of methane combustion chambers the conclusions drawn confirmed the principle that CFD was capable of modelling methane air ignition processes reasonably accurately.

### 3.8.3 Modelling of Sub Surface Fires

Since the spread of sub surface fires in tunnel networks and mines present one of the most serious hazards within sub surface ventilated spaces, a number of researchers have reported studies related to the spread of fire and combustion products such as smoke and noxious gases using validated CFD models.

Woodburn and Britter (1996) detailed the results of sensitivity studies conducted on a CFD model of a tunnel fire. The model was a representation of a series of experiments carried out by the fire and thermofluids section of the Health and Safety Laboratory (HSL) in Buxton, UK. The experimental tunnel was longitudinally ventilated from inlet to outlet by a force ventilation fan. The CFD model simulations concentrated on the area immediately around the seat of the fire and the area immediately downstream of the fire (figure. 3.14). It was reported that the upstream propagating smoke was sensitive to the velocity profile, the ventilation velocity rate, the heat input and the turbulence model used. The standard k-e and buoyancy modified k-e were both employed to model the resultant ventilation flow.

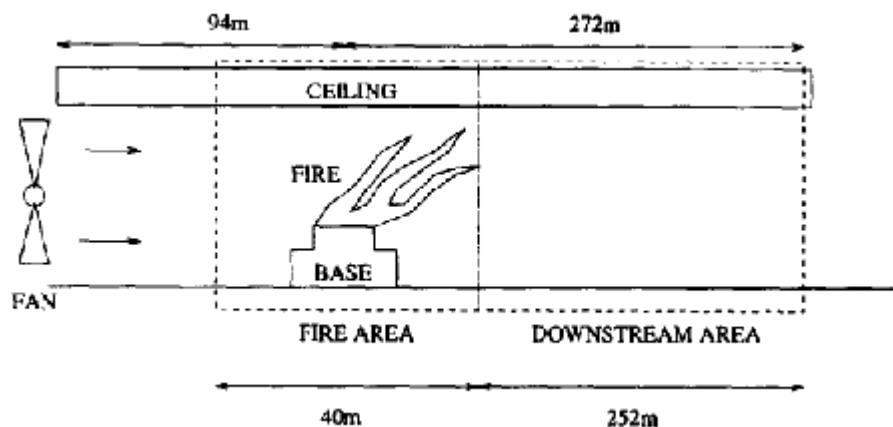


Figure 3.14 Woodburn's experimental tunnel fire model (Woodburn and Britter 1996)

The CFD code used to model the experiment was Flow3D™, later to become CFX™ from AEA technology. Although a general agreement was

found between the CFD results and the experimental study in terms of smoke propagation, the study illustrated the high degree of sensitivity such simulations have with regard to input boundary conditions such as velocity and heat.

A report from the National Institute of Standards and Technology from Madrzykowski and Vettori (2000) detailed a building fire case study into the use of a transient CFD based fire simulator. The model was intended to investigate the mechanism by which a *flashover* occurred in instances where an under ventilated fire is subjected to a sudden oxygen rich environment. It was found that the model exhibited a reasonable correlation with reports from the actual incident proposing a possible mechanism for the spread of the fire and the thermal conditions within the building.

#### **3.8.4 Evaluation of Alternative Ventilation Configurations**

CFD models are in a constant state of evolution owing to the continuing rapid advancements of the computational hardware to which the boundaries of any model are set. The work initially conducted by Moloney et al (1999; 1997) was further developed by Hargreaves et al (1998) and Hargreaves and Lowndes (2000) to include more representative computational models to accommodate higher levels of geometrical accuracy. Hargreaves et al (1998) and Hargreaves and Lowndes (2000) conducted a series of CFD simulations to calibrate the computational models employing a grid of point velocity measurements obtained from the use of an ultrasonic anemometer within a modified full scale surface training gallery located at Welbeck Colliery, UK. Hargreaves draws a distinction between calibration and validation defining the former as a process of incrementally modifying the CFD model so that the predicted data fits the available experimental measurements to within an acceptable level of accuracy. Hargreaves proposed that validation assumes a priori knowledge of the data. It was further proposed that once a basic model has been calibrated it could be applied to model similar ventilation and mining configurations with greater confidence.

Following extensive numerical exercises, Hargreaves concluded that in comparison to the more sophisticated turbulence models, that the standard  $k-\epsilon$  provided the best agreement between the predicted and measured flow data. The form of representation of the gallery wall roughness was also investigated, that resulted in the use of a 0.05m roughness value used to represent irregularities in the tunnel wall, floor and roof surfaces. Well defined surfaces such as equipment panels were treated as smooth surfaces. Initial models were developed to represent the flow regime within an empty, unobstructed training gallery using the structured mesh version of CFX™ with a mesh independent cell count of 150,000. These were used primarily to attain a degree of confidence that the main qualitative aspects of the flow regime were being predicted accurately (Figure 3.15).

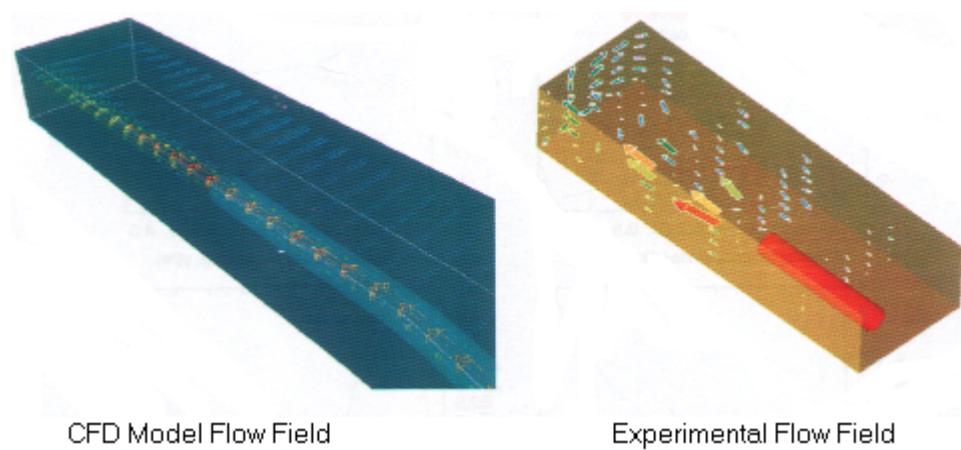


Figure 3.15 Qualitative ventilation flow comparisons (Hargreaves et al 2000)

Quantitative comparisons were made using point samples from a series of ultrasonic ventilation traverses made across the flow domain, an example of which is illustrated in figure (3.16).

Whilst general agreement was reported between the initial CFD models and the measured data there were localised positions within the computational model that were reported to bear little resemblance to those values taken from the measured data. The roughness of the gallery walls was found to contribute little to the bulk flow characteristics.

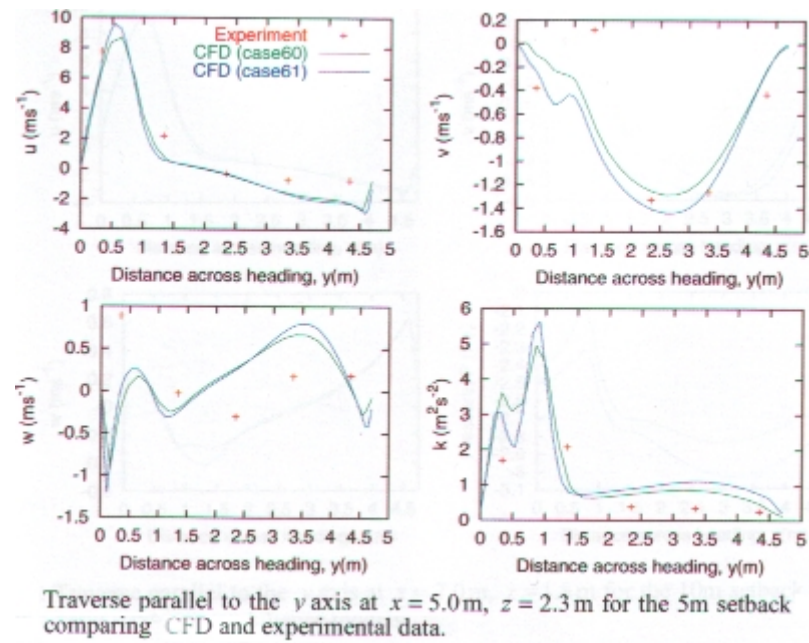


Figure 3.16 Quantitative evaluations of ventilation flow using point samples (Hargreaves et al 2000)

Further analysis conducted by Hargreaves concentrated upon the application of more advanced CFD models to a series of underground ventilation surveys conducted within an underground rapid development drivage at Welbeck Colliery, UK. The particular drivage was 3.1m high by 5.3m wide. A CAD representation of the Jeffrey 1038HH continuous miner (figure 3.17) was imported within the CFD models to replace the earlier simple flow obstruction models used in earlier work by Moloney (1997) and Hargreaves and Lowndes (2000). As a result of the increased geometric accuracy of the models the mesh density was reported to be in the region of 1,000,000 cells. In addition to the conventional forcing duct, an on board scrubber system was also employed and incorporated into the CFD model.

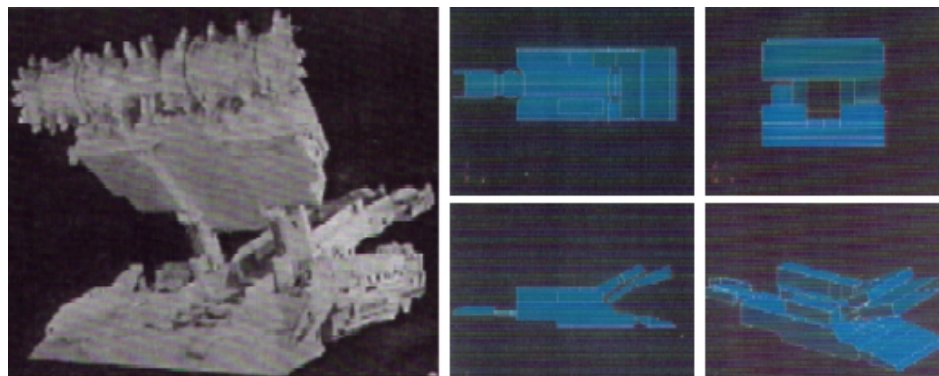


Figure 3.17 Hargreaves CM representation (Hargreaves et al 2000)



The intent of this study was to evaluate and compare the dilution characteristics produced by a variation in the configuration and duty of the ventilation and mining models used within the CFD simulations. Firstly, the physical position of the miner was changed to simulate a face advance in 3 stages of 2.5m each. The face was advanced in two cuts, firstly by taking first a full-face cut followed by the removal of the remaining adjacent *buttock* side cut. The operation of the scrubber was treated as an on/off variable at a fixed flow determined by a fixed body force included as a boundary model within the scrubber duct. Finally, the orientation of the boom during a cut cycle was represented both a fully up and fully down position. It should be clarified that the models constructed by Hargreaves were steady state in nature owing to the impracticality of a transient simulation modelling, for example, the downsweep of the boom. CFD simulations of all possible combinations of these variables were conducted for both the operator and buttock side of the drivage, figure 3.18 illustrates the different stages of the cutting cycle modelled by Hargreaves.

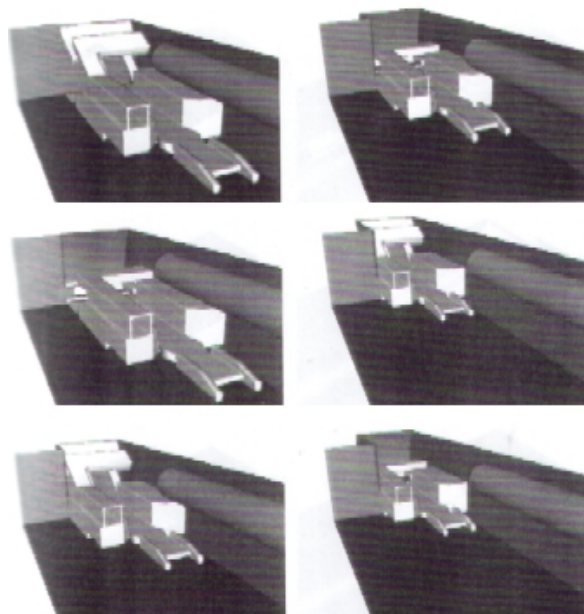


Figure 3.18 Cut cycle modelled by Hargreaves (Hargreaves et al 2000)

Hargreaves raised some important points in his conclusions. These primarily concerned the interpretation of the data obtained from the CFD studies as being qualitative in nature owing to uncertainties in the use of the methane

tracer gas. It was stated that as a result of the complexity of the flow in the region of the face a quantitative interpretation of methane dispersion patterns would be severely limited. It is however clear, that the large number of CFD models created accommodating the interaction of work place variables such as boom orientation, scrubber operation and advance position provides a useful insight into qualitative influence of physical changes to the environment. It can also be stated that despite some minor identified irregularities the consistency of the validation with controlled experimental measurements confirms the growing acceptance of the application of CFD to evermore complex sub surface ventilation problems.

### **3.8.5 Discussion**

The results produced and conclusions drawn from a number of CFD studies have been reviewed to provide an insight into the current research activity in the field of mine ventilation. There are several common conclusions drawn by these authors.

The CFD model studies conducted to address a range of ventilation problems all conclude that the simulations provided the same 'general agreement' with the experimental data. A number of investigators (Moloney 1997), Hargreaves and Lowndes (2000), Ren et al (1997) and Woodburn and Britter (1996) have used both qualitative and quantitative approaches in their evaluation to highlight the potential inadequacies of the CFD models employed. Although these often have little influence on the area of interest they do serve to highlight the caution to which one must treat CFD results.

In terms of turbulence modelling it is clear that from the evidence of a number of studies ((Moloney 1997), Hargreaves et al (1998), Hargreaves and Lowndes (2000), Woodburn and Britter (1996), Jazbek (1999) and Gilham (1997)) the standard k-e turbulence model has been confirmed as the most acceptable general purpose turbulence model.

In conclusion, it is evident that the data produced by CFD over the last decade has shown a clear and consistently increasing level of accuracy. The data produced from the work of Hargreaves and Lowndes (2000) has demonstrated the ability of CFD to provide a wide range of flow solutions incorporating a number of domain variables quickly, economically and accurately. However, it is also clear that if the vast amounts of data produced by these models are to be used effectively, there must be further developments in the interpretation and graphical representation of this data.

### **3.9 Summary**

The work reviewed in this section is representative of the current state of research with regard to the application of CFD modelling to the study of tunnel ventilation and associated issues.

The fundamental equations describing fluid motion, including the continuity equation, the Navier-Stokes equations and the energy equation have been discussed in terms of the simple fluid volume principle. Turbulence modelling has been discussed in terms of the four main turbulence models available in commercial code, the respective advantages and disadvantages have also been outlined, and their approximate or empirical nature has also been discussed.

To validate the CFD models developed most of the studies reviewed have incorporated some form of experimental correlation. Early studies from Moloney (1997) used established experimental visualisation techniques to validate 3D CFD simulations of a simple drive using unobstructed and later simply obstructed flow domains. Hargreaves et al (1998) reported an extension of this work to consider a larger more complex flow domain by the incorporation more geometrically accurate representations of the CM machine, the auxiliary ventilation systems and the drive geometry. The results of the work of both Moloney (1997) and Hargreaves and Lowndes (2000) summarised in this Chapter have illustrated the gradual

improvements to the CFD models to represent the auxiliary ventilation of rapid development drivage, achieved over a relatively short period of time. Other model validation work conducted by Uchino and Inoue (1997) and Konduri et al (1997) concerning full scale validation and modelling of jet fan characteristics respectively, have drawn similar conclusions and demonstrated a cautious but generally positive evaluation of CFD as a reliable source of flow information.

The flexibility of CFD has also been assessed, examples of ambitious fire simulations from Woodburn and Britter (1996) and Madrzykowski and Vettori (2000) have demonstrated the potential for complex transient thermodynamic simulations to be undertaken and validated to a satisfactory degree. The models of Hargreaves et al (1998) have illustrated a qualitative method of simulating steady state methane gas dispersion within a ventilated drivage.

This chapter has served as both an introduction to the fundamental principles of the development and use of CFD modelling, and as an indicator of the current level of confidence the scientific community has with the process as a validated source of flow information for the analysis of sub surface ventilation characteristics.

The subsequent data sets produced by CFD methods are much larger than those produced through traditional analytical or simple network computational methods.

To interpret and communicate this data to a wider audience requires the development of improved visualization methods. The next chapter provides a detailed insight to the methods used by the scientific and engineering community to interpret and visualise such large and complex data sets.

## CHAPTER 4

### VISUALISATION

#### 4.1 Introduction

This chapter outlines the development of tools with which to visualise large and complex data sets, such as produced by the CFD simulation of ventilation flows within rapid development drivages. *Visualisation* is a term used to describe what is conceptually a very simple process, that of displaying data in a presentable manner. It is the objective of visualisation, in its broadest definition, to make the process of analysing the range, trends and patterns within large data sets easier. This involves displaying data in a manner recognisable to the human observer, who is usually skilled in the art of visual pattern recognition whilst being less talented in the field of direct feature extraction from raw multi dimensional numerical data. Globus (1994) makes some basic statements defining how the contemporary scientist defines *visualisation excellence*:

- Consists of complex ideas communicated with clarity, precision, and efficiency.
- Is that which gives to the viewer the greatest number of ideas in the shortest time with the least ink in the smallest space.
- Requires telling the truth about the data

Globus goes on to define exactly what visualisations should do:

- Avoid distorting what the data have to say
- Present many numbers in a small space
- Make large data sets coherent

Given these simplistic definitions it would be understandable to assume the process itself cannot be too complex, certainly not in the same league as the

complexity of the processes, simulations and experiments that produce the data in the first place. This was arguably true in the context of the early years of computational analysis where data sets comprised small numbers of variables representing small 1D or perhaps 2D domains. The enormous data sets produced by the current generation of computationally fast workstations produce output files comprising millions of lines of data representing complex 3D, often transient, domains. The use of a 2D or 3D graphical plot is no longer sufficient to communicate effectively the information produced.

Since the 1980's advances in the fields of experimental and computational analysis of all types of application has led to the production of data sets of increasing size (Rosenblum 1994). Rapid increases in the production of volume data are an inevitable consequence of improved hardware resolutions for experiments involving any kind of scanning or imagery, and memory capacity and speed for computational experiments. It is often the case that the increases in data output represent increases in the levels of accuracy rather than any increase in the physical size of the experiment. For example, wind tunnels have not suddenly got any bigger whereas the data output from them has increased many times over. Visualisation has therefore had further demands placed upon it in terms of efficiency, feature extraction and accuracy.

These demands have generated a specialised area of research dealing exclusively with visualisation as opposed treating the subject as a sub-class of other areas, for example the data output generated by CFD simulation models.

The visualisation of data produced from computational sources often comprises data values at fixed points in space normally described in Cartesian co-ordinates. Experimental data is usually taken from a lesser number of sampling locations or is entirely qualitative. Whatever the source, the fact that data is only described at finite locations requires some kind of approximation to be made as an integral part of the visualisation process. It is this necessary approximation that introduces a further level of inaccuracy

within the whole analytical process, in addition to those present during the pre-processing and solution stages of a CFD modelling process. Approximation in various forms is therefore an important aspect of the process of visualisation.

The task of visualisation is far from simple. Once the purpose of the visualisation has been defined a number of processes must be carried out, collectively described as *post-processing*. These associated methods will be discussed thoroughly in the following sections.

## 4.2 History

Since the process of visualisation and visualisation as a science is a relatively new concept the number of potential applications is constantly increasing as increases in computational power opens the door to more thorough, in depth visualisation methods. To accommodate for the growing international audience dedicated to the research and evaluation of advanced visualisation algorithms a number of specialised conferences were born. The IEEE visualisation conference first held in 1990 has become the primary conference dedicated to the discipline of visualisation for scientific research. In Europe, the annual Eurographics workshop on scientific computing provides a similar platform for visualisation researchers.

One of the earliest driving forces of visualisation methodology was the need for the newly emerging process of CFD to have a standard set of visualisation tools for displaying the data produced during a simulation. CFD emerged as a valid method of analysing fluid flow during the 1970's and 1980's. 2D visualisations of fluid flow began to appear regularly during the 1980's. Rosenblum (1994) has identified the two main growth areas of visualisation as volume visualisation and fluid dynamics visualisation. Arguably there is a degree of crossover, the former being a sub set of the latter. It is clear however that the exploration and visualisation of volume data sets introduced by recent advances, primarily in medical imagery, has

driven the recent surge in numbers and variety of volume visualisation algorithms. Since this process is by its nature highly computational the development of visualisation techniques has gone largely hand in hand with the recent strides forward in computational processing power.

In last decade visualisation has achieved greater flexibility and availability than ever before with the development and introduction of module based visualisation systems such as the IRIS<sup>TM</sup> Explorer from NAG Ltd, IBM data Explorer<sup>TM</sup> from IBM Systems Ltd. and the Visualization Toolkit (VTK<sup>TM</sup>) from Kitware, enabling scientific researchers to create tailor made visualisation applications to suit the requirements of their particular data making use of widely utilised standard visualisation algorithms.

### **4.3 Data Sources & Formats**

For the purposes of an evaluation of the most prominent visualisation techniques an understanding of the sources and formats of the raw data is necessary. There is no standard for data of any number of dimensions describing any type of variable. There are however a number of common formats derived from a relatively small number of data sources. Commercial visualisation environments tend to restrict themselves to these common formats leaving specialised data to be converted by the individual.

#### **4.3.1 Medical Scanning**

The development of medical scanning, such as the application of nuclear magnetic resonance pioneered at the University of Nottingham, has contributed greatly to the development of a particular area of data visualisation, that of volume visualisation. Data produced by this method is volumetric in nature as its intent is to produce 3D representations of human anatomy. Typically the scanning device reads material density. The data is obtained by a series of scan lines that together form a 2D slice. A number of these slices then together form the full 3D volume data set. The scanning



itself is achieved by one of a number of methods including *Computed Tomography* (CT), *Magnetic Resonance* (MR) and *Single Photon Emission Computed Tomography* (SPECT) (Lorenson 1987).

The format of the data is therefore of a uniform 3D gridded nature of points falling at regular intervals defined by the resolution of the scanning equipment in use. Typical data sets produced by this method detail a material density variable only with no Cartesian co-ordinates. Since the volume data set is often cubic and varying in order of x then y then z including the co-ordinates is unnecessary.

The medical establishment uses this method primarily to visualise structures such as bone that exhibit a relatively constant material density. Visualisation of the data sets produced by this method requires the isolation and 'wrapping' of regions within the data set either at a set value or within a range of values. Complex internal structures can thus be visualised by isolating the particular material density of the required region be it bone or soft tissue exhibiting differing densities.

The data set is therefore relatively simple being a 3D regular volume of equal proportions comprising a single density variable. The visualisation algorithms required to undertake the task of isolating and representing internal patterns and structures are less simple but represent an important contribution to the development of volume visualisation. These will be covered in a later section.

#### **4.3.2 Computational Simulation Sources**

Computational modelling now produces vast amounts of raw simulation data. These data sets primarily originate from the well established finite element simulations of solid stress mechanics in addition to the finite volume techniques used widely in CFD. It is typical for data sets originating from CFD models to be large, often measured in gigabytes (Kenwright et al, 1996). Data reduction or efficient organisation has thus become an active

research area as data set sizes outstrip computational processing capabilities. Computational methods such as CFD produce solutions to a number of variables at fixed points in a domain known as nodes. These nodes together comprise the computational mesh introduced in Chapter 4. It follows therefore that data produced from these simulations is as varied as the mesh used to generate the solutions. Data sets can be roughly classified into structured and unstructured data sets but the non-uniformity of inter node spacing makes even the structured data set a complex source. A typical modern CFD analysis would produce a series of unstructured co-ordinates bounding an irregular complex geometry. Resolution would be irregular concentrating at regions of interest or where local velocity gradients are high requiring greater numbers of nodes in order to resolve the complex flow phenomena.

It is normal for commercial CFD applications such as CFX<sup>TM</sup> from AEA Technology and Fluent<sup>TM</sup> to offer an output of raw data in the text format detailing co-ordinate information, variables, cell connectivity and boundary condition information in a single file for use in custom visualisation applications.

The CFD ventilation modelling studies of Hargreaves (1998) generated unstructured data sets comprising of around 1,000,000 data points with each point comprising seven independent variables occupying an unstructured tetrahedral based grid.

## **4.4 Pre-Processing**

Pre-processing is normally associated with the initial stages of setting up a CFD simulation. The term is also used less extensively to describe some numerical processes undertaken in the initial stages of a visualisation procedure. These processes are concerned with the steps taken to provide a value for any given point within a data set of finite points. The processes required are therefore defined as point location and interpolation.

#### 4.4.1 Point Location

Data produced from CFD simulations provides information regarding variable values at specific points within the flow domain. It is desirable to enable the analyst to request variable values at any point in the domain rather than be restricted to the finite points provided by the solution. If an interpolative solution is to be used based upon the cell within which the point lies then an algorithm is required to perform the task of searching the entire data set and returning the cell and constituent nodes surrounding the point. This process is referred to as *point location* or *cell searching*.

The process of cell searching is normally carried out on the basis of the natural co-ordinate system, sometimes referred to as the canonical system, rather than the usual physical co-ordinate system. Calculations based upon the natural co-ordinate system are more computationally efficient since they are normalised and transformed to the origin. Ueng et al (1996) demonstrated significant savings in both computational processing intensity and memory usage over the same process using the physical co-ordinate system. It should be noted however that this co-ordinate transformation only delivers computational savings when applied to a tetrahedral based mesh, Sadarjoen et al (1994) applied the transformation to a deformed hexahedral based mesh and found significant increases in computational cost. Ueng et al (1996) has suggested that the coefficients of the co-ordinate transformation for the deformed hexahedral cells cannot be accurately calculated using simple differencing methods and the consequent need for more sophisticated methods increases the computational cost.

Kenwright and Lane (1996) presented an efficient point location function, using a non dimensional natural co-ordinate system. Given an arbitrary point  $x$  described in dimensional physical co-ordinates, the aim of the function is to firstly express that point in natural co-ordinates. Figure 4.1 illustrates a tetrahedral cell expressed in both physical and natural co-ordinate systems together with the arbitrary point  $x$ .

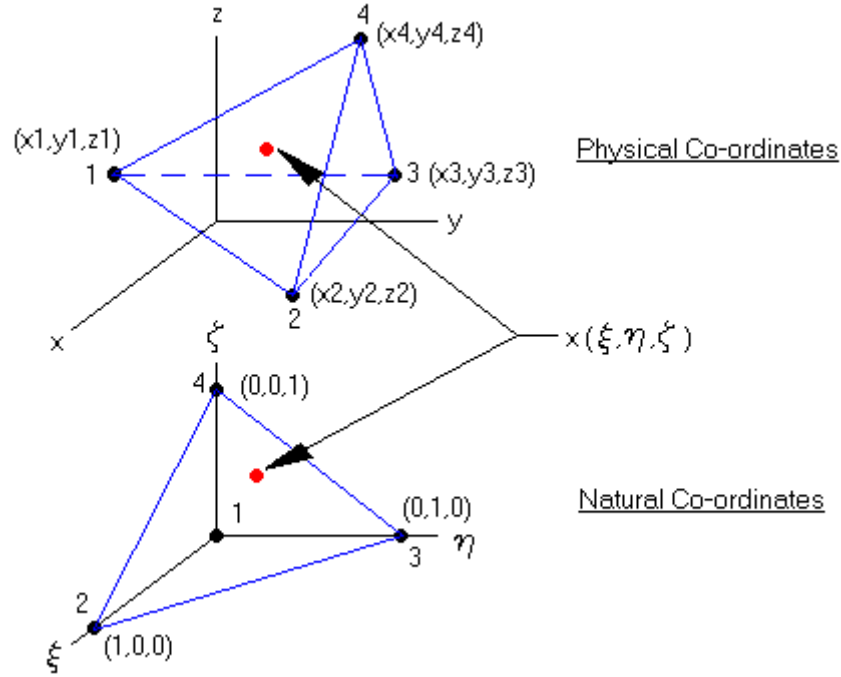


Figure 4.1 Tetrahedral cell physical and natural co-ordinate numbering

Kenwright and Lane (1996) used a linear interpolation function in order to map from the natural co-ordinate system to the physical co-ordinate system, expressed mathematically by equation 4.1.

$$x(\xi, \eta, \zeta) = x_1 + (x_2 - x_1)\xi + (x_3 - x_1)\eta + (x_4 - x_1)\zeta \quad (4.1)$$

Since the reverse procedure is required a simple inversion of equation 4.1 may be carried out analytically as there are no non-linear terms. Equation 4.2 gives the solution for the natural co-ordinates for a given point  $(x_p, y_p, z_p)$  expressed in physical co-ordinates.

$$\begin{pmatrix} \xi \\ \eta \\ \zeta \end{pmatrix} = \frac{1}{V} \begin{pmatrix} a_{11} & a_{12} & a_{13} \\ a_{21} & a_{22} & a_{23} \\ a_{31} & a_{32} & a_{33} \end{pmatrix} \begin{pmatrix} x_p - x_1 \\ y_p - y_1 \\ z_p - z_1 \end{pmatrix} \quad (4.2)$$

The constants in the above 3 X 3 matrix are given by;

$$\begin{aligned}
a_{11} &= (z_4 - z_1)(y_3 - y_4) - (z_3 - z_4)(y_4 - y_1) \\
a_{21} &= (z_4 - z_1)(y_1 - y_2) - (z_1 - z_2)(y_4 - y_1) \\
a_{31} &= (z_2 - z_3)(y_1 - y_2) - (z_1 - z_2)(y_2 - y_3) \\
a_{12} &= (x_4 - x_1)(z_3 - z_4) - (x_3 - x_4)(z_4 - z_1) \\
a_{22} &= (x_4 - x_1)(z_1 - z_2) - (x_1 - x_2)(z_4 - z_1) \\
a_{32} &= (x_2 - x_3)(z_1 - z_2) - (x_1 - x_2)(z_2 - z_3) \\
a_{13} &= (y_4 - y_1)(x_3 - x_4) - (y_3 - y_4)(x_4 - x_1) \\
a_{23} &= (y_4 - y_1)(x_1 - x_2) - (y_1 - y_2)(x_4 - x_1) \\
a_{33} &= (y_2 - y_3)(x_1 - x_2) - (y_1 - y_2)(x_2 - x_3)
\end{aligned} \tag{4.3}$$

The matrix determinant V is given by;

$$\begin{aligned}
V &= (x_2 - x_1)[(y_3 - y_1)(z_4 - z_1) - (z_3 - z_1)(y_4 - y_1)] + \\
&\quad (x_3 - x_1)[(y_1 - y_2)(z_4 - z_1) - (z_1 - z_2)(y_4 - y_1)] + \\
&\quad (x_4 - x_1)[(y_2 - y_1)(z_3 - z_1) - (z_2 - z_1)(y_3 - y_1)]
\end{aligned} \tag{4.4}$$

Using these functions the natural co-ordinates ( $\xi, \eta, \zeta$ ) may be evaluated from the given physical co-ordinates of the fixed point x. Kenwright and Lane (1996) suggest this can be achieved in 104 floating point operations, a figure which can be halved if common terms are pre computed prior to evaluating the matrix coefficients and determinants. Now that the natural co-ordinates have been defined all that remains is to perform a cell search. Kenwright and Lane (1996) propose four conditions that must be met for a point to be defined as lying within a given cell. These are:

$$\xi \geq 0 \quad \eta \geq 0 \quad \zeta \geq 0 \quad 1 - \xi - \eta - \zeta \geq 0 \tag{4.5}$$

If one or any combination of these conditions is not valid then the point must lie outside the cell under consideration. The process can be exemplified via a 2D representation, illustrated in figure 4.2.

This approach to cell searching proves extremely useful when applied to *particle tracing* algorithms. Since particle tracing requires the constant tracking of a particle through adjacent cell boundaries information regarding which neighbouring cell the particle has crossed into would greatly reduce computational costs. By a consideration of which of the four conditions is violated first, the particular face the particle has crossed can be identified. For example, if the particle crossed the  $\xi = 0$  face then the violation would be on the condition relating to  $\xi$ .

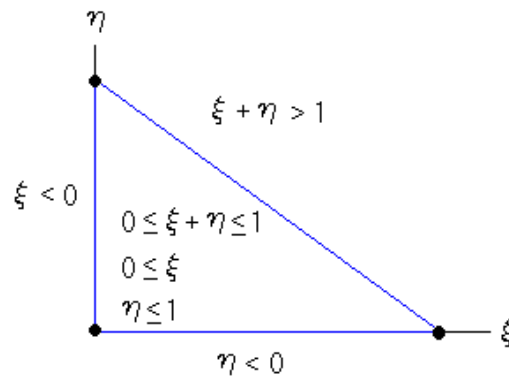


Figure 4.2 Cell search conditions

This cell searching algorithm has been used extensively for the purposes of CFD flow visualisation by a number of authors (Kenwright and Lane 1996), (Ueng et al 1996) and (Lohner 1990), with very little modification to suit individual applications.

Some important issues were identified by Kenwright and Lane (1996) regarding possible problems with the approach specific to its application within particle tracing schemes. On occasion where the particle crosses a face near a corner of the cell two or more conditions may be violated, in cases such as these the worst violator is used to predict the adjacent cell. It was reported that tests in a number of mesh data sets never failed to locate the bounding tetrahedron using this cell search scheme.

#### 4.4.2 Interpolative Methods

One of the most important issues in volume data set visualisation is that of interpolation. Since for the most part, and certainly for the purposes of CFD visualisation, the data is given only at a finite number of points to produce a continuous visualisation between those points some degree of approximation is required. This approximation is almost always based upon some kind of interpolative method. Interpolative methods require more computational processing and memory usage but arguably produce a more accurate visualisation.

##### 4.4.2.1 Hill Climbing

Often CFD engineers require visualisation of variables on 2D planes within the dataset. Using an interpolative method ensures that the data displayed on such a plane is influenced in appropriate amounts by those nodes nearest to it. Methods employed where computational resources are scarce use a simple process of adopting the values of the nearest node based upon linear distance. This process is referred to as *Hill Climbing* (HC).

The process of hill climbing is less computationally intensive as the number of floating point operations required to define a value for a given arbitrary point is relatively low since the previously described cell search scheme is not required. It is however, unsuitable for data sets comprising millions of data points. A refinement reported by Hultquist (1995) uses a multipass approach whereby the data is scanned at an initial coarse grid resolution and incrementally converged on to the true nearest point. Figure 4.3 illustrates this process in simple terms.

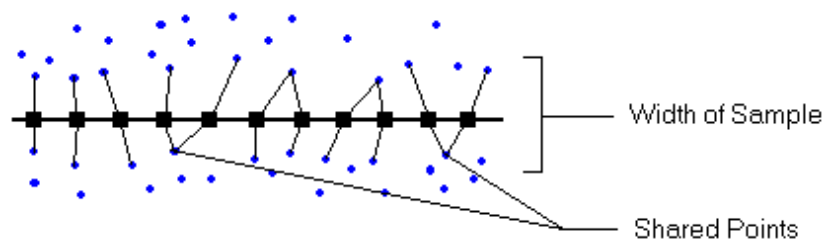


Figure 4.3 Depiction of hill climbing approximation

Although hill climbing is unquestionably fast the process does introduce a degree of error the significance of which is dependent upon the type of visualisation being conducted. For example, in particle tracing visualisations the scheme may terminate a trace that is in close vicinity to a boundary. This causes the particles to *stick* to stationary objects within the domain reducing the number of traces and thus the quality of visualisation. Another problem, again regarding particle tracing, concerns the propensity of the hill climb scheme to jump across solid thin boundaries. The particles thus appear to pass through solid walls. For static visualisations the same problems apply though with less severe consequences. Hill climbing does therefore present some serious drawbacks, however, in cases where the mesh density is suitably high, the error may be minimal and the reduction in computational cost may then be worthwhile. It should therefore be applied with caution and of course correlated with other more accurate schemes.

#### 4.4.2.2 Spatial Interpolation

Having identified the cell within which a point lies a value must be assigned to that point with due consideration to the influence of the surrounding nodes that make up the bounding cell. This is referred to as *spatial interpolation*. Three possible techniques have been proposed. These are, *physical space linear interpolation* (Chung 1977), *linear basis function interpolation* (Dhatt 1984) and *volume weighted interpolation* (Buning 1989). It has been shown mathematically that all three approaches are equivalent and produce identical interpolative functions (Kenwright, 1995;1996). Kenwright, (1995) also demonstrated the linear basis function interpolative scheme to be the most efficient owing to its re-use of the existing natural co-ordinates defined during the previously described point location process.

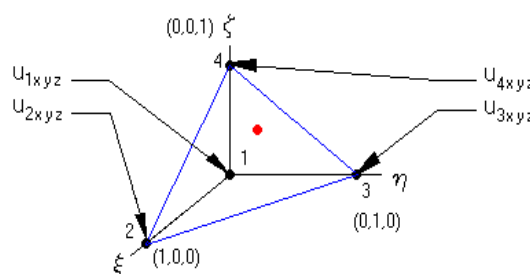


Figure 4.4 Single tetrahedral cell node numbering scheme



If a single cell such as that illustrated in figure 4.4 is considered, the spatial interpolation based upon the linear basis function approach is given by equation 4.6 using the node numbering scheme given in the illustration.

$$u(\xi, \eta, \zeta) = u_1 + (u_2 - u_1)\xi + (u_3 - u_1)\eta + (u_4 - u_1)\zeta \quad (4.6)$$

Note the use of the existing defined natural co-ordinates  $(\xi, \eta, \zeta)$  and  $u_{1..4}$  representing the velocities at each respective node. Equation 4.6 is repeated for each of the three velocity vectors or just once in the case of single scalar variables.

## 4.5 Data Optimisation

Following the growth of the application of CFD and other finite computational methods, the size of data sets produced has presented even the most up to date processing hardware with difficulties in producing good quality visualisations economically in terms of computational time and memory usage. As CFD has achieved acceptability in the design process, the need for the turnaround of simulation, results and feedback to be achieved as quickly as possible has never been more apparent (Kuhner et al 2001).

### 4.5.1 Simplification

To aid the visualisation of large volumetric data sets several authors have presented studies into the efficient reduction of data set size whilst maintaining the relevant features and accuracy of features within that data set. Cignoni et al (1996) terms the process of 3D mesh simplification for the purposes of faster visualisation times as *decimation*, the reverse being described as *refinement*, a process usually used prior to solving in order to improve accuracy. There are a number of algorithms published for the purposes of mesh decimation, many such as that presented by Renze and Oliver (1996) use the simple principle of vertex removal, the voids left in the

mesh after the vertex removal are then re-triangulated with a coarser tetrahedral based mesh. This type of decimation is conducted randomly to ensure a constant degradation across the volume. No consideration is given to the error produced by such a process. A method proposed by Trotts et al (1998) takes into consideration the predicted error in resultant approximation when a cell is removed. The process can then prioritise each cell for removal based upon minimising the resultant error.

Many of these mesh decimation techniques make prior assumptions regarding the data set topology, for example, the method proposed by Trotts et al (1998) cannot cope with complex irregular geometries since boundary cells are often removed. Cignoni et al (1996) presents an evaluation of some of the most common mesh decimation techniques allowing a comparison by incorporating error evaluation into the study. Cignoni defines two measures of error induced by mesh decimation, *domain error* and *field error*. The former concerns itself with the degradation of domain geometry, or the removal of boundary cells. Whilst the latter, perhaps more importantly, measures the scalar data field error induced by mesh decimation. By using a number of different error evaluation algorithms Cignoni was able to demonstrate on a 3D CFD data set that mesh decimation in 3D data sets produced high local peak errors in the region of 50-60% with much lower mean square errors in the region of 1-3%.

The process of mesh decimation is therefore only to be used with due caution particularly where single point sampling is conducted. Cignoni also states that decimation processes should only be used in cases where the practitioner has access to the original data such that locally defined areas can be viewed with more confidence.

Kuhner (2001) presents a method of data set reduction based upon the representation of volumetric data in 3D regular Cartesian co-ordinates using an *octree data structure*. This type of process differs to mesh decimation in that it does not aim to preserve the mesh structure itself, the existing data is examined and re-ordered in such a way that redundant data is eliminated, the

process is therefore far more robust than the previously described mesh decimation techniques and considerably easier to implement into post processing routines. A similar method is demonstrated by Ueng et al (1997) where tree based data structures are used to assist in the efficient construction of streamlines.

Kuhner (2001) identified the growing need for interactive visualisation by non-specialised practitioners as a key factor in the justification of such a procedure. The data sets studied by Kuhner were developed to be incorporated within a virtual reality environment. Kuhner's octree data structure optimises the original data set by creating an incrementally coarsened grid (figure 4.5) in areas where the error induced by doing so falls below a set value.

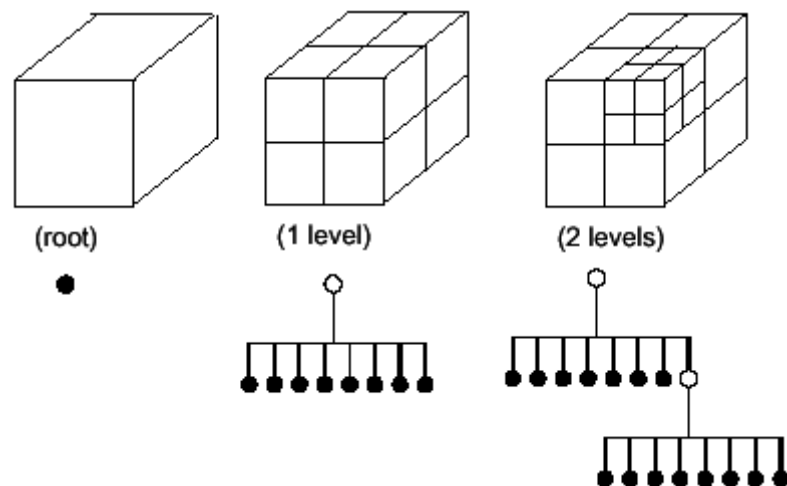


Figure 4.5 Octree based data reduction procedure (Kuhner et al 2001)

Each incremental coarsening step is conducted on a 1:2 ratio starting from a defined *root cell* comprising of an increasing number of *child cells*. The reduction is only conducted if the curvature describing the velocity function does not exceed a pre-defined value. This error control process is illustrated in simple terms in figure 4.6.

For a fuller description of the use of coarsening algorithms the reader is referred to Kuhner (2001) and Clark (1976). To exemplify the principle of

tree based data reduction figure 4.7 illustrates how a simple 2D mesh could appear prior to and after such a procedure.

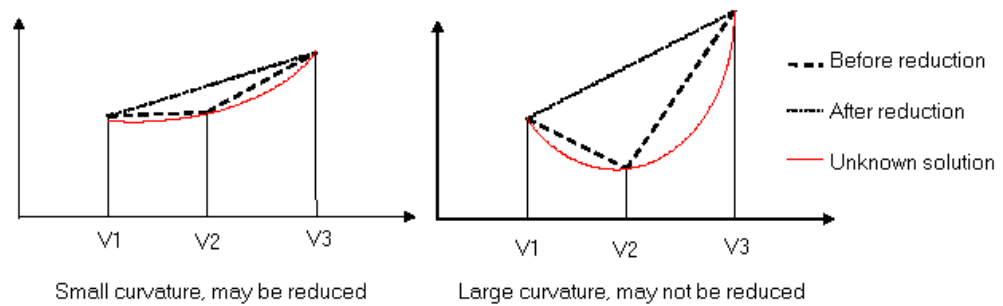


Figure 4.6 Octree based reduction criteria

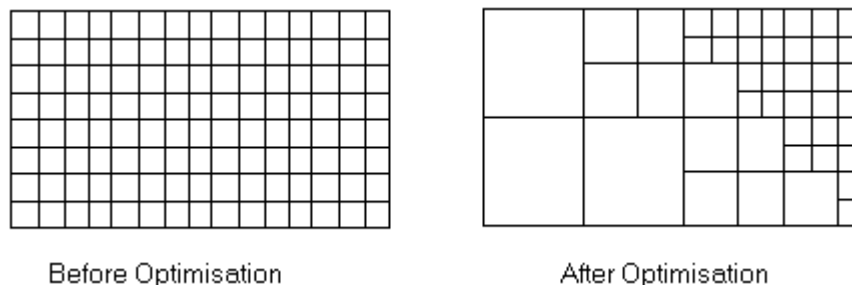


Figure 4.7 Example of tree based reduction applied to a 2D regular mesh

An example of data reduction is given by Kuhner (2001) as a 2D grid of 7469000 nodal points coarsened to 88963 nodal points whilst preserving the overall variable visualisation and distribution. The savings in computational cost are therefore significant, it is also clear that hierarchical data structures contribute greatly to the efficient display and post processing of CFD data for the purposes of interactive VR visualisation. It should however be considered that in cases where the flow field is such that velocity gradients are high throughout the domain, such as in highly turbulent flow, the process may offer little data reduction as in order to preserve the steep curves between nodal points any degradation would not be possible. In practice flows such as these are not commonplace, flow fields generated by sub surface ventilation in particular comprise large areas of laminar type flow in addition to highly turbulent regions.

#### 4.5.2 Feature Extraction

*Feature extraction* is another sub set of visualisation that has been the subject of a number of recent studies (Walsam et al (1996); Huang and Menq (2001) and Samtaney et al (1994). The objective of these studies was to improve the efficiency of the process of pre-defining those areas of interest within a data set. In simple terms, the process of feature extraction conducts the task of classifying which flow features are of interest using a customised algorithm to scan the volume data set for their presence. It is typical within the data sets produced by CFD simulations that the area of interest only comprises a small fraction of the total volume of data (Walsam et al 1996). Although it is common for feature extraction algorithms to be applied to 2D data sets there is much less application to large 3D data sets due to the increased complexity. The examples that have been applied to such data sets tend to be derived from medical scanning applications (Samtaney et al 1994).

There are many methods of classifying features, Samtaney et al (1994) identifies *threshold clusters*, *critical points* and *vector field lines* as being those most commonly used for the purposes of CFD visualisation.

The simplest and most often applied form of feature extraction, used by Walsum et al (1996), is the generic process of defining a sub set of  $N$  nodes, defined through the evaluation of a simple *evaluation function*  $F(N)$  applied to the entire data set. The evaluation function can define an exact value or a range or be a Boolean combination of characteristics. If the node  $N$  satisfies the function then it becomes a member of that particular subset. By producing a number of evaluation functions a number of data sub sets representing individual or combinations of features can be produced.

Although this method of feature extraction requires an initial sweep of the entire data set the classification of all features of interest at an early stage can produce significant timesavings in the long run. The process can also

benefit through the application of data optimisation techniques such as mesh decimation and octree structuring described in the previous section.

## 4.6 Flow Visualisation Methods

In the field of contemporary CFD based flow visualisation there are a number of methods used extensively in commercial and other generic post processing applications. Flow characteristics are represented by common visualisations specific to variable types, usually classified into vector and scalar variables in 2D and 3D data sets. Although there are small variations between post processing applications these methods are for all purposes universal. The following sections introduce the most common methods used for the visualisation of flow features originating from 3D CFD data sets.

### 4.6.1 Glyph Based Visualisation

A *glyph* is a common term used within visualisation circles to describe a graphical object representing one or more variables through characteristics such as geometry, orientation and colour. A precise definition (Oxford (1992)) is 'an image or sign which has a characteristic in common with the thing it signifies'. In practice it is more convenient to use the term *icon*, since this is more consistent with computational terminology, the two are however interchangeable.

Iconic representation is not however restricted to the visualisation of flow features, the process has also been used extensively in the field of statistical analysis (Chambers et al 1983) and in pictorial information systems (Chang 1989).

Walsum (1996) defines the parameter or degrees of freedom of an iconic representation as being classified into three groups. These three groups represent the number of parameters that can be separately bound to data quantities, they are listed as follows;

- Spatial parameters
  - Position and orientation
- Geometric parameters
  - Control the shape of the object
- Descriptive parameters
  - Colour, texture, transparency or sound

Walsum goes on to further classify icons as either fixed shape or amorphous template. Fixed shape icons have a number of variables such as length, height and width that physically define the dimensions of the icon whilst retaining a fixed overall shape, velocity vectors are an example of fixed icons. Amorphous icons have no predefined shape being fully defined by the local properties of the data, streamlines are an example of amorphous icons. Icons can also be defined as being either *passive* or *interactive*, the former type is a representation of flow properties at a fixed point in space where as the latter's position can be moved by the user analogous to a probe.

The use of icons is well established in the field of CFD visualisation and universally recognised by researchers of a number of other disciplines. The characteristics of icons are also increasingly designed to accommodate the non-specialised observer thus greatly easing the communication of complex flow data to a wider audience. The following sections discuss individual iconic representations in detail.

#### **4.6.1.2 Vectors**

The display of static velocity data is almost exclusively performed by *fixed point vector icons*. Typically an icon is displayed at each data node, the position and number of the data nodes is dependent upon the type of mesh, interpolation scheme and definition of the practitioner.

Vector icons come in a variety of shapes and sizes, fundamentally they take the universal arrow form with various application specific modifications based upon this foundation. Figure 4.8 illustrates the main vector icon types used in contemporary fluid flow visualisation.

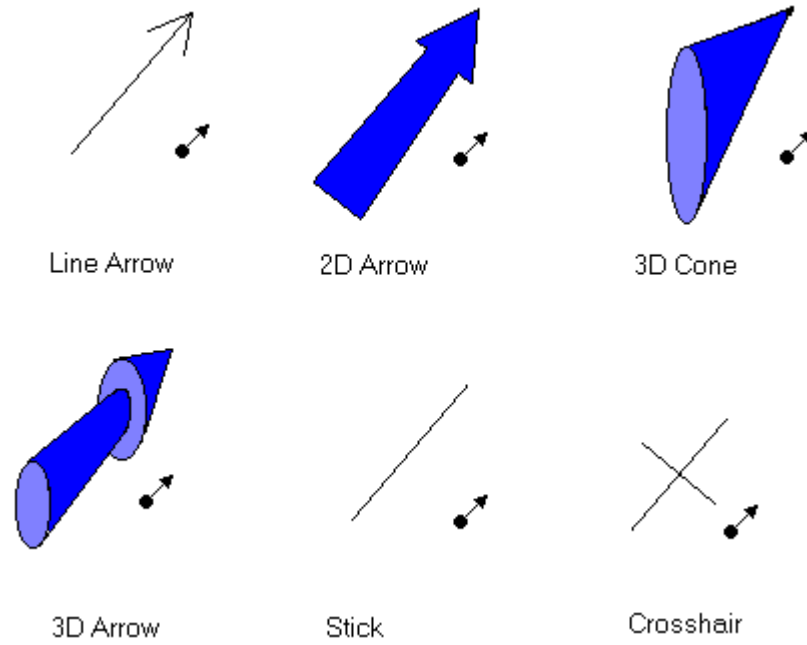


Figure 4.8 Contemporary vector glyphs used for fluid flow visualisation

In the previous section a number of parameters were identified that define the visual characteristics of iconic visualisations. *Static vectors* are perhaps the clearest example of linking data characteristics to icon shape and appearance. The scalar vector value determines overall dimension or overall colour on a graded scale usually from red (high) to blue (low). It is normal for these characteristics to be either combined or used independently.

The application of vector icons to fluid flow is not however straightforward. Being a basic graphical representation of data point values vector plots are perhaps the most primitive of visualisations. As such they present serious problems in the case of modern large volumetric data sets for which they were not designed. The large amount of data, each point of which is represented individually, creates confused and cluttered images (Garcke et al 2001). Some attempts have been made to replace large vector fields with



smaller numbers representing vector 'clusters' exhibiting similar characteristics (Garcke et al 2001) and (Westermann 2001).

Vector plots work extremely well on 2D planes cut through a 3D data set plotted on points clearly defined on a regular grid, (figure 4.9).

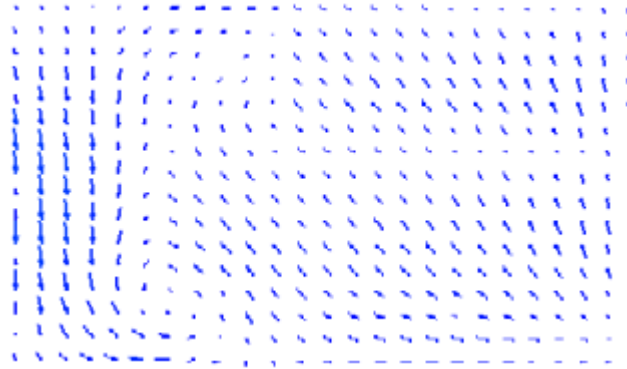


Figure 4.9 Vectors on a 2D plane

When plots are produced on 2D planes using the plane intersections with the mesh as a plotting point the resultant images often become either too *busy* where mesh densities are high, or largely empty where, in the converse case, mesh densities are low (figure 4.10). In cases such as these where there is a high local variance it is often helpful to normalise the vectors to the same scale, colour gradation also assists in producing an effective visualisation.

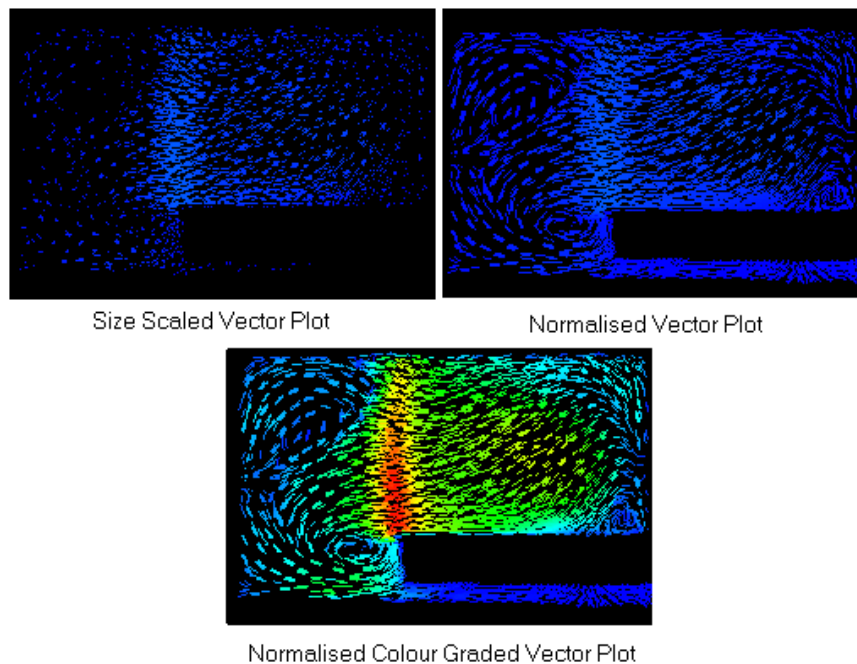


Figure 4.10 Vectors plotted according to mesh intersections in 2D

Vectors are not recommended for the visualisation of 3D data plotted on 3D grids due to serious perceptual problems, there is simply too much data displayed for the observer to extract any global or local patterns. For this reason, vectors are restricted primarily to displaying data on carefully selected 2D sampling planes within 3D data sets, an example of which is illustrated in figure 4.11.

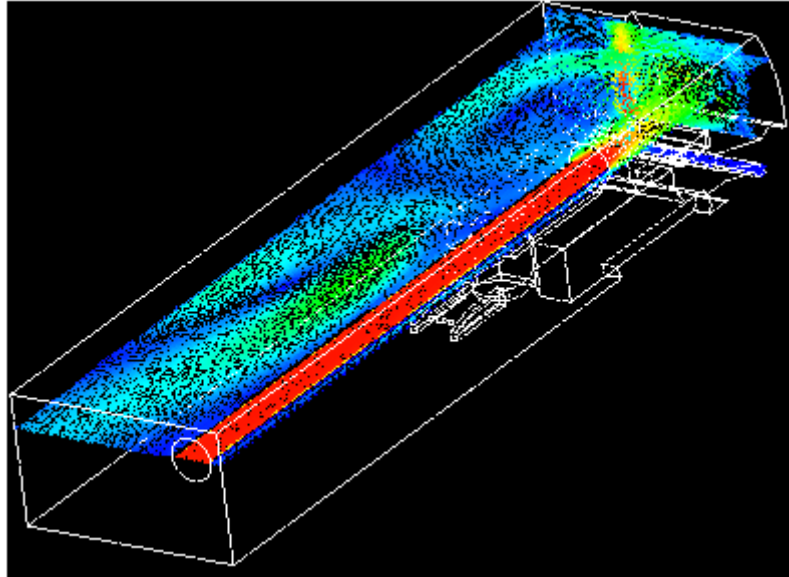


Figure 4.11 Combining 2D vector sampling planes in a 3D domain

#### 4.6.1.3 Particle Tracing

*Particle tracing* refers to the process employed in order to track a massless particle through a velocity field, the resulting path obtained over a given time ( $t$ ) is referred to as a *streamline*. There are a number of differing concepts and terms regarding particle tracing in experimental visualisation. To clarify, these are summarised as follows;

- Time Line
  - Trace of a line of particles released at the same time
- Streak Line
  - Trace of a continuous injection of particles from a fixed point
- Path Line

- Trace of a single particle path

In terms of computational data visualisation we are purely concerned with the generation of streamlines, referred to as pathlines in experimental visualisation. The definition of a streamline within computational terms is that of a line everywhere tangential to the local velocity vector.

The tracking of a single massless particle through a 3D computational velocity field is based upon the solution to a simple equation that can be derived from the particle illustration in figure 4.12.

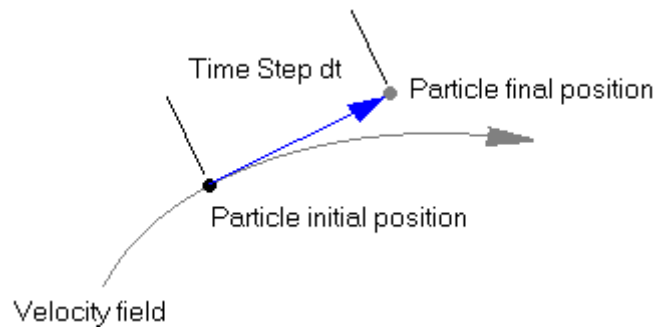


Figure 4.12 Time stepped particle tracing

For a single particle described in Cartesian co-ordinates  $x, y$  and  $z$  whose velocities are  $u, v$  and  $w$  respectively, given a time step  $dt$ , the equation describing the construction of a streamline can be expressed as the differential equation 4.7.

$$\frac{dx}{dt} = u(x) \quad (4.7)$$

This expression can therefore be integrated in terms of time,  $dt$ , yielding equation 4.8;

$$x(t) = x(0) + \int_0^t u(x(t)) dt \quad (4.8)$$

Equation 4.8 is the fundamental building block of a streamline construction based upon progression using a number of small time steps. A number of authors have developed streamlining algorithms based upon this fundamental expression (Volpe 1987, Wilkes and Mathew 1986 and Buning 1988).

To create a streamline based upon this expression requires a solution to the ordinary differential equation (ODE), equation 4.8. Since ODE's occur frequently within engineering numerical methods there are a number of solutions that have been applied in differing situations with varying degrees of success. The most commonly applied methods within the field of flow visualisation are Euler's Method (first order accurate) and higher order methods specifically the Runge-Kutta 2<sup>nd</sup> order (R2K), sometimes referred to as the Huen Method or the Improved Euler Method and the Runge-Kutta 4<sup>th</sup> order (R4K). All methods essentially are evolved from the fundamental principles exhibited within Euler's Method.

Euler's Method involves the direct substitution of finite differences within the particle tracing equation; the curve exhibited by the true streamline is therefore approximated with a tangentially true line governed by the size of time step. The potential for error when applying this method is obvious, assuming a fixed time step it is easy for the particle to diverge from its true

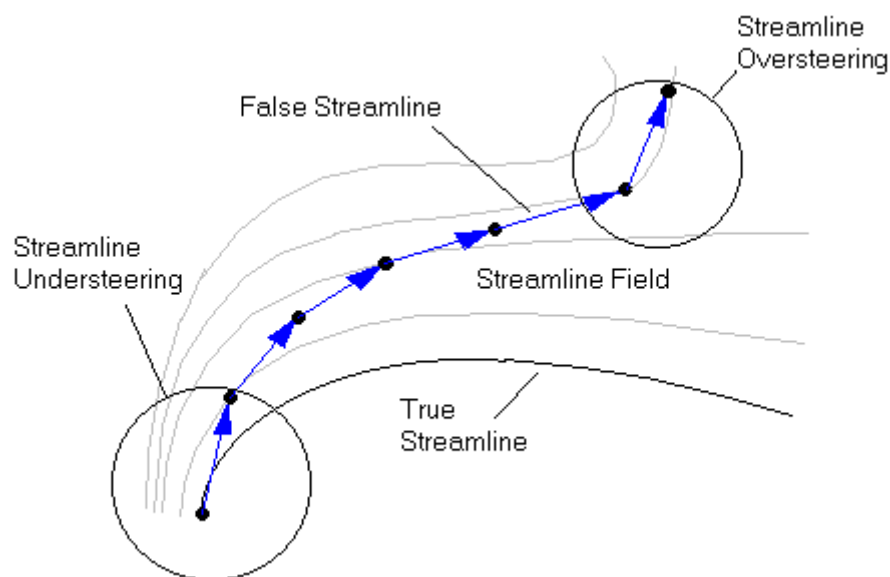


Figure 4.13 Particle steering error

course. This well known characteristic manifests itself in the particle either *understeering* or *oversteering* round sharp bends causing the trace to, in effect, jump across independent streamlines, figure 4.13.

The application of Eulerian approach to particle tracing is a good indication of how a small error at the point interpolation stage can give rise to serious errors when the cumulative effect is considered. The application of higher order methods such as the R2K and R4K (Appendix I) involves the integration step being divided into a number of intervals. The derivative is therefore given by a weighted average of these derivatives over the original interval. The accuracy, in terms of proximity to the true streamline, is therefore largely dependent upon the integration method and time step size.

The choice of integration scheme must be made with due consideration to an acceptable trade off between required accuracy and computational expense. Higher order schemes offer greater accuracy but require greater computational effort, for example, the R4K scheme requires the integration to be performed at three time values as opposed to the single step used by the Eulerian approach. Given the application of the above equations there are a number of potential sources of error. Kenwright and Mallinson (1992) have identified these as being either independent of the tracing algorithm such as severe grid distortions and poor convergence or due to the tracing algorithm, such as the choice of numerical integration scheme used to solve equation 4.8.

Error analysis studies reported by Darmofal and Haines (1994) focus on local and global errors produced by a large number of alternative advanced integration schemes (modified RK schemes) applied to large unsteady data sets. Sikorski et al (1995) used a modified RK scheme for the faster construction of streamlines for steady flow on unstructured grids. Other work by Ueng et al (1996) and Kenwright (1995,1996) identifies the R4K as being a reliable and reasonably accurate method when applied to multi gigabyte unsteady data sets. Kenwright (1996) does however accept that the

excessive computational costs of the R4K method over lower order schemes do prohibit its application in certain situations.

Studies by Buning (1988) evaluated a number of integration schemes including the first order Euler and RK schemes finding the first order Euler scheme to present misleading information in 2D vortex flows where a fixed time step was used. However, much greater accuracy was achieved in 3D flows by altering the time step where necessary thus eradicating the need for a universally small time step.

The majority of so-far reported studies have utilised either standard RK schemes or modified RK schemes for the construction of streamlines within large multi gigabyte time dependent data sets where error minimisation and the significance of the cumulative effect is significant. Existing applications and studies related to smaller steady data sets where computational resources are limited have made use of the Eulerian approach with a greater emphasis on time step modification to reduce error (Brodie 1999; Buning 1988).

#### **4.6.1.3.1 Variable Time Stepping**

The integration time step is of crucial importance if a representative particle trace is to be constructed. There are a numerous methods of achieving this by the adoption of slightly different methods. Buning (1988) achieved an *adaptive step size* by considering the size of the cell containing the particle and the inverse of the velocity magnitude at that point thus taking into consideration irregularities in mesh density throughout the domain. This method was also investigated by Darmofal and Haines (1992) for similar purposes. A universal error tolerance scheme known as *step-doubling* has been implemented in a number of recent studies. Step-doubling involves the particle being progressed initially by a full single time step, then twice progressed again from the initial point by half the initial time step. The difference in position of the two final particle positions based upon this technique serves as the error tolerance. If the tolerance is greater than a specified amount, usually defined through trial and error, then the step size is

halved and the process repeated over again. This tolerance may be measured in terms of the angle between the two vectors or as the linear distance between the two particle trace endpoints, figure 4.14.

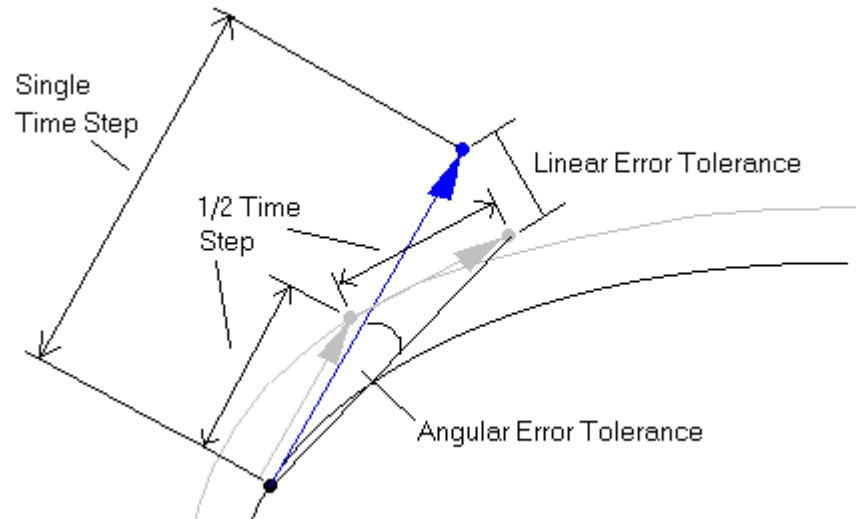


Figure 4.14 Adaptive time stepping using step-doubling

Either technique produces the same result. Step-doubling has been successfully applied in more recent times by Kenwright and Lane (1995;1996) and Ueng (1996;1996).

#### 4.6.1.3.2 Streamlines, Ribbons & Tubes

The *streamline* is the universal method of displaying particle traces within CFD data sets. However, there are two other stream based visualisations which while being based upon the stream line offer further flow information. These are referred to as *stream surface*, *ribbons* and *tubes*. The principle upon which these are constructed is usually a straightforward extension of the methods used to produce streamlines. For example, a *stream ribbon* can be constructed based upon the same method as that used for a streamline with the addition of rotation based upon local streamwise vorticity. Two streamlines are thus created with the second being restrained to a fixed distance (Hulquist 1995). A stream ribbon is thus defined as a streamline with width in a single plane, in this way rotation can be visualised in addition to velocity. The two-streamline approach can cause a number of

problems primarily concerning the effects present in high shear flows where one velocity stream exceeds the others by a large amount causing a large difference in the number of time steps of each stream. This is not so much a numerical problem as a graphical problem since the ribbon surface is usually formed by triangles whose vertices intersect the time step points on the streamline, figure 4.15. Time step adapting schemes may reduce this effect.

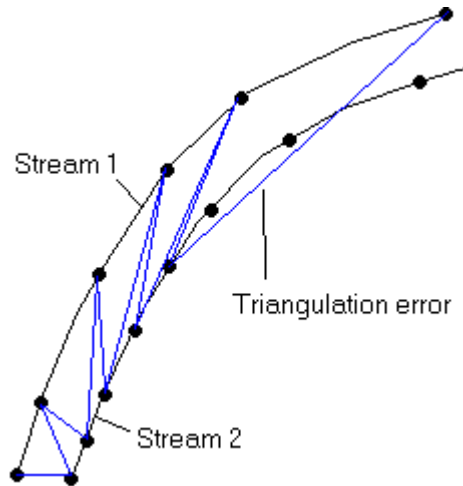


Figure 4.15 Two-streamline triangulation error

*Stream tubes* are another variation on stream ribbons, Batchelor (1967) defines a stream tube as 'the surface formed by all the streamlines passing through a closed contour'. It's perhaps more intuitive to think of a streamtube as being the surface formed when the streamribbon surface is rotated 180 degrees. Stream tubes present the same problems in construction as stream ribbons, they do however present the same advantages in displaying more information than the streamline about a given flow. Advanced efficient techniques used for the construction of stream ribbons and tubes have been presented by Darmofal and Haimes (1994), Hultquist (1994) and Ueng (1996).

The question of whether or not to use these adapted streamlines is really only answerable by the level of information that is considered relevant, the graphical complexity of these types of surfaces may also prohibit their use due to restrictions in certain visualisation environments.



#### 4.6.1.4 Contours

*Contouring* generally refers to 2D plots of a scalar variable on a plane such that a number of value ranges are isolated by lines, each line is referred to as a *contour*. The process has been used successfully for many years in a range of fields from geographic applications to the familiar CFD visualisations using an equally wide range of numerical techniques (Sabin, 1986).

The visual characteristics of contour plots are normally determined by the number of contours, i.e. the number of isolated ranges displayed on the plane. Figure 4.16 illustrates a typical series of shaded and unshaded contour plots

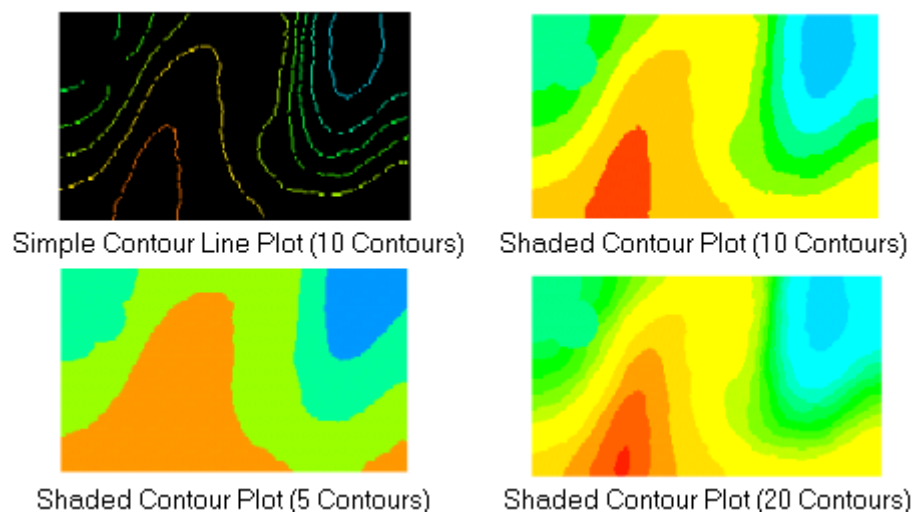


Figure 4.16 Typical 2D plane scalar contour visualisations

In general, the process is most simply explained in terms of a regular grid of scalar data on a 2D plane. Volume data sets from CFD sources are often unstructured in nature thus creating an irregular scattering of data points. It is however possible using the interpolation techniques previously explained to pre-process this data such that a regular 2D grid can be formed prior to contouring. The contour itself is comprised of a line where a given scalar variable is constant. In general the contouring algorithm produces the contour line by progressively comparing each node of each cell to a



scheme at the cost of further computational resources, it is reported though that higher order interpolation required special attention at boundaries (Sabin 1986).

#### 4.6.1.5 Isosurfaces

It follows that a contour restricted to a 2D surface could be extended into 3D thus creating a true *volume contour*. An *isosurface* can therefore be considered as the 3D equivalent of a 2D contour, it is a 3D surface corresponding to a constant scalar value within 3D scalar data field. The simplest method of construction is the basic addition of a number of parallel 2D contour planes spaced at regular intervals, this creates the fundamental wireframe surface which can then be joined by a method such as triangulation. A similar method was implemented by Keppel (1975) for the construction of complex surfaces. Although simple, this method is inefficient and numerically clumsy, it also suffers from ambiguities that can arise when more than one contour exists on a single plane, concerning which contours to connect (Fuchs et al 1977). The method now considered as the standard approach to the creation of 3D isosurfaces was first presented in Lorensen and Cline (1987) and is referred to as the *Marching Cubes* method (MC). The underlying principle is referred to as the *divide and conquer* approach. This method is now regarded as the universal solution to the old problem of surface extraction (Montani et al 2000). Stytz et al (1991) surveyed a large number of surface tracking algorithms, and concluded that the MC method was the most practical and simple in terms of implementation for wide range of applications.

The MC method as presented by Lorensen and Cline (1987) was originally developed specifically for application in the field of medical imaging. In this application, 3D images were required of internal anatomical features such as bone structures. The data produced by this application was introduced in a previous section. Lorensen's MC algorithm is a *case table* method that, in its original form, was restricted to processing data in medical scan line order. Formatting any type of data is not problematic but it should be noted that

medical scanners produce data corresponding to a regular 3D grid, Lorensens MC algorithm was thus restricted to regular gridded data.

In general terms the algorithm proceeds by examining every cell within the data set and classifying each cell according to the state of the scalar value at each cell node, whether they are above (+) or below (-) the given threshold value, figure 4.18.

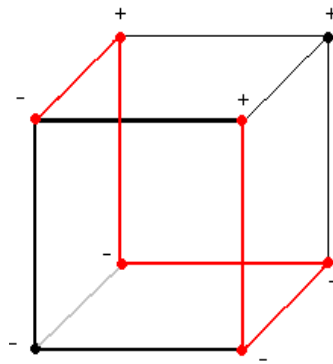


Figure 4.18 Single cell case, nodes defined as above or below threshold

If a single cell within a regular (hexahedral, 8 nodes) grid is considered there are  $2^8 = 256$  possible permutations for the + and - condition at each of the cell nodes. This number represents all possible ways an isosurface can cross a cell assuming that the variable function follows a linear approximation across each cell edge. These permutations, or cases, are stored in a case table, sometimes referred to as a *lookup table*. Each case determines the topology of a surface crossing that cell for the given permutation, the precise intersection of the surface along each edge is determined at a later stage through linear interpolation. Figure 4.19 illustrates the first fourteen triangulation cases utilised in Lorensen's case table.

The permutations stored in the case table are identified by a number in the range 0-255, once the correct permutation index has been identified the corresponding edges can be interpolated and joined to form the individual triangles which together form the isosurface.

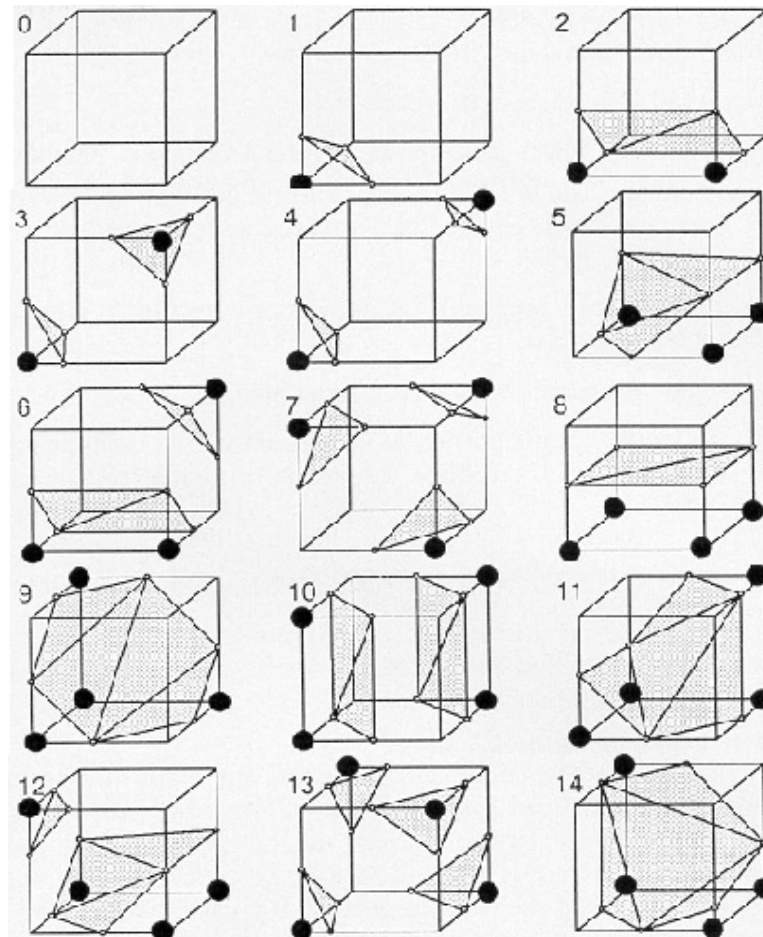


Figure 4.19 Triangulation cases from Lorensen's case table (Lorensen and Cline 1987)

To summarise the procedure Lorensen identified the following key steps to the MC algorithm.

- Read four *slices* into memory
- Scan two *slices* and create a cube from four neighbours on one slice and four neighbours on the next slice
- Calculate an index for the cube by comparing the eight density values at the cube vertices with the surface constant
- Using the index, look up the list of edges from a pre-calculated table
- Using the densities at each edge vertex, find the surface edge intersection using linear interpolation
- Calculate a unit normal at each cube vertex using central differences. Interpolate the normal to each triangle vertex
- Output the triangle vertices and vertex normals

The initial stages of the MC process as proposed by Lorensen refers to the reading of *slices*, this is a reference to the format of medical scanning data and should be considered as data input in more generalised terms.

Lorensen experimented with higher order interpolants to identify the intersection point on each edge but found that since the MC algorithm created at least one and, as many as four triangles per cube the higher order interpolants produced no significant improvements over the linear interpolant.

Although the MC algorithm continues to find growing universal approval for the application to 3D isosurfacing there have been a number of modifications proposed to the original algorithm. One of the problems inherent in the MC approach concerns the visitation of non isosurface cells, specifically it is desirable to reduce this to a minimum as this represents wasted computational resources. Itoh et al (2001) proposed a *volume thinning* algorithm which enabled the isosurface construction process to skip non isosurface cells leading to a reduction in processing time. Other work by Gallagher (1991) and Giles and Haines (1990) proposed pre-processing techniques such as scalar cell classification for the purposes of speeding up the MC algorithm for interactive applications. All of these methods require additional data preparation; as such they are only applicable where real time visualisation is necessary.

#### **4.6.1.5.1 Volume Rendering**

*Volume rendering* is a computationally expensive procedure, which aims to produce visualisations exhibiting far more information than the more commonly applied isosurfacing methods introduced previously. A comparison of contemporary methods is given by Ebert et al (1994) and examples of its application can be found in Williams (1998) and Shen and Johnson (1994). The process is rarely associated with integration into interactive environments, but is rather more focussed upon producing static high quality images. A recent study by Kniss et al (2001) demonstrated

volume visualization at interactive rates, but relied heavily upon state of the art parallel computers to achieve the results.

## **4.7 Summary**

This chapter has introduced and discussed the fundamental concepts and methodologies applied in current practice to the visualisation of 3D flow field data generally derived from CFD model simulations.

Data sources have been discussed with regard to computational and experimental sources, mesh types and formats. Data originating from medical scanning techniques has also been covered due to its historical influence over certain volume visualisation techniques now universally used for the purposes of CFD visualisation.

The chapter has identified the key numerical methods fundamental to visualisation applications. These primarily concern the processes of point location within unstructured tetrahedral based meshes and the subsequent interpolation required to defined a value at any given point within a data set comprised of finite points as reported by Kenwright and Lane (1996), Ueng et al 1996 and (Lohner 1990). Common interpolative schemes based upon nearest neighbour (Hill Climbing) and spacial interpolation have been introduced and compared.

The growing trend for large 3D data sets to be produced by processes such as CFD as identified by authors such as Rosenblum (1994) and Kenwright has led to a growing area of research into data preparation and optimisation prior to visualisation. The process of mesh decimation has been reviewed with reference to error evaluation and prediction (Cignoni et al 1996). More robust methods have been identified as being concerned with data tree structures as applied by Kuhner et al (2001) and Ueng et al (1997).

Individual visualisation techniques have been defined within the context of the concept of glyph-based visualisation or iconic visualisation. Vectors, streams, contours and isosurfaces have all been defined together with all relevant construction methods. The acclaimed marching cubes algorithm (Lorenson and Cline (1987) isosurface construction method has been discussed and clarified step by step.

The chapter has introduced the concepts and methods necessary to produce high quality visualisations from raw 3D data sets. The graphical nature of visualisation methods has led to close development alongside 3D computational methods such as Virtual Reality (VR). VR as a visual display medium serves many applications. A general introduction to the application of VR technology as a medium within which to visualize, communicate and interpret the information contained in the large data sets produced by CFD simulations is provided in the following chapter.



## CHAPTER 5

### Virtual Reality

#### 5.1 Introduction

Broadly, *Virtual Reality* (VR) may be defined as an immersive 3D environment allowing real time interaction with simulated real world objects (Feiner and Thalmann 2000). Brooks (1999) defines VR as an experience in which the user is effectively immersed in a responsive virtual world, which implies user dynamic control of the viewpoint. There are other types of immersive computer environments as reported by Tamura et al (2001) such as *Augmented* and *Mixed Reality* (AR and MR) which generally superimpose VR onto the real world. For the purposes of this thesis the discussion will be restricted to what has been defined as VR.

VR currently encompasses a branch of visual simulation that has only recently proven itself, largely owing to the huge increases in computing power and corresponding decrease in cost that has been witnessed in recent years.

The relative novelty of VR has led to a flourishing background of active research in various aspects of the area spanning novel applications and the basic technology required to deliver them. Brooks (1999) defines a number of key technologies as being crucial to the development and application of VR;

- The visual (aural and haptic) display that immerse the user in the virtual world and that block out contradictory sensory impressions from the real world.
- The graphics rendering system that generates, at 20 to 30 frames per second, the ever changing images.

- The tracking system that continually reports the position and orientation of the head and limbs of the user.
- The database construction and maintenance system for building and maintaining detailed and realistic models of the virtual world.

These four key technologies together form the basis for a VR system. It is often the case that research is carried out with a focus on one particular constituent technology and the contribution it makes to the whole. The application of VR has found its way into numerous areas such as military, civil, education and entertainment with the latter being perhaps the current driving force behind the technology. As the boundaries imposed by the limits of computing power of the day are constantly pushed back, the depth and number of applications increases at a rate unique for a new technology. As a result of this, the research community is faced with the ongoing task of creating evaluating and evolving new applications constantly.

This chapter will concern itself with the technology and construction methods necessary to build a virtual environment, and provide an evaluation of current applications and summarise key VR related research issues.

## **5.2 History of the *Immersive Environment***

VR as an idea is not the new concept many contemporary publications claim it to be. Sutherland (1965) is widely credited as providing the first formal definition of the immersive environment, what we refer to today as VR;

*Don't think of that thing as a screen, think of it as a window, a window through which one looks into a virtual world. The challenge to computer graphics is to make that virtual world look real, sound real, move and respond to interaction in real time and even feel real.*

Given the computer technology that existed at the time Sutherland's contemporaries would be forgiven for thinking him somewhat optimistic. The original challenge has, however, finally been realised and applied with a significant degree of success. It is not uncommon however for media friendly technologies such as VR to be *hyped* leading to unrealistic expectations and consequent disappointment (RosenBlum et al 1998 and RosenBlum 2000).

Initial VR development was restricted to highly specialised research communities associated with government organisations such as the military or large corporations with equally large budgets who saw the potential for its application in the home entertainment industry alongside the introduction of the first home computers in the late 1970's and early 1980's and consequent development of the now universal desktop metaphor. Military application primarily concerned aircraft simulation where the use of VR offered a safe economic training ground reducing risk exposure for inexperienced pilots. VR only became practical in the early 1990's as affordable and capable desktop computers began to appear (Goebel et al 2001). Goebel defines the success of VR over the last decade as resulting primarily from the following four areas;

- Stable hardware and reasonably priced software that resulted in more powerful and successful VR demonstrations and applications.
- Stable graphics Application Programming Interfaces (API's)
- Continuously increasing performance, allowing larger datasets to be processed in real time.
- Curious researchers exploring for industrial applicability.

The initial interest generated by VR led to numerous studies focussed on areas of the technology such as force feedback interfaces, 3D audio, novel interaction methods etc. However, a lack of customer delivered applications of the technology led to some serious questions being raised about its validity (Rosenblum et al 1998). Recent times has seen a more level headed,

application driven approach to VR development with more authors presenting realistic proposals for the use of VR and what might be achievable in the near future (Prajapati 2000, Robinson and Webster 2001, Shiratubin and Thabet 2001 and Rosenblum and Macedonia 2000).

## **5.3 The Human Interface**

*Human interfacing* is a global term used to describe the various methods a user employs to communicate with a computer and conversely for a computer to communicate with a user. Since VR aims to provide a realistic immersion it is charged with the task of providing maximum sensory feedback through vision, audio and touch. The following sections cover the necessary technologies and methods utilised for this purpose.

### **5.3.1 Colour & Computer Graphics**

Most current active research has used the mid-1960's as a reference point for the development and general advancement of computer graphics since this is when computer displays first found prominence. Early foundation research setting the challenges for the following decades is typified by authors such as Sutherland (1966) who defined ten unsolved problems in Computer Graphics (CG). Foley (2000) is one of several contemporary authors to continue this approach using a *top ten* problem definition within computer graphics. Some of the key problems identified by Foley are creative information display, the display of more pixels and truly immersive VR. The latter two are typical of many problems identified by current authors, which may be solved over time by the provision of more raw computing power, the former refers to a subjective process of using technology in a novel manner to solve current problems. Foley identifies data visualisation as one of the most important areas in recent times given the explosion in computer based information and data storage.

In terms of what is relevant to effective visualisation the discussion of CG is focussed upon the use of colour. Although often considered a trivial issue, the uses of colour in CG features a number of complex issues concerned with how the use of colour can improve information visualisation or conversely substantially impair it. There are clear scientific reasons why certain colours are used for certain visualisations. McDonald (1999) presented a study into the issues dictating the effectiveness of colour in CG in terms of *human perception*. Colour in CG is usually controlled via the RGB interface, differing colours, shades and hues are created by altering the intensity of each of the three channels. Human vision is trichromatic by nature having three distinct classes of photoreceptor. The spectral sensitivity of each photoreceptor differs for each of the three RGB values. It has been shown (Mc Donald 1999) that the relative sensitivity of these receptors RGB follows the ratio 40:20:1. The practical implications of this mean that human vision is far more sensitive to red than it is to blue (Hunt 1998), a fundamental statement which often governs the colour mapping of CFD visualisations where dominant variable values are almost always red and weaker variables blue. This relationship can be illustrated by superimposing the spectral relative sensitivities of the RGB spectrum with the relative sensitivity of human vision to spectrum colours, figure 5.1.

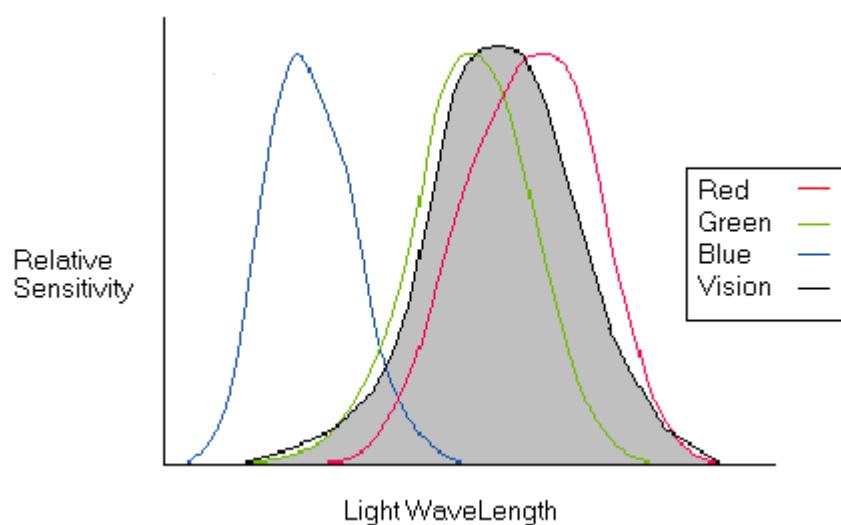


Figure 5.1 Human sensitivity to light spectrum colours

It is also known (Mc Donald 1999) that red wavelengths converge beyond the retina thus in order to perceive them the lens must become convex, conversely the shorter wavelengths of blue and green converge in front of the retina thus requiring a less convex and hence more relaxed lens. Red and blue thus evoke markedly different reactions in the observer. The use of colour for the purposes of complex information visualisation should therefore be considered in light of these relationships rather than be left to chance.

Some colours are detailed in figure 5.2 along with their respective RGB constituents.






	White	R G B
	Blue	R G B
	Yellow	R G B
	Red	R G B
	Green	R G B
	Black	R G B

Figure 5.2 RGB colour control

### 5.3.2 Current Visual Technology

*Human cognition* is suggested as being the primarily orientated around vision (Kosslyn (1994)). It is therefore this type of interface that has received most attention and development. There are two key requirements for a visual interface to provide effective visual feedback; these are depth perception and the accuracy of the field of view. Truly immersive visual interfaces must therefore provide a true stereoscopic view allowing for such factors as eye convergence, parallax motion, perspective correct textures and shading. An approximate specification for an effective field of view can be defined by

consideration of the human field of view, being around 180 degrees horizontal by 110 vertical not allowing for head and eye movement.

To accommodate these factors a number of *Head Mounted Displays* (HMDs) have been introduced such that the perceived display offers total immersion and completely blocks out external influences. The use of these devices has been limited by a number of factors such as low resolution, limited field of view, ergonomic weakness, heavyweight and the associated discomfort caused by sensory confusion (Rosenblum et al 1998). In addition some degree of movement tracking is required with these systems, early efforts created system latency between user movement and image movement of around 500ms, whereas it has been shown in flight simulators that latencies of 50ms are perceptible (Brooks 1999). To counter these effects, a number of large projection based vision systems were introduced throughout the 1990's such as the Cave Automatic Virtual Environment (CAVE) system developed at the University of Illinois, Chicago. A typical projection system consists of three to six large displays orientated in a semi circular fashion around the user providing the illusion of immersion while maintaining a sensory link to the real world thus eliminating the motion sickness associated with HMDs. Typical projection systems provide visual resolution of about 4 minutes of arc compared to human vision which, for perfect vision, is around 1 minute of arc.

For economical VR applications the desktop screen still provides the universal interface. However, a number of factors have been identified that limit the validity of describing such systems as VR (Brooks 1999). These are the inability to block out the real world, the inability to present objects as life size and the consequent inability to present a *true* illusion of immersion. It is however stated by Brooks that such specialist visual systems such as HMDs and CAVE type systems, whilst improving in performance, are still uneconomical if a practical utilisation of VR is required. Desktop VR currently presents the most realistic medium for the creation of any application driven VR project. DeLeon and Berry (2000) created a series of

interactive *virtual museums* based upon the desktop display with a high degree of success in terms of user experience.

### **5.3.3 Haptic and Audio Feedback**

The provision of haptic (touch & motion) feedback will probably complete the total VR immersive experience, the complexities of such a task have prohibited any practical applications to date but active research is ongoing. Haptic interfaces have however been developed for use in medical applications (Bardorfer et al 2001) for the purposes of measuring movement but the technology is still in its infancy.

Audio feedback is simpler to implement requiring technology of no more complexity as that of graphics. In the past VR has however tended to concentrate upon unimodal systems offering interactive vision only. Modern technology has been applied to this problem resulting in the provision of 3D soundscapes within virtual worlds. It has been shown (Larsson et al 2001; Lombard and Ditton 1997) that the provision of sound within a VR world greatly increases the users sense of *presence*.

## **5.4 3D Environment Building**

The success of virtual environments depends to a great extent upon the accuracy and realism of those models and objects contained within it. Although the last decade has seen considerable improvements to the methods used to create such models the process of building is still a highly involved process and considered generally as a *major task* (Brooks 1999). The methodology, whilst containing a number of steps is however reasonably straightforward comprising a number of issues which will be discussed in the following sections.



#### 5.4.1 Concept of Primitives: The *Top-Down* Approach

The requirements of virtual environments for realistic models to be created accurately and efficiently has led to the production of universal software based object creation applications such as 3D Studio MAX™ from Kinetix. These applications follow a universal object creation procedure based upon the premise that most complex geometric entities can be created by the Boolean addition and subtraction of a number of fundamental volumetric objects known as *primitives*, illustrated in figure 5.3.

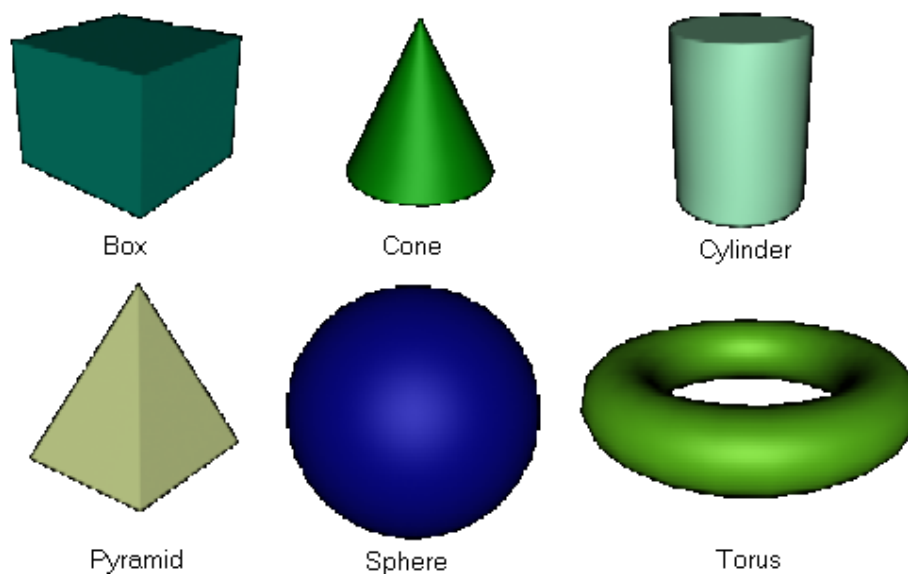


Figure 5.3 Primary primitive entities used in conventional 3D modelling

These primitives form the basis by which objects of much greater complexity can be formed. The primitives form a basic topology that can be adjusted via length, height, width, radius etc such that almost any shape or curvature can be formed by combining them in a specific manner. The approach of Boolean interaction between primitives by starting with a single volume and progressively subtracting primitives to create curves and planes is often referred to as *top down* modelling and provides an extremely efficient method of model construction.

### 5.4.2 WireFrames, Faces & Volumes

3D modelling software creates simple objects like the primitives described in the previous section based upon the formation of a number of polygons, or faces, which together form the volume. These polygons are defined by an underlying entity within the volume referred to as a wireframe and comprise of a number of constituent co-planar points upon which is built a surface. The wireframe can be thought of as the most basic constituent element of a 3D model being the skeleton defining the basic topology of the object. If a simple primitive such as the regular box is considered the basic wireframe structure would take the form of that illustrated in figure 5.4, comprising six wireframe quadrilaterals. In accordance with the structure of the wireframe six polygons would attach themselves to the wireframe creating the 3D solid object. Since a regular box contains no curves a bare minimum of faces is required to produce the required appearance.

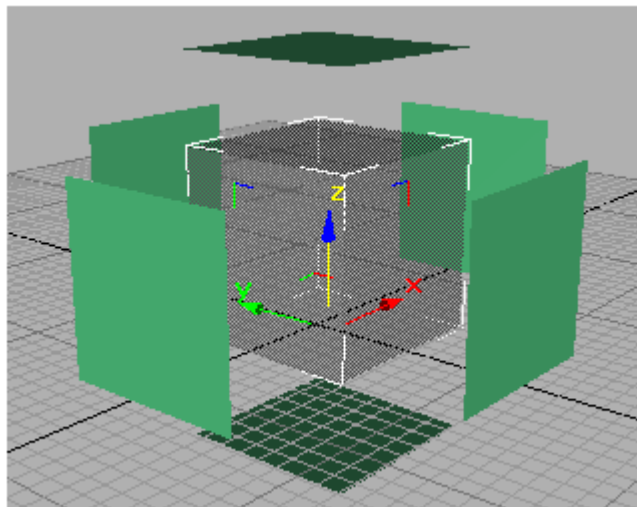


Figure 5.4 Primitive wireframe representation of a box

A more complex object such as the cylinder introduces the need for curves. Curves are not strictly defined as a true arc in 3D modelling, they are approximated by a number of straight line segments in the wireframe, hence the greater the number the more accurate the appearance of the curve. Figure 5.5 illustrates the principle.

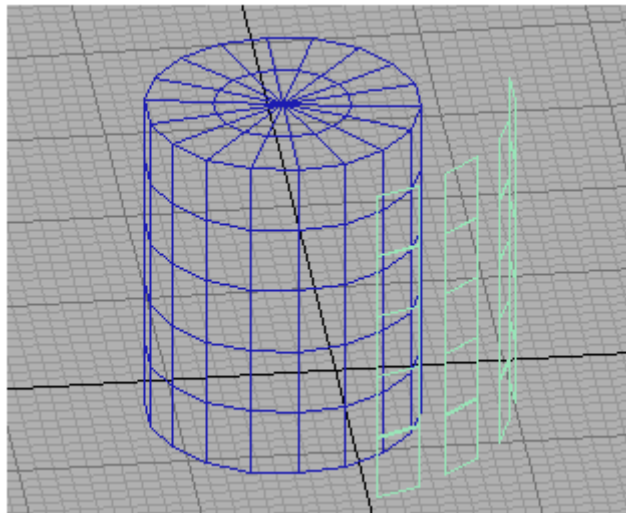


Figure 5.5 Approximated curve using line segments on a cylinder

### 5.4.3 Object Optimisation

Since 3D models are comprised of hundreds or thousands of polygons, most of which are spent approximating curves, if the model is to be rendered in real time allowing interactivity the number of polygons must be kept to a minimum thus easing the pressure on the rendering hardware.

The process used to reduce complex 3D model geometries is generally referred to as *polygonal simplification* or *optimisation*. The aim of such a procedure is to reduce the number of constituent polygons within a model such that the visual appearance maintains a satisfactory degree of realism whilst the polygon count is low enough such that the graphics rendering hardware is able to update the 3D scene at a rate consistent with perceived realtime, approximately 20-30 Frames Per Second (FPS). The process first found prominence as early as the 1970's when Clark (1976) stated the benefits of displaying graphical models at varying resolutions. Commercial and military flight simulators have also used such processes to create multi resolution aircraft models since their introduction in the 1970's (Cosman and Schumacker 1981).

Luebke (1997) presented a recent overview of some of the common recent approaches to model optimisation identifying three main approaches as;

- Augmenting the raw polygonal data to convey more visual detail per polygon.
- Using information about the model to cull large portions of the model that are obscured from view.
- Polygonal simplification methods directly reducing the number of polygons in a model.

Luebke identifies the four main approaches to polygonal simplification as, *sampling*, *adaptive sub-division*, *decimation* and *vertex merging*. *Sampling* concerns an approximation to the original model, built by taking a sample of points on the surfaces of the model in question. The simplified model is then constructed around these points using the number of sample points as a control variable. *Adaptive sub-division* involves the creation of a simple base model that is subjected to incremental division until a model within a prescribed tolerance is achieved. Adaptive sub-division often fails to capture complex details within a model and should therefore be applied to models incorporating simple surfaces (Hoppe 1996). *Decimation* is analogous to the process used to refine CFD data sets introduced in Chapter 5, a process of removing vertices and re-triangulating the resulting hole. Finally, *vertex merging* involves the merging of two or more vertices such that the associated faces can be represented by a single face thus reducing the overall polygon count. Luebke (2001) presents a thorough evaluation and decision tree specifying a number of different simplification algorithms suitable for certain types of model from curve rich organic models to sharp edged mechanical models. Whatever the method, the resulting model should consist of fewer polygons, this is particularly useful in the context of perspective detailing (figure 5.6).

Commercial software applications such as 3D Studio Max™ from Kinetix incorporate polygonal optimisation based upon edge and/or face collapse. A

user-defined threshold is used to identify which entities to *collapse*; these are then replaced by larger polygons.

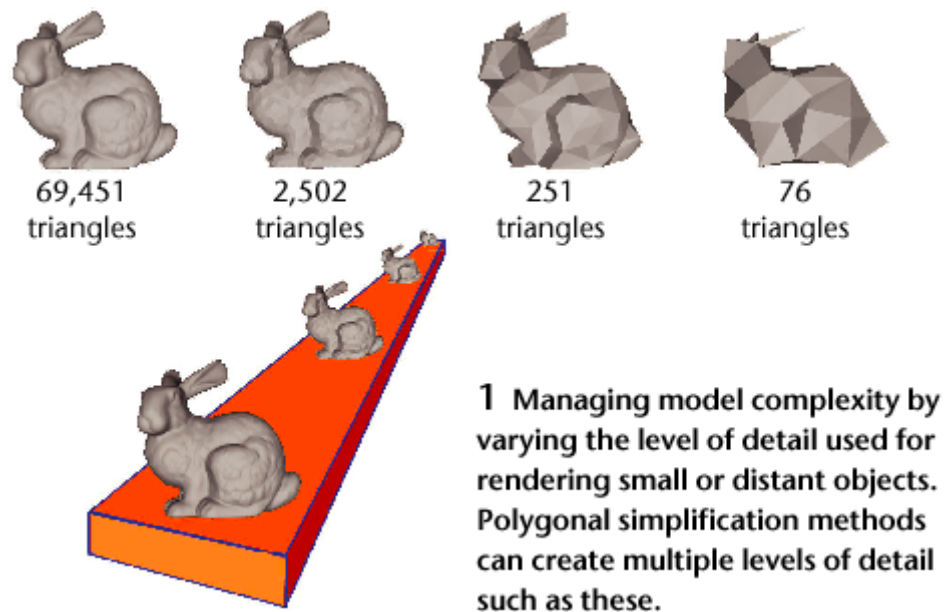


Figure 5.6 Example of polygonal mesh simplification (Luebke 2001)

#### 5.4.4 Realism; Textures and Surface Maps

There are a number of techniques that have been developed in order to give a 3D model the appearance of more detail and *realism*. The most prominent and widely used method is referred to as *texture mapping*. *Texture mapping* enables simple objects to attain a degree of realism beyond what might be thought possible with a low polygon count. Applying a texture to an object involves the simple mapping of an image onto the faces of that object. The image typically consists of surface detail relating to the object as it is in the real world. An example of a texture applied to an object would be that of a brick wall, the underlying object is thus allowed to be constructed with an absolute minimum of complexity whilst the texture applied to the surface faces creates the illusion of detail. The illusion of depth due to irregular surfaces is likewise given by the colour gradation of the texture. Other examples include grass, woodgrain and metal, figure 5.7.

The process of mapping a texture image onto an object is dictated by the underlying mesh defining the construction of that object, the alignment of faces and the mapping method defined by the user. Mapping methods vary but primarily concern how the image is wrapped around the volume of the object.



Figure 5.7 Bitmaps used for texture mapping

3DStudio Max™ uses a number of texture wrapping techniques including *face*, *planar* and *sphere wrapping*. The method chosen is purely determined by the required appearance of the model. The final appearance and orientation of the texture is also influenced by the face topology of the object. For example, for a surface comprising a repetitive pattern such as metallic surfaces, the face wrapping method would *tile* a metallic texture on every face of the object. The lower the number of faces the lower the resolution of the texture. *Tiling* is therefore an efficient method for the creation of realistic surfaces using small repeated images.

#### 5.4.5 Light Sources and Shading

A key component contributing to the realism of a rendered 3D environment is the realistic interaction of environment objects with a source of light. In the real world light provides a sense of perspective through shadowing and shade. Light sources within a 3D world must vary according to the environment being constructed. Variables associated with light sources within the 3D world control factors such as light intensity and distribution. Aside from the general ambient lighting there are three main types of light source used in the construction of 3D environments. The first is the point light source which corresponds to a single point source in space from which light is emitted radially in all directions sometimes referred to as an omnidirectional light source. An unshielded light bulb would be the real world equivalent.

The second is analogous to natural sunlight and is often referred to as a sunlight system or infinite light source. This light system requires a definition of the direction of the emitted light.

The final type of light source falls somewhere between the latter two and is referred to as a spot light source defining both point source and direction of emitted light and being analogous to a real world shielded spot lamp. Figure 5.8 illustrates the three aforementioned lightsources.

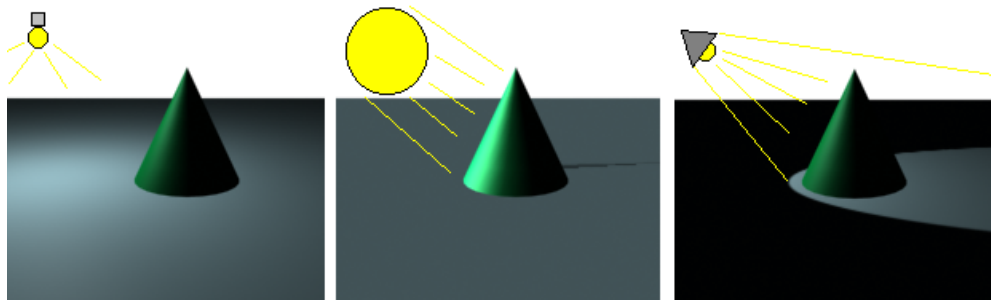


Figure 5.8 Point light (left), Sunlight (centre) and Spot light (right) sources

Techniques for shading also play a great role in controlling the realism and efficiency of rendered 3D objects. The basic shading technique is known as *flat shading* and comprises the simple application of a uniform colour to each face of the object governed by its orientation in relation to the light source. This is considered to be the crudest form of shading and least hardware intensive. Increasingly advanced methods such as *Gouraud* or *Phong* shading produce a much more realistic rendering of an object by providing a gradated colouring across the faces of the object, these are referred to as 'smooth' shading methods and are associated with higher computational costs, figure 5.9.

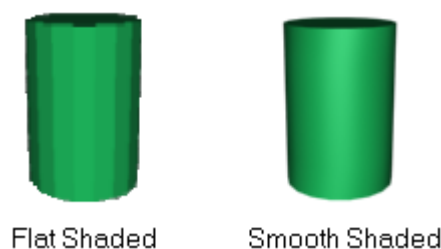


Figure 5.9 Examples of flat (left) & smooth (right) shading

## 5.5 3D Formats and Standards

The flourishing world of 3D modelling over the last decade has led to the creation of a large number of dedicated modelling applications. This in itself has spawned an active industry dedicated to producing efficient and accurate conversion utilities. Whilst the number of formats is large there are a few which have emerged as international standards over recent years, the most important and established formats for the storage of 3D models will be covered in the following sections.

### 5.5.1 Virtual Reality Modelling Language (VRML)

The *Virtual Reality Modelling Language* (VRML) was developed during 1994-95 by a community of 3D computer graphics professionals as a method of extending the text capabilities of the newly emerging *World Wide Web* (WWW), or internet, to the display of interactive 3D environments. Although introduced relatively recently, in the world of web-based computer graphics VRML is perhaps one of the pioneering formats for the network transport of complex 3D objects over the internet. In 1997 an updated version of VRML, VRML97, became an ISO standard (ISO/IEC 14772) and despite the introduction of numerous other more advanced formats remains a universal standard owing largely to its intuitive structure and flexibility. Today, VRML is used extensively for the purposes of internet marketing, engineering demonstration, architecture, entertainment and visualisation (Nadeau 1999).

VRML is a text-based format allowing the construction of 3D worlds containing a number of primitives, sounds, textures and simple levels of interactivity. Its primary display is through universal web browsers such as the Microsoft Internet Explorer™ and Netscape Navigator™ range using freely available plugins such as Cosmoplayer™ from Cosmoworlds. The browser serves as an interpreter for the VRML file providing a user interface and displaying the world. The VRML file itself is identified by its file



extension, *wrl*, an abbreviation of *world*. The intuitive design of the structure of a VRML file can be demonstrated by opening a simple VRML file in a text editor, figure 5.10 illustrates the VRML file for a simple box geometry.

```
#VRML V2.0 utf8

# Comments go here!
# A simple VRML BOX file

DEF Box01 Transform {
  translation -23.38 0 0
  children [
    Transform {
      translation 0 35 0
      children [
        Shape {
          appearance Appearance {
            material Material {
              diffuseColor 0.651 0.898 0.898
            }
          }
          geometry Box { size 70 70 70 }
        }
      ]
    }
  ]
}
```




Figure 5.10 VRML '97 text format for primitive box object

The first line is referred to as the *header*, which informs the browser or other application what format the file is in (this is the same for all VRML97 files). The comment lines are followed by the actual description of the scene. The scene is constructed using a number of *nodes*. These nodes represent different aspects of the environment. For example, some common geometry nodes include box, cone, sphere, indexed face set, indexed line set and point set. Other nodes include, appearance (*texture*, *lighting*, *transparency* etc), *animation* (colour, position etc) and *interaction* (proximity sensor, touch sensor etc). There are a total of 54 basic nodes, a full listing can be found in Wernecke (1996) and Appendix II.

Despite being extremely simple at its fundamental level VRML is a highly capable 3D programming language capable of building realistic 3D scenes using the image based surface texturing techniques described in the previous section. Recent examples include the use of VRML to create 'virtual

campuses' for university promotional purposes and interactive mapping (Jin and Wen 2001), Figure 5.11.



Figure 5.11 The 'Virtual University' (Jin and Wen 2001)

Other VRML based projects have included media presentation and weather reporting (Lawton 1999) and scientific applications such as magnetic field visualisation (Bartsch et al 2001).

VRML is now considered obsolete in terms of new application development being superseded by the X3D syntax, which is commonly described as the next generation open standard for 3D on the web. The accepted specification as published by the Web 3D Consortium of X3D is as follows:

- Compatibility with existing VRML content, browsers, and tools.
- Extension mechanism to permit introduction of new features, quick review of advancements, and formal adoption of these extensions into the specification.
- Small, simple "core" profile for widest-possible adoption of X3D support, both importing and exporting.
- Larger, full-VRML profile to support existing rich content.
- Support for other encodings including XML for tight integration with Web technologies and tools.

- Architecture and process to advance the specification and technology rapidly

At its heart, X3D and its syntax XML works upon an extensible principle thus allowing application developers to incorporate the required components of the specification rather than the entirety as with VRML. It is this flexibility, which has allowed the X3D specification to widen its use in media related application development.

Despite the obvious advantages of X3D from the point of view of an application, VRML remains a widely used format in its ISO standard form for specialised applications, such as those developed for the purposes of academic research where the compatibility requirements associated with marketed applications are largely irrelevant. It is also the case that developments on the leading edge of 3D format research take time to filter through to downstream users hence the continued application of VRML by users outside the specialised 3D development community.

### **5.5.2 CAD Based Formats: IGES and DXF**

The proliferation of the use of CAD from the 1970's onwards led to the requirement of an interchange format such that data representing a mathematical description of a 2D or 3D drawing could be exchanged between applications and systems. An *Initial Graphics Exchange Specification* (IGES) was developed in the late 1970's through the collaboration of a number of competing vendors as the result of demands from the user engineering community. The IGES format describes an object through classification of geometric and non-geometric entities and is based upon the text format thus allowing universal transfer across previously incompatible systems. It is primarily used today for the interchange of engineering drawings.

The DXF format was popularised by the AutoCad™ suite of engineering drawing applications from AutoDesk. Like IGES, it stores the mathematical information necessary to reconstruct an engineering drawing in the text format allowing inter-system transfer. It may also be stored in a binary form. Both IGES and DXF are used extensively for the purposes of engineering technical drawing.

### **5.5.3 Direct X™**

Direct X™ was developed by Microsoft and released in 1995 as a component of the Windows operating system. It is essentially a suite of Application Programming Interfaces (APIs) allowing the developer to access hardware features directly. These APIs allow direct communication between software applications and hardware components such as high performance 3D graphics cards, sound cards or input control components such as joysticks or computer mice.

It is currently accepted in the application developer's community as the standard for media rich application development, based around the Windows operating system that currently holds a dominant market position. The majority of available 3D acceleration graphics hardware is Direct X™ compatible and most 3D related media applications, including VRML/X3D browsers, support the technology.

## **5.6 Applied Virtual Reality**

Over the last decade VR has been applied to a wider range of applications than ever before resulting in the publication many studies relating to a wide range of disciplines both academic and industrial. The following sections provide a summary of those application areas of most significance to the subject of the thesis.

### 5.6.1 Education & Industrial Training

One of the key areas that VR has been applied with measurable success is within that of education field, spanning from elementary school to specific procedural training within hazardous industrial environments.

Johnson et al (2002) published a report from studies relating to the introduction of a prototype-learning environment for elementary age group school students. The VR system re-created a number of external environments for the purposes of allowing students to conduct scientific experiments and measure natural phenomena that would have otherwise been impossible, dangerous or uneconomical. The project was intended to augment traditional learning techniques rather than replace them. The authors found that using VR greatly assisted the teachers in that it provided them with a higher degree of control over the learning environment. Distractions could be eliminated and the *virtual experiments* designed specifically to communicate scientific phenomena clearly without the ambiguity often found in field studies. Although only qualitative assessments were made on the experiences of the students, all were positive, leading to improvements on the expectations of the teachers when the students finally conducted the same experiments in the real world.

Noor and Wasfy (2001) took a similar approach using VR to simulate real world physical experiments concerning wind tunnel testing and structural testing for aerospace systems. The virtual environment reflected a high specification immersive system comprising back projected surround screens, head tracking input devices and surround verbal input capabilities. To construct the environment an object orientated VR toolkit, IVRESS, was used to enable the definition of object properties and event handling routines. The resulting environment consisted of a number of *virtual laboratories* within which users could interactively conduct experiments in a risk free environment. Noor also states that some integration with FEA and CFD is used to provide results for various aspects of the virtual laboratory such as structural testing and wind tunnel aerodynamics. No detailed

specification of the CFD or FEA parameters was included in the report. Since real time CFD or FEA analysis for complex 3D systems is beyond the realms of modern computing it must be assumed that the models represented within the virtual laboratories were extremely simple representations.

Tam et al (1998) produced an early desktop-based VR system for the purposes of operator training in the electric power utility industry. The application, ESCOPE-VR, differed to many of the time being budget desktop based as opposed to relying upon high cost dedicated workstations. It was found that the high cost associated with specialised workstation machines prohibited the commercialisation of the software completely. The hardware used was thus a standard *off the shelf* 60Mhz Pentium™ class, rendering a 3D model containing 8175 polygons. Although slow by present standards, specification of hardware provides a useful indicator of progress. The VR training application focussed upon the familiarisation with procedural tasks, which have been identified as being particularly suitable for VR training methods. The application included a 3D model of a power station, 3D sound immersion, verbal input via speech recognition and an interactive help system. The application was developed through a Virtual Environment (VE) toolkit (MIRAGE), which was essentially a software application that provided all the necessary tools for a user to construct a VR training environment. By developing a specialised toolkit the authors greatly eased the production and development of the application. The interaction of the user within ESCOPE-VR was based upon what the authors describe as a *major loop* assessing user input and making the necessary amendments to the environment.

In a follow investigation, Tam et al (1999) produced a similar VR *learn by doing* training system (SEDA-VRML) for the maintenance and trouble shooting of industrial power systems. The trainee was required to undertake virtual inspections of power equipment. This application was built around the web based VR system of VRML and the Java programming language with the intent of increasing accessibility beyond high-end workstations. It

was found that the application functioned well via the internet and local intranet systems using a Pentium™ class 75 MHz PC. The main aim of the application was to demonstrate the potential for VRML web based VR training systems as a lower cost alternative, in this respect the application proved the technology of the day perfectly capable of delivering such applications.

McClaren et al (1995) reported on studies relating to the application of VR methods to aid risk assessment in the subsurface mining industry. The studies proposed the use of real time risk analysis algorithms at each point in the simulation considering a number of variables and providing a quantitative estimate of risk exposure to the user. Procedural operations simulated within the virtual environment concerned the use of Free Steered Vehicles (FSVs) for the purposes of materials and equipment transport underground. The simulation used Computer Generated Individuals (CGIs) to represent personnel interacting with the position of the FSVs through a finite number of decisions available to them. The degree of risk was evaluated and visualized by the use of two risk regions surrounding the FSV, one representing high risk, the other representing medium risk. The trainee could therefore operate the FSV and interact with a number of CGIs who were able to react in a number of different ways to the actions of the trainee. The simulation was therefore able to demonstrate to the trainee how risk can be minimised and how dangerous situations develop in relation to their own actions. The hardware used was based on a 486 DX (pre-Pentium™) computer architecture. Further related studies by Denby et al (1998) and Squelch (1998) continued the successful application of similar VR methods to hazard awareness training in the mining sector using a virtual reality toolkit *SAFE-VR™* developed exclusively for the construction of hazard awareness related virtual reality based training environments.

### 5.6.2 Scientific Data & Information Visualisation

As a result of the ever increasing size of volumetric data sets and advances in data gathering technology the intuitive interface that VR can provide has seen application to the visualisation of complex data and information. Early studies by authors such as Stone et al (1994) and Ribarsky et al (1994) had identified the potential for VR to assist data visualisation stating the intuitive manipulation of data by human operators as the key to its future success. Since then a number of applications have been produced some of which will now be discussed.

Sarathay et al (2000) developed a prototype VR based visualisation tool for the visualisation of multi gigabyte data sets produced by FEA and CFD codes in a manner open to the non expert user. A combination of advanced data mining and feature extraction techniques were employed within the system such that the user would be presented with only the most relevant features characterised within the data set. User navigation was achieved via a simple *fly through* method where the user could explore the data set internally with no restrictions on movement planes. Disorientation where physical model references were absent was a significant problem. The work of Sarathay et al was conducted with the aim of demonstrating to the engineer the transfer and manipulation of standard engineering data in a VR world, to demonstrate the effects of design and changes and finally to evaluate the effectiveness of such a system in terms of aiding engineering analysis.

Russ and Wetherelt (1999) used VRML to construct a VR interactive representation of a large sub-surface mine network comprising a complete and accurate mapping of all tunnels and link roadways. The objective of the study was to explore the possibility that the interpretation and mapping of complex mine networks, inherently 3D, could be made significantly easier through the use of interactive 3D maps based upon VRML as opposed to the traditional storage of 3D mine networks plans on 2D maps. A case study, based upon the South Crofty Mine in Cornwall (closed in March 1998), was



considered using data from electronic surveys, paper maps and other reports. It was estimated that the total mileage of all tunnels and workings would come close to 200 miles. The model, at the time of publication, occupied 17 Mbytes of computer memory and in order to allow real time exploration detail levels had to be reduced considerably. The initial models, as expected, provided a fully spatial appreciation of the mine layout. Specific regions could be identified quickly and easily in the context of the local tunnels and the mine as a whole. Although Russ and Wetherelt experienced significant *teething* troubles these were mainly symptomatic of inadequate computing power which, given the rate of development, rarely proves to be a permanent obstacle.

Schultz et al (1998) produced a VR post processing environment designed to address the deficiencies of traditional FEA and CFD post-processors using car body dynamics as a case study. Schultz found that at a large automotive manufacturer (BMW) it was typical for engineering computational simulation time to be divided as 30% pre-processing, 10% solving and 60% post-processing or data analysis thus identifying a strong incentive to provide more efficient data analysis tools for the engineers. The structure of the system is illustrated in figure 5.12.

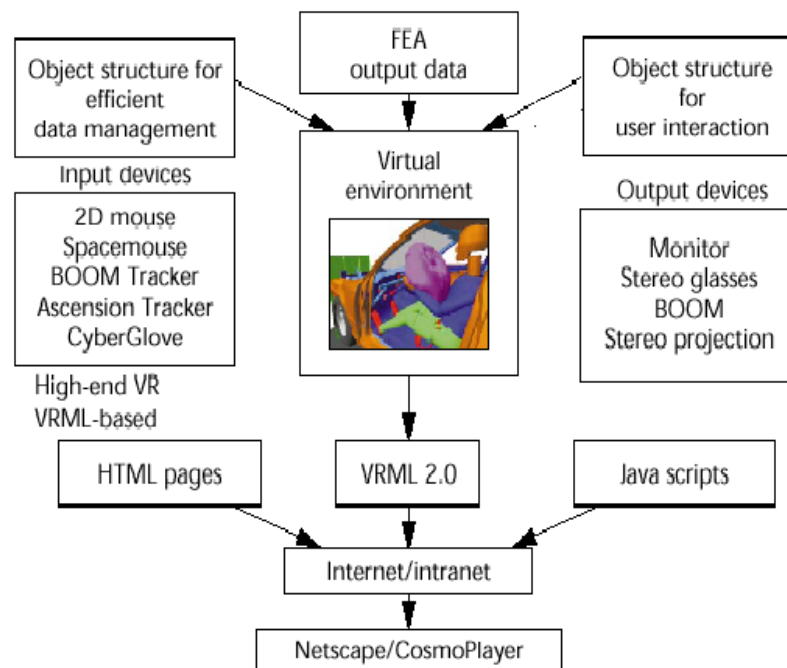


Figure 5.12 Schultz's virtual environment for FEA data analysis (Schultz et al 1998)

Since large time dependent data sets in the order of 20-25 million cells were the subject of the visualisation system Schultz used data reduction algorithms to produce optimisations of around 50% allowing the maintenance of a minimum 10Fps to preserve interactivity. FE data was loaded into the environment and visualisations were calculated in real time at the request of the user who also controlled all visualisation parameters. Although the system relied upon high-end graphics workstations the option of VRML output allowed widespread network communication through web browsers.

Svidt et al (2001) presented a similar environment for the visualisation of pre-solved CFD results data within a VR environment, the application was the ventilation of a livestock building. A six sided CAVE type projection system was implemented for the display of the VR environment, the data originated from the commercial CFD code FLUENT™ V5 simulating both airflow and CO<sub>2</sub> concentrations within the building. 2D contour planes and vectors were used to represent the flow variables. Although interaction was limited to the simple display of 3D results the use of VR technology was found to greatly assist the communication of results to non-expert audiences.

Walsha (1999) produced a VR based application for the simulation of mine fires and display of simulation data within a virtual mine. Walsha used cell based ventilation network analysis data as opposed to CFD data owing to practical limitations. At the time of publication, and presently, the modelling of a complete mine network considering airflow, thermodynamic properties and gas diffusion is well beyond the realms of available hardware. Walsha did however demonstrate the potential of this type of integration with a small test application concerning an enclosed ventilated room. The modular network modelling routines were capable of simulating a range of fire related scenarios such as open fires, strata fires, methane explosions and ignition. The simulation data was displayed within a virtual representation of

the mine network via various icons denoting airflow, temperature and relative gas concentrations.

### 5.6.3 Discussion

It has been shown that VR has been applied successfully to a number of educational and training applications using a variety of methods and technologies. This in itself dictates that VR cannot be exclusively defined in terms of a single piece of technology such as surround CAVE projections, HMD's or simple desktop screens. Most authors covered in this review have all defined VR in their own terms, although there is general agreement concerning the limited sense of presence associated with desktop systems. Desktop based VR has however been shown to demonstrate great potential for the purposes of industrial training (McClaren et al 1995 and Tam et al 1998) beyond the financial economics of the more technically advanced systems (Noor and Wasfy 2001). For economic industrial application driven research the current candidate must therefore be desktop based if any chance of commercialisation is to be realised.

Although most publications reported positive *qualitative results* from the studies it is difficult to measure the success of these VR training applications in an accurate quantitative manner. Most studies presented the VR applications as prototypes, therefore reducing the need for any formal product evaluation and relying upon experience based opinions to base performance judgement. Since the application of VR technology is still in its early stages this is to be expected. The VR applications surveyed all demonstrated the potential for VR to be used extensively within the industrial training *learn by doing* environment. There is little to dispute that real world experience is the best method of learning hence any system that approximates to that whilst reducing or eliminating the disadvantages such as risk, cost and lack of absolute control offers significant gains for the purposes of training. Where VR applications offer additional advantages have been well demonstrated by the work of McClaren et al (1995), Denby et al (1998) and Squelch (1998) where a simple VR recreation of real

world situations and decision making within the mining industry has enhanced the learning experience of the trainee, via the incorporation of active risk assessment and risk visualisation methodologies not hitherto demonstrated within real world training systems.

In terms of data visualisation, the majority of the applications considered here demonstrate a unified approach to the problem of large data set visualisation by tackling the individual problems associated with this task. A recurrent theme of many studies (Schultz et al 1998 and Sarathay et al 2000) is that of the level of data optimisation and feature extraction required to enable an immersed human observer to make any sense of the data displayed. With data sets produced by FE codes regularly outputting multimillion point data sets, any attempt to construct such an environment should therefore pay due attention to identifying, extracting and displaying those segments of data which exhibit distinctive qualities and thus communicate specific characteristics of the data set as a whole.

Effective and efficient VR visualisation should be distinguished from simple 3D post-processing. Studies typified by Svidt et al (2001) demonstrate how the usual functions of a CFD post processor can be extended by the simple addition of a navigable 3D display. Defining this as VR is questionable. Although this may allow the user complete freedom of real time movement, allowing the viewing of a 3D model to be a lot less tedious, the ambitions associated with VR as a concept go beyond this rather simplistic approach. At the very least, a VR based data visualisation system needs to create the link between the scientific data displayed and the associated consequences within the real world. At its most simple level this is achieved by simply placing the data in context through the addition of a realistic 3D representation of the physical environment. Data displayed independently of its defining physical boundaries makes little or no sense with no *a priori* knowledge. Therefore, to extend complex data visualisation to a wider audience the visualised data defined as an *effect* should be associated with a *cause* manifested via the physical characteristics of the real world. It is this factor, which should separate what could be considered as an *advanced post*

*processor* and an interactive VR data display system. Walsh (1999) demonstrated this by incorporating scientific data display into a VR mine where scientific variables were given greater meaning and relevance through direct representation in the appropriate environment.

It has also been shown that VRML continues to provide a foundation for both distributed network VR based training applications (Tam et al 1999) and more prominently as a primary and secondary format for the visualisation of complex geometric data (Russ and Wetherelt 1999) and FE based scientific data (Schultz et al 1998).

## 5.7 Evaluation of VR

A number of studies have, in recent times, attempted to demonstrate the effectiveness of VR for training applications through consideration of a number of psychological issues and experimental comparisons.

The term *presence* is used extensively in such studies as a psychological construct used to describe the feeling a user has of actually *being there* to various degrees. Mowafy (1993) presented the results of a psychological evaluation of three differing types of visualisation media used for the integration of complex spatial information into a mental model. These were orthographic 2D representation, fixed 3D rendering and real time virtual format. The application concerned the extrapolation of critical information from 2D Head Up Displays (HUDs) used by fighter pilots, an example of AR. The results were reported as having *substantial differences*. It was suggested these differences were directly related to the level of *presence* experienced by the trainees using different methods.

*Knowledge retention* is another term widely used when considering the effectiveness of VR training in terms of psychology and memory functions. Since the purpose of training is very much concerned with the amount of information that is recalled and applied correctly in the real world, the

evaluation of the degree of knowledge retention is a valuable assessment of the impact of VR methods upon human subjects. Hall et al (1998) reported on an experiment similar to that of Mowafy incorporating two methods of information display, one 2D, the other fully immersive 3D VR. The objective of the experiment was to attempt to measure knowledge retention as a function of the particular training method. The case study involved the operation of machinery and devices. It was found that after allotted practice times the VR group demonstrated a much greater ability to perform the tasks in the real world than the 2D group suggesting greater immediate knowledge retention. However, since the VR study was based around a technically advanced fully immersive system involving HMDs, trackers and VR gloves the participants expended greater effort in familiarisation with the various interfaces than the training itself.

A study by Boud et al (1999) used experimental comparison to assess the suitability of VR and AR as a training method for specific tasks primarily involving spatial awareness such as assembly tasks. Boud's study concerned the eight-stage assembly of a water pump and compared a greater number of VR, AR, 2D and combination methods than previous studies. These were, conventional 2D drawings, desktop VR, desktop VR with stereo 3D glasses, immersive VR using HMD, and finally, context free AR. The results considering eventual time taken to complete the task in reality are illustrated in figure 5.13.

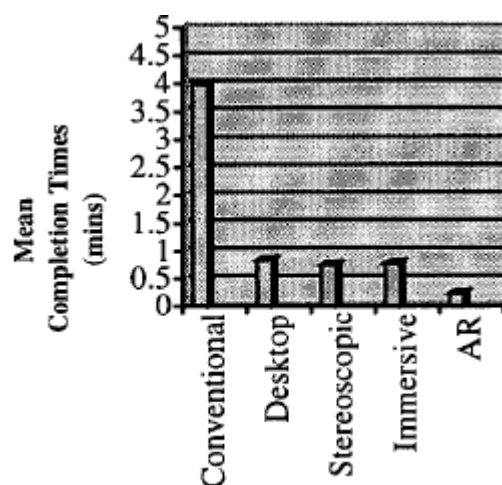


Figure 5.13 Task completion times based on alternative VR formats (Boud et al 1999)

Although it is clear that the conventional method is significantly outperformed by all VR related methods the initial suggestion points toward AR as being the most effective technique for these tasks. Upon questioning the users cited poor responsiveness and clumsy interfacing as a major problem for the immersive VR technologies. Again, therefore, familiarisation with the training technology is shown to severely impede application effectiveness.

Much has been made of the evaluation of VR directly, Philbin et al (1998) took the approach of evaluating task appropriateness for VR training as an initial step prior to any assessment of VR methods applied to that task underlining the principle that VR methods are suitable for a specific range of tasks rather than as an all encompassing solution to all training problems. Philbin states that 'VE's alone will never fulfil the training needs for every task'.

Task appropriateness as defined by Philbin appears to have figured in most published VR evaluations since all focus their efforts upon tasks involving spatial awareness typified by procedural tasks undertaken in the manufacturing industry. Wittenburg (1995) presented another such evaluation concerning a manufacturing process the results of which are summarised in figure 5.14. The process itself concerned the operation of a machine divided into four procedures, set-up, start-up, running and shutdown.

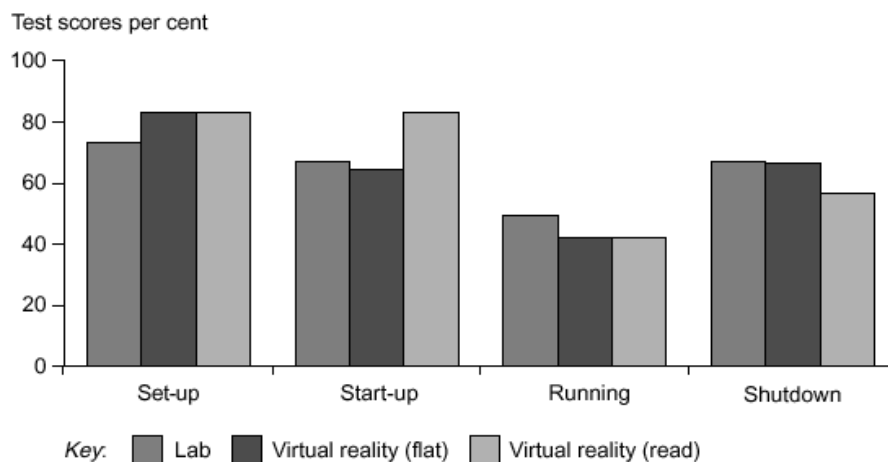


Figure 5.14 Comparisons of alternative learning techniques (Wittenburg 1995)

Compared to Boud et al (1999) Wittenburg's results are much less decisive. The experiment was conducted based upon 486DX 66Mhz computers using flat screen (desktop) and HMD based displays running at 10 fps in addition to the conventional lab training using a total of 21 participants.

Most studies considered so far have concentrated upon the effectiveness of recreating real world procedures in a purely visual manner. Duffy (1999) evaluated the ability of a VR based training application, incorporating risk adaptive sound, to influence the users *perception of risk* whilst undertaking a procedural Computer Aided Manufacture (CAM) machining task. Real exposure to risk is of course impossible within the virtual world hence it is difficult to simulate risk effectively. Duffy used accurate sound levels associated with high-risk scenarios such as tool breakage to emphasise risk levels within the VR training application. The results of the study were qualitative but indicated that simulation of high-risk scenarios incorporating appropriate sound improved decision making. The study was based upon 24 participants.

Evaluation is a specialised issue in terms of the assessment of VR for purposes of training in all areas. It represents an individual research subject in its own right as exemplified by the authors detailed above. Since the continued success of the application of VR to training in industrial environments depends very much upon past evaluations much of current research in the area has focussed upon structured evaluation such that VR training applications can be accurately compared to other, more traditional, training techniques. D'Cruz (1997) highlighted the need for a regulated evaluation process focussing upon such relevant factors as audience specification, user abilities and management issues such as resource availability in the form of time, money, people and equipment. Proper evaluation in this context therefore goes beyond the scope of this thesis, however the issues raised are relevant to the design and specification of the application.



## 5.8 Summary

This chapter has reviewed the current position and capability of available hardware to deliver authentic VR based simulations of real world events specifically for the purposes of worker training.

The chapter has summarised all relevant methods necessary to construct, optimise and interact with a virtual world from scratch using methods most proven within the VR research and applications industry. Attention has been paid to polygonal simplification methods, essential if the critical frame rate range is to be maintained at interactive levels (20-30 fps). Realism has also been introduced with respect to light sourcing, shading and conventional texture mapping.

The rate at which VR based technology progresses is unique amongst scientific areas and renders such a summary or review as being highly temporary in nature. Studies reviewed in this chapter separated by a few years (DeLeon and Berry 2000 and Tam et al 1998) appear to have advanced disproportionately. Most of the advances are however concerned purely with ergonomics and realism. The underlying applications and concepts advance at a much more sedate rate.

Evaluation has been covered with reference to a number of studies, some considering psychological effectiveness such as levels of *presence* and *knowledge retention* (Mowafy 1993 and Hall et al 1998), others performed evaluations based upon structured experiments (Wittenburg 1995 and Boud et al 1999). Results indicate a general positive trend towards the acceptance and adoption of VR as a more effective training format. However, it is often the case that the low number of experimental participants may adversely influence the results and any conclusions based upon them. Evaluation has been shown to be a separate discipline from the design and construction of such applications requiring a focussed and structured approach.

VR has been generally demonstrated to perform well for procedural tasks with a high number of successful applications within the mining industry (McClarenon et al 1995, Denby et al 1998, Squelch 1998, Walsha 1999 and Russ and Wetherelt 1999).

The Chapter has provided the technical background of VR alongside a summary of recent applications and, importantly, a survey of recent structured evaluations. The combined consideration of all the areas introduced within the Chapter serves to indicate that VR as a technology is only just finding productive application as an economical solution to industries training requirements. Despite there clearly being some way to go as far as the development of economical fully immersive systems is concerned desktop VR has been shown to deliver viable training solutions within the context of heavy engineering industry.

This Chapter represents the final section that summarises the background necessary to give an appreciation of all methods and technologies required to fulfil the objective of this thesis.

## **CHAPTER 6**

### **INITIAL SPECIFICATION AND EVALUATION STUDIES OF CFD/VR INTEGRATION**

#### **6.1 Introduction**

This Chapter summarises the research work conducted to determine the hardware and software specifications required to construct interactive VR world representations of a conventional rapid development driveway within which to view the ventilation and pollutant dispersion data predicted by CFD simulation models.

As CFD and VR methods were primarily developed as independent tools, there are currently no computational methods or software applications available that can directly integrate the two technologies. The integration of these technologies to develop an improved ventilation planning and training tool is the primary objective

The focus of the work reported in this Chapter is the critical evaluation of the integration of the CFD visualisations with the VR world models and interactive control systems, using methods previously developed and applied to the independent application of CFD and VR. The strengths and weaknesses of these methods and applications are highlighted.

#### **6.2 Summary of Literature Review**

The technical background behind the analysis, modelling, design, planning and training associated with the application of conventional auxiliary ventilation systems to the ventilation of rapid development drivages were reviewed in Chapters 2 to 6.

Figure 6.1 illustrates both the various planning procedures and engineering design tools that may be currently used to assist in the planning and operation of such auxiliary ventilation systems, and highlights the further proposed integration of CFD and VR technologies to further improve the design, operation and training processes.

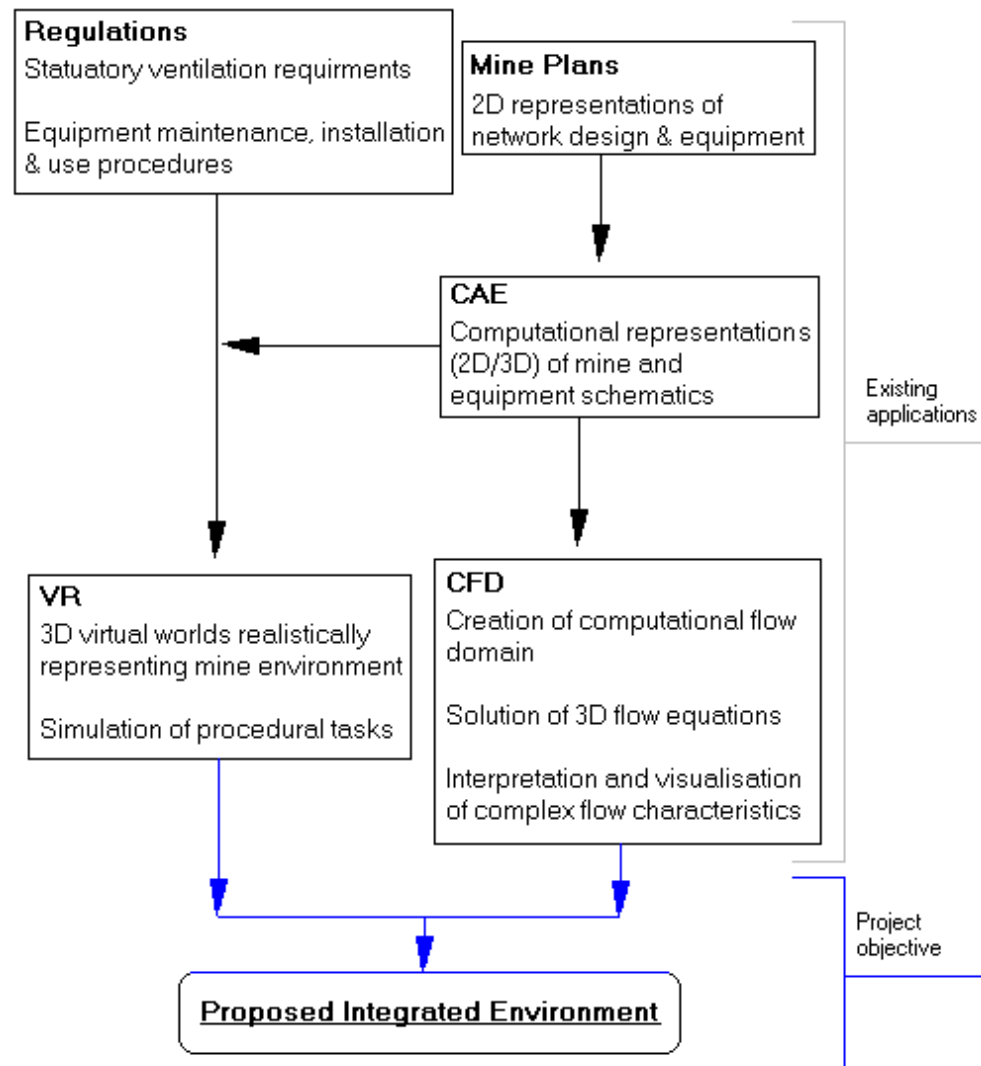


Figure 6.1 Project objective in context of key technological applications

### 6.3 The Technical Specification of the Real World Models

To develop a realistic VR world representation of the physical geometry and equipment layout within a typical UK rapid development driveage, a series of

consultation meetings were held with the Head Quarters Environmental and Safety Engineers of UK Coal plc (formerly RJB Mining (UK) Ltd). A combination of the technical data, obtained both from previously published studies and from the information supplied by the company engineers, was used to ultimately construct a series of VR models within which to view the CFD ventilation and pollutant dispersion simulations. CFD ventilation model simulations were performed (detailed in later Chapters) for a selected range of conventional auxiliary ventilation configurations that may be used during each stage of the mining cycle. The development of these models allows the cause and effects of the potential environmental hazards that may be encountered to be visually communicated to the design engineer, supervisory officials and miners. These environmental hazards may be caused by a variety of means, including natural, man made and/or equipment failure. The natural hazards are principally caused by the abnormal emission of gases, water or mineral into the mine workings, which results in increased pollutant loads being placed onto the ventilating air. Often the remedial action enacted is the isolation of the machine-cutting power, the maintenance of the fresh airflow delivered to the heading and the evacuation of the workforce. The heading may be then recovered by employing a combination of degassing and salvage procedures. Man made hazards are principally caused by non compliance to the operational and maintenance procedures specified in the local managers rules, governing the operation of the auxiliary ventilation system. The managers rules normally include: the specification of: the minimum/maximum force duct and exhaust duct air quantities; the maximum and minimum set back distances from the face, of the outlet and inlet of the force and exhaust ducts respectively; the staged advance of the auxiliary ducts and fans to follow the advance of the machine. Thus, the environmental hazards that may occur due to a non compliance with these operational rules may include: a non advance of the force or exhaust ducts, which may create an increase in gas and dust concentrations due to inefficient gas mixing or dust capture.

A comprehensive environmental monitoring system is installed within rapid development drivages. These systems primarily monitor the gas

concentration levels within the general body within the head of the drivage. Methane transducers are often installed on the cutting boom, the inlet to the exhaust fan and hung from the roof of the drivage above the cutting machine. The methane transducers are often interlocked through an outstation to the electrical power delivered to the cutting machine and the exhaust fan. Should the methane concentration exceed a permitted level (often set at 1.25% general body) the power to the cutting machine and the exhaust fan may be isolated, and not restored until a manual inspection confirms the return of gas levels to below this level. In addition to methane monitoring, transducers are often also installed within headings to monitor total oxygen, carbon monoxide and Products Of Combustion (POC).

The fresh air delivered by the forcing duct and quantity drawn by the exhaust duct may be monitored by the installation of Duct Velocity Meters (DVMs) or differential pressure transducers. These transducers can be connected to both visible and audible alarms to warn of a reduction in airflow.

Should these monitoring systems fail to alarm or isolate power to equipment an environmental hazard in the form of increased gas or dust levels may be created within the drivage.

The ability to effectively simulate both the cause and effect of a potential environmental hazard greatly assists the safety awareness and understanding of the workforce, and reinforces the need to comply with the operational ventilation standards specified by the local managers rules. In addition, the capability to simulate the beneficial effects of enacting a remedial ventilation system response to a potential hazardous situation, such as the restoration of the force duct setback distance from the face or the repair of a damaged duct, will improve the safety awareness and training of the workforce.

In summary, the key stages involved in the development of such an integrated safety awareness and training tool were identified as:

- The construction of representative VR world models of a rapid development drive.
- The creation of the various physical stages of the mining process and the associated auxiliary ventilation system configurations.
- The identification of the range of potential environmental hazards that may be experienced within a rapid development drive.
- The CFD simulation of the various ventilation and pollutant dispersion patterns for each potential auxiliary ventilation pollutant emission configurations.
- The incorporation and viewing of the above events within the VR world.
- The identification of the range of remedial measures that may be enacted on the occurrence of a potential environmental hazard.
- The subsequent CFD modelling of the beneficial effects produced by the enactment of the above remedial methods.
- The translation and representation of the simulation of these remedial methods within the VR world.
- The development of an educational tool with to train and evaluate the training of mine workers, in order to enhance the use of best practice and effect improved environmental control within rapid development drivages.

Given the hardware and software capabilities available during the development of this research project, it was decided to define a minimum acceptable specification to be met by the training application:

- Practicability
  - The application must make use of standard desktop hardware architectures or *off the shelf* hardware. Many VR training applications were found to be based upon advanced specialist workstations. It was considered unrealistic to demand the associated high rates of expenditure. The objective was to construct a *user* application *not* a demonstration.
- Ergonomic
  - The application must offer a detailed representation of the working drive environment. Frame rates must be maintained such that no system latency was detectable. The environment must be representative of the drive configurations experienced by the mine workers.
- Data Display
  - The complex flow and concentration data produced by CFD processes should be displayed in an intuitive and recognisable form such that the user requires no prior understanding of CFD or any processes involved in the generation and visualisation of the data. This was considered imperative if the user was to gain an appreciation of the link between ventilation characteristics, their own actions and any associated change in the level of risk.
- Interact ability
  - The user should be able to interact with the models to investigate the potential beneficial/detrimental effects produced by changes to the various equipment configurations, ventilation flow rates and pollutant emission rates. These models could be used to reinforce good and bad ventilation practice.



To achieve the minimum specifications outlined above, the following three key constituent components were identified, figure 6.2.

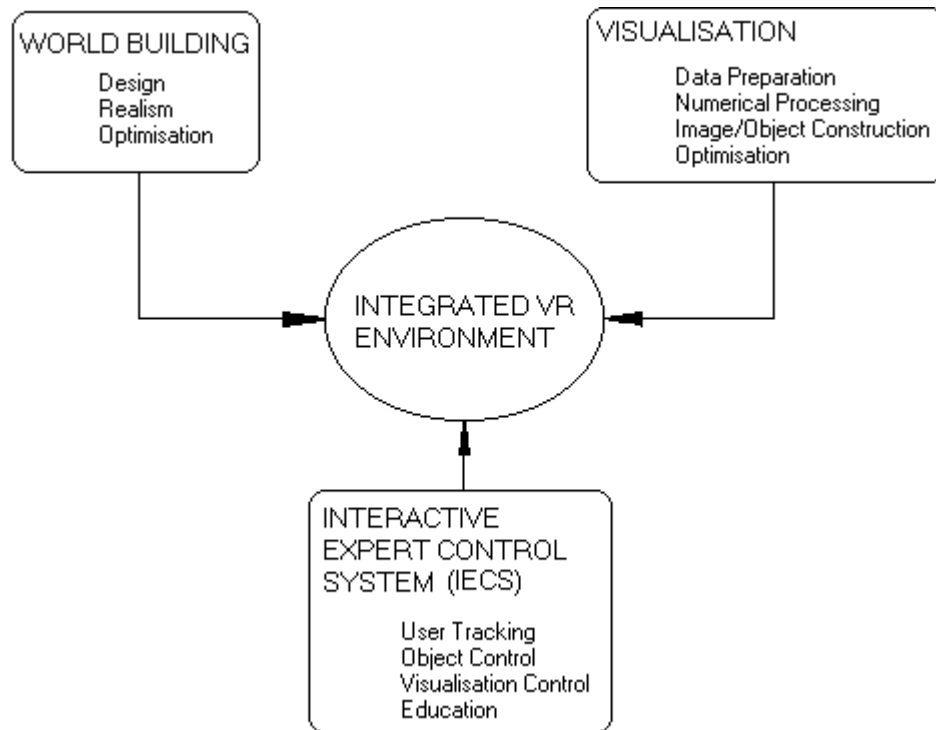


Figure 6.2 Components of proposed integrated VR environment

The following sections detail the degree to which the methods and applications available at the outset of the project were able to satisfy these requirements.

## 6.4 Evaluation of Supporting Software

To provide a foundation for the development of an integrated VR environment, the identification of a suitable generic software VR world viewer was required. Two major current applications were assessed. The first application considered was *SAFEVR™*, a propriety VR simulation builder, designed specifically for hazard assessment within the process industries. The second application considered was the general purpose universal 3D world programming language, VRML.

### 6.4.1 Introduction to World Building using SAFE-VR™

SAFEVR™ is a virtual reality based simulation builder developed specifically for the purposes of the creation of VR training applications focussing on hazard identification and assessment within the extractive and process engineering industries. The application was developed and is distributed by the AIMS research group within the School of Chemical, Environmental and Mining Engineering at the University of Nottingham.

This application allows complex interactive VR environments to be built, using an integral Boolean based logic control system. This control system takes the form of a visual programming language, which allows the user to define precisely how the user interacts with the objects, sounds and animations within the VR environment. The control system makes use of a number of *operators* represented by visual icons that are used to construct the hierarchical logic networks. These operators are available as either input or output states. Each of these states generates a binary (on/off) condition. A network can therefore be built such that an output(s) is delivered on condition of any number of inputs. The operators available are detailed in figure 6.3.

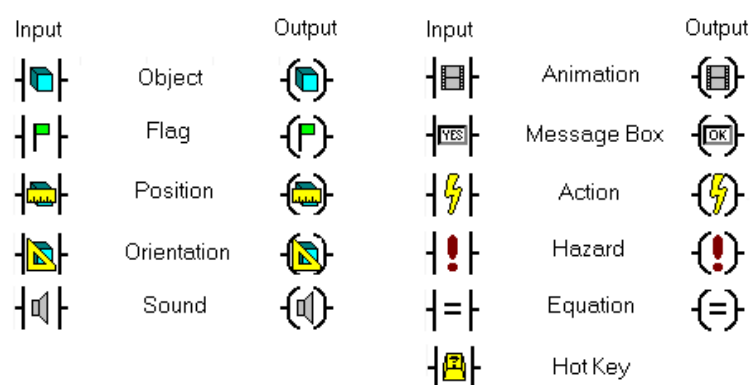


Figure 6.3 Operators used for interactive control within SAFEVR™

Flag operators represent a defined condition, for example the stage of an animation at a point in time. The complexity of the network may be greatly reduced should a flag be used to represent more than one operator condition.

The operators can be combined in any number of configurations, to produce complex network controls functioning in the background. Figure 6.4 illustrates a simple example.

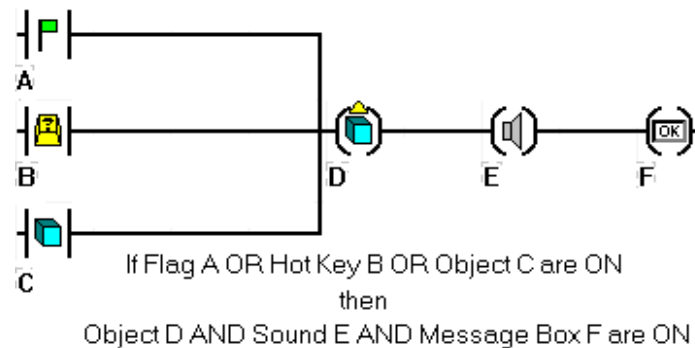


Figure 6.4 Example of implementation of SAFEVR™ operator

To display objects within the VR world, SAFEVR™ supports both the Microsoft Direct X™ format and the AGT™ format from GAMUT. Both of these formats are universally employed for the purposes of VR world building. Objects representing world details and scientific data visualisations are pre-built and loaded into the application to form a library. The application can display any number of objects retained within the library according to the instructions embedded within the control network designed by the user. SAFEVR™ does not offer the ability to post-process scientific data in real time.

#### 6.4.2 VRML

VRML is a more general purpose application than SAFEVR™. VRML was primarily developed for the visualisation of 3D objects, rather than for specific simulation purposes. Therefore VRML possesses limited interactive control in comparison to SAFEVR™. Interaction with a VRML based environment, may be achieved through a *point and click* basis. Objects, sounds and animations can be initiated through this method or by means of VRML nodes such as the proximity sensor node. There is no control language within VRML equivalent to that incorporated within SAFEVR™. The VRML 97 ISO standard does not accommodate nodes enabling real

time processing of data. However, a literature survey identified limited applications capable of delivering real time post-processing based upon a modified VRML format.

### 6.4.3 Discussion

To assess the merits of both of the above VR software supporting platforms, the performance of each was evaluated against the specification criteria detailed in section 6.2.

- Practicability
  - VRML offers the most practical option, as the software is based upon a web browser plugin distributed freely. VRML is also *platform independent*, capable of running on a wide range of available hardware. SAFEVR™ is a specifically developed application and as such incurs a one off cost. However, SAFEVR™ is also developed specifically to run on desktop architectures to minimise the cost of supporting hardware.
- Ergonomics & Data Display
  - Both VRML and SAFEVR™ platforms are capable of displaying the same 3D objects to the same level of detail. There is no distinction between the two as regards data or object display. Currently, neither SAFEVR™ nor VRML offer real time data post-processing as standard, though some developers have demonstrated that modifications may be made to VRML to enable this to occur.
- Interact ability
  - SAFEVR™ offers a powerful control programming language capable of creating complex interactive control networks. A variety of responses can be generated with regard to the users

actions and position within the environment. This control system is also easily accessible enabling greater development and evolution. VRML offers only limited interactive control embedded within the VRML programming language, though it does offer the potential for active post processing capabilities.

Although there was a capital cost associated with the purchase and use of the VR tool SAFEVR™, this cost was minimised by its use of conventional desktop architecture. It was also considered that the application should be capable of responding to the interaction of the user, to enable guidance to be given to the user in response to their actions. This feature would enhance the educational experience. Unfortunately, the inclusion of this help feature was not possible to the same extent from within a VRML based environment.

It was concluded that the facility to perform real time data post-processing of the CFD data would be an advantage. This feature would not need the computer memory capacity required to store the pre-processed CFD visualisation objects. However, as the developer would be familiar with CFD methods, a fixed number of visualisations forming a library could be selected to illustrate particular critical airflow characteristics and pollutant dispersion.

The inclusion of real time data post-processing would also require some degree of training with regard to data visualisation and CFD methods. This would specialise and thus narrow the audience for which the application could be designed. For these reasons, SAFEVR™ was chosen as the platform upon which the application would be based.

For the purposes of world building, a much more established application area, the software application program 3D Studio Max™ was chosen as it offered all the tools required to build, detail, optimise and format 3D world objects.

## **6.5 Preliminary Model Studies**

To develop the preliminary application, it was decided to develop VR worlds within which to view the results produced by CFD simulation models.

Use was made of an existing library of simulation data produced during the execution of a preceding research project. This previous ECSC project employed validated CFD modelling to examine the effectiveness of alternative auxiliary ventilation configurations to ventilate the cutting cycle of a continuous miner system (Hargreaves et al 2000). The data library contained a series of steady state analyses of the ventilation and pollution dispersion patterns for a progression of stages of the cut utilising both sole forcing and combined forcing and a CM mounted exhaust scrubber unit.

The available data described both the flow field within the domain in addition to describing the dispersion of methane gas. The gas dispersion model was limited in that density effects were not accommodated. The methane was introduced at the face at a constant rate and dispersed by the flow field. This did however offer a qualitative appreciation of the dispersion capabilities of each ventilation configuration and was therefore considered suitable for integration within the training application.

## **6.6 Construction of Preliminary Prototype**

### **6.6.1 Introduction**

The initial prototype model was constructed using the methods available at the time to integrate the display of CFD data within VR environments. The methods applied were evaluated against the outline specifications detailed in section 6.3, and any deficiencies noted. To enable this evaluation to be performed, a representative CFD simulation data set was employed to produce standard visualisations within the VR world. Since this model would be required only as an aid to assessing the methods and effectiveness

of standard CFD visualisations the data produced from the ECSC project (Hargreaves et al 2000) was not used for this purpose since this contained high levels of geometric detail which would be required to be duplicated within the VR environment thus requiring resources to be spent upon detailed 3D modelling irrelevant to the current objective.

The computer application program SAFEVR™ version 1.3 was used as the simulation platform into which objects and visualisations were imported. The prototype VR application was simple but versatile in design, allowing the user to switch on or off a number of visualisation objects. The assessment criterion upon which the performance was evaluated was based upon the computational efficiency of the process. This was a measure of the memory storage required to represent both the visualisation of the objects, and the ability of the application to maintain interactive frame rates, related to visualisation object polygon counts. In addition, a qualitative judgement was made based upon the extent to which the standard CFD visualisations could be interpreted within the 3D VR environment.

#### **6.6.2 CFD Prototype Test Model**

A 3D CFD model representative of the ventilation of a particular stage of the cutting cycle within the development drive investigated by Hargreaves et al (2000) was constructed. The ventilation simulation and pollution dispersion data produced by this model was employed as the source of visualisation data for the test application. This model was designed to exhibit the general flow characteristics expected within such an auxiliary ventilated rapid development drive. Figure 6.4, presents the simplified layout of the drive, which incorporates a single forcing duct system eccentrically slung on the left hand side of the roof of the drive. The outlet to the forcing duct is positioned 5m from the face. The continuous miner is represented as a simplified rectangular obstruction located at the head of the drive. The model was constructed, solved and post processed using CFX v5™ from AEA Technology.

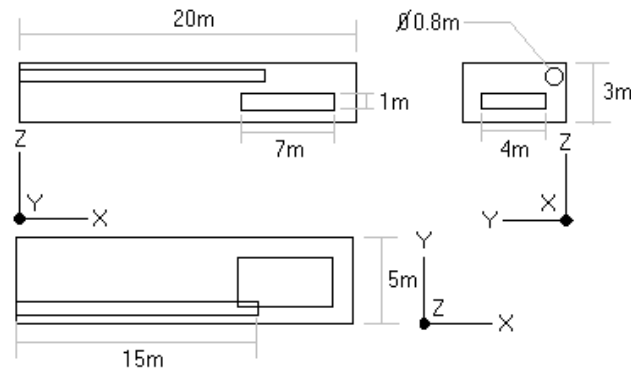


Figure 6.5 CFD model geometry used for evaluation

The following model parameters were set to specify the CFD model and the subsequent model simulations:

- ***Turbulence Model***
  - *Default k-e two equation model*
- ***Inlet Boundary (Airflow delivered through forcing duct)***
  - *6 m<sup>3</sup>/s*
- ***Outlet Boundary (Mass flow balance)***
  - *Outbye defined as 'Opening'*
- ***Wall Roughness***
  - *Assumed to be zero on all surfaces*
- ***Fluid Medium***
  - *Single phase, air*

It should be noted that it is normal practice in the construction and analysis of a CFD model, to perform mesh sensitivity analyses, to identify the minimum mesh density to ensure the solution is independent of the numerical approximations inherent to a finite cell based approach. This is necessary where the solution is required to accurately represent a real flow situation such that an engineering evaluation can be performed upon the results. The test model was designed to provide a generic data set that exhibits general flow characteristics and *not* to investigate a particular flow scenario in detail.



As the purpose of this exercise was to evaluate the effectiveness of the visualization of the graphical representation of the CFD data within the VR world s mesh sensitivity test was not performed.

The test model was solved using the CFX v5™ solver and a state of convergence attained where all residuals were below target criteria. The results file was post-processed using the CFX v5™ post-processor, *CFX Visualise™* to create a series of graphical plots detailing airflow characteristics and the representative gas dispersion, using the default available vector fields & isosurfacing techniques within CFX Visualise™. Streamlines generated from within CFX Visualise™ were not used, as the 1D graphical line glyphs used to construct these were not at the time supported within the 3D environment of SAFEVR™.

### **6.6.3 Construction of SAFEVR™ Simulation**

An identical physical geometry of the layout of the driveway used to produce the CFD simulation data was constructed using 3DStudio Max™. The model was detailed with arbitrary textures, exported into the DirectX™ format and imported into the SAFEVR™ simulation builder.

The graphical plots produced by CFX Visualise™ were exported using the built in CFX v5™ exporter and written in the VRML'97 format. To allow the plots to be imported into the SAFEVR™ simulation builder they first had to be imported into 3dStudio Max™ application and subsequently exported into the appropriate Direct X™ format. The graphical plots were then imported into SAFEVR™ as individual visualisation objects.

The design of the SAFEVR™ control system was limited to simple control of the visualisations using specified *hot keys*, as only a basic assessment was required. This enables the user to view a single or combination of visualisations from the library of visualisation objects within the VR environment.

## 6.7 Evaluation of Preliminary Prototype

### 6.7.1 Results

Figs 6.5-6.7 illustrate some screen captures of the test VR simulation detailing the different flow visualisations.

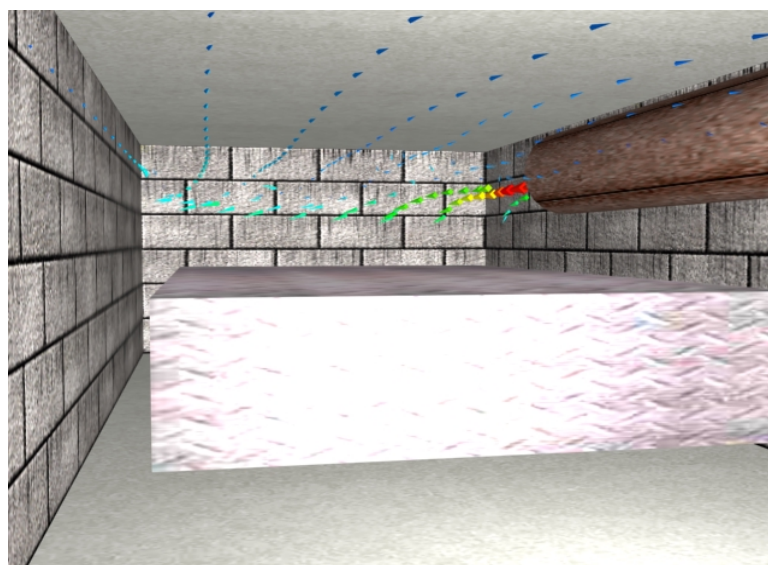


Figure 6.6 Longitudinal vector plot

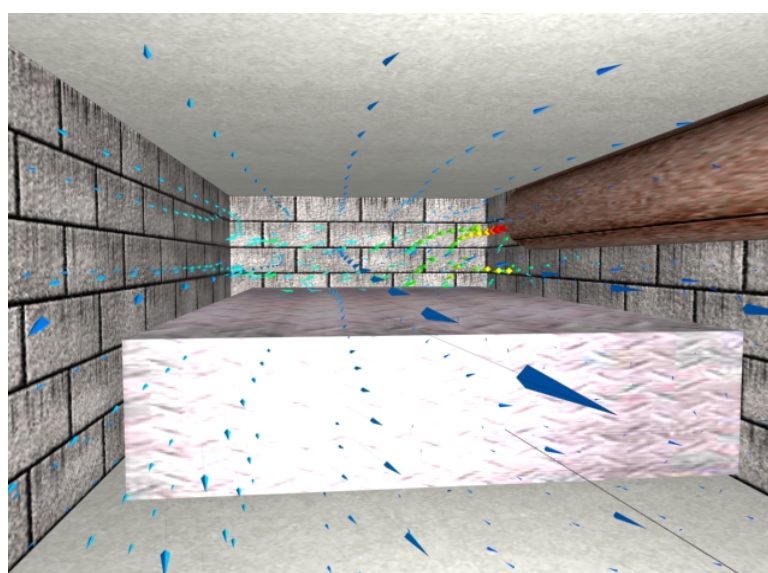


Figure 6.7 3D combination vector plot

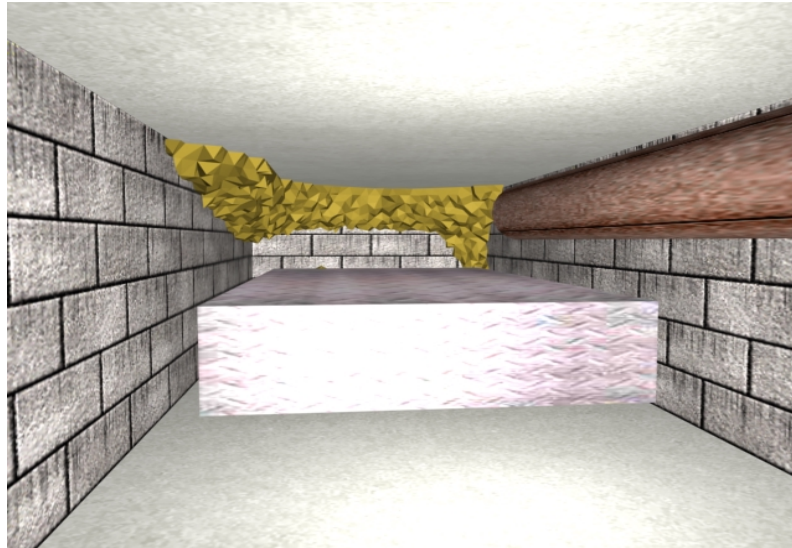


Figure 6.8 Isosurface gas dispersion plot (1%)

### 6.7.2 Assessment of Computational Efficiency

The polygon counter within the 3Dstudio Max™ software environment gave an indication of the number of polygons used to build each visualisation. This is proportional to computational memory storage requirements and influences the frame rate at which the hardware is able to update the scene interactively, i.e. with no discernable time lag, the lower the number of polygons used, the greater the *computational efficiency* of the visualisation object.

It was found that all the visualisations produced from the CFD application were associated with high polygon counts. As an example, the single longitudinal vector plot illustrated in figure 6.5 contained 31,702 distinct polygons. This was equivalent to a budget of around 77 polygons per glyph, clearly uneconomical for the purposes of interactive VR viewing. It is difficult to define a precise budget from which polygon counts can be referenced, as hardware capabilities can vary widely. A good comparative assessment may be made by recreating the same glyph or object, to a comparable level of visual quality, within a 3D object building environment such as 3DStudio Max™. A simple vector glyph can be created within 3Dstudio Max™ containing no more than 8 distinct polygons. Thus, the

aforementioned plot could potentially be recreated to contain no more than 3,200 polygons, a reduction of 90%.

The combined vector cloud illustrated in figure 6.6, contained over 190,000 polygons. Due to the high polygon counts the hardware exhibited difficulties in maintaining interactive frame rates for all visualisations. Excessive system latency was experienced when more than one visualisation at any one time was displayed within the VR environment.

The isosurface visualisations, one of which is depicted in figure 6.7, performed better than the vector representations. The surface depicted in figure 6.7 contained 8562 distinct polygons, a reasonably low count for such a large visualisation. Although no information was available regarding the numerical approach employed by CFX v5<sup>TM</sup> to generate such isosurfaces, it was apparent that the size of the constituent surface triangles followed the gradation of the CFD mesh. The author was, at the time, aware that some isosurfacing approaches were developed specifically for unstructured meshes. Whilst this approach is valid for the production of scientific visualisations, it is uneconomic for the purposes of computationally efficient visualisations. Localised high mesh resolutions produce equally high polygon densities, invisible to the observer, thus offering no benefit in the context of visualisation whilst demanding high hardware resource allocation.

### **6.7.3 Visualisation Effectiveness**

To assess the visual effectiveness of the visualisations a qualitative evaluation was performed. This would assist in determining how the visualisations could be improved to suit the immersed 3D VR environment perspective.

Chapter 5 introduced many of the difficulties experienced by data visualisation practitioners with respect to the intuitive display of 3D flow data. These difficulties were confirmed by the test application primarily with regard to the representation of dynamic data forms such as airflow. The

vector plots depicted in figure 6.5 were designed to be viewed normal to the plane on which they are plotted. This is problematic in a VR environment since for the simulation to represent a real world experience, it is desirable to limit the users ability to view the environment at angles and orientations that can be replicated in reality. It is also difficult for the user to constantly re-orientate within the VR world to view each visualisation. The visualisation should ideally present itself intuitively to the user in a natural viewing position. Vector plots generated normal to the users point of view do not suffer from this problem. Although the amount of information they provide is still inherently 2D. Increasing the number of viewing planes to address this problem, to create a 3D visualisation produces a cluttered image, especially at a distance, making any kind of pattern recognition difficult or impossible, (figure 6.6).

The vector plots were also limited in terms of providing a true appreciation of air velocities. The use of an indicative colour and or measure scale does inform in a scientific manner but this is not immediately intuitive to a non-expert observer. Scaling can also mislead due to the effects of distance perspective in VR. The movement of air is dynamic, and thus representing this in a static manner presents obvious limitations.

The isosurfaces presented in figure 6.7 were an ideal visualisation technique for use in a VR context, as they exhibited a true 3D representation of data and formed a single volume easily identified by the user. This however is only suitable for static data such as the steady state gas concentration clouds depicted in figure 6.7. The uses of 2D concentration contours provided the same clarity, but were limited in their potential application as they depicted only a portion of the available data.

#### **6.7.4 Discussion**

The evaluations detailed in the previous sections demonstrated clear deficiencies in the application of standard scientific graphical visualisations within a VR environment. In the context of the CFD post-processor, CFX

Visualise™, the graphical visualisations were able to communicate complex data to an engineering audience effectively in terms of visual clarity. However, to view the same data within a VR world application with a high degree of visual clarity and in a computationally efficient way requires the visualisations to be modified to suit the VR context.

The effectiveness of the visualisations is a subjective issue. However, the issues raised were reaffirmations of statements made by previous researchers detailed in the literature review. By combining this with the quantitative evaluation concerning polygon usage a clear and justifiable overall evaluation was achieved.

## 6.8 Conclusions

The preliminary evaluation work and associated discussions reported in this Chapter led to the following conclusive statements regarding the extent to which currently available methods could achieve the outline specification detailed in section 6.3.

- *The use of a specialised VR simulation builder, SAFEVR, was chosen on the basis that the required level of interactive control could be incorporated quickly and easily using desktop architectures.*
- *The CFD visualisations produced from within the CFD post-processing environment were shown to lack the optimised structure required for use within VR environments*
- *The CFD visualisations also demonstrated poor clarity under certain conditions apparent from within an immersed VR perspective*
- *In order to successfully integrate CFD visualisations within a VR environment the visualisations must be generated specifically for that environment in terms of computational efficiency (polygon usage and*

*memory storage requirements) and in terms of visual clarity and ability to communicate clear information from a scientific source to a wider audience.*

## **6.9 Summary**

The work reported in this chapter presented an evaluation of the methods available at the outset of the research project to create a VR world environment representation of an auxiliary ventilated rapid development driveway, within which to view scientific airflow and pollutant dispersion visualisations sourced from a finite method based 3D CFD simulation code. Three key constituent technologies were identified as critical for the construction of such an environment: the VR world building application and procedures; the visualisation of the CFD simulation data; and the method of controlling the world objects, visualisations and user interactions, from within the VR environment.

A brief overview of World building was given, as this was a highly developed area of VR environment construction. It was identified that there were a wide range of universal applications suitable for the task. For the purpose of this project it was concluded that 3Dstudio Max™ offered the functionality to construct the required complex 3D representations of the rapid development driveway.

Two platforms were evaluated for their ability to serve as a foundation for the VR application. These were, the international 3D programming language, VRML 97, and the specialised VR simulation builder developed at the University of Nottingham, SAFEVR™. Attention was given to a number of factors, practicality, ergonomics, data display and interactivity. SAFEVR™ was chosen as the most suitable foundation upon which to represent the VR world simulations.

CFD software applications have developed significantly over the last decade. A representative commercial application was used for the purposes of generating a data set containing flow characteristics representative of those exhibited within a dead end ventilated driveway. The standard visualisation processes used within the CFD application were used to generate a series of visualisations that were incorporated within a simple VR simulation. It was shown that the standard visualisation graphics produced by the CFD post processor, CFX Visualise™, lacked the required computational efficiency and visual clarity when placed within a VR world context.

Consequently, it was concluded that it was necessary to construct an interface capable of producing flow visualisations, based upon CFD simulation data, and specifically designed for efficient and effective operation within a VR environment. The following two Chapters present both the background behind the development of a more suitable interface and its subsequent application to the production of a tool to assist in the optimal design and operation of auxiliary ventilation systems within rapid development drivages



## CHAPTER 7

# DESIGN AND EVALUATION OF THE VISUALISATION INTERFACE

### 7.1 Introduction

This Chapter summarises the results of the research work conducted to develop a single interface with which to import and process raw CFD simulation data and produce a series of flow visualisations suitable for display and interpretation within an immersive VR environment.

The methods adopted were built on the foundation of the various numerical techniques introduced in Chapter 5. The appropriate numerical processing algorithms were identified and then applied to the CFD simulation data. The comparative performance of a number of alternative methods employing a single reference data set was conducted to identify the best numerical method in terms of accuracy and computational economics.

However, in the context of the visualisation of complex volumetric data the term *accuracy* may be misleading. In this case the absolute accuracy is defined as the *trueness of fit* to the original data, which invariably implies trueness to any errors implicit within the original data.

The visualisation of complex 3D data sets inherently contains varying degrees of approximation, since there are a large number of algorithms that may be implemented at any stage of the process available for a given data type. The application of each method will introduce a quantifiable error. The error introduced may be global, indifferent to characteristics of the input data, or local, being dependent upon such factors as data point density, boundary proximity or the degree of change between neighbouring points (areas of high gradients). The generation and treatment of these errors are discussed with reference to both vector and scalar data.

The form of data visualisation is discussed with particular focus upon performance within VR environments. For example, the display of gas concentrations in an intelligible yet intuitive manner, presented the greatest challenge, since the volumetric plot of gas clouds required the rendering of large amounts of data. A number of alternative 3D gas volume plots were evaluated in terms of their ability to communicate the maximum information at the minimum computational cost. In addition the animation of airflow patterns placed high demands upon the computational hardware.

The chapter concludes with the definition of the final specification of the performance capabilities required of the developed CFD/VR interface program and of the evaluation criteria used to judge the levels of scientific accuracy and perceived accuracy (that which can be recognised by an observer).

## **7.2 Summary of the Airflow and Pollutant Dispersion Features**

To produce an effective representation of large 3D CFD data sets requires a prior knowledge of the precise flow features that dictate effective ventilation and pollutant dispersion. The following section summarises those flow features that primarily influence the mixing and dispersion of pollutants, including methane and fine dust clouds within the head end of rapid development drivages.

- *Dead Flow Zones*
  - These are regions of relatively low air velocity that may in some cases deteriorate into stagnation zones. Any reduction in the fresh air delivered to the seat of a pollutant emission will increase the concentration of the resultant diluted pollutant cloud.

- *Local Recirculation Zones*
  - These are regions in which the pressure regime induces a recirculation of airflow, which may under some conditions allow the concentration of a given pollutant to increase.
- *Flow entrainment*
  - In the vicinity of the fresh air jet issuing from the end of the forcing duct, polluted air returning from the head of the drivage may be entrained into the jet flow, thus introducing an additional pollutant load to the head of the drivage.
- *Face Flow Characteristics*
  - The effective ventilation of the face cut, is ensured provided the direction, quantity and velocity of the delivered fresh airflow are maintained. This ensures an effective scouring of the face to rapidly dilute and remove the gas and dust liberated in the vicinity of the face of the heading. Any deterioration in the orientation, quantity and velocity of the delivered fresh air may produce local increases in pollutant concentration in the vicinity of the cut.
- *The pollutant concentration levels*
  - The mixing of any gaseous or particulate pollutant emission will be influenced by both the location and rate of emission. For example, if the pollutant emission source were located at site obstructed from the ventilation flow, this would produce a higher concentration profile.

### **7.3 The Specification and Design of the Numerical Algorithms Governing the Visualisation Interface**

The output simulation data produced by the majority of commercial CFD codes (including CFX v5™ from AEA Technology) may be produced in the form of basic text data (*raw* data). It was therefore decided that the interface program would be developed to use a text based data input.

The interface utility was initially developed and coded using the C++ programming language as a console application within the Microsoft Visual™ programming environment. The hardware platform used during the initial development of the interface was a 450Mhz Pentium™ II desktop computer with 256Mb RAM running Microsoft Windows™ '98 O/S. All versions of the interface utility were based around and tested upon this hardware architecture.

The interface utility was designed using the most universal, and proven, data visualisation algorithms identified in Chapter 5. The functionality of the utility was such that the process was divided into a series of steps. At each step a decision could be made with regard to the choice of algorithm or method to employ. The two most widely used point variable definition methods; Hill Climbing (HC) and Volume Space Interpolation (VSI) were employed to evaluate the comparative performance of each of the methods. Control over global and variable time stepping was provided to provide an evaluation of streamline airflow data.

During the development of the initial interface, provision was made for the storage of output data in a regular text format to allow a direct comparative evaluation to be made of the performance of the various methods. In the later versions of the interface program, actual 3D visualisations were produced and outputted to files for use within the VR environment.

The process followed to develop the initial specification of the interface utility is illustrated in the flow diagram, figure 7.1, below. This flow sheet details each of the main operation and decision points. The process was designed to assess the numerical accuracy of each of the various algorithms, and hence the output data at this stage was restricted to text files. The interface was designed to accept input data directly from a CFX v5™ text output file.

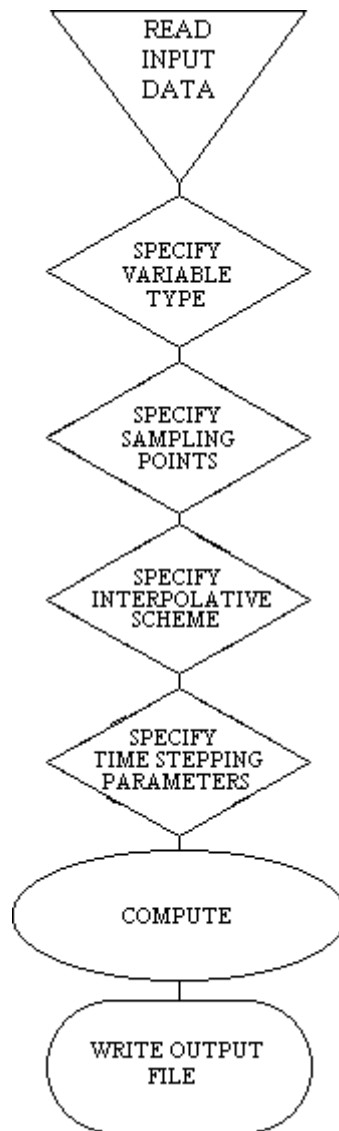


Figure 7.1 Numerical side of interface flow diagram

Each decision stage represents a choice of number of alternative solution routes by which the utility could complete the visualisation process. The primary decision stages within the process were, the specification of variable

type, the choice of the sample points, the choice of the interpolation scheme and if applicable, the specification of the time stepping parameters. These stages are described in more detail in the following sections.

### 7.3.1 The Variable Type

The CFD data produced for the range of simulation exercises formed were stored in a library. For each simulation exercise the library contained airflow data in vector form together with methane concentration data in a scalar form. This therefore allowed the processing of three primary visualisation types, scalar point samples of velocity and methane, and time dependent particle traces (figure 7.2).

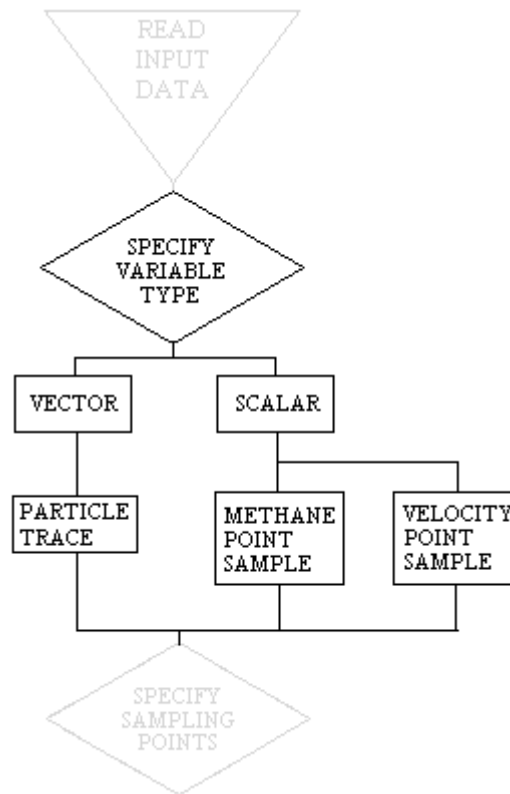


Figure 7.2 Specification of variable type sub flow diagram

### 7.3.2 Sample Data Points

The sample points chosen could be defined in regular or scattered (random) orientation on 2D planes parallel to any axis or within defined 3D volumes.

The standard random number function within C++ was used to generate a random set of sample co-ordinates. The spacing for each regular sample sets was a fixed globally defined variable. In addition, the option of processing a text coordinate listing was also incorporated. If no sample plane were defined then the data would be simply displayed at the coordinate points given within the data set (a *node point* plot). To maintain computational efficiency, and produce a reduction in the total size of the processed data, a further option of eliminating every  $n^{\text{th}}$  point was implemented. This option was only available for the representation of fixed data points (static data), as particle tracing uses a smaller number of sample points at the initial trace location, (Figure 7.3).

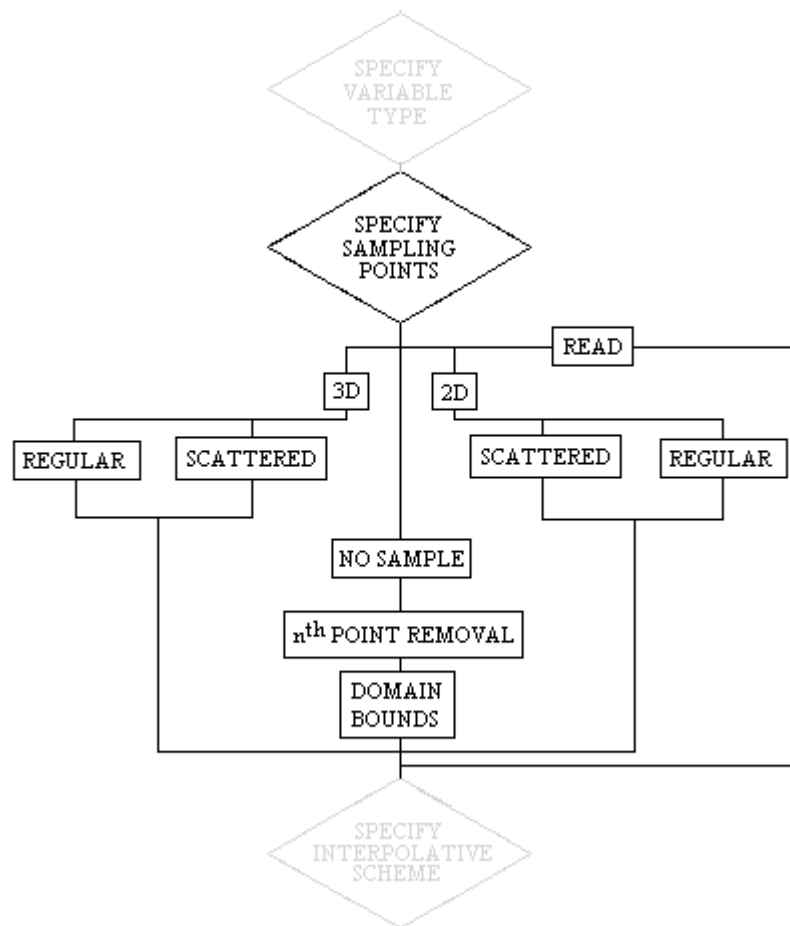


Figure 7.3 Specification of sampling points sub flow diagram

### 7.3.3 Interpolation Scheme

The choice of the interpolation scheme used was based upon the HC and VSI schemes as introduced in Chapter 5. This option only applied if a sampling set had been defined in the previous step, otherwise no interpolation would be required, (figure 7.4).

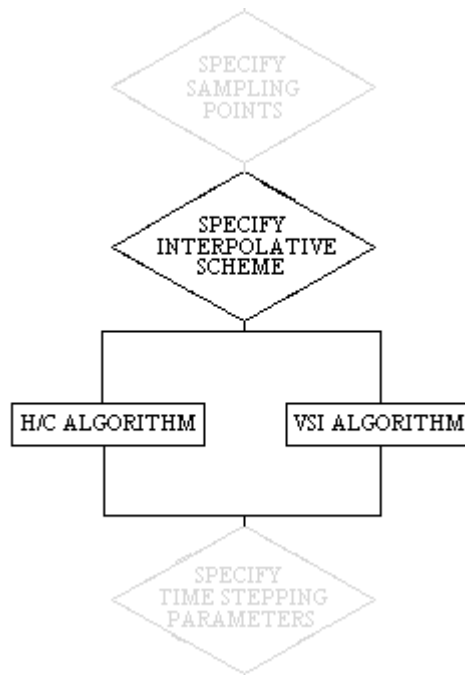


Figure 7.4 Specification of interpolative scheme sub flow diagram

### 7.3.4 Time Stepping Parameters

For the purposes of creating particle traces upon which graphical streamlines could be built an Eulerian approach was applied to particle progression. This offered the most computationally efficient method. However, to accommodate for the inherent error introduced in the first order Eulerian approach a variable time step with adjustable global linear error tolerances was implemented alongside a fixed time step approach whereby the global time step was defined prior to processing, (figure 7.5).



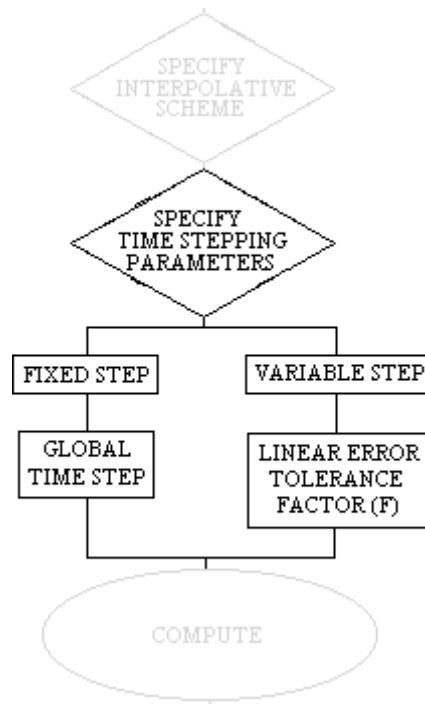


Figure 7.5 Specification of time stepping parameters sub flow diagram

## 7.4 Visualisation Calibration & Residual Error Analysis

In order that the visualisations produced by the interface utility, exhibited an acceptable degree of accuracy, it was necessary to evaluate the two point interpolation algorithms and the time stepping parameters employed. This would provide an indication of the performance in terms of the error produced by each individual method and combination of methods. This is of particular importance with regard to the production of particle trace data, as small step errors may lead to significant and visually perceptible cumulative errors.

Since the approach taken to the application was to minimise the dependence upon high specification hardware, it is desirable to use the least processor intensive methods whilst maintaining acceptable accuracy. The results of the error evaluation exercises would provide sufficient evidence to justify the selection of a particular method. The evaluations were based upon the numerical output of the utility as specified in section 7.2.

#### 7.4.1 Identification of Reference Data

To test the performance of the algorithms incorporated within the interface utility a representative reference data set was employed. A single data set was used for all tests to maintain continuity and enable the calculation of accurate residual errors. The data set was chosen arbitrarily from the library of available real case simulations, rather than the simplified model data used for the evaluation exercises discussed in Chapter 7. It was crucial that the utility was evaluated against a representative range of flow characteristics, mesh densities and gradients expected within the available library. Since the accuracy of interpolation algorithms and particle trace functions is heavily influenced by computational mesh node spacing and, in the case of particle traces, local velocity gradients, the testing of the utility against a data set exhibiting a limited range of flow characteristics and uniform mesh resolution would not provide a clear indication of relative performance.

The data set used for the testing and evaluation of the interface originated from the simulation data generated from the ECSC project (Hargreaves et al 2000) detailed and discussed in Chapter 4. This study considered the computational modelling of an auxiliary ventilated rapid development drive, employing a Jeffrey 1038HH continuous miner machine. The face of the drive was advanced in a two cut sequence. First, a full boom cut was advanced on the driver's side of the CM to a maximum of 6 metres. The machine was then withdrawn and the remaining pillar, on the left hand side of the drive was cut. The machine was then withdrawn back from the face, the roof and walls scaled and bolted and/or meshed as appropriate. The heading was primarily ventilated by a force fan delivering  $6\text{m}^3/\text{s}$  of fresh through a 1m diameter duct slung eccentrically on the right hand side of the roof of the heading. The force duct was not advanced as the face cut advanced. In addition to the force duct, a machine mounted exhaust scrubber fan unit was mounted on the left hand side of the machine. This exhaust scrubber fan drew  $4\text{m}^3/\text{s}$  of air through two duct vents located under the cutting boom of the machine to effect dust control. A range of CFD models and ventilation simulation exercises were performed to provide a scientific

insight into effectiveness of the face ventilation at each stage of the cut cycle. This study, correlated by both scale gallery and underground ventilation survey data, produced a large number of simulation data sets each representing a different stage of a cutting cycle. Two steady state ventilation simulations were performed at each stage of the cutting cycle, one with the boom fully raised at the top of a cut, and the other with the boom fully down on the apron at the end of a cut.

The data set selected from the aforementioned range is henceforth referred to as the 'CM21' data set.

#### 7.4.2 Scalar Data

A comparison between the performance of the HC and VSI schemes demonstrated the degree by which the HC algorithm lagged behind the VSI algorithm in terms of accuracy. Although the HC scheme is appreciably faster and more efficient in terms of computational storage and processing costs, the VSI scheme is inherently more accurate in pure analytical terms. A test was therefore designed to quantify this difference. Should the difference be shown to be significant, the VSI scheme would be chosen over the HC scheme.

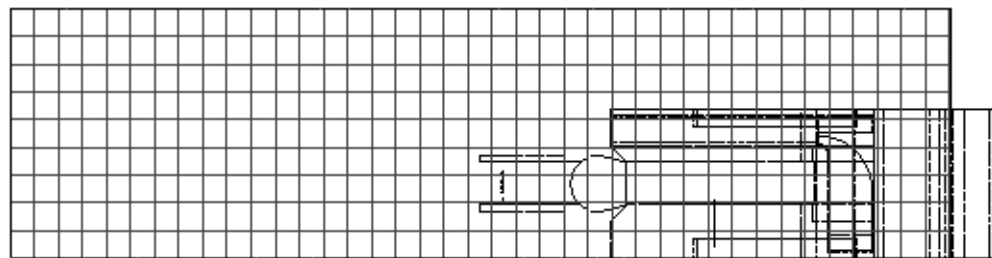


Figure 7.6 Sampling grid taken from CFX v5™

The tests were carried out by specifying a regular 2D horizontal sample plane parallel to the X and Y-axis of the model, at a height of 2.35m on the Z-axis. The chosen plane was co-incident with the centre line of the force ventilation duct. This would expose the utility to the width of the range of scalar velocity values present within the domain. A fixed number of grid

points were defined (namely 40 in the X direction and 10 in the Y direction) to maintain a fixed ratio between grid square sides. Figure 7.6 illustrates the velocity sample plane in the context of the CFD generated wireframe model.

#### 7.4.2.1 The Performance of the HC & VSI Interpolation Schemes

The interface utility was tested using the reference data set, CM21 (outlined in section 7.4.1), employing both the HC and VSI schemes applied to the velocity data located across the prescribed sample plane and grid resolution. The resulting processing produced two output files, each consisting of 400 sample points, detailing the co-ordinate and velocity data. The velocity data was transformed into a single scalar value and the linear residuals between the two were calculated. The linear residuals were plotted against the sample point numbers (figure 7.7).

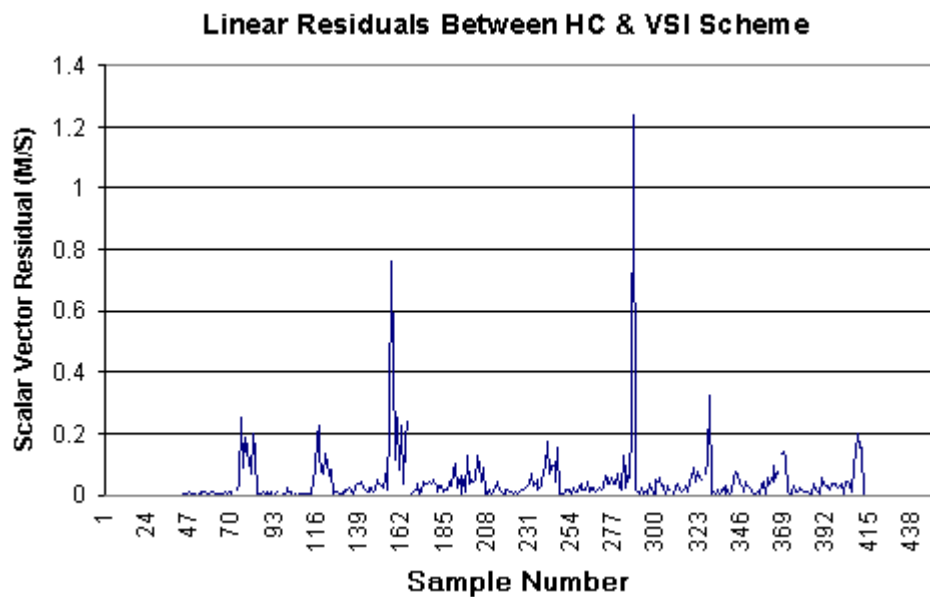


Figure 7.7 Graph depicting linear residuals between HC and VSI interpolation

An analysis of the residuals displayed in Figure 7.7 demonstrates a predominant fluctuation in the plotted residual of less than 0.2m, with a number of isolated and random higher peak residuals. On further analysis it was determined that the mean linear residual error was 0.037 m/s, which was considered as negligible. However, the residuals plotted as a percentage error against the VSI scheme at each point demonstrate a much more severe

error in relation to the local scalar value with a mean percentage residual error of 5.91% which peaks in places, at a value of 100% (figure 7.8).

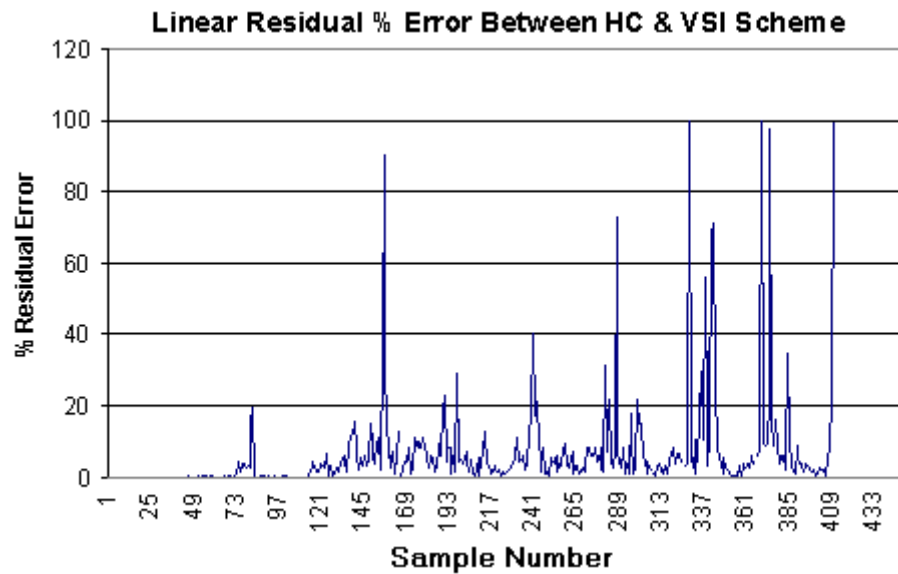


Figure 7.8 Graph depicting linear residuals percentage error between HC and VSI

In addition to conducting a numerical residual analysis to highlight peak errors, residual error visualisations across the sample plane were created using VRML. The images represent a conversion of the residuals into an RGB graded linear colour scale designed to indicate the relative degree of error experienced across the processed sample domain. Figure 7.9 illustrates the distribution of the linear residual values.

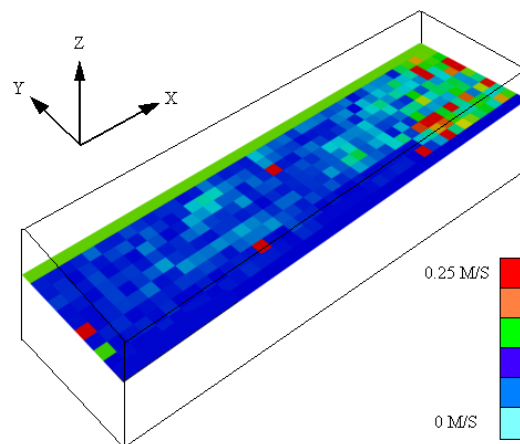


Figure 7.9 Residuals plotted in wireframe model context

The plot clearly demonstrates a cluster of high residual points in the vicinity of the face of the heading, co-incident with a high data point density, high velocity gradients and the presence of a large number of boundaries in the vicinity. The respective local percentage plot demonstrates a more cluttered residual dispersion although clearly the three wall boundaries produce a consistently high discrepancy (figure 7.10).

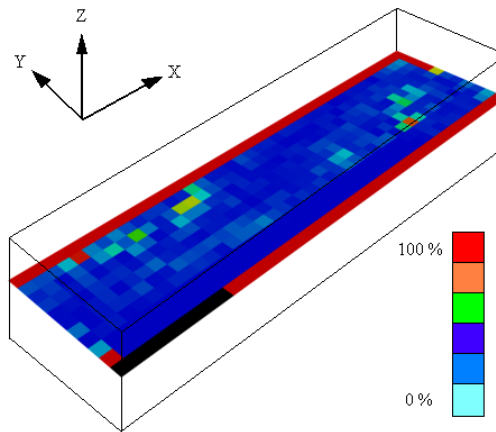


Figure 7.10 Residual plotted as percentage error in wireframe context

#### 7.4.2.2 Discussion of Results

On an analysis of the both of the results plots, illustrated on figures 7.7 and 7.8, a small number of peak errors were determined to exist between the performance of the two schemes. This is best illustrated in the local percentage error plot (figure 7.8) since each error is localised to its own range giving a more accurate measure of the numerical error. The number of these relatively high error peaks is low given the 400 total sample points. However, the occurrence of these peak errors warrants further discussion.

The HC scheme is inherently sensitive when used in close proximity to boundaries, since it seeks the nearest adjacent node, and is unable to distinguish between boundary nodes and internal nodes. This characteristic may explain the clustering of high residuals in the region of the face of the heading, where the geometric boundaries of the CM are prominent and in close proximity to the sample plane. The medium range of the residual

values observed along the far side of the sample plane, also supports this hypothesis due to the proximity of the wall.

A more accurate comparative assessment of the two methods may be found on an analysis of the local percentage residual plot, illustrated in figure 7.10. In this case, the computed residuals do not demonstrate any clear clustering, except at the wall boundaries of the sample plane. This would appear again to be a result of the proximity vulnerability of the HC scheme. Although the sample nodes in these regions are co-incident with the boundaries and therefore should be zero, the HC scheme seeks the nearest adjacent node, which, may or may not be situated on that boundary. It is apparent, that the HC scheme has identified internal domain nodes rather than boundary nodes thus a 100% error is produced.

In real terms this does not create a severe problem, since the domain nodes selected in error by the HC scheme have very low velocities due to their proximity to the no-slip wall boundary. The linear residual plot shown on Figure 7.9 illustrates this point. This boundary effect is of course a characteristic restricted to the velocity variable. However, it is reasonable to expect the methane variable to behave similarly since the concentration will diffuse slowly over distance hence there will be no abrupt changes between node neighbours.

The remaining anomaly requiring explanation is that of the linear residual clustering evident at the face end of the domain. Although it has already been suggested that the characteristic clustering may be due to boundary proximity, it was observed that in this region the velocity field undergoes a series of abrupt changes in direction and magnitude. This is not the case further outbye, along the X axis of the domain, where the flow exhibits a slower more laminar characteristic, where both local percentage and linear residual errors are small. Since the complex geometry representative of the continuous miner machine extends into this region, it was surmised that boundary proximity could not be the sole cause of the clustering at the coalface. Following further investigation it was concluded that it was the

presence of the high velocity gradients in this region, where the difference between node neighbours is the greatest, makes a major contribution to the error produced by the HC scheme. It is also apparent that the higher mesh density in this region is not sufficient to eliminate error caused by the HC scheme.

The results have demonstrated some clear error characteristics in terms of the position of the sample in the domain, the local variable conditions and the mesh density. The mean residual error was found to be relatively low across the sample, although it became more concentrated in the face region, thus increasing its significance.

In addition, a distinction needs to be drawn between error defined as numerically significant and error defined as perceptible. Although the mean local percentage residual error of 5.91% is numerically significant, it may be imperceptible to the human observer. The data obtained from the CM21 utility test was converted into a VRML visualisation. Simple sphere glyphs were used to denote velocity magnitude, the sphere radius and colour was in linear proportion to the velocity magnitude (figure 7.11).

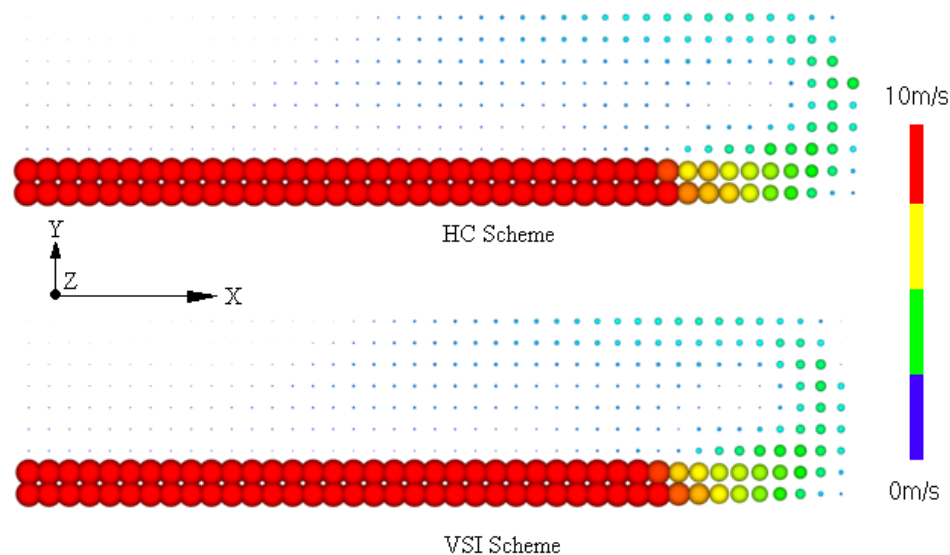


Figure 7.11 Sphere glyph visualisation demonstrating imperceptible error

Evaluating the residuals in terms of perceptible error almost eliminates the more severe numerical errors identified previously. At a glance the



visualisations appear identical. Certainly the bulk flow characteristics are identical in both cases, the flow through the duct illustrated in the red trace on the bottom of the traces, the gradual scour of the flow across the face on the far right and the stagnation points are common to both plots. The residual errors are only apparent upon close examination. Viewed in this fashion, the errors do not influence the overall visualisation in any significant manner and thus may be ignored. Consequently, this suggests that the numerical benefits offered by the VSI algorithm do not translate themselves at the perceptible level. Since the data produced by the utility is designed for the purpose of visualisation, the advantages of the more advanced VSI scheme cannot be realised. Therefore the increased computational costs incurred by the use of this method cannot be justified. It was concluded that the HC scheme could be employed for the visualisation of the fixed scalar data within the application.

### **7.4.3 Particle Trace Generation**

#### **7.4.3.1 Introduction**

The generation of particle trace data for the purposes of constructing streamlines, which describe the airflow characteristics, is far more sensitive to local step error. Since this error will be magnified in cumulative terms over the lifespan of the trace.

As the method used to create the particle trace becomes less computationally accurate, the resulting trace will diverge from the true trace. A *true trace* may be defined as that obtained using an infinitely small time step. To evaluate the performance of the algorithms incorporated into the interface utility the divergence of the traces can be measured against the most analytically accurate parameter setting employed for each specific method.

The evaluation concerns the application of both HC and VSI schemes for point variable interpolation along with fixed time stepping, variable time stepping and error linear tolerance parameters. A series of independent

evaluations of the method using the HC and VSI schemes were conducted, employing in turn fixed and variable time stepping. A comparative analysis of the relative performance of the two methods was also conducted.

The evaluation studies were conducted using the data set, CM21, used in the previous tests. A single particle was traced through the domain for a period of 10 seconds released at a point co-incident with the outlet plane of the forcing duct at a position approximately on the centre line of the duct, to maximise the exposure of the released particle to a representative range of flow conditions.

#### **7.4.3.2 HC Stream Divergence Using Fixed Global Time Step Change**

The visualisation interface was used to generate a particle trace at the prescribed initial starting co-ordinates for a life span of 10 seconds. The HC algorithm was used to generate the point interpolation in conjunction with a series of fixed global time steps, equivalent to 2FPS, 5FPS, 10FPS, 15FPS, 20FPS, 25FPS and 30FPS. Employing the application program 3DStudio Max™, the particle traces were normalised to 25FPS to allow the calculation of the step residual errors. The residuals at each time step were calculated against 30FPS and the results plotted in terms of linear residual against time step number (figure 7.12).

The number of time steps for each series of computation exercises was set at 250, though at lower FPS values this causes the trace to terminate prematurely. The first termination occurred at time step 61, it was therefore decided to terminate all subsequent calculations at this time step.

Figure 7.12 clearly demonstrates the severe divergence that occurs for the traces employing the lower frame rates. At frame rates below 10FPS the divergence is immediate, above 10FPS the divergence is small until approximately the 50<sup>th</sup> time step where the rate of divergence increases dramatically.

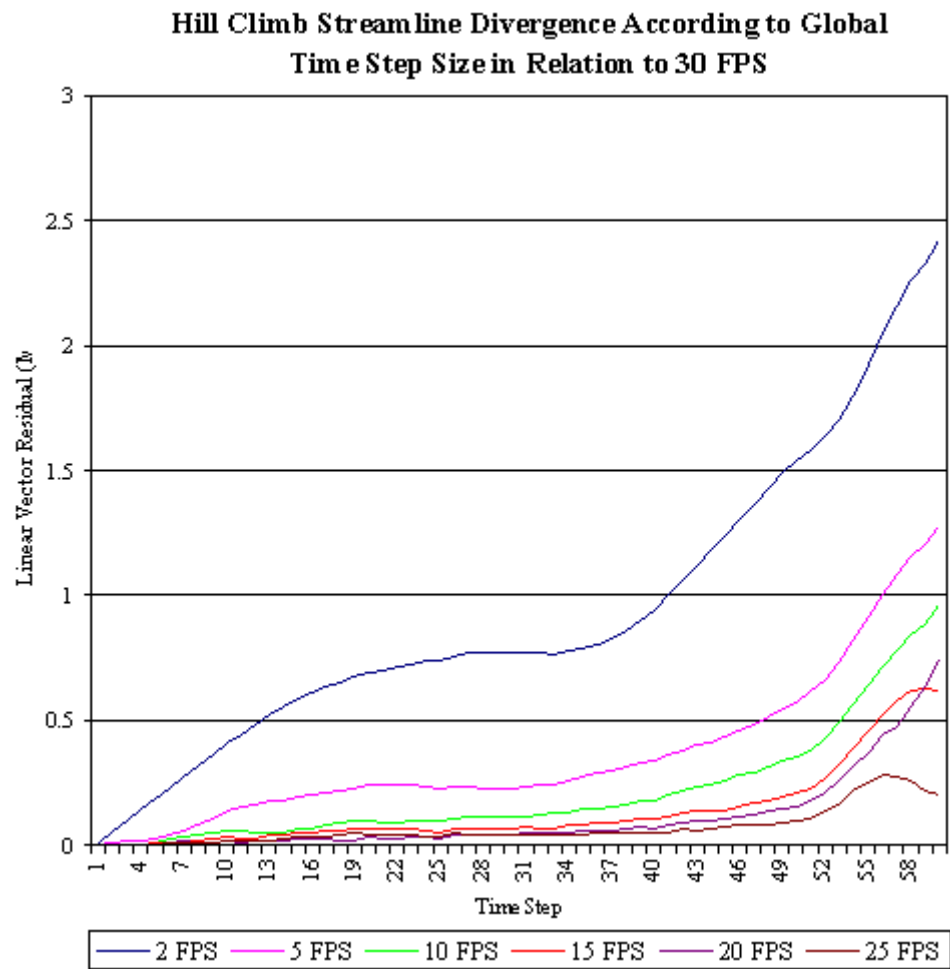


Figure 7.12 Graph depicting stream divergence for HC fixed time step scheme

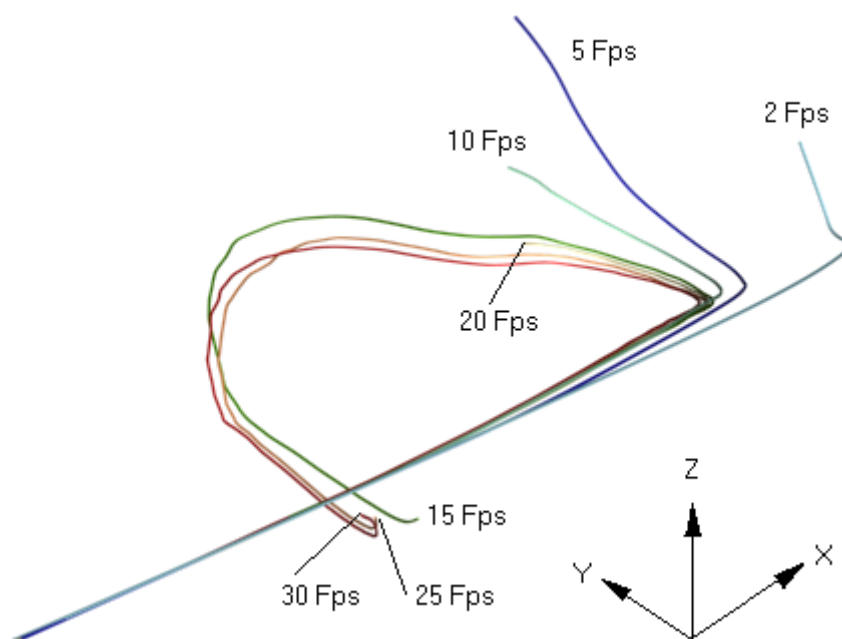


Figure 7.13 HC fixed time step stream divergence visualisation

Figure 7.13 illustrates the particle traces demonstrating the degree of visually perceptible trace divergence with respect to altering the global time step. The location of the 50<sup>th</sup> time step region can be placed into context clearly occupying the region where the bulk flow separates from the wall adjacent to the forcing duct and begins to turn across the face. Evidence of trace understeering was apparent within this region for the lower frame rate traces. The results also indicated that divergence occurs up to a frame rate of 30FPS. It was thus concluded that a higher top-level frame rate was required in order to minimise trace divergence further.

#### 7.4.3.3 VSI Stream Divergence using Fixed Global Time Step Change

The same test was performed using the VSI point interpolation scheme. The trace was made of a single particle released from the same duct centre line position for a lifespan of 10 seconds.

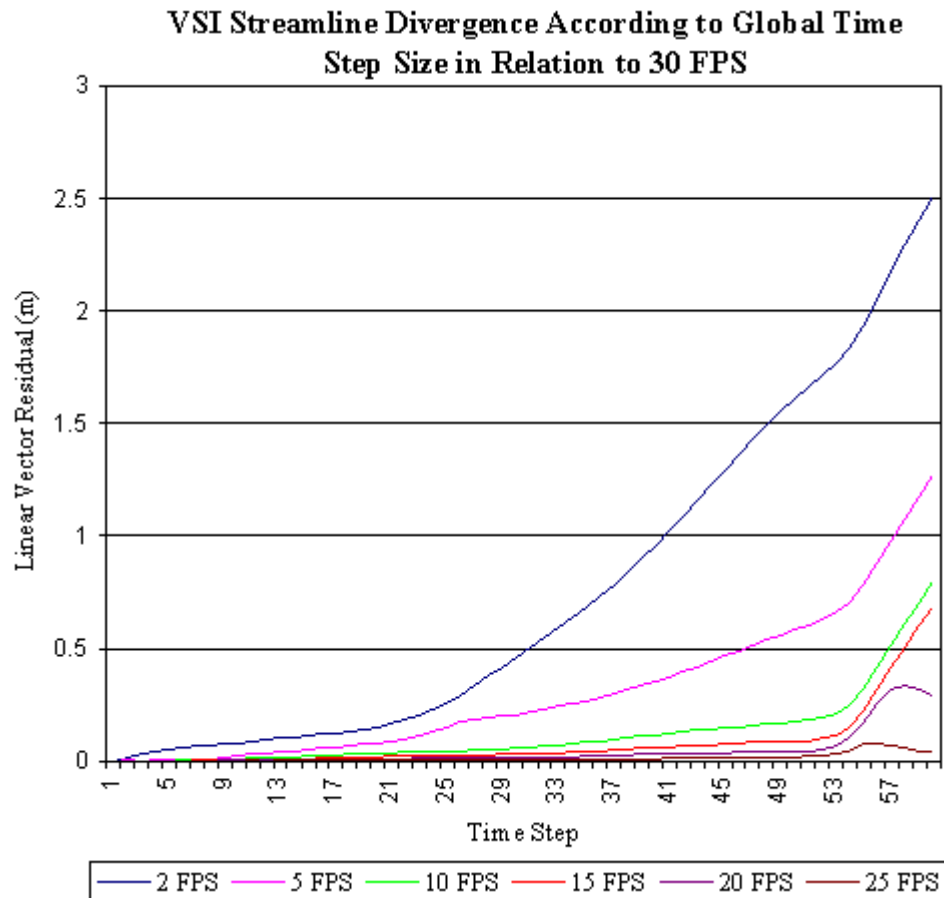


Figure 7.14 Graph depicting stream divergence for VSI fixed time step scheme

Equivalent fixed time steps in the range of between 2FPS to 30 FPS were used. Residuals were calculated using the 30FPS trace as a reference. Plots of the residuals against the time step number are illustrated in Figure 7.14.

The lower FPS values were again observed to produce a premature trace termination in the same region as the HC test. The residuals were therefore again terminated at the 61<sup>st</sup> time step. An analysis of the results concluded that a severe immediate divergence was observed for frame rates below 10 FPS. The rate of divergence was observed to increase rapidly at the 50<sup>th</sup> time step, and again exhibit understeering. Figure 7.15 illustrates a visualisation of the traces, which demonstrate the increased lifespan of the trace corresponding to 30 FPS

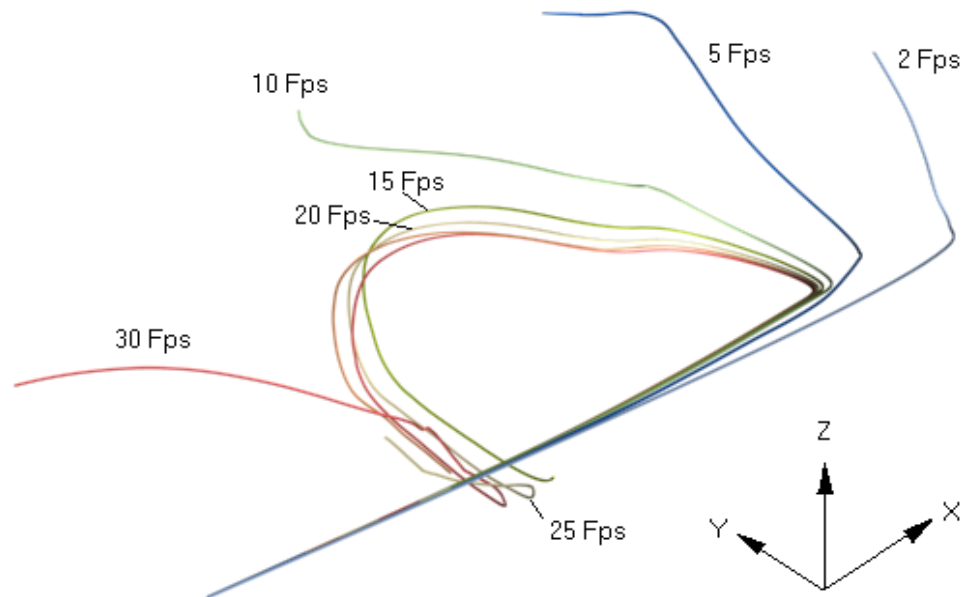


Figure 7.15 VSI fixed time step stream divergence visualisation

#### 7.4.3.4 Vector Residuals from VSI & HC Scheme at Fixed Global Time Steps

Having calculated residuals for each respective scheme with reference to its own parameters, the difference between the two schemes were evaluated by comparing the residuals generated at each time step for each method. The objective of this analysis was to investigate whether there was a frame rate at

which the traces generated by both the HC or VSI schemes would become indistinguishable, i.e. at which point would the utility become insensitive to choice of interpolation scheme. The results were plotted against the time step number, (figure 7.16).

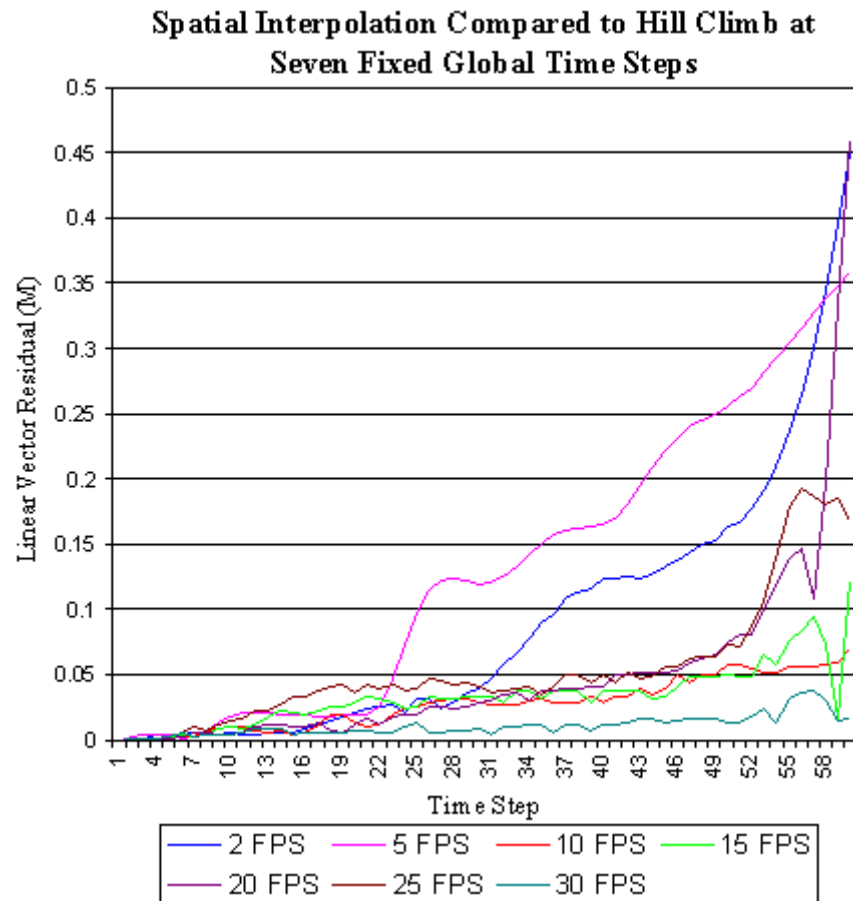


Figure 7.16 HC & VSI fixed scheme residual divergence graph

In the initial stages of generation the trace produced by both schemes demonstrated little difference, thereafter the trace produced by both schemes began to slowly diverge. The results indicate that at frame rates of 25FPS and below, both schemes exhibited a divergence from each other. At 30 FPS the divergence, aside from isolated spikes, does not exceed 0.05m, although there is a clear relatively constant rate of divergence, which may therefore lead to the residual exceeding 0.05m later in the trace lifespan. It was concluded that to minimise the inherent error associated with the HC scheme that a minimum frame rate of 30 FPS should be adopted if this method were to be used.

A qualitative comparison may be made by comparing the 30 FPS particle traces visually as depicted in figure 7.17.

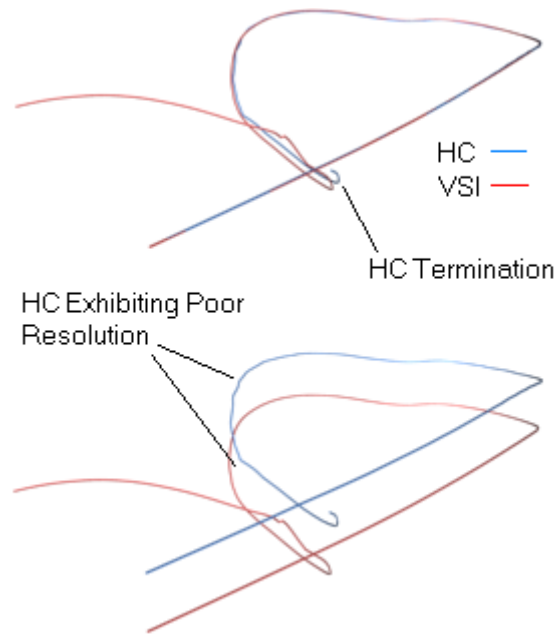


Figure 7.17 HC and VSI 30fps stream divergence visualisation

It is clear that although both the HC scheme at the higher frame rate and the VSI scheme at the same frame rate demonstrate little difference, the quality of the VSI trace is superior in terms of continuity and the smoothness of the stream trace produced. In addition the HC generated trace terminates prematurely and exhibits clearly visible direction changes, suggesting the use of much higher frame rates to generate a smoother trace.

#### 7.4.3.5 Variable Time Step HC Streamline Divergence According to Error Tolerance Change

Although, in the previous sections, the HC scheme demonstrated poor capabilities with regard to the production of smooth continuous particle traces, it was decided that a variable time stepping procedure should be applied to assess whether this would improve the smoothness of the trace produced. The same test was performed using the parameters specified for the fixed time step HC test (section 7.5.3.2) on the basis of a adaptive

variable time step step doubling scheme governed by a linear error tolerance factor (F). The error tolerance was varied over the range 0.1, 0.05, 0.025 and 0.0125m. The results (Figure 7.18) indicated that the variable time step scheme had little influence upon the tendency for early termination, but did produce particle traces exhibiting much smoother characteristics.

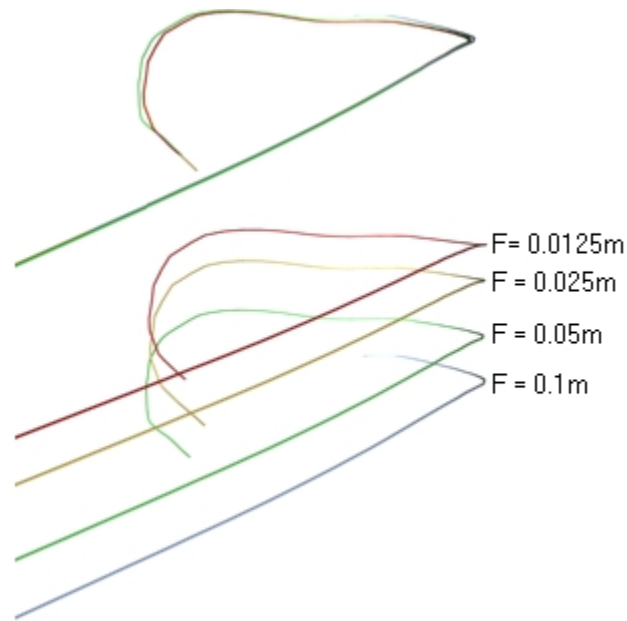


Figure 7.18 HC scheme variable time step stream divergence visualisation

A variation of the error tolerance factor was demonstrated to have no discernable influence. This is most likely due to the fact that halving the time step does not necessarily mean the variable at the alternate nodal point selected has a different value. The nearest nodal point identified by the method may well be that picked originally. This hypothesis would explain the negligible impact of varying the error tolerance.

#### 7.4.3.6 Variable Time Step VSI Streamline Divergence According to Error Tolerance Change

The test described in the previous section was applied with the VSI interpolative scheme. The step doubling variable time step scheme was applied with the same range of error tolerance factors, outlined in section 7.4.3.5 above. The residuals were calculated against the smallest tolerance factor as previously. The results are illustrated in figure 7.19.



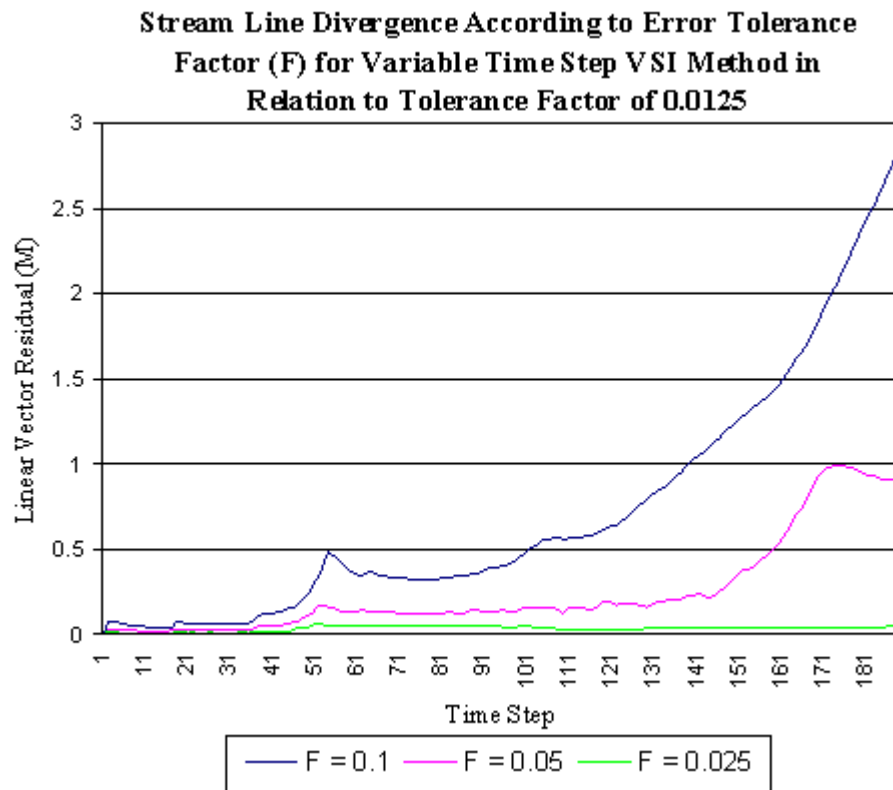


Figure 7.19 VSI variable time step streamline divergence

The results obtained from the variable time step trial provided a much better foundation for analysis since premature trace termination was minimised, the minimum lifespan of the traces were extended to 191 time steps enabling a more thorough evaluation than that possible with the fixed time step trials. The results indicated clearly that a tolerance control factor of no less than 0.025 m would be necessary to eliminate any trace divergence. Tolerance factors greater than this were shown to produce high rates of divergence. The use of a tolerance factor of 0.025m did not exhibit any significant divergence, suggesting that the procedure had been improved. The residual

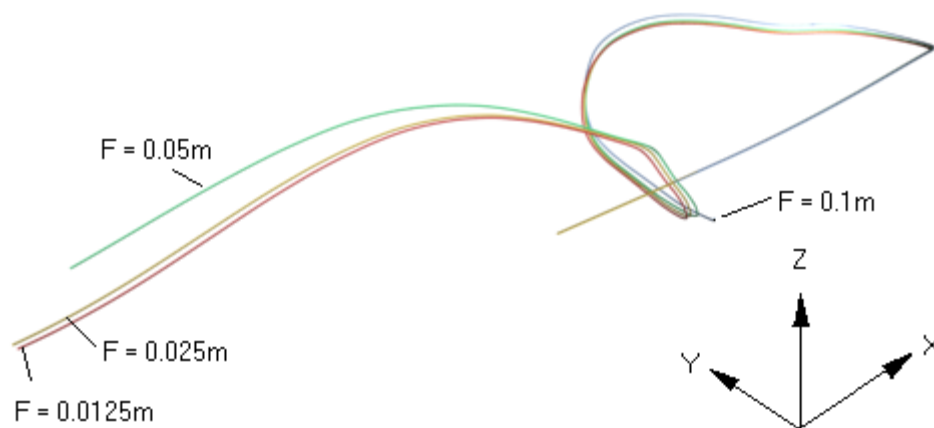


Figure 7.20 VSI scheme variable time step stream divergence visualisation

for this tolerance factor was shown to be restricted to a limited range across the sample. Figure 7.20 illustrates the trace divergence supporting these observations.

It is clear that the error tolerance has a direct impact upon the divergence of the traces when using the VSI scheme as opposed to the HC scheme tested in the previous section. This is due to the fact that step doubling will always produce a new variable value at the new nodal point, as it is defined through interpolation and will thus always have a slightly different numerical value. When the same test was applied to the HC scheme for an error factor of 0.1m, a termination was observed in approximately the same region as the terminations observed in the previous section.

A further model sensitivity analysis was conducted to determine as to whether there was a frame rate that would maintain the prescribed error tolerance factor. The variable time step scheme automatically converges upon the required frame rate by doubling the frame rate. Understandably therefore, given a low starting frame rate of 5 FPS the maximum frame rates may reach high values. The frame rates generated by the variable time step scheme were plotted for each of the error tolerance factors against time in order to provide an insight into the levels of accuracy the algorithm required in order to maintain the respective tolerance factors, (figure 7.21). The values were sampled for each of the factors at intervals of 0.5s.

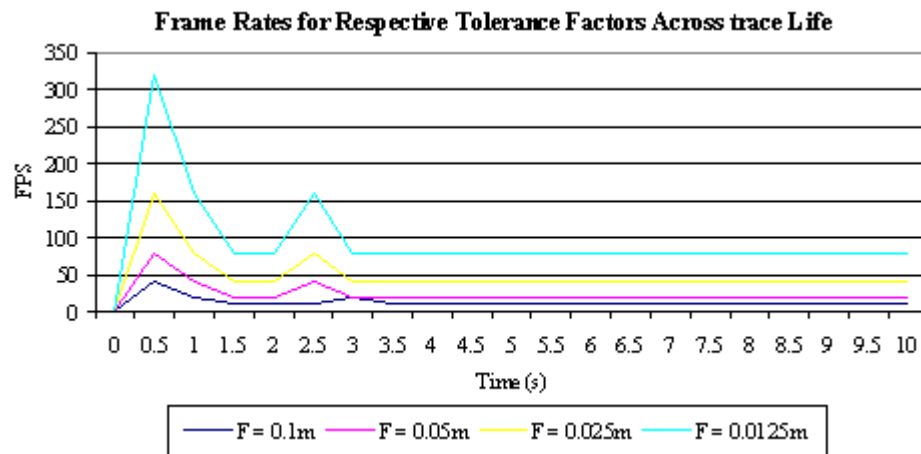


Figure 7.21 Frame rates produced by step doubling scheme across trace life

#### 7.4.3.7 Variable Time Step HC & VSI Comparison

Due to premature termination of the HC traces, little can be concluded from a comparison of the HC and VSI scheme traces for variable time steps. Figure 7.22 illustrates a visual comparison of the smallest error tolerance (0.0125m). There is no visible difference aside from the early termination of the HC trace. This suggests that up until the termination of the HC trace the choice of HC or VSI interpolation is visually insignificant if a variable time step is being used.

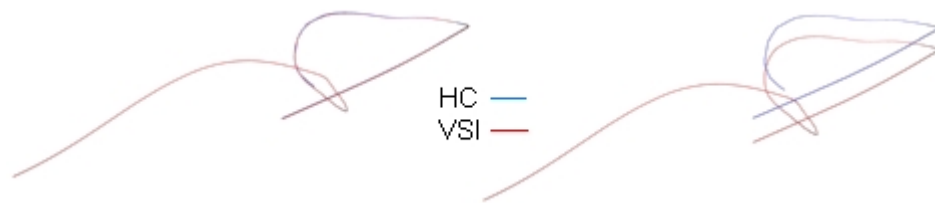


Figure 7.22 HC and VSI streamline visualisation using error tolerance of 0.0125m

#### 7.4.3.8 Combined Residual Analysis Compared to Optimum Theoretical Method

The previous sections demonstrated the characteristics of a number of alternative approaches to particle trace construction in terms of divergence from the most analytically accurate for each particular approach. A parametric study was conducted to investigate the performance of each of the methods.

To aid decision-making a comparison was made between the performance of a selected number of the approaches and the identified optimum analytical method, the VSI variable time step with error tolerance of 0.0125m. Not all the approaches and parameters were investigated, since some clearly demonstrated poor performance, included all the fixed time step approaches for the HC scheme with frame rates below 20 FPS, and the fixed time step VSI scheme below 15 FPS. In addition, since the HC variable time step scheme demonstrated no significant change in terms of error tolerance only one tolerance factor was considered, namely 0.0125m.

The residuals were plotted on one graph against the time step number (figure 7.23). Stagnated traces were deleted from the termination point onwards and all traces were plotted up to a 1m residual ceiling to preserve clarity.

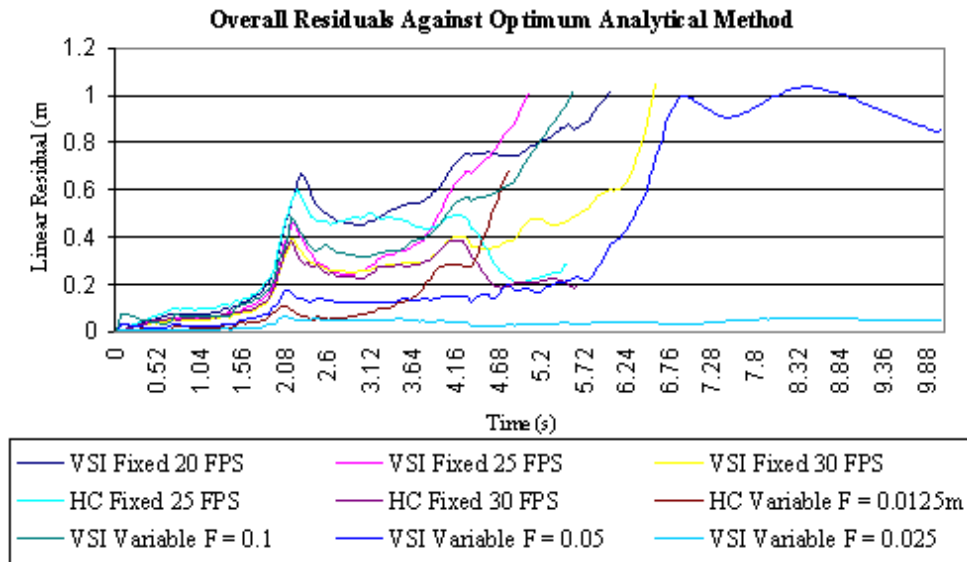


Figure 7.23 Overall stream divergence residual graph

The qualitative visualisation is depicted in figure (7.24) detailing all the above traces. Since the difference between traces is small they have not been individually labelled.

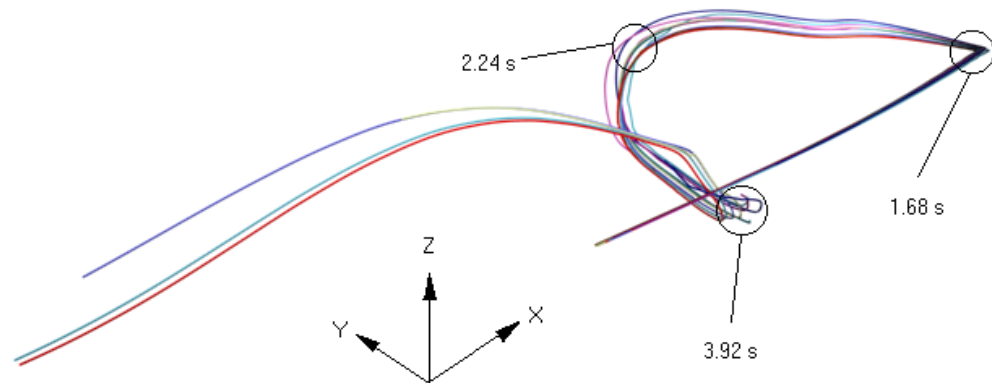


Figure 7.24 Overall streamline divergence visualisation

The chart and qualitative visualisation demonstrate limited visual divergence for all methods, significant divergence only occurred over approximately half of the total trace lifespan of 10 seconds. The divergence was more pronounced when viewed in the plotted form, but it is clear where within the

domain the limitations of certain approaches become significant. All approaches demonstrate a vulnerability to error in regions of high vector gradients. This is demonstrated by consideration of the chart (figure 7.23) at the time of approximately 1.68 to 2.24 seconds where a sharp divergence is evident. This coincides with the first sharp turn of the flow (figure 7.24). Between 2.24 and 3.92 seconds there is a period where the error drops and stabilises as the flow enters a laminar region. From 3.92 seconds onwards the flow is again subject to high gradients causing another sharp rise in divergence rate.

Although the HC schemes have demonstrated an ability to maintain an acceptable error in the early stages of the trace the tendency to stagnate precludes them from use. All of the VSI based schemes have demonstrated extended lifespans. It is concluded that the VSI scheme with a variable error tolerance of 0.025m needs to be employed to maintain the visual accuracy across a typical 10 second trace.

#### **7.4.4 Conclusions**

The analyses conducted in the previous sections support the following conclusions.

- *In order to maintain confidence in the visual accuracy of particle traces an evaluation of divergence is necessary.*
- *Frame rates lower than 20 FPS (0.05s) cause significant particle trace under-steering in regions of high velocity gradients.*
- *Traces constructed using a HC based scheme are vulnerable to stagnation and perceptible changes of direction.*
- *Variable time stepping has no appreciable impact upon HC based traces.*
- *For no appreciable visual divergence a VSI variable time stepping scheme with a tolerance of 0.025m is required.*

## 7.5 Graphical Representation of Numerical Data

In order to effectively display the methane and air flow velocity variables to the user a number of alternative iconic representations were evaluated in terms of their computational efficiency and effectiveness in communicating the flow forms and gas concentration profiles. For this purpose a VRML visualisation output process was incorporated into the interface producing a variable parameter visualisation in the VRML format. Methane and airflow were considered independently, and their treatments are described in the following sections.

### 7.5.1 Methane

Five methods of visualisation were evaluated for the purposes of methane data display; node point plots, uniform point distributions, random point distributions, 2D contouring and polygon based isosurfacing. Despite their title, the three versions of the point-based plots did not make use of point glyphs. Points were actually represented by the use 2D regular quadrilateral planes. This was because within the functionality of SAFEVR™, one-dimensional glyphs such as points and lines were not, at the time, supported.

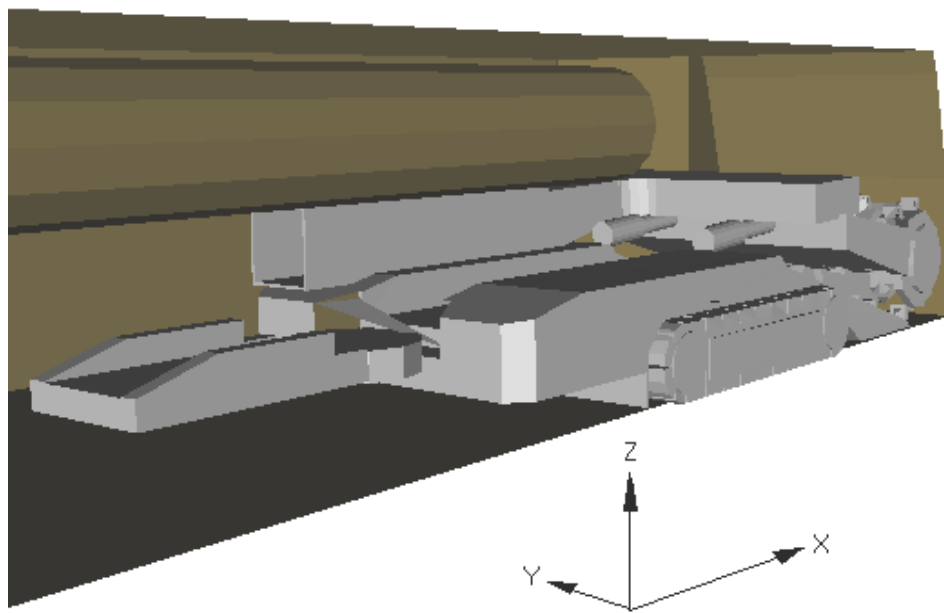


Figure 7.25 CM21 Data set VRML representation

These were therefore replaced with small 2D planes, to create the illusion of point clouds. The disadvantage of this approach is the increase in computational power required to update this type of glyph as compared to the use of true point entities. The differing methods of visualisation are displayed for the benefit of the reader within the familiar context of the rapid development drive.

A simple VRML model was constructed for this purpose based upon the parameters of the CM21 configuration data set. The model is displayed in figure 7.25. For clarity, the viewpoint is maintained constant for the each illustration and wireframe models for solid objects within the drive are used to assist clarity of view. The threshold limit value for the methane gas concentration for each visualisation was set at 1%.

#### **7.5.1.1 Node Point Plots**

The node point plot was the simplest of the visualisation methods, being based around the display of a single point co-incident with its parent data node. The density and position of the points were therefore entirely dependent upon the nodes within the data set. As such, it is the most computationally efficient since no interpolation or point location is required.

The parameters that may be adjusted to assist in the communication and interpretation of the visualisation concerned the gradation of the colour scale to highlight high concentrations of methane. The glyphs could also be adjusted in terms of global size to indicate the relative magnitude of the methane concentration. Figs 7.26-7.28 illustrate some of the variations evaluated. The colour graded plots (figures 7.27, 7.28) used a gradation representing the maximum methane concentration of 1% as red graded down to blue (0.25%) representing the lowest concentration within the local sample.

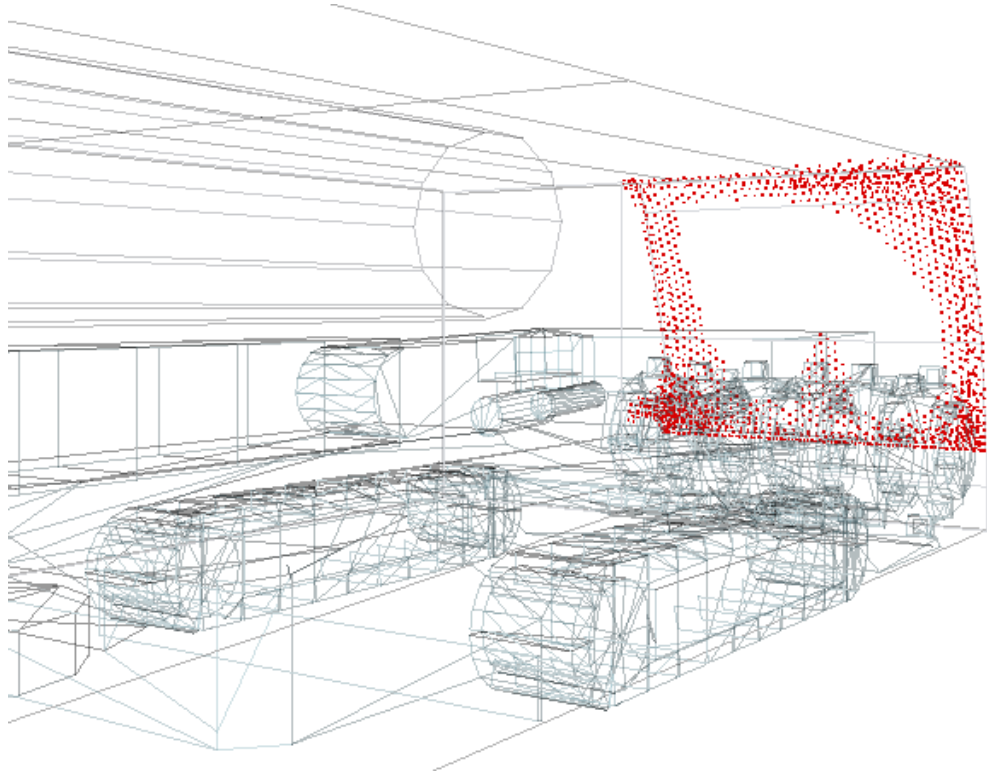


Figure 7.26 Node dependent point gas dispersion plot (1%)

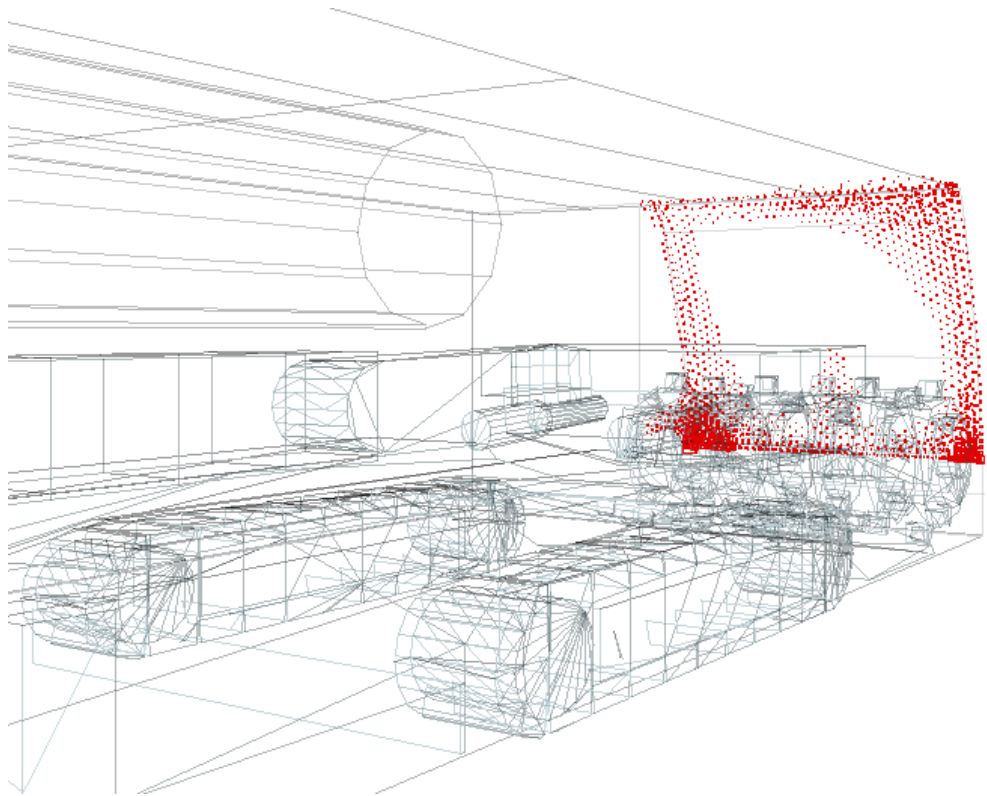


Figure 7.27 Node dependent scaled point gas dispersion plot (1%)



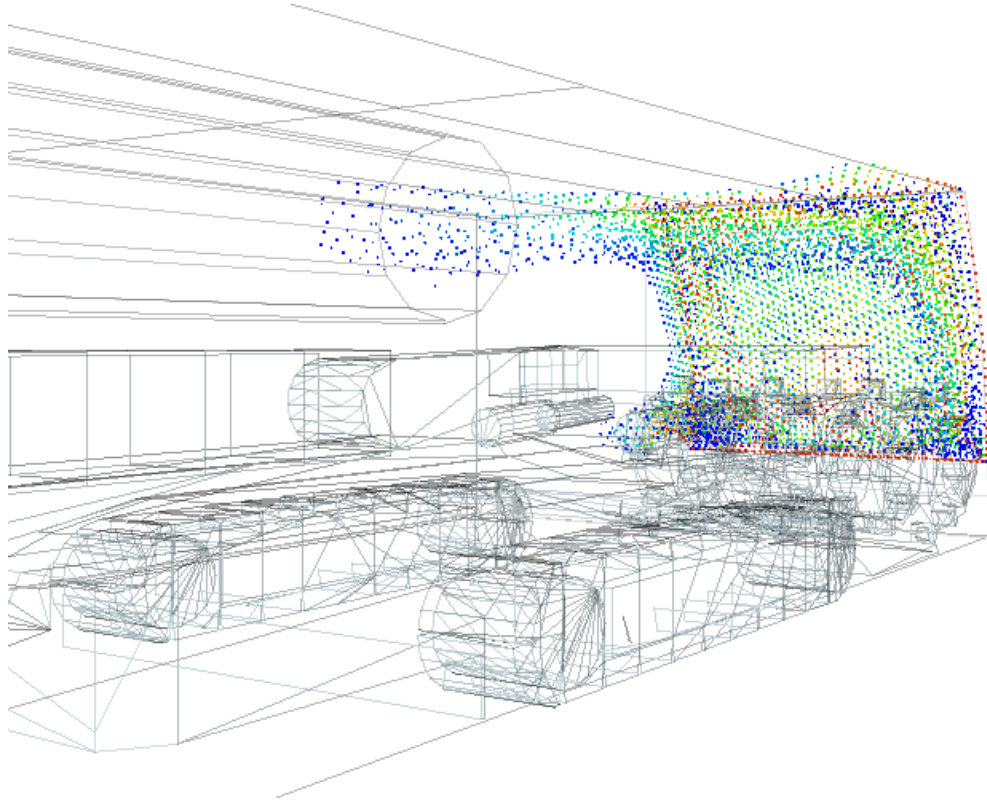


Figure 7.28 Node dependent colour graded point gas dispersion plot (1%-0.25%)

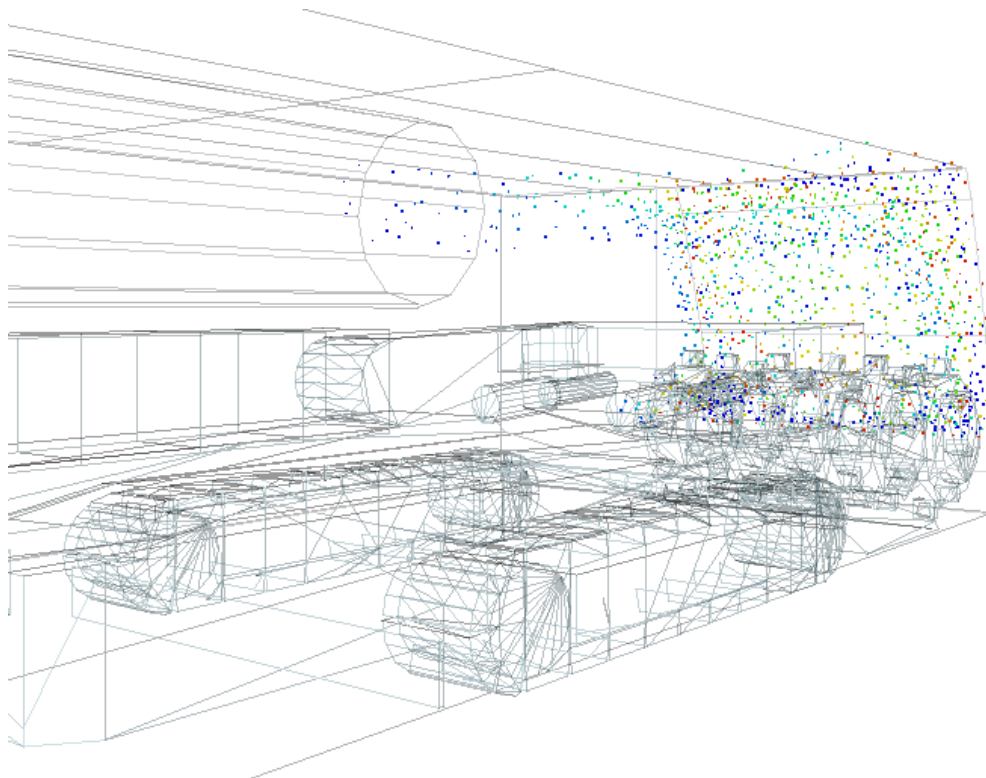


Figure 7.29 Node dependent reduced colour graded point gas dispersion plot (1%-0.25%)

The node point plots depicted in the previous pages are representative of the kind of visualisations produced using this method. The number of potential variations is high considering factors such as nth point removal, varying the colour gradation bounds and applying autoscaling locally or globally. The conclusions drawn during the assessment can however be supported, for the purposes of this thesis, by consideration of the aforementioned representative plots.

The major drawback with this approach is the lack of control over the number and density of glyphs, this being totally dependent upon mesh density. This can cause misleading visualisations. Figure 7.26 demonstrates a degree of clustering due to mesh density in specific areas of the plot. This can be corrected, as shown in figure 7.27, by scaling the glyph dimensions to the plot variable. Here the true high concentrations are clearly depicted. Colour gradation is also shown to assist in highlighting high local methane levels as depicted in figure 7.28. However, to provide a sufficient range of colour gradation, a larger number of glyphs must be used below the upper bound (1%) leading to a much greater strain being placed upon computational resources. Removal of points on a random distribution method does address this problem but the reduction is clearly detrimental to the visualisation, as this may remove important concentration features and produce a confused visualisation, as depicted in figure 7.28.

The polygon count used to produce these type of plots varied from 3,382 up to 11288 for the colour graded plots.

#### **7.5.1.2 Uniform Distribution**

By performing a careful selection of the sample points, a close control may be exercised over the density and positioning of plot points. For this purpose, the interface was designed to generate a regular 3D sample field, on which point data could be displayed. This method requires the generation and interpolation of a large number of points hence is computationally expensive in terms of processing time and memory usage.

As a consequence of the positive assessment of the HC algorithm for static point visualisations, this algorithm was used to generate a field of points at which the methane concentration and airflow variables would be plotted.

The plots produced by the regular grid approach eradicated the problems associated with data clustering as depicted in figure 7.29. The polygon count could also be controlled; typically counts of less than 1,000 could be achieved. The plot depicted in figure 7.29 contains 966 distinct polygons. Using this method similar benefit could be realised for both scaling and colour gradation methods.

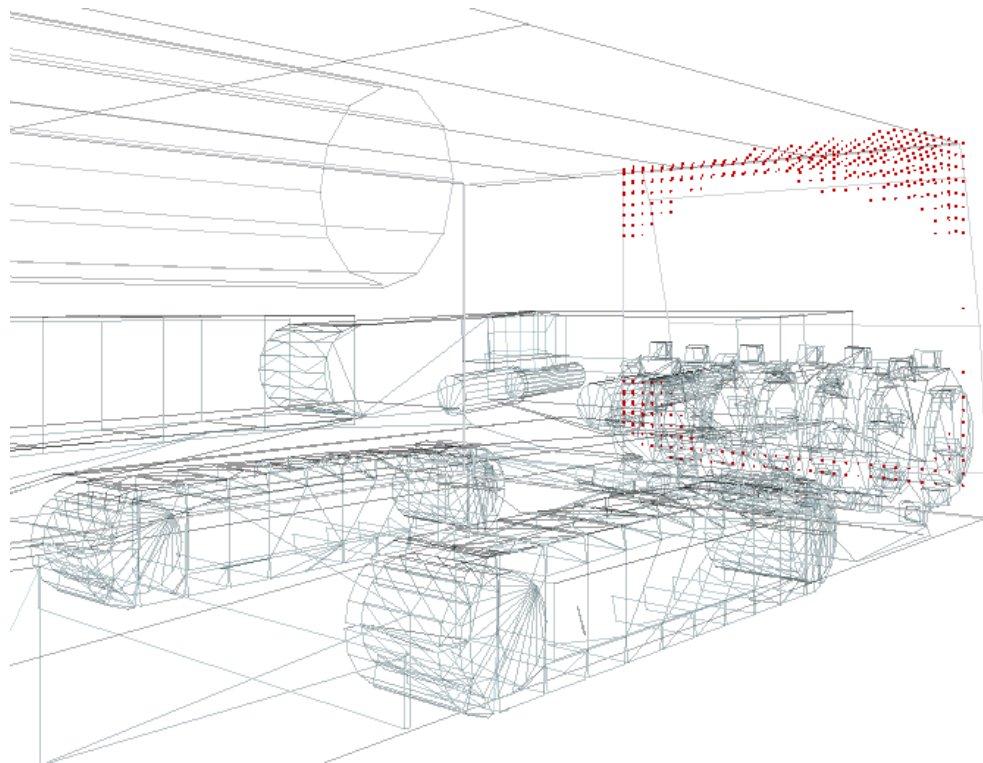


Figure 7.30 Regular sampled scattered point gas dispersion plot (1%)

The regularised plots did however present problems when viewed in a real time 3D environment. The primary problem concerned the tendency for large numbers of points to become hidden when viewed along the exact level plane. In terms of achieving a more qualitative evaluation, the regular positioning of the glyphs produced a less than natural cloud. The node plots of the previous section did not present this problem. In terms of performance in a 3D environment the regular grid plots were however far superior to the

node plots requiring much less computational effort in order to maintain an interactive frame rate.

#### 7.5.1.3 Random Distribution

In an attempt to combine the individual advantages of each of the two previous methods and eliminate the disadvantages of both, a randomised point sample approach was evaluated. The control parameter of this approach was the density of points defined within a specific volumetric region. Thus control over the polygon count could be achieved as with the regularised plots. The interface generated a number of illustrative plots, two of which are depicted in figs 7.30 and 7.31.

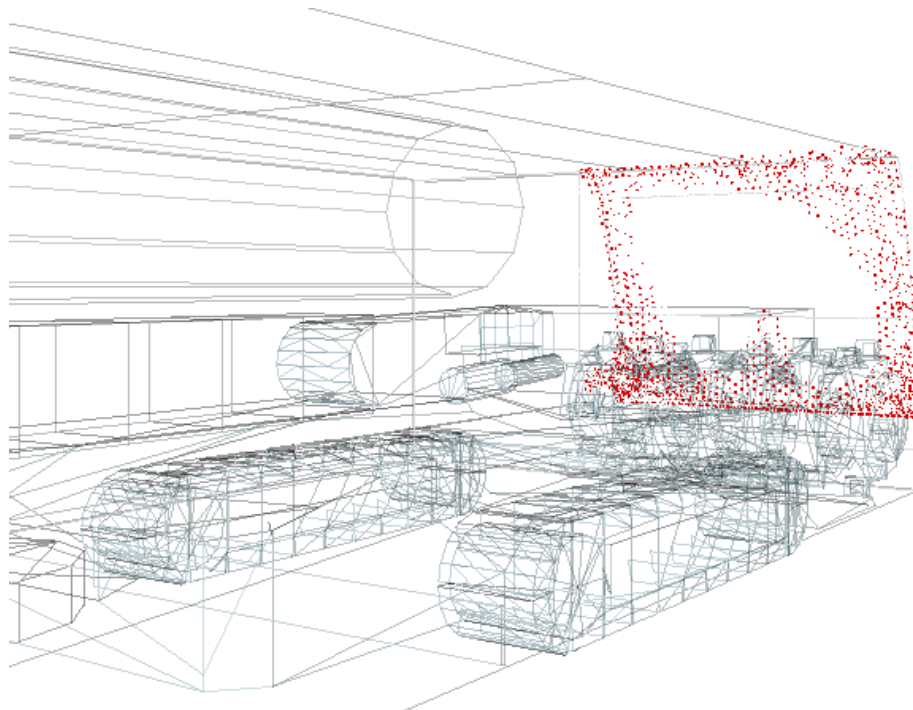


Figure 7.31 Dense random point gas dispersion plot (1%)

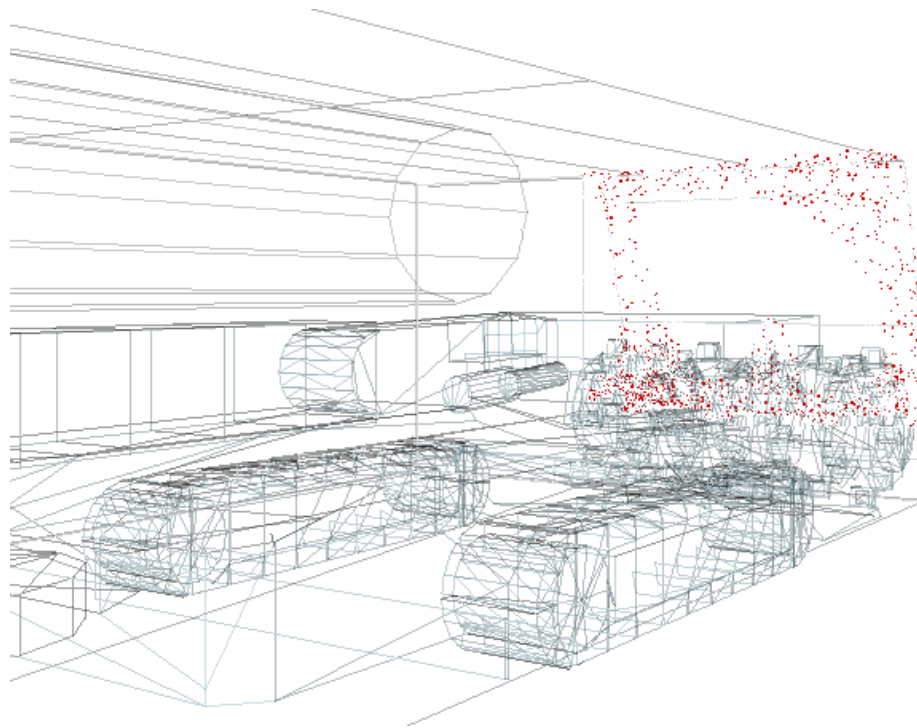


Figure 7.32 Low density random point gas dispersion plot (1%)

#### 7.5.1.4 2D Contouring

For the purposes of producing 2D planar contour representations of the simulation data, the interface was programmed to initially generate a regular 2D grid at specified intervals using the HC scheme. The process used to generate the contours followed a cell-by-cell examination approach. The four values of the data located at the constituent nodal points, delineating each cell, were examined and compared to the threshold values, these could either be input by the user or defined locally or globally by the interface. The points at which the contour lines would cross the cells were defined by a linear interpolation along each edge. These points were used to generate polygon faces using the VRML *indexed face set* node. The polygon faces were coloured according to a linear RGB variable linked scale. The user could specify the number and hence spacing of the contour surfaces.

Figure 7.32 illustrates the flow diagram representing this process. Figure 7.33 illustrates the output of the interface for differing grid densities with a total contour count of 10.

The contours produced by the interface were all associated with low face counts typically less than 500.

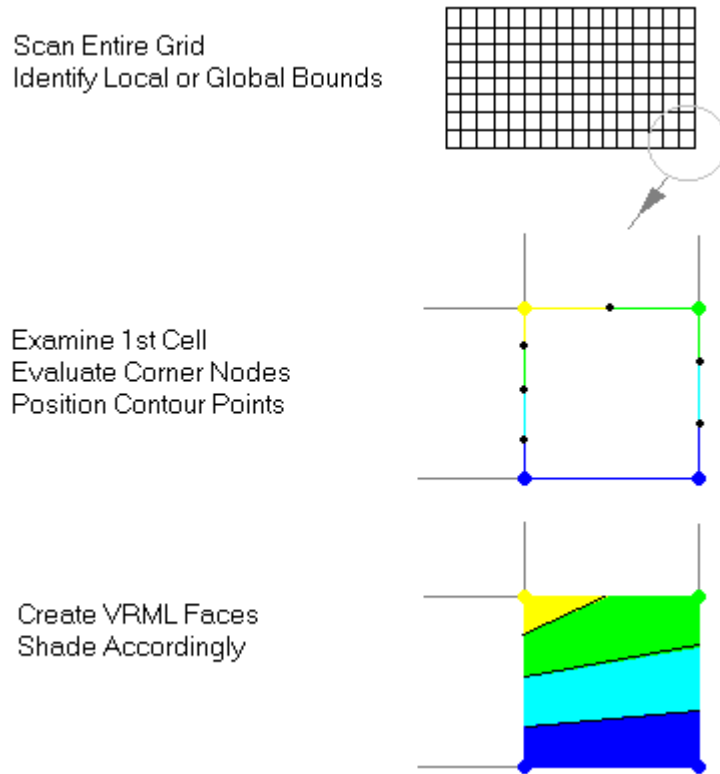


Figure 7.33 2D planar contouring scheme using

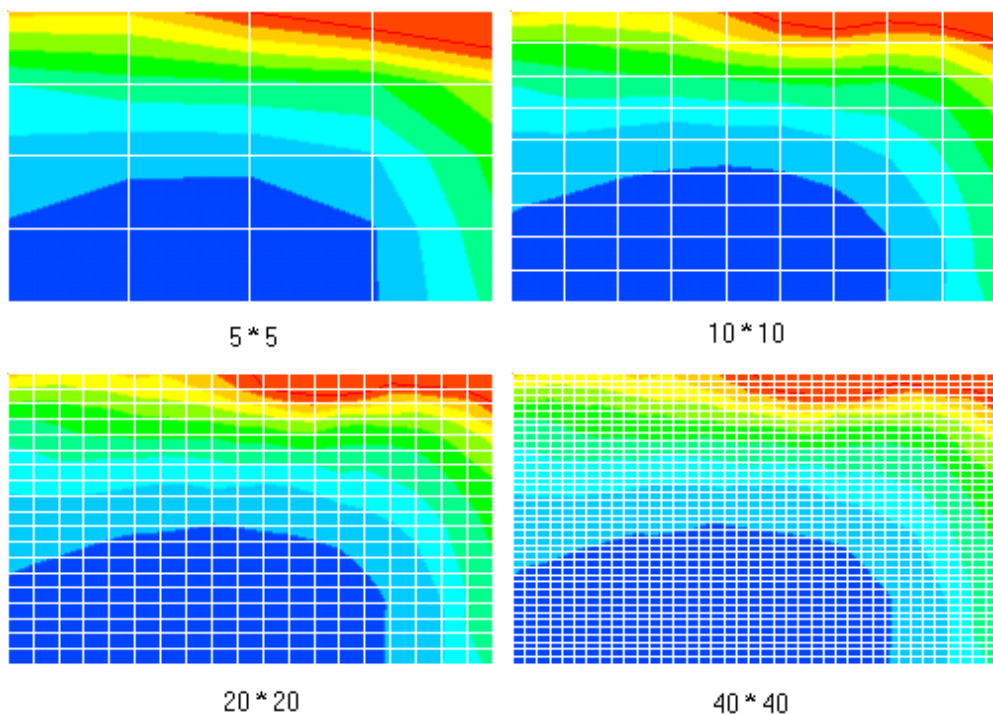


Figure 7.34 Examples of contours produced using VRML displayed with grid detail

### 7.5.1.5 Generation of 3D Isosurfaces

For the purposes of producing 3D isosurfaces, the *Marching Cubes (MC) algorithm* was implemented, which was introduced in Chapter 5. Since the MC algorithm creates a polygon-based isosurface from a structured data source, a regularisation procedure was applied to the original unstructured CM21 mesh data set. For this purpose the VSI scheme was used owing to the susceptibility of the HC scheme to produce errors close to boundaries.

The original case table used by Lorensen (Lorensen 1987) was implemented within the interface. For the construction of the graphical surface the *indexed face set* node incorporated within VRML was used, such that the three constituent points of each triangle plane were associated with the points linearly interpolated from the corner nodes of each cube.

The MC algorithm was not originally developed for the purposes of isosurface creation within volumes which contain internal structures. The medical scanning datasets for which the algorithm was developed were of the form of a continuous 3D block of data. Since the regularised grid will inevitably cause cells to overlap internal geometry areas, in regions where the isosurface wraps an internal geometry, there may be a degree of inaccuracy. Practically, this does not present a visualisation problem as the overlapped region hides these areas. Correction may be achieved through the use of Boolean object subtractions within the 3DStudio Max™ software environment.

Three levels of grid density were tested in order to obtain a balance between visual quality and polygon usage. Incremental increases in grid density were achieved by successively halving the inter nodal distance from 0.25 to 0.125 and then to 0.0625m. The threshold value for the creation of the isosurface was, in all cases, set at the equivalent of 1% general body volumetric concentration of methane gas in air as with the point plots detailed in sections 7.5.1.1-3. The output from the interface utility was combined with a

wireframe and opaque surface VRML™ model of the CM21 configuration simulation data set geometry for clarity. The results obtained are illustrated in figures 7.34-7.36.

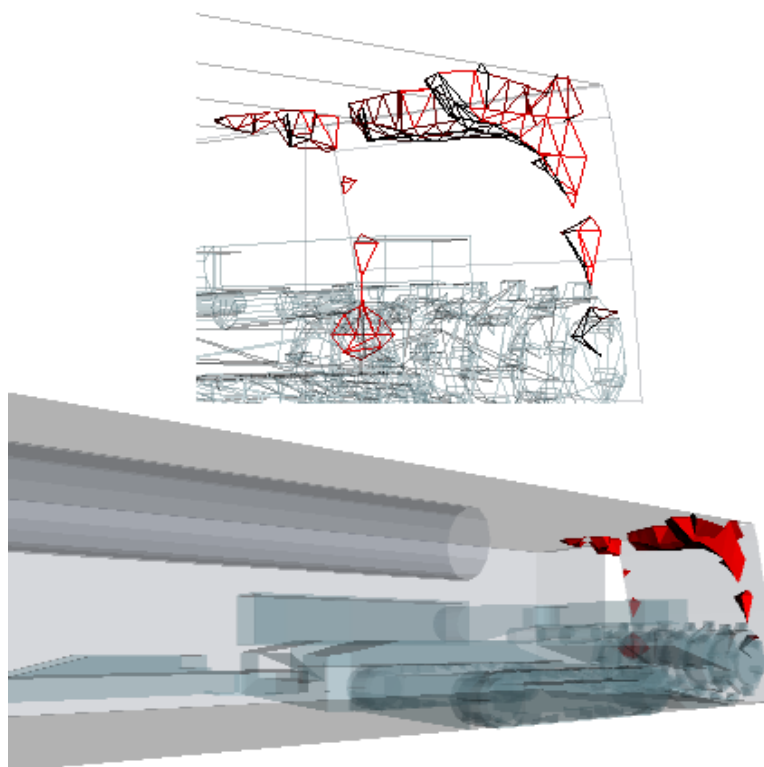


Figure 7.35 MC generated isosurface using coarse 0.25m spacing

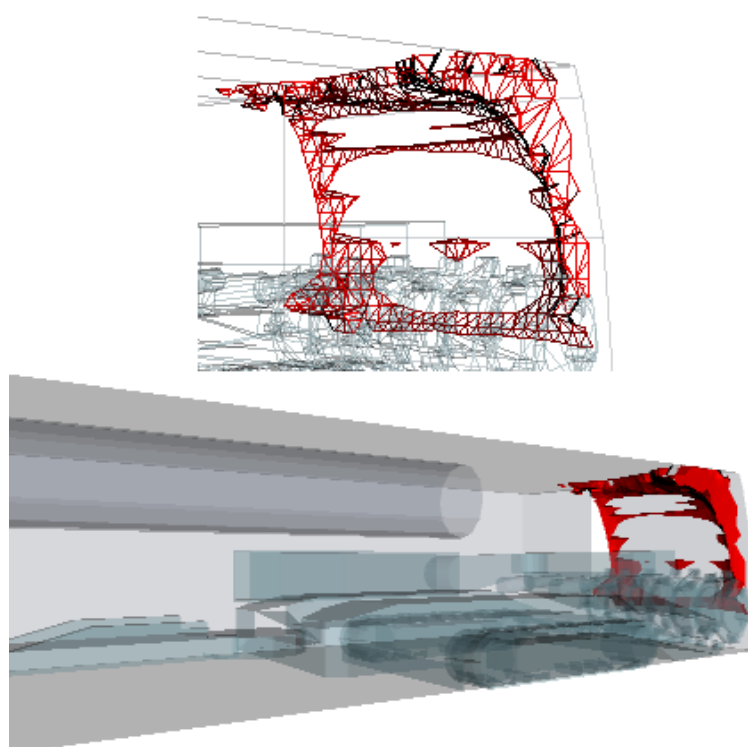


Figure 7.36 MC generated isosurface using 0.125m spacing



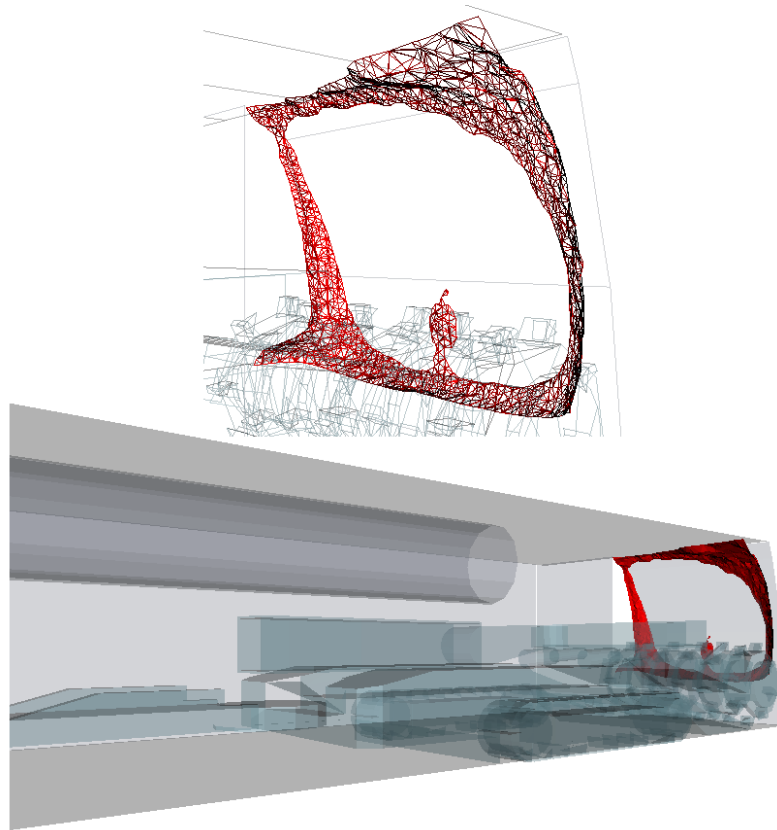


Figure 7.37 MC generated isosurface using fine 0.0625m spacing

On examination of the plots above, it is clear that to obtain a continuous smooth isosurface, a high grid density is required. The low grid density represented in figure 7.34, exhibits severe discontinuities and fails to communicate important areas of methane concentration such as those present directly above the cutting head. It is likely that in this case there are simply too few points at or above the threshold value within each cube to form a triangular facet of the surface.

The medium density grid, represented in figure 7.35, demonstrates clear improvements. This grid density communicates a clearer picture as to the extent and range of the methane concentration and distribution. However, the surfaces are not smooth and continuous, demonstrating several *data* holes and jagged edges. The much higher density grid, represented by the results shown in figure 7.36, illustrates good visual quality. A smooth continuous 3D surface adequately communicates distribution of the gas concentration within the 3D environment. The computational cost is however high, with a polygon face count of 4,803 faces as opposed to 333 &

2215 for the low and medium density grids. This does however compare well to the point plots discussed in the previous sections and is computationally comparable in the context of the other methods discussed.

### **7.5.2 Airflow**

#### **7.5.2.1 Animation of Ventilated Airflows**

In order to recreate the effect of a tracer material being introduced into the flow domain a large number of particles were seeded at the grid points across a locator plane defined at specified regions within the domain. As with the static methane point plots small 2D planes were used in the place of true points for the reasons previously outlined. The interface program was programmed to generate the numerical trace co-ordinates in terms of time. The parameters used for the trace generation were as follows;

- |                        |                        |
|------------------------|------------------------|
| • Interpolation Method | VSI                    |
| • Time Stepping        | Variable Step Doubling |
| • Error Tolerance      | $F = 0.025m$           |
| • Initial Frame Rate   | 5 FPS                  |
| • Lifespan             | 4-10 Seconds           |

All traces were animated within a simplified VRML environment for the purposes of evaluation. Since the focus of the project was to highlight the relationship between airflow and pollutant gas concentration the seed points of these traces were selected according to where in the domain the most critical gas and airflow mixing occurs. Two planes were selected for this purpose. The first was coincident with the outlet of the forcing duct equivalent to that used for the purposes of the trace testing detailed in section 7.4.3. This would indicate to the user the bulk dispersion characteristic of the airflow issuing from the forcing duct. The second locator plane was positioned in the region of the cutting face 0.1m from the

face itself. Both planes are depicted in figure 7.37 in the context of the CM21 configuration simulation data set for clarity.

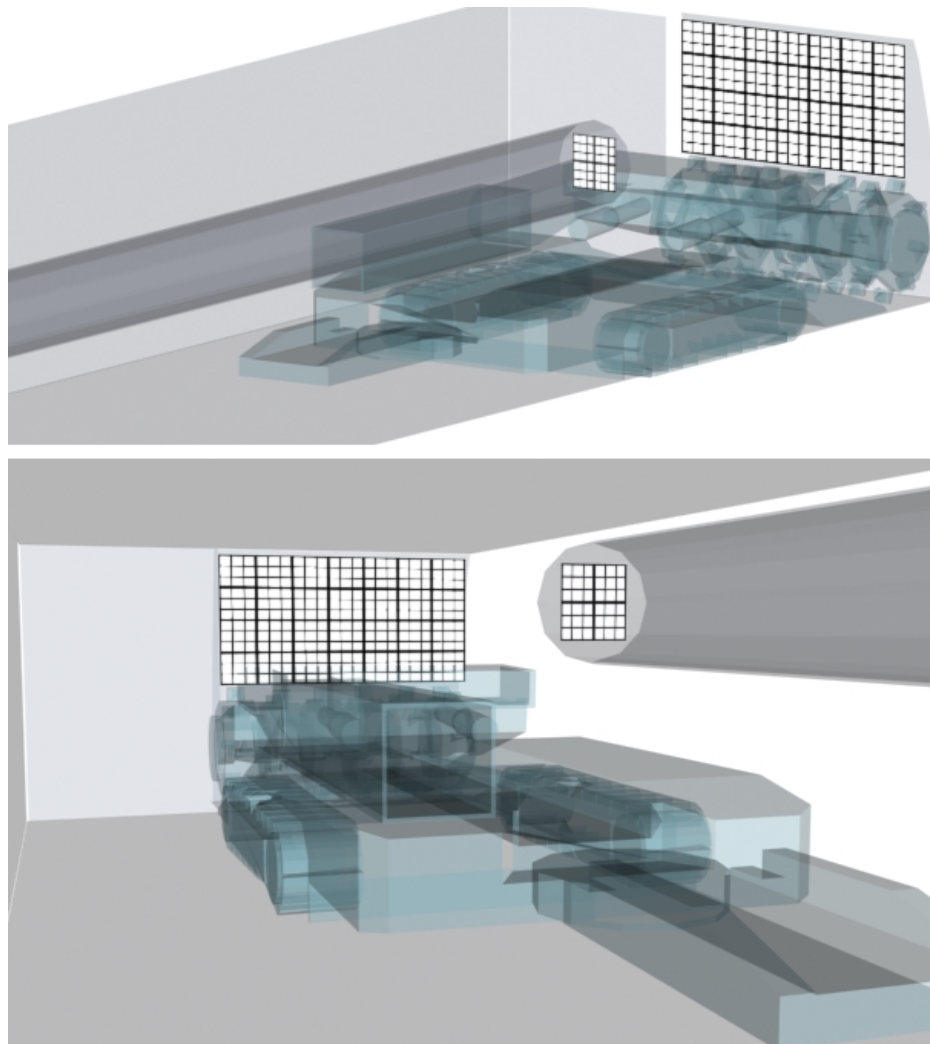


Figure 7.38 Seed point planes used for particle stream animation

The locator plane positioned adjacent the face cutting region was used to represent direct face ventilation thus the lifespans were relatively short (4 seconds). The locator plane positioned at the duct would be required to trace the airflow throughout the domain hence a longer lifespan of 10 seconds was used for the traces. A pulse function was incorporated into the interface utility such that particles could be released from the same position at a fixed release rate. This was intended to produce a line of particles originating from each seed point at specified intervals such that a greater appreciation of the form of the streamline could be gained. It was found that releasing single particles communicated limited information with regard to both the bulk and

specific flow characteristics within the heading. By pulsing the particle releases 5 times a short trace history could be observed at any point in the trace allowing the visualisation to be paused at any stage and studied by the user (figure 7.38).

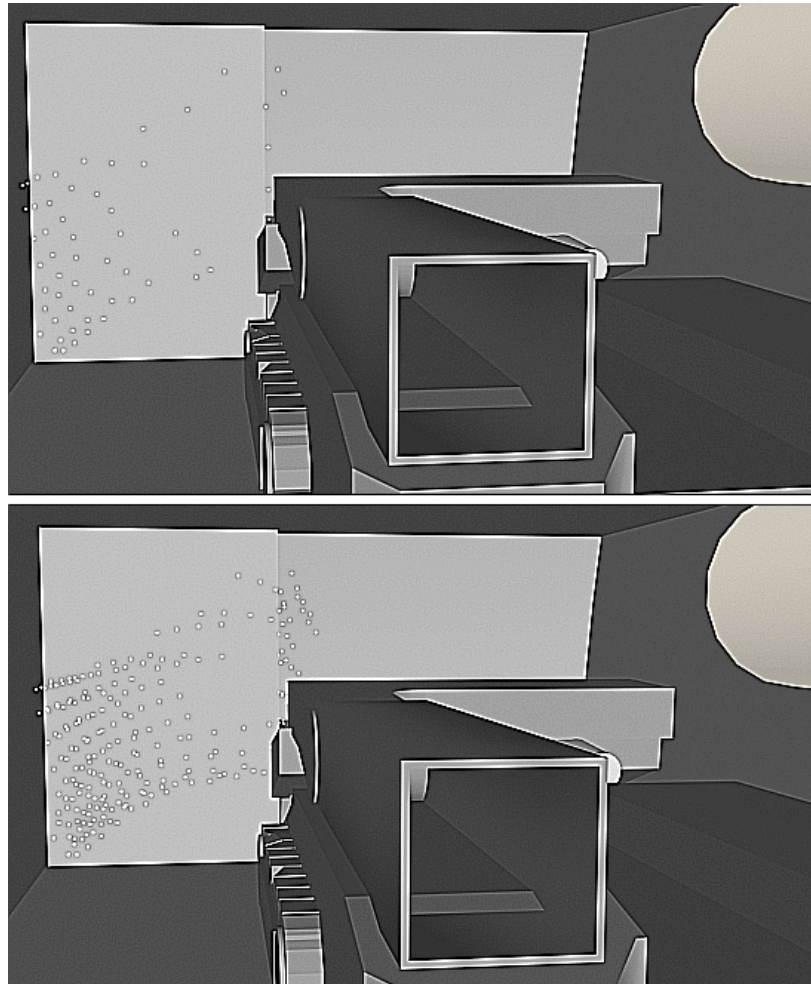


Figure 7.39 Single (above) and pulsed (below) duct particle animations

However, this approach does reduce the effective grid spacing to the number of particle added at each pulse. This procedure was not required for the face locator traces since the objective of this trace was to illustrate the dispersion characteristic caused by the face ventilation airflow rather than airflow direction itself. Figure 7.39 illustrates the results of the face locator trace over four time intervals demonstrating how the face dispersion characteristic is visualised.

Although the polygon face counts were typically low (less than 1,000) the animation of each individual face along an independent trajectory placed high demands upon the rendering hardware.

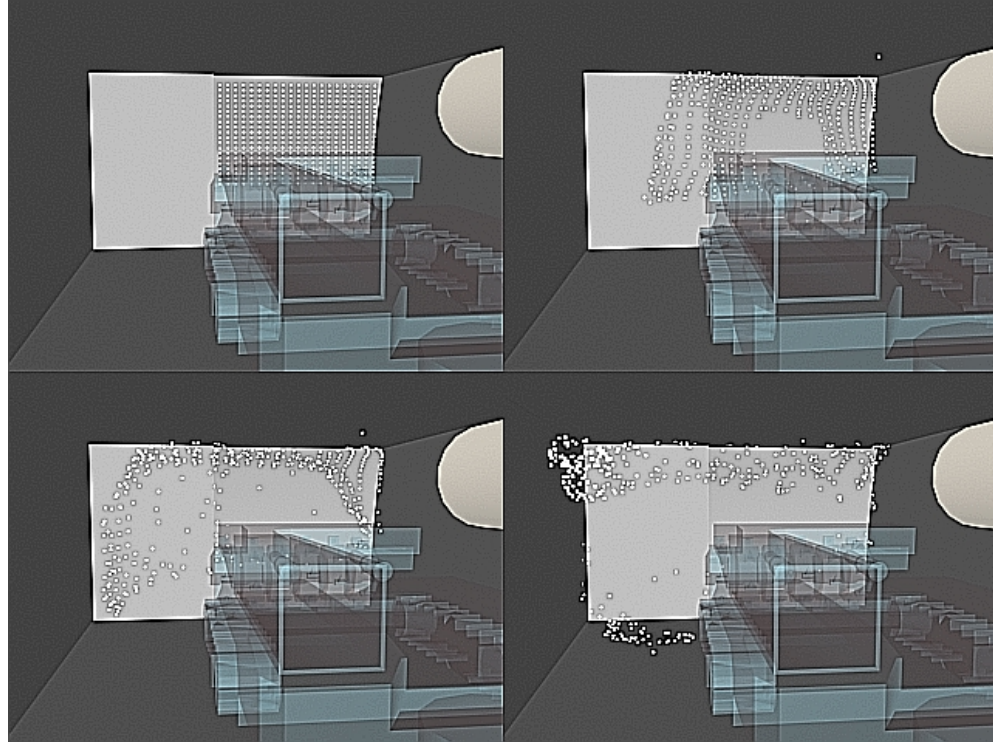


Figure 7.40 Face seeded particle animations at four time intervals

By performing a series of parametric studies, that considered variations to, the pulse rate, the number of particles, grid densities and trace lifespan, the following blend of parameters were found to provide a good balance between visual quality and the ability of the hardware to maintain an interactive frame rate.

- Face Seed Grid
  - A mesh grid of 24 X 24 seed points
  - A trace life span of 6 seconds
  - The use of a single release pulse

- Force Duct Outlet Seed Grid
  - A mesh grid of 24 X 24 seed points
  - A trace life span of 8 seconds
  - The use of a five consecutive release pulses

The animated particle trace visualisations proved useful in providing a real time visualisation of the ventilation characteristics. The number of particles was found to be limited to around 700 if interactive frame rates were to be maintained.

#### 7.5.2.2 Streamline Generation

In addition to the dynamic animated airflow visualisations, the particle traces were also used to create a static streamline based upon the trajectory and lifespan of each of the traces. This approach was only applied to the longer lifespan traces produced from streamlines issuing from the locator plane at the outlet to the forcing duct. This was due to the fact that at the later stages of the trace lifespan some of the particles were observed to diverge and scatter to such an extent that the visualisation lacked meaningful interpretation. Since the lifespan of the traces generated at the face locator were relatively short and the velocities low, the particle animations produced coherent visualisations.

The streamlines were constructed by extruding a 2D plane normal to the trajectory along the entire length of its lifespan. The *indexed line set* node could not be used since SAFEVR™ did not at the time support this display mode. The number of traces displayed was reduced to 25, as higher numbers cluttered the display, which might adversely affect interpretation. The polygon count employed for the 25 traces was in the region of 150,000.

Figs 7.40-7.43 illustrate some of the visualisation views produced through this method in the context of a VRML™ model.

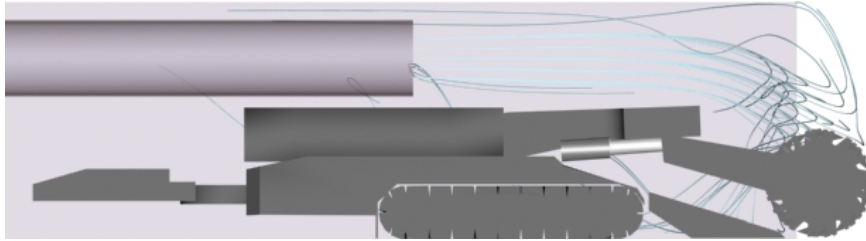


Figure 7.41 Side view duct seeded extruded streamlines

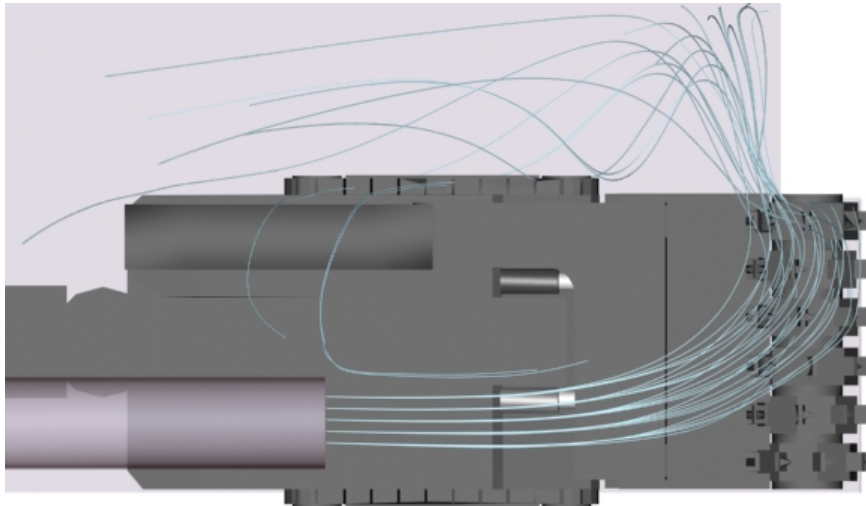


Figure 7.42 Plan view duct seeded extruded streamlines

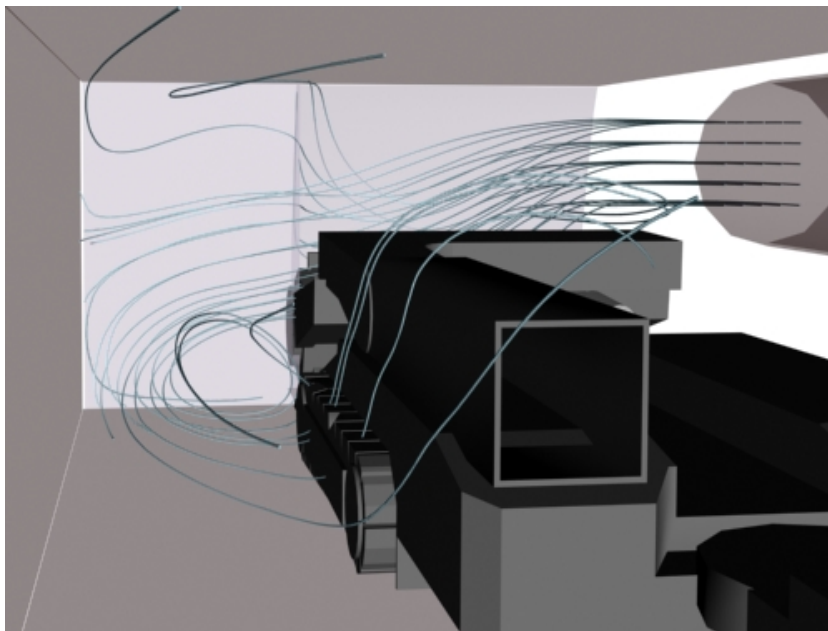


Figure 7.43 Internal view (1) duct seeded extruded streamlines



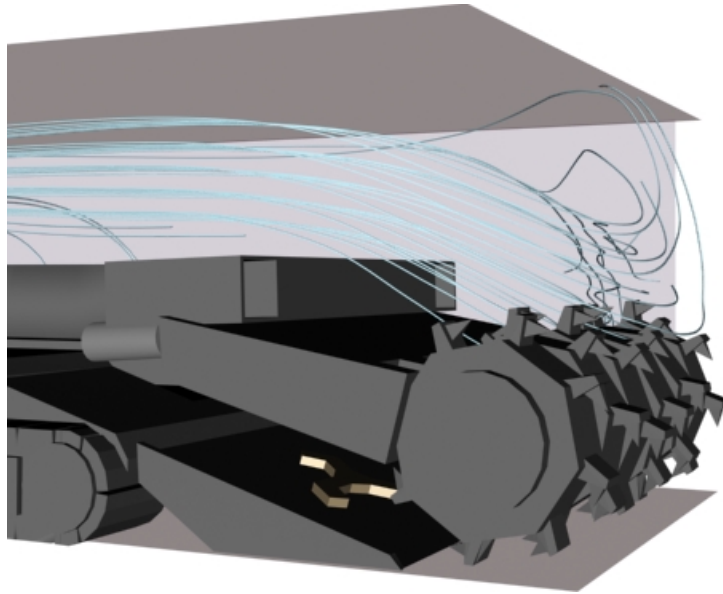


Figure 7.44 Internal view (2) duct seeded extruded streamlines

The prohibitively high polygon count was a direct result of the high number of time steps taken to maintain an error tolerance of 0.025m. This process is illustrated in figure 7.44.

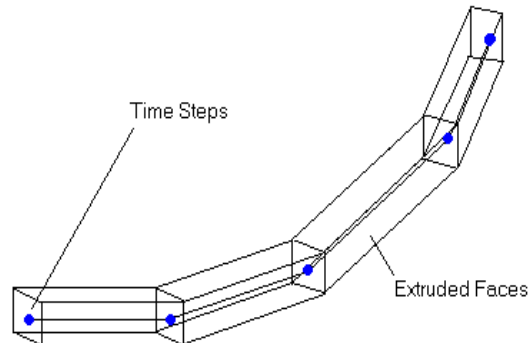


Figure 7.45 Stream line extrusion face construction process

## 7.6 Final Definition of Interface Capabilities

In addition to the specification of the upstream numerical processing capability of the interface detailed in Section 7.3 of this Chapter, the graphical functionality of the interface is summarised in the flow diagram depicted in figure 7.46.



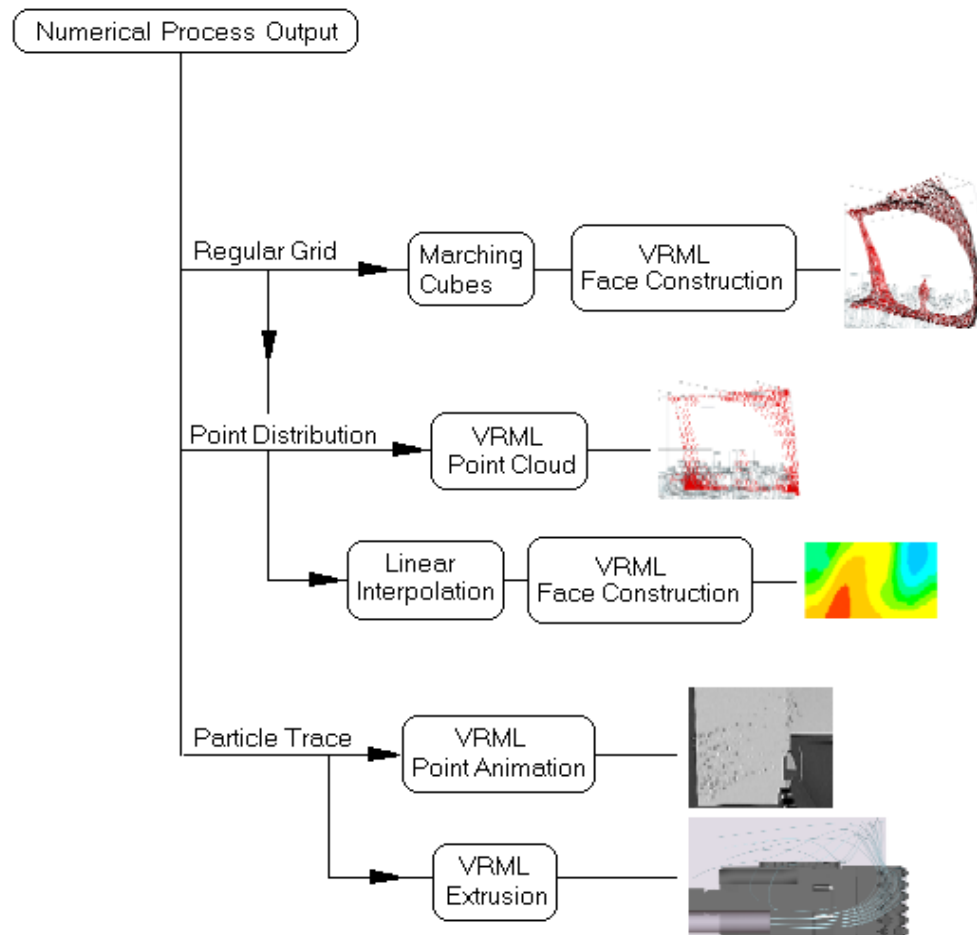


Figure 7.46 Final definition of interface capabilities and graphical output

## 7.7 Summary

This chapter has covered the work undertaken to test and evaluate the approaches available for the visualisation of 3D flow data and the production of computationally efficient visualisations specifically suitable for display within interactive 3D environments. This section has summarised the results of the exercises performed to identify the optimal combination of computational and graphical components to be included in the development of the interface utility.

The performance of each computational algorithm considered, was compared against that of a chosen standard method. All of these evaluation exercises used a single representative data set to enable the performance to be judged against a common reference point.

The results of the residual error analyses conducted were used to highlight the advantages and disadvantages of each of the numerical approaches. It was concluded that schemes of limited analytical complexity such as the HC interpolative scheme performed well for static data plots, when judged on the basis of perceptible error. For dynamic plots the limitations of the HC scheme were demonstrated and the superior qualities of the VSI scheme were manifested in the production of visually higher quality plots.

The graphical form of display glyphs was also evaluated in terms of visual impact and computational efficiency. A variety of methods including point plots, 2D contouring and 3D isosurfacing were evaluated for the purposes of methane concentration visualisation.

The chapter has provided an in depth evaluation of post processing procedures that formed the basis for the final specification and construction of the application. The analysis performed has served to both quantify the degree of numerical and visual error inherent in CFD data visualisation, and identify methods suitable for minimising the impact of such errors. These optimum methods available within the interface utility were used to the construct the CFD visualisations present within the VR training application detailed in the following chapter.

## **CHAPTER 8**

### **APPLICATION DESIGN & DEVELOPMENT**

#### **8.1 Introduction**

This Chapter summarises the results of the research work undertaken to complete the design and development of the final integrated CFD and VR prototype training application. The process of the specification, design and construction of this application, is built on the foundation of both the results of the evaluation studies presented in Chapter 7 and the components of the interface programme identified in Chapter 8.

The introductory sections detail the specification and design of the application, which employs a comprehensive library of CFD simulation model data to replicate the wide range of ventilation and methane concentration patterns that may occur within a representative rapid development drive. The precise specification of the various CFD models used to simulate the ventilation and pollutant dispersion data, at the various stages of the cutting cycle within the heading was provided in Chapter 8, section 8.4.1. Amongst the various scenarios available within the CFD simulation data library, are a number that model the occurrence of a potential ventilation hazard and allow a range of potential remedial measures to be explored.

This Chapter details the two development phases used to construct the VR application. All elements of the process are detailed including the post-processing of the CFD simulation data, the VR world building, the representation or animation of the simulation data within the virtual world, and the design and implementation of the Interactive Expert Control System (IECS). The IECS employs the visual logic language implicit within the SAFEVR™ simulation builder application.

The first phase of development includes an evaluation of the application and a number of conclusions are drawn, upon which the second phase of the application development was built.

The operation of the prototype training application is illustrated using an extensive range of computer screen shots. The Chapter concludes with a section that discusses the performance of the application with respect to the original requirements and the specifications detailed in Chapter 7.

## 8.2 Outline of the Development Process

The development of the final VR application was comprised of a number of separate stages. The flow diagram illustrated in figure 8.1 details the intermediate products delivered at each stage, and places them in context of the whole development process. The process begins from the selection of a particular simulation scenario from the available library of CFD model data. Once the scope of the application had been mapped, dictated by the range of simulation exercises available from within the CFD data library, there was no further inter-dependence between each of the remaining stages of the development process. This enabled each stage of the processes to be conducted in any order or in parallel.

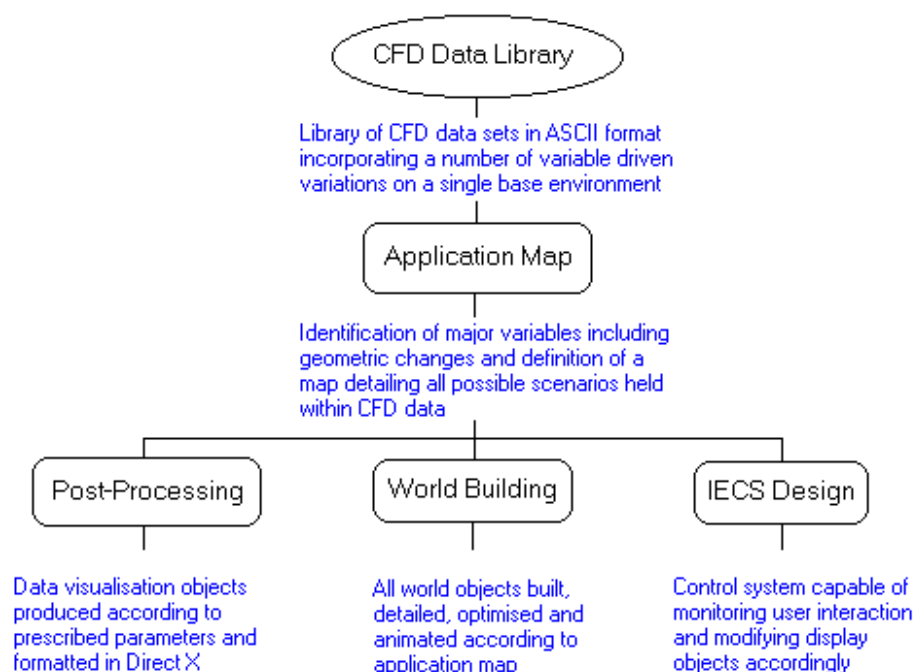


Figure 8.1 Outline development procedure flow diagram

The procedures, illustrated in Figure 8.1, outline all the stages involved in the construction of the application. Two commercially available applications were employed, 3DStudio Max™ for world building and SAFEVR™ for the purposes of simulation building. The third application necessary was the post-processing interface utility, developed as part of this research project.

## 8.3 CFD Data Library Specification

### 8.3.1 Data Library Map

The initial range of CFD simulation data was available from the published results of a previous research project (Hargreaves et al (2000)), summarised in Chapter 8, Section 8.4.1. The range of different mining and ventilation configurations within this simulation data library is depicted in figures 8.2 & 8.3.

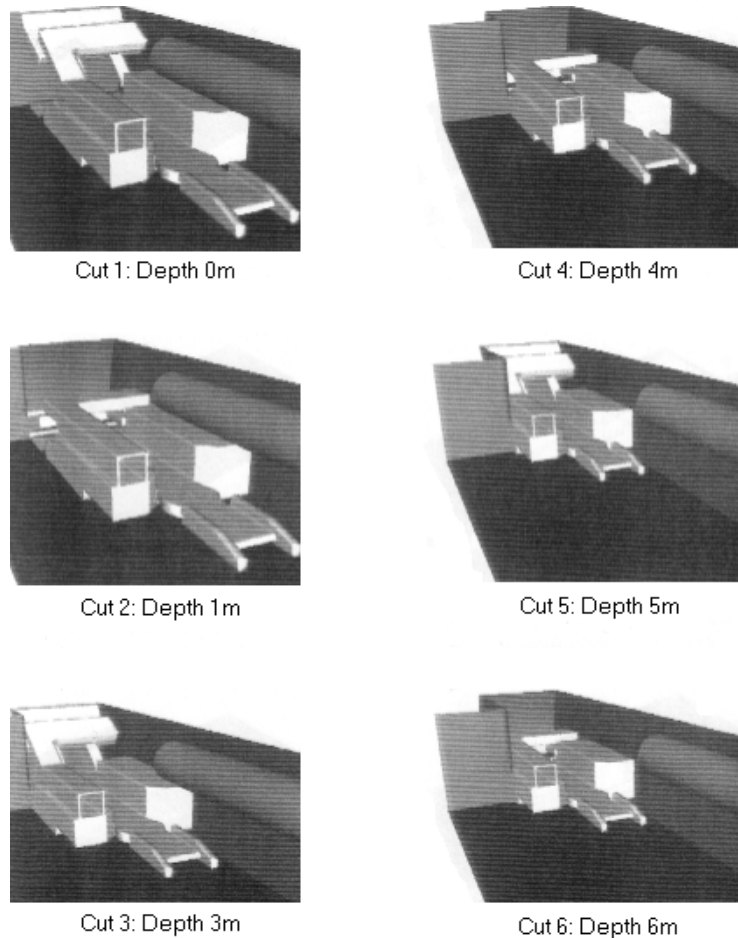


Figure 8.2 Operator side CFD data model representation (Hargreaves et al 2000)

For each of the twelve cutting stages, two ventilation simulation exercises were performed, one with the exhaust scrubber operating the other with the exhaust scrubber fan off. This provided a total library of 24 CFD simulation data sets. A more detailed discussion is also provided in this thesis in Chapter 4, Section 4.8.4.

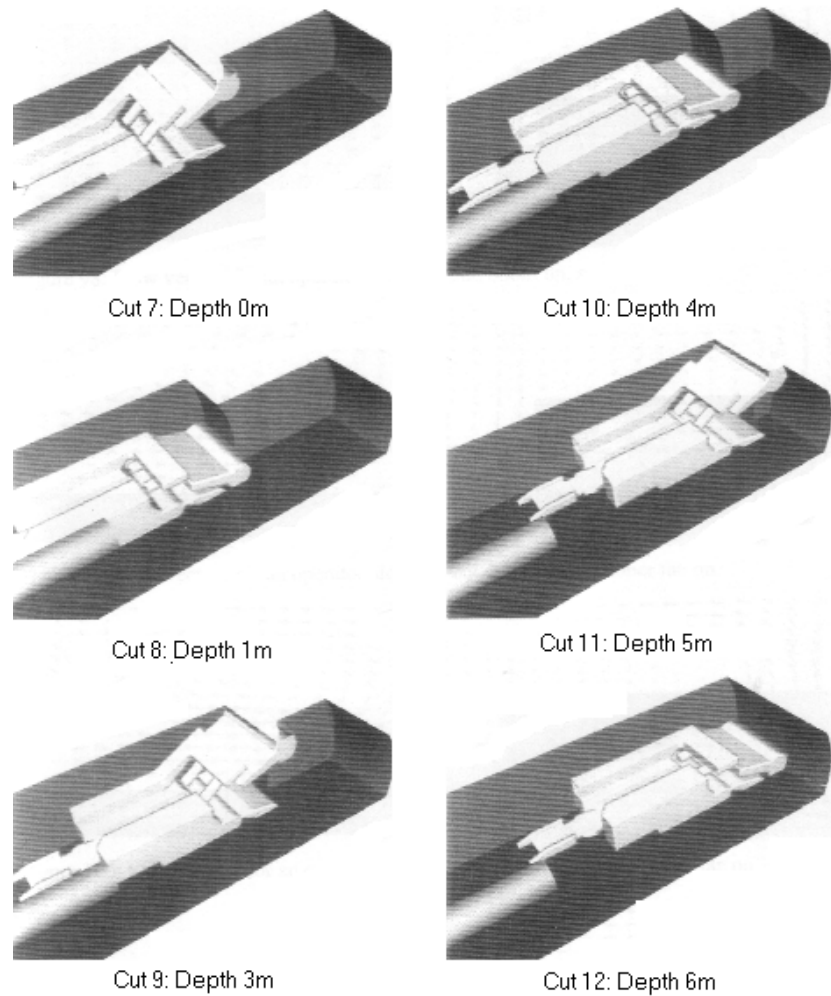


Figure 8.2 Buttock side CFD data model representation (Hargreaves et al 2000)

### 8.3.2 CFD Model Parameters

Hargreaves et al (2000) used a single base model to calibrate the CFD parameters and the mesh sensitivity. The parameters used for the CFD models were identified as follows.

- Turbulence Model
  - The standard k-e turbulence model was employed

- Carrier Fluid
  - Air was employed as the carrier fluid
  - The viscosity of the air was set at  $1.725 \times 10^{-5}$  kg/m/s
  - The density of the air was set at 1.284 kg/m<sup>3</sup>
- Wall Roughness
  - The depth of the wall roughness function was set at 0.05m

### 8.3.3 Classification of Variables

The data library was classified in terms of the variables used to generate the 24 individual data sets. Each cut cycle model consists of 6 cut sequences, which in reality may be viewed as 3 pairs, as each of the two raised or lowered positions of the cutting boom, only slightly increases or decreases the cut depth. Figure 8.4 depicts a record tree representing the structure of

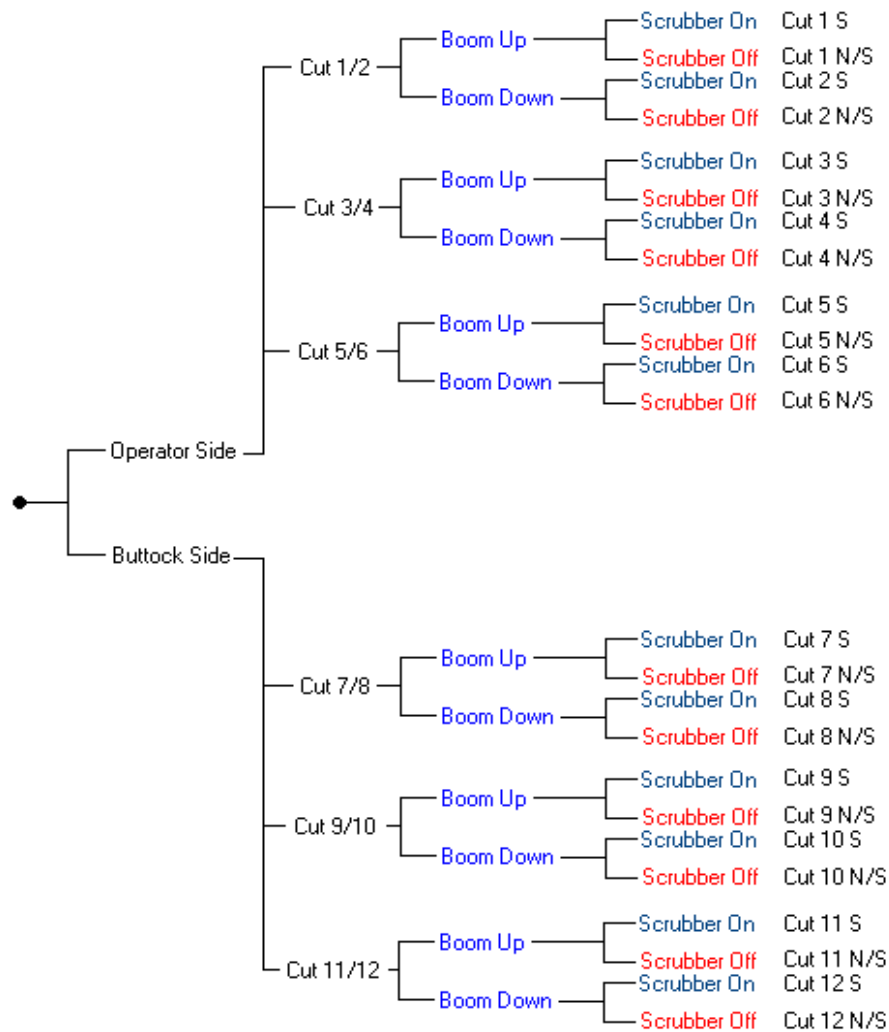


Figure 8.4 CFD data library

the data library in terms of the available geometric and boundary variables, and data set classification.

This tree representation of the data library is indicative of the range of possible simulation scenarios the user could employ using the CFD data library. A variation in the mining or ventilation configuration is enacted by a change to the three major variables, the boom position, the exhaust scrubber fan power and the cut depth.

#### *8.4 The Identification and Classification of the Potential Hazards*

A *potential hazard* is defined by this study, to be those events present within the rapid development driveage that can directly influence the mechanism of airflow delivery and/or methane emission pattern. The CFD data simulation library, contained variables that described both the airflow and methane concentrations at fixed points within the flow domain. Thus the focus of the study of hazards using the application, was on those variables within the CFD models that directly or indirectly influence the effective delivery of the ventilation air and the resultant mixing and dispersion of any methane within the driveage. The degree of dilution of the methane emitted, was represented by the general body concentration calculated at each nodal point in the domain.

A literature review of previous studies of the application of VR to industrial training applications concluded that these investigations were concerned with identification of physical hazards, such as the proximity of workers to mechanical equipment or to procedural factors. The primary objective of this investigation was to extend this approach to develop an application, to permit the study of the potential environmental hazards associated with the operation of auxiliary ventilation systems within rapid development drivages.

A major educational benefit afforded by the ability to simulate potential environmental hazards, is the facility to both visualise the *cause* and *effect* of



a hazard. The cause of a hazard may be created due to a non compliance with an operational procedure, or the failure/damage to an environmental monitoring transducer or ventilation fan or ducting. The hazard may be manifested as a reduction in the fresh air delivered to the face of the heading, due to a puncture in the duct further outbye or deterioration in fan performance. The effect produced in this case, would be a significant increase in the methane concentration experienced in the vicinity of the cut. The coincidence of a critical gas concentration (methane 4-15% general body concentration) and a source of ignition may result in a flame or explosion. Consequently, any mechanism that results in a reduction in the fresh air supply delivered to the face and/or an increase in the methane emission may be termed a potential hazard.

This approach enables the user to gain an appreciation of the influence that certain crucial environmental and system variables may have on the methane dilution and removal within the environment, and helps establish a clear educational link between the cause and effect in terms of the creation of a potential atmospheric hazard.

## **8.5 Phase One Simulation Construction**

### **8.5.1 World Building**

The VR environment was constructed in its entirety within the commercial world building application, 3DStudio Max™. The world was designed to offer as realistic a representation of a typical rapid development drivage as possible, to enable the user to navigate and interact naturally within the world, as they would within such a heading underground. This required the specification of a high level of geometric accuracy and texture detail. Since the world is also required to act as a context within which CFD simulation data is displayed, the world also was required to be coincident with the physical boundaries defined within the CFD model. CFD models often do not recreate the real world geometry to a high level of detail, since the level

of geometric detail required by the CFD model is that which exerts a tangible effect on fluid flow modelled. The inclusion of any further detail is superfluous in the context of a CFD analysis, since influence upon the flow field is minimal. In addition, the inclusion of small geometric details greatly complicates the meshing process, which may lead to significant increases in mesh densities, and consequent increases in both processing and memory storage requirements. Although satisfactory for the purposes of performing a scientific CFD analysis, the 3D model used for the initial CFD simulations was primitive by the standards of 3D VR modelling, where high levels of detail are expected. The immersive VR model was therefore created using the CFD geometric boundaries as a template. This included the drivage walls, the ducting and the CM itself. The geometry file used for the CFD models was exported from CFX v5™ into an IGES format and imported into 3DStudio Max™ whereupon the VR recreation was constructed around the original IGES geometry. From this point the model environment was detailed. Care was taken to ensure that any additional physical geometrical details added to the VR model did not alter the boundaries significantly since this would detract from the CFD visualisations ability to replicate the true flow and concentration fields within the environment. This is of particular importance with dynamic flow animations since the particles often move in close proximity to the boundaries thus any inaccuracies would become

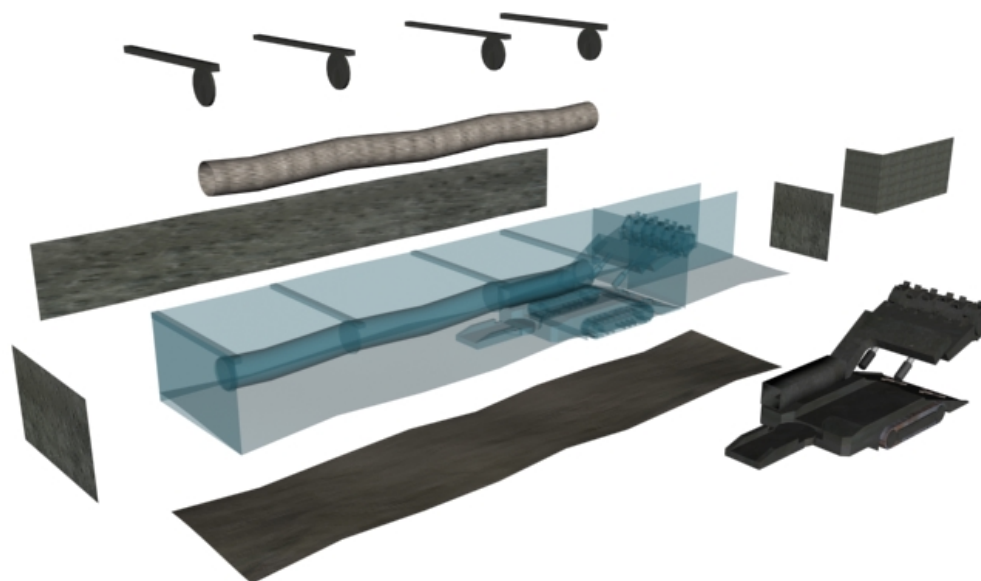


Figure 8.5 Constituent 3D model parts

immediately apparent to the user. Figures 8.5 & 8.6 illustrate the model construction and a comparison between the final detailed VR models constructed within the application, and the original CFD model geometry. Details of the textures employed are included in Appendix III. In addition, an optional opaque version of the CM machine was included to enhance the visual clarity of the airflow and resultant methane concentration viewed within the VR world representation of the drivage.

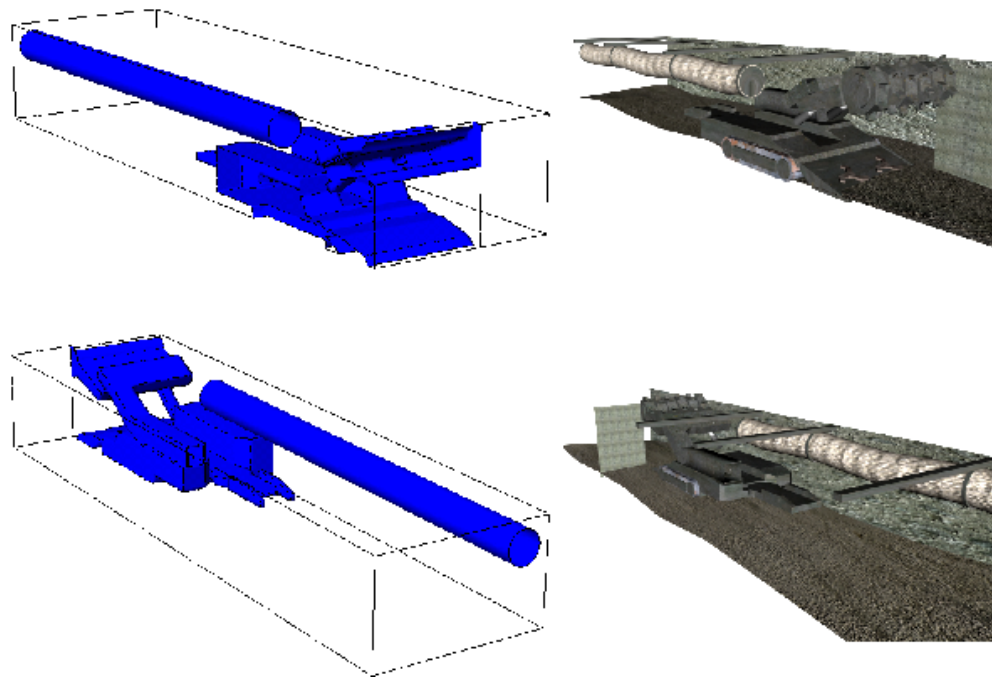


Figure 8.6 CFD geometry (left) and detailed 3D representation (right)

### 8.5.2 Animation Map

At the outset of the project, it was anticipated that due to the limitations imposed by the specification of the hardware available, (Chapter 8, Section 8.3), that there would not be sufficient capacity with which to enable the complete range of data library simulations to be included within the application. For this reason, the first phase of the development of the application concentrated upon the replication of the ventilation and methane dispersion patterns experienced during the extraction of the main operator side cut only.

The VR world created for the simulation was animated in accordance with the precise boundary changes demonstrated within the CFD data library. For each side of the cut executed, this included the steady state simulation of the two boom orientations, and three main cutting depths. The animation was therefore mapped from Cut 1 to Cut 6 accordingly as depicted in figure 8.7.

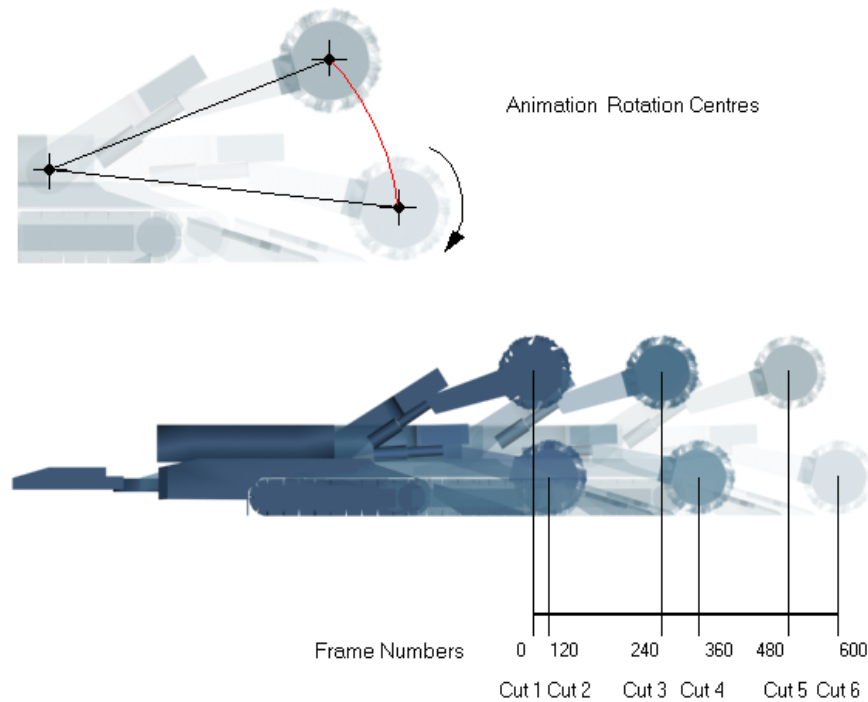


Figure 8.7 CM animation detail and

For all of the animations processed a default frame rate of 30FPS was used. Since the CFD data library consisted of a series of steady state simulation data sets, the animation of the movement of the equipment between each cutting stage was included purely for the purposes of realism. The animations included the rotation of the cutting head, and the raising and lowering of the cutting boom. Each animation was given a reference such that the geometric variables could be reconfigured according to a frame number. The animated movement of the CM between each cut stage was included purely as aesthetic detail, as there was no transient flow and pollutant dispersion data was available.

The change in the drivage walls were animated to represent the advance of the cut, in accordance with the boundaries of the CFD model and moved in tandem with the movement of the CM machine as illustrated in figure 8.8.

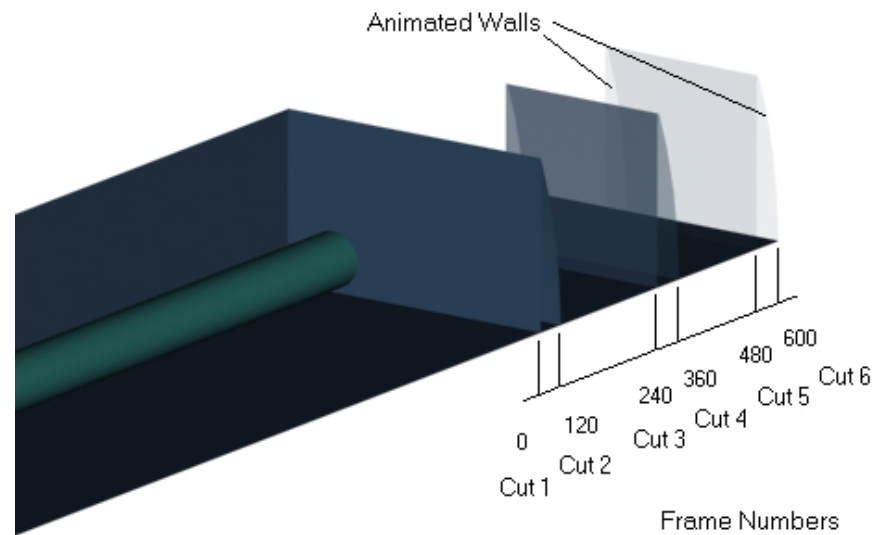


Figure 8.8 Drivage animation detail and frames

### 8.5.3 The Post-Processing of the CFD Simulation Data

Visualisation objects were created using the interface utility developed specifically for the task. Isosurfaces and animated particle traces were generated as described in Chapter 8 with considerations detailed in the following sections.

#### 8.5.3.1 Selection of Visualisation Graphical Form

For the purposes of animated particle traces the procedure outlined in Chapter 8 was employed. For the purposes of isosurface creation, one threshold level was used in the creation of each isosurface for each data set. UK coal representatives had stated favour towards a colour-graded visualisation for the purposes of the display of methane concentrations. This enabled the display of more detailed technical data and increased the ability of the application to communicate methane dispersion characteristics. Since

the use of particle clouds had been precluded through the evaluation carried out in Chapter 8, it was decided to initially use single isosurfaces representing a 1% general body concentration of methane in air. This would allow the future incorporation of further graded threshold ranges of methane concentration isosurfaces should the hardware capacity be enhanced.

#### **8.5.3.2 Visualisation Parameters**

The following parameters were used for the generation of visualisations from the CFD data simulation library.

- Particle Traces
  - Particle traces were generated in the region of the forcing duct outlet and face cut region. The duct traces were seeded on a 10 X 10 regular grid central to the duct, using a total of 121 seed points repeated over 5 pulses for a particle trace life span of 8 seconds. The face traces were seeded on a 24 X 24 regular grid, using 625 seed points for a single pulse, for a particle trace life span of 6 seconds.
- Isosurfaces
  - Isosurfaces were generated for the display of steady state methane concentration clouds, employing, three graded threshold values representing a general body concentrations of 1% (upper threshold limit), 0.5 % and 0.25 % methane in air. Each of the three isosurfaces was coloured red, orange and green, respectively. Each isosurface was displayed at a 40% opacity level to assist clarity.

### **8.5.4 Interactive Expert Control System (IECS) Design**

#### **8.5.4.1 Specifications**

The following specifications were outlined for the purposes of the design and implementation of the IECS, which was constructed using the SAFEVR™ visual logic language.

The IECS provides a user interface with which to select a particular configuration of the VR world environment, in which to view a particular simulation.

- User Control
  - To facilitate user control of and interaction with the VR world environment, it was specified that the user should be able to perform the operator side cut, proceeding from the initial face to the final depth of the cut.
- Scientific Data Visualisation
  - The user on request could view an individual or sequences of pre-processed visualisation scenarios, stored within the simulation library.
- Tracking
  - To ensure that the application would display the correct sequence of visualisations, the IECS was designed to track the scenarios requested by the user. This was accomplished by the assignment of 'flags' to each configuration such that the correct visualisation(s) could be displayed automatically.

#### **8.5.4.2 IECS Decision Making Process Map**

The three key decision making processes embedded within the construction of the application are illustrated in figure 8.9. below.

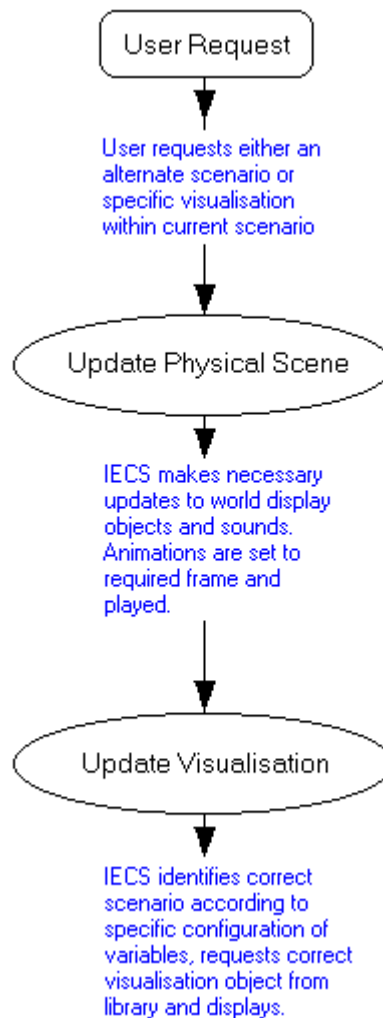


Figure 8.9 IECS design outline

For each of the three key stages, a network was created using the visual logic operators within the SAFEVR™ simulation builder. The number of objects stored within the application largely determines the size of each network, since each object requires its own branch and unique series of decision processes.



The largest network capacities are required on the generation of a visualisation update, since the visualisation library contained the greatest number of possible display objects. The implementation of a user request to update a physical scene configuration is by comparison relatively simple, since these deal with a smaller number of objects representing the physical environment. An example of a network that represents a user request is illustrated in figure 8.10.

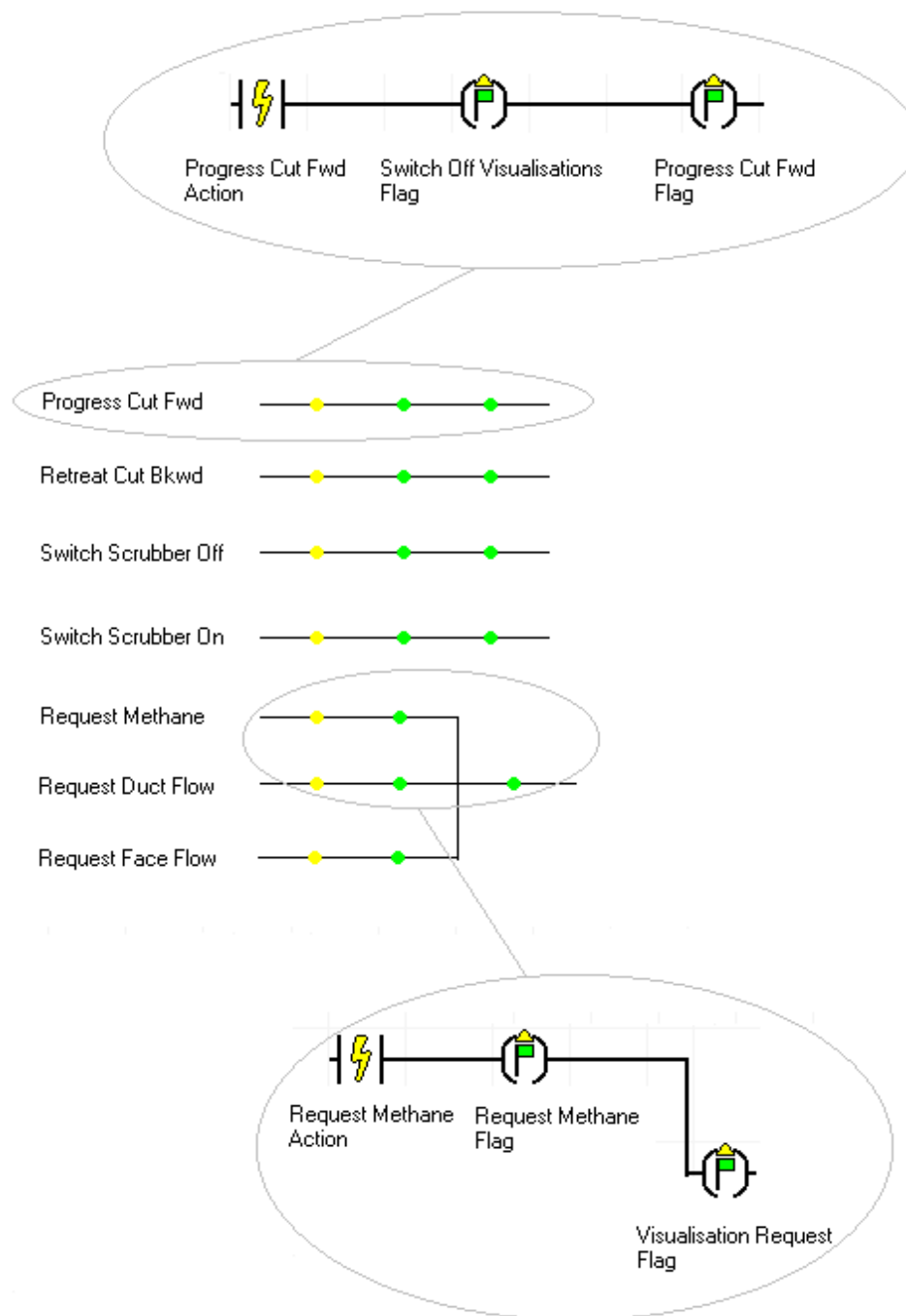


Figure 8.10 User request control paths

The user may choose to select in turn, one of a total of seven available interactions within each simulation scenario; three visualisations and four configuration changes. Each action requested switches on a corresponding flag on the governing logic tree. For example, in the case of a physical advance of the face cut and/or the associated movement of the CM machine, the resultant flag(s) are then passed to the physical world update stage. However, as the activation of the exhaust scrubber fan and the associated visualisation request require no physical changes, these flags are passed directly to the update visualisation stage. The logic tree governing both the physical world update and visualization stages associated with the advance of the CM machine cut is illustrated in Figure 8.11.

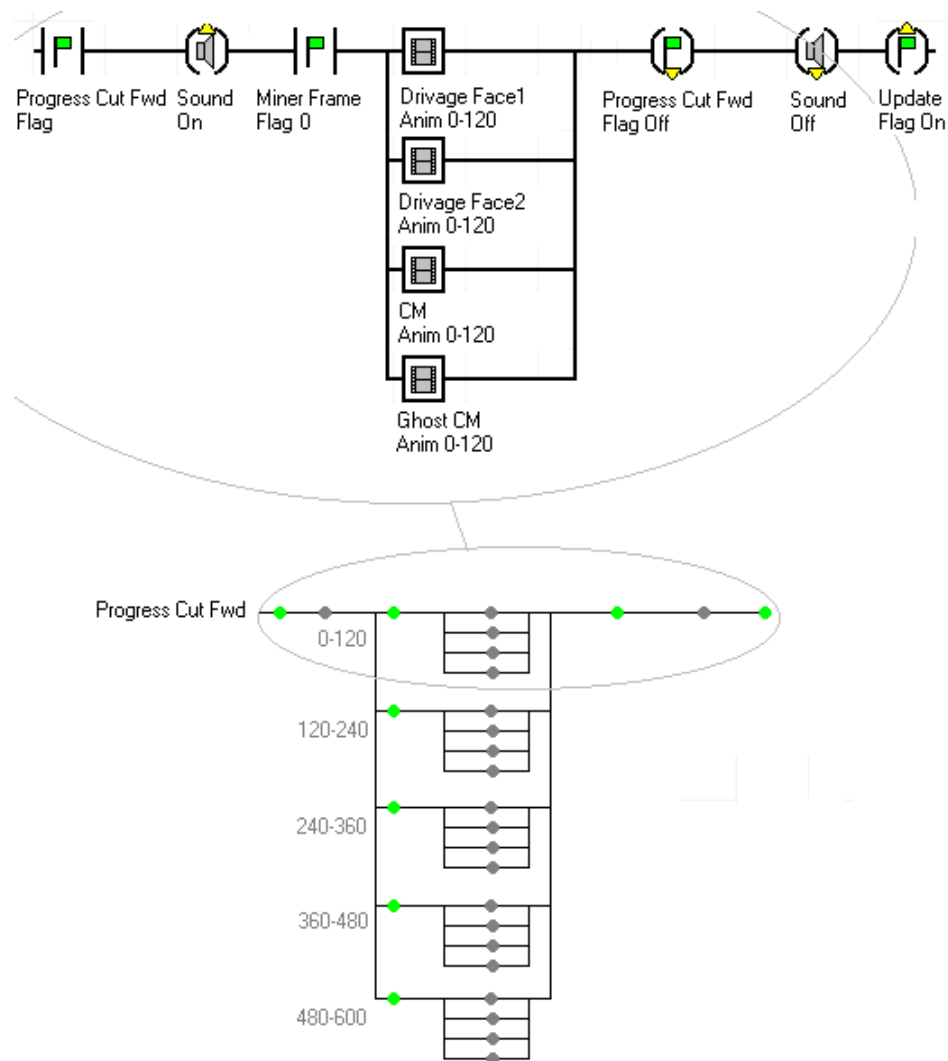


Figure 8.11 Physical world update paths

The logic tree associated with the both the ventilation simulation and physical world changes associated with the withdrawal of the CM machine, once the cut has been advanced to its maximum cut depth, are not illustrated as they are structurally identical.

Once the required animation is complete the request flag, in this case the forward progression of the cut and CM machine, is turned off. An update flag is then turned on that transfers the process to the visualisation update stage. The update flag is used where a physical configuration of objects was changed whilst a visualisation was active. This would enable the application to recall which visualisation was active and display the appropriate object in

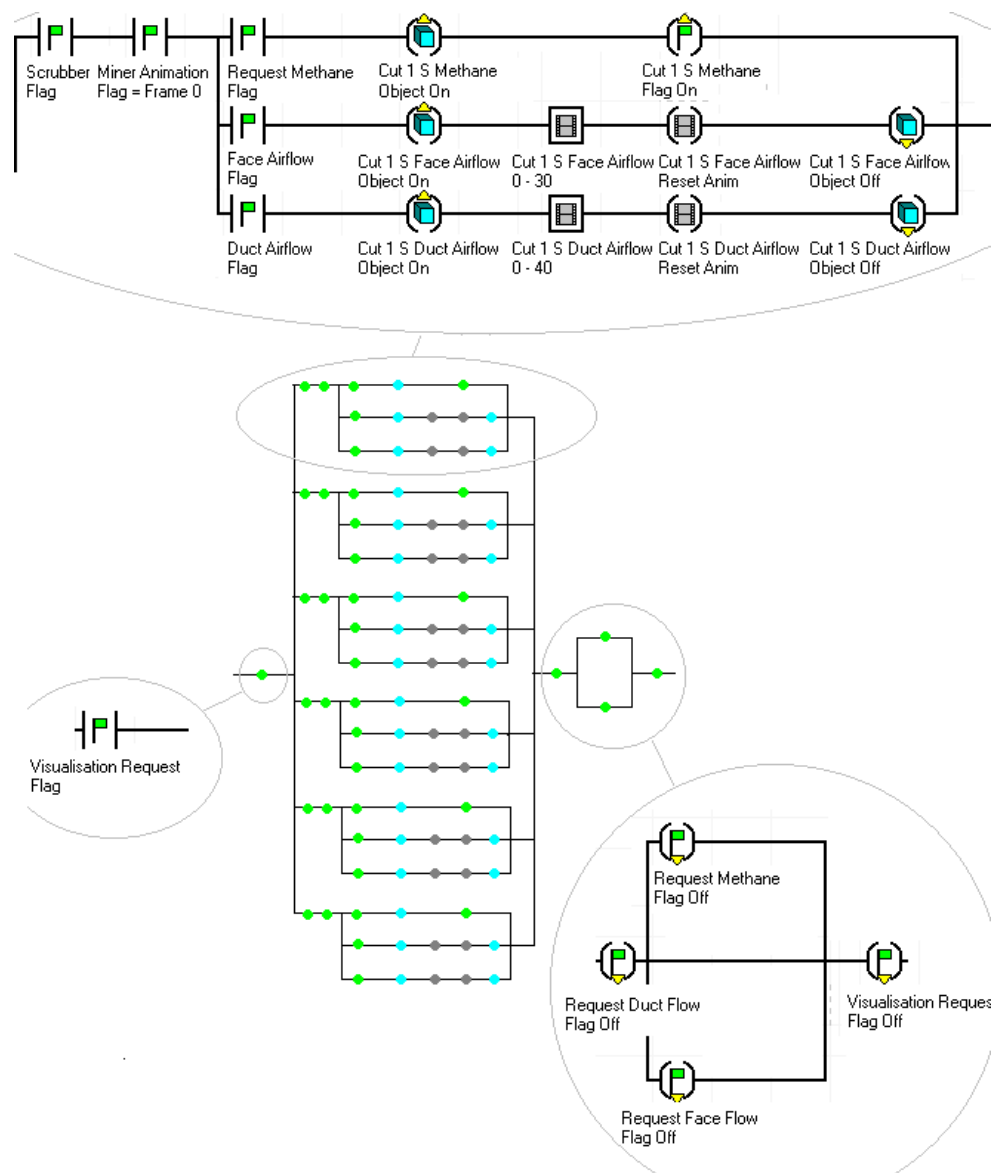


Figure 8.12 Visualisation update paths

the next scenario. To accomplish this, each steady state visualisation required its own active flag. The visualisation update is the final major stage, the logic control network for six simulation scenarios is illustrated in figure 8.12.

Either the visualisation request flag or an update flag passed from the physical scene update stage initiates the visualisation update stage. The correct visualisation is displayed through the use of a decision tree using flags to determine the correct path. The flags will be conditioned according to the output of the previous two stages. Finally the request flags are reset to refresh the process, allowing subsequent simulation choices to be viewed

The three integrated logic networks represent the key stages of the operation of the IECS system. Other smaller logic networks were created to control sound effects, to switch off all visualisations and to set the animation frame flag, all of which play a role within the simulation. Although, due to space constraints it is not possible to display the whole logic network associated with the development of this application, this section has presented examples that are representative of the general approach and initial design structure of the IECS for the first phase of development.

#### **8.5.4.3 User Control Methodology**

To enable the user to control on screen, the viewing of the scenario configuration changes, the visualisations and effect a *ghosting* of the CM machine (making the machine transparent to assist the visualisation of the airflow and gas concentration data), an on screen button panel was developed. This enabled the user to *point and click* on icon buttons on the panel, each of which enacts different actions and requests. These buttons were constructed as foreground objects in the physical VR world and were loaded into SAFEVR™ and treated as objects in the same way as all other constituent parts of the VR world. To maintain the buttons position relative to the user as they navigated around the environment, orientation and

position operators were used within the IECS, to maintain a fixed distance and orientation, using the view port of the user as a constantly updating reference point. The control panel incorporated five buttons that control the forward and backward movement of the CM machine, the switch on or off of the exhaust scrubber fan and the ghosting of the CM machine. In addition , five other buttons control the different forms of the airflow and gas concentration visualisations that may be viewed.

Figure 8.13 illustrates the control panel buttons including the original three methane level buttons (later reduced to one). The layout of the panel was later modified for purely aesthetic reasons.

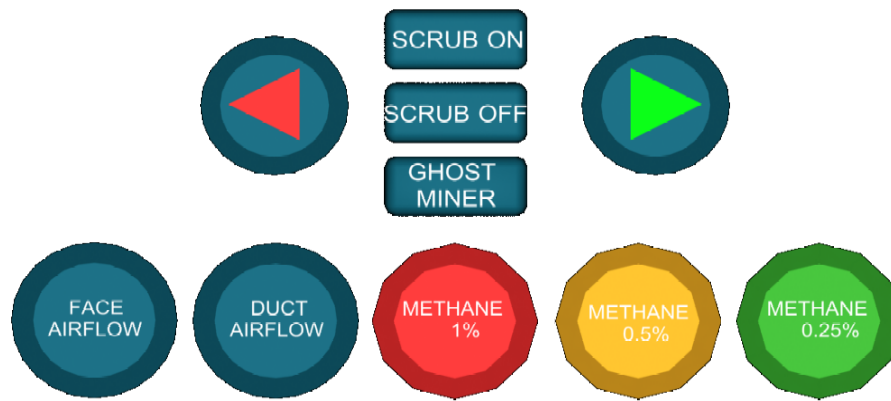


Figure 8.13 User control panel used in VE

The controls were designed to enable to user to control every available physical configuration variable and experience a view of the changing flow regime effectively in real time. The controls developed for the application were kept as simple as possible to facilitate ease of use.

### 8.5.5 Application Screen Shots

The application was run from within the SAFEVR™ environment. Figures 8.14-8.21 illustrate the use of the application by the use of a sequence of representative screen shots demonstrating a number of representative computer screen views.

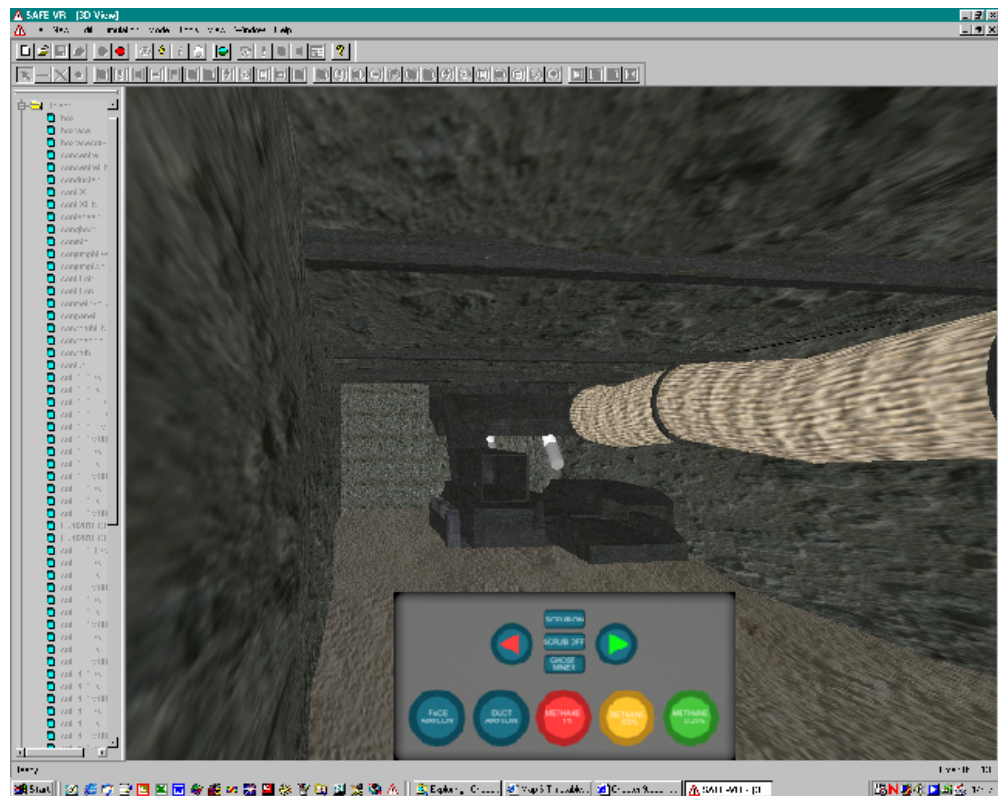


Figure 8.14 Startup screen detailing VR driveage at initial cut stage

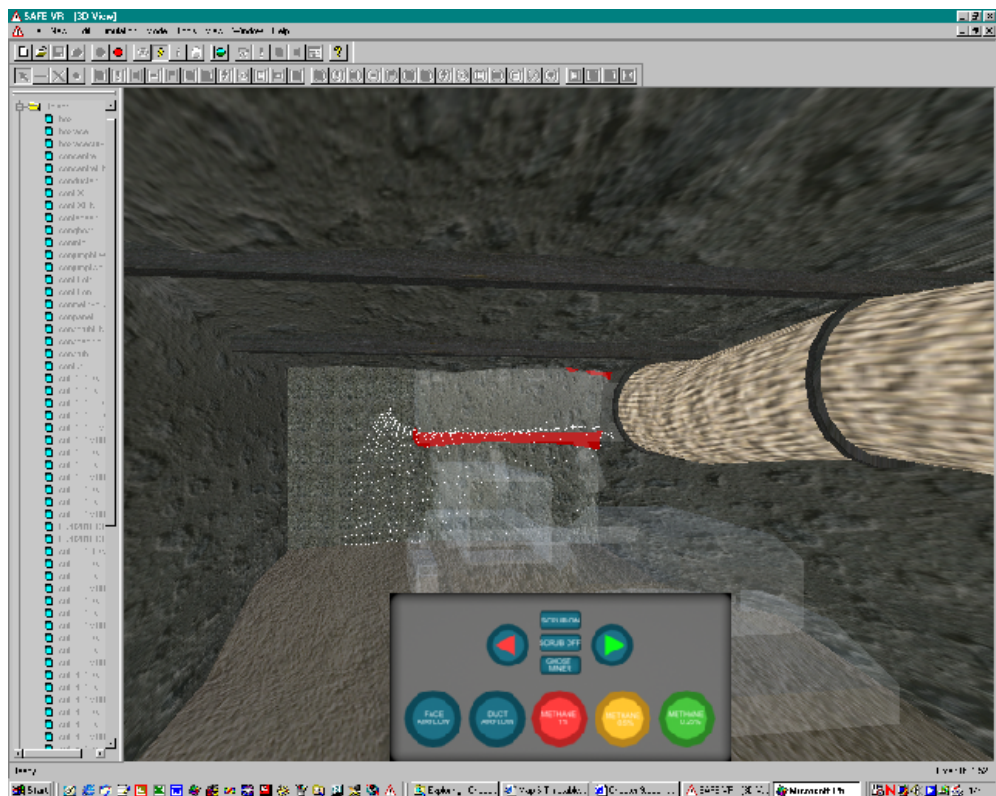


Figure 8.15 Cut 1, boom raised, face particle flow and methane concentration



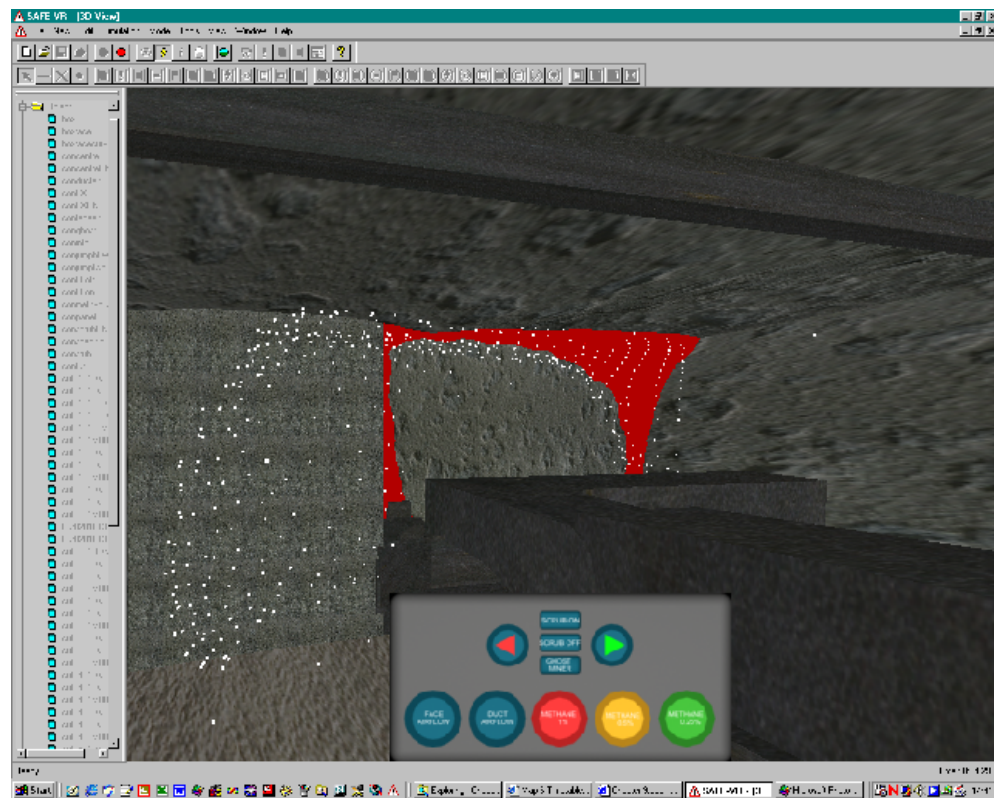


Figure 8.16 Cut 2, boom lowered, face particle flow and methane visualisation

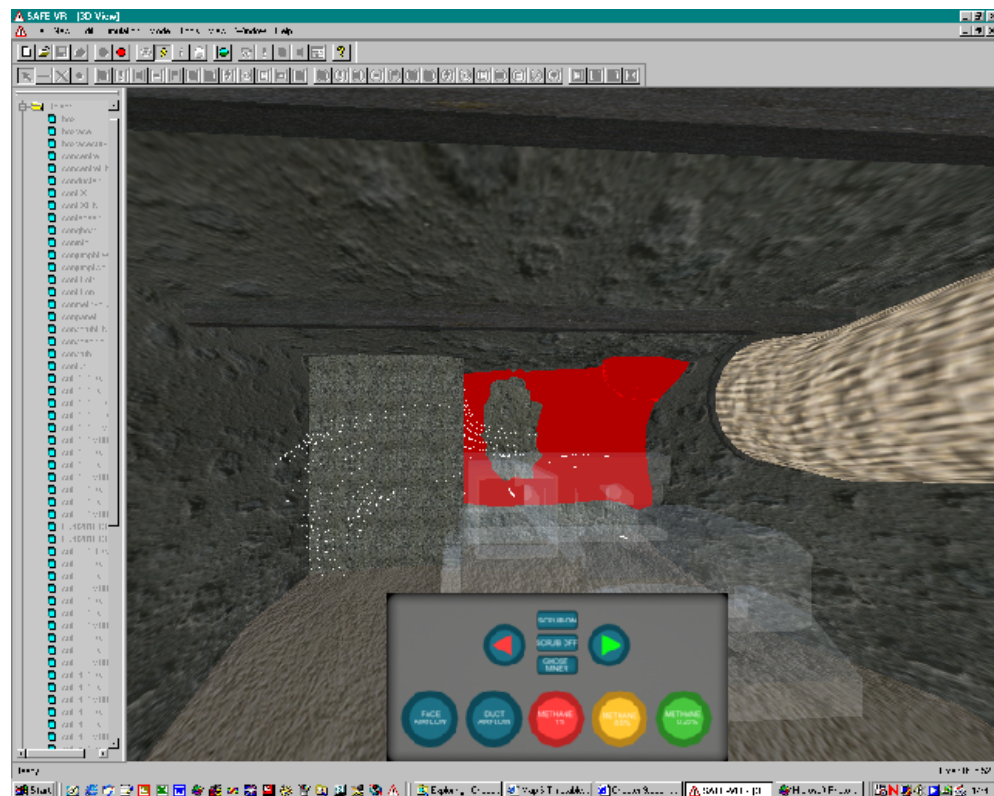


Figure 8.17 Cut 4, boom lowered, duct particle flow and methane visualisation

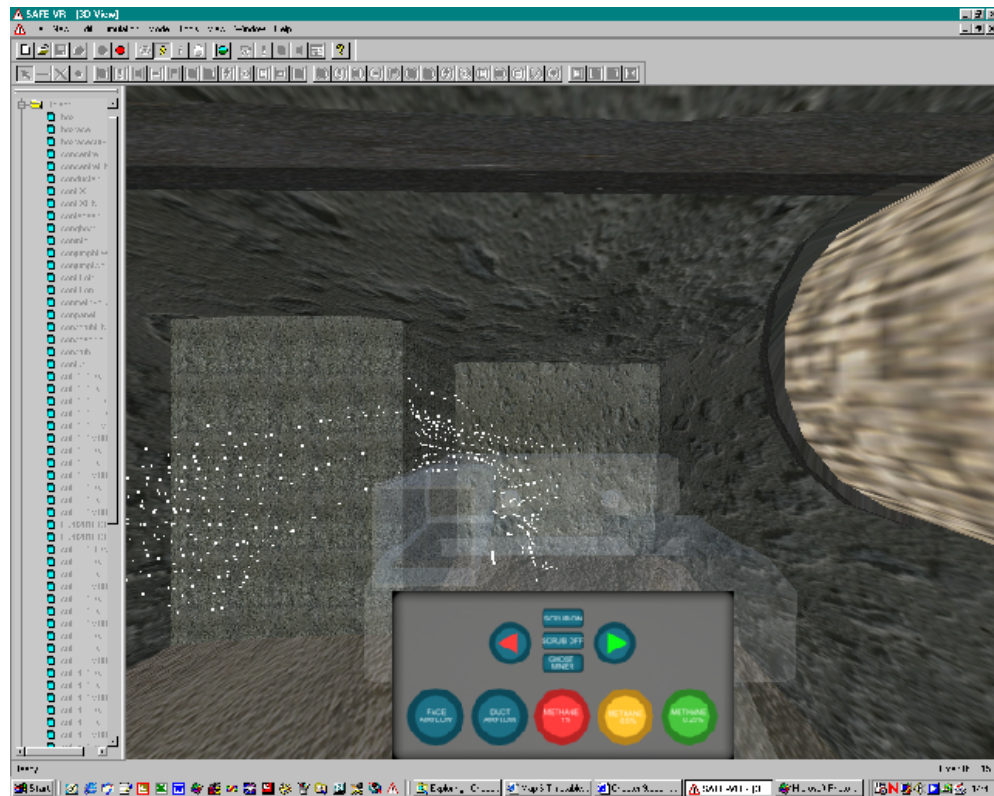


Figure 8.18 Cut 6, boom lowered, duct airflow detail

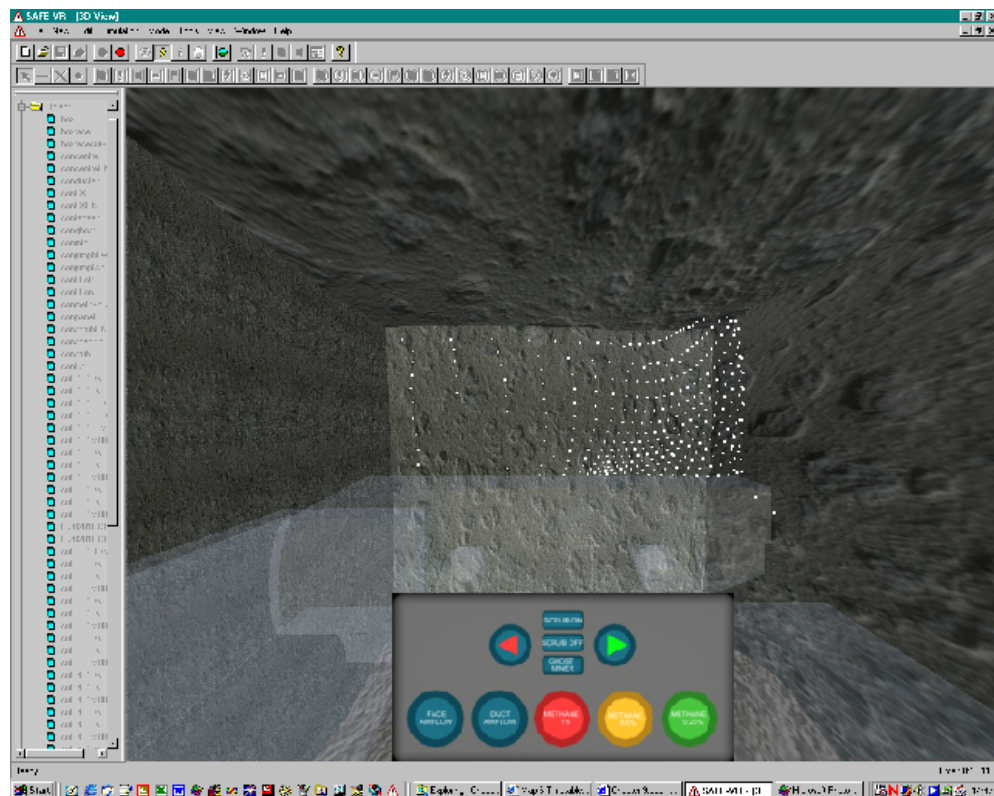


Figure 8.19 Cut 6, boom lowered, face particle flow detail



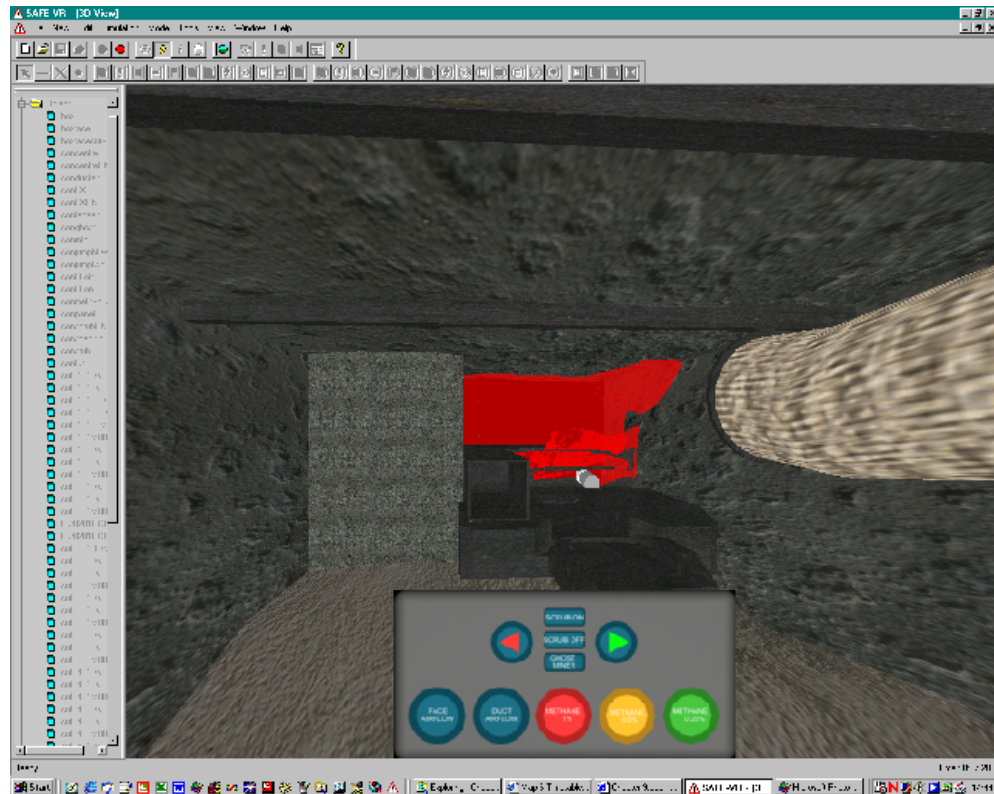


Figure 8.20 Cut 6, boom lowered, methane detail

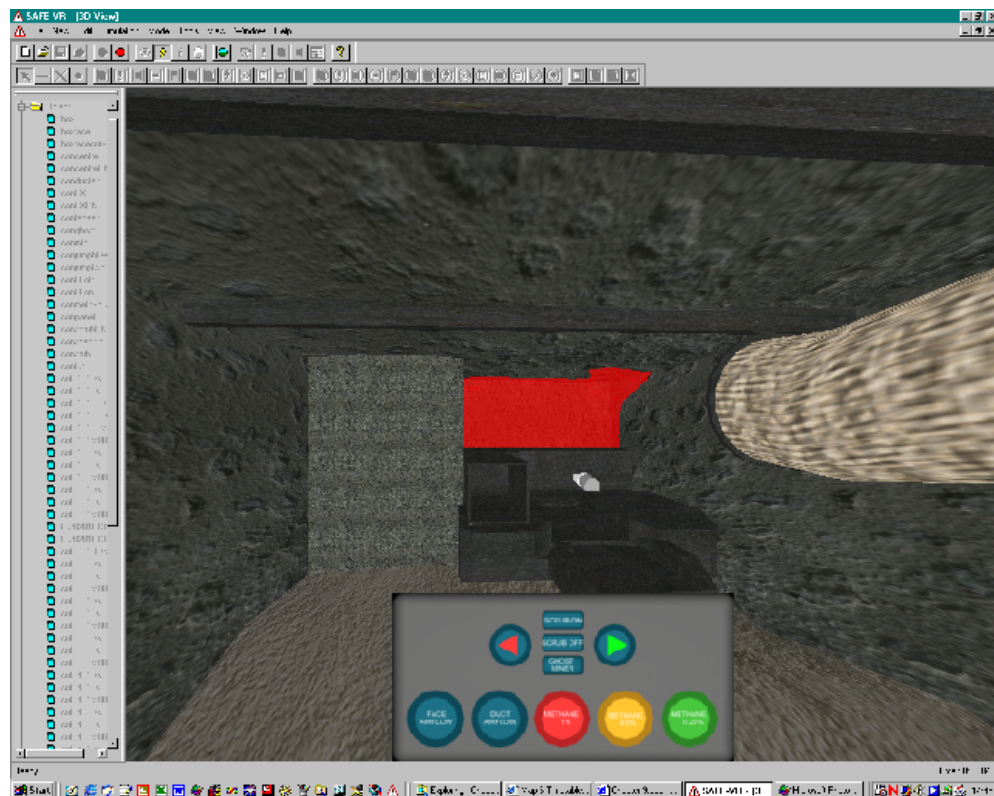


Figure 8.21 Cut 6, boom lowered, scrubber activated, methane detail

### 8.5.6 Preliminary Assessment of the Application

The operation of the early versions of the application, suffered greatly from a lack of both processing and memory storage power afforded by the original specified computer hardware platform (outlined in Chapter 8, Section 8.3). To allow the application to run interactively on this hardware platform, it was necessary to reduce the size of the object library. This was achieved by considering only the simulation scenarios that replicate the development of the driver side cut up to and including Cut 4 (Figure 8.2.) and incorporating the operation of the exhaust scrubber fan. This restricted data set, represented the visualisations of 8 CFD simulation data sets, thus the maximum number of simulation scenarios was defined as 8, assuming 3 visualisations of the type used for each scenario. To further reduce the number of objects required for visualisation, the option of viewing the range of three threshold methane gas concentration isosurfaces (0.25, 0.5, 1.0 %) was reduced to a single isosurface (1.0 %).

To perform a preliminary evaluation of the application, two identical versions of the application were developed, each of which operated on one half of the available CFD simulation data library scenarios. This allowed each application to be run interactively on the original hardware platform without suffering the problems of system latency. This enabled all the intended functions of the application to be tested. The application was run through each stage of the simulated cut on the operator side. Visualisations were viewed and evaluated individually at each step and in sequences of steps. At all times the application maintained adequate frame rates and functioned to the design specification. It was concluded that the limit of performance was primarily due to the memory storage requirements of the large number of visualisation objects, which exceeded the available 256Mb and not to the total polygon count as objects were only ever displayed in small numbers.

### 8.5.7 Developments

Following this preliminary evaluation the project hardware was upgraded to a Pentium™ III specification. incorporating a 1.7 Ghtz processor, 512Mb RAM and a 64Mb Radeon ATI™ accelerated graphics card displaying at 800 ×600 screen resolution. Using this hardware configuration, the complete application was able to be operate with none of the system latency problems associated with the original lower specified hardware.

### 8.5.8 Discussion & Conclusions

The first phase of the development of the application defined the precise boundaries of the capability of certain hardware configurations. To enable the application to be a successful training tool, it was considered critical that the user be exposed to as great a number of alternate simulation scenarios as possible. The adoption of the upgraded hardware enabled the trainee to be exposed to a total of 12 distinct simulation scenarios. Each separate scenario demonstrated the ventilation and gas dilution characteristics associated with different mining and ventilation configurations. Experience gained testing the application in its limited form using the lower specification hardware indicated that a number of scenarios lower than this exhibited a lack of depth within the application where the users options were too restricted. One possible approach would be to develop a more efficient use of the original CFD simulation data library. For example, using data sets at extremes of the variable ranges in addition to the inclusion of customised CFD models. The following conclusions were drawn based upon the performance of the application.

- *The preliminary application displayed the visualisation objects efficiently but the memory storage requirements of the hardware proved a limiting factor to the number of visualisations that could be viewed.*

- *The three-stage process of the IECS was proven to function reliably, enabling the user to efficiently interact with the VR world environment and request and view visualisations of the airflow and resultant gas concentrations. It was concluded that no modification would be necessary to the structure of the IECS..*
- *Given the advent of recent improvements in available desktop computer hardware architecture, it was concluded that a maximum 20-25 representative simulation data sets should be included in the next generation of the application. This would allow the viewing of all of the original CFD simulation data sets.*
- *It was decided that a wider range of scenarios should be incorporated within the application to highlight the consequences of following bad practice, with respect to the operation of both the mining and auxiliary ventilation system. The application should also include examples of the simulation of remedial measures that may be enacted to recover a hazardous situation. The inclusion of simulation examples that demonstrate these two facets would greatly increase the educational and training value of the application.*

These conclusions were subsequently used to construct an outline specification for the second phase of the application, whose construction is detailed in the following section.

## **8.6 Phase Two: Simulation Construction**

### **8.6.1 Introduction**

The objective behind the second phase of the development of the application was to address any deficiencies identified from the assessment of the performance of the initial first phase prototype development.

I

Once again, the hardware platform upon which the application would be further enhanced, was upgraded to the highest available specification defined within a desktop architecture. The new platform specification was a dual processor Intel Xeon™ 2Ghz  $\times$  2 based machine, with 2Gb of Random Access Memory (RAM). The graphics were displayed through the use of a generic NVIDEA™ 64Mb accelerated graphics card with a 800  $\times$  600 resolution. This represented a considerable improvement that would greatly extend the limits of the application defined in the previous section. However, it should be noted that the second phase of the development of the application reported in this Chapter, was constructed on the previous generation of hardware. Since the dual processor machine was only made available at a very late stage of the project for the purposes of evaluation.

It was apparent that the original objectives of the application were not achievable to any satisfactory extent at the time they were outlined early in the project considering the limits of the hardware originally available. Since the objectives have not changed, it has been shown in previous sections and the next that hardware capabilities had caught up with the objectives of the project over the project duration. This has been shown to be a characteristic of the development of this type of application over an extended timescale. However, the work carried out and reported in the coming sections reflects an evolution of the methodology behind the application, not purely an expansion to fill the ever-widening boundaries of modern computational architectures. The author had found it beneficial to consider those problems concerned with fundamental design methodology, separate from those concerned with pure computational capacity. Since the latter were generally solved by the evolution of processing power, whilst the former required greater attention and were essentially independent of hardware capability.

### **8.6.2 Additional Specifications & Proposed Enhancements**

Following the development of the original application it was concluded that although the program performed well, there were a few deficiencies that

required attention. The following sections discuss the changes and modifications subsequently made to the application.

#### **8.6.2.1 Data Library Map**

The CFD simulation data library contained the visualisations for a total of 24 scenarios, each of which would contain 3 separate visualisations. However, the computer memory capacity required to store the entire CFD simulation data library during the development of the first phase of the application exceeded that available on the hardware platform used.

To maintain the width of the educational and training experience offered by the application, it was decided to reduce the number of scenarios spread across the entire cut cycle on both sides of the drivage sides, and maintain the number of visualisations per scenario. It was also decided to limit the number of scenarios that permitted the activation of the exhaust scrubber fan unit, since this facility effectively doubled the scenario number. The range of scenarios chosen were selected on the basis of the ability to clearly indicate significant airflow and/or gas dilution characteristics. Where the comparison of two scenarios demonstrated little difference, only one of the scenarios was included in the new data simulation library. For example, on the operator side, the mid point cut depths (cut 3 and 4) were removed since the highest depth (cut 5/6) demonstrated similar, but more extreme, airflow and gas dilution characteristics. In a similar fashion the beneficial effects of the use of the exhaust scrubber fan were illustrated for a single cut sequence, which reduced the overall number of visualisations that needed to be stored for each cut scenario.

Figure 8.22 illustrates the original CFD simulation data library indicating the scenarios selected for inclusion within the second phase of the application. Given the limitations exposed through the first phase of the application it was considered that this more efficient use of available data would demonstrate the same range of characteristics present within the complete CFD data library at a much reduced computational cost.

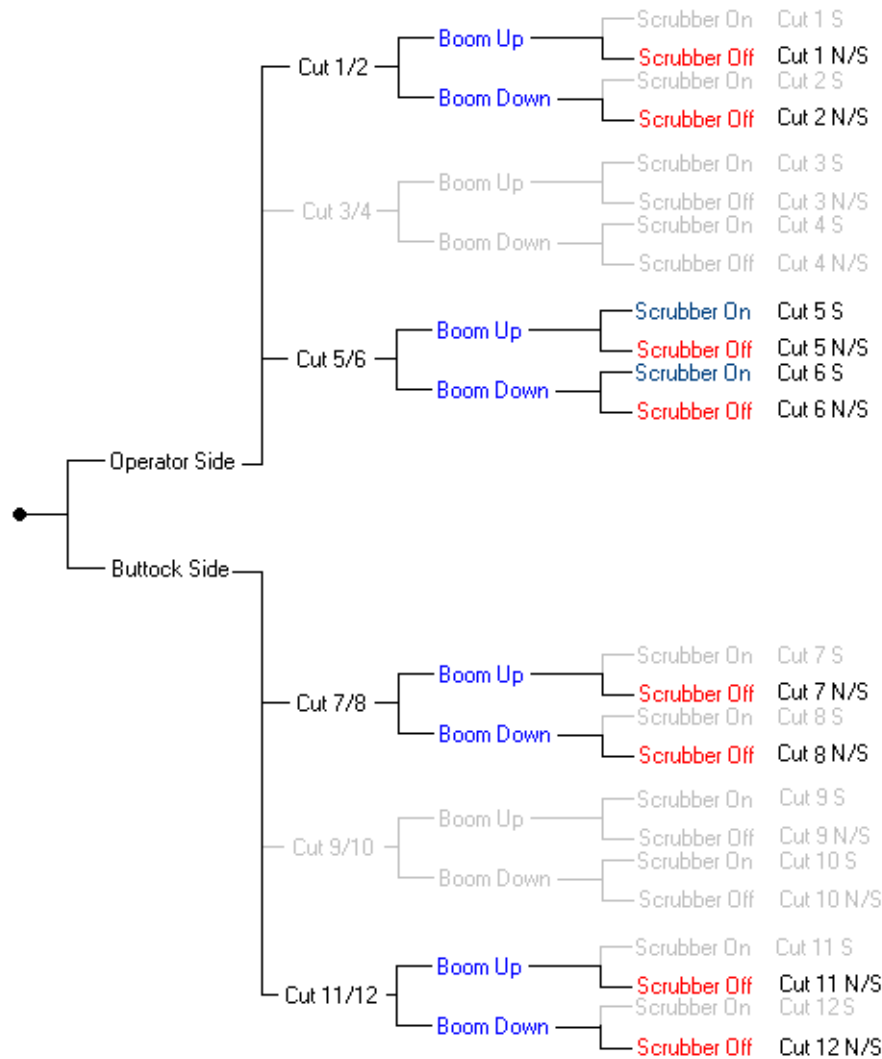


Figure 8.22 CFD data library data sets included in second phase

### 8.6.2.2 Use of HTML Media for Online Assistance

Throughout the development of the application a principle of constructing a self-explanatory application had been adopted. This is inherent to many VR applications, since they replicate reality little instruction, aside from that required to operate the computer, is required for those familiar with the subject environment. It was however decided that the inclusion of an active guide would greatly enhance the educational capabilities of the application.

To enhance the training and self-learning experience of the application, it was decided to develop a supportive help facility as an integral part of the application. SAFEVR™ includes an external application initiation operator that can be included as part of the IECS. Through the use of this operator, a

number of media documents can be viewed in response to a direct request from the user or be prompted by the interaction of the user with the environment.

For example, an HTML document may be automatically displayed when the user performs a specific action that may lead to the creation of a hazard, the document could detail the effects/consequences of that action and suggest corrective remedial procedures.

Consequently, three levels of supportive information were included in construction of the application. The first level provided a description of the physical layout and operation depicted by the particular scenario detailing variable configuration data such as the current cut depth. The second level provided a general document indicating basic user control methodology. The third level, presented a precise description and explanation of the simulation scene the user is observing through the view port. The application tracks the sequence of simulation scenarios viewed by the user, through the use of condition flag operators, which upon request prompt the display of the appropriate document.

An additional number of buttons were incorporated onto the control panel, to allow the user to request the display of appropriate level of information. The help facility was developed using HTML documents due to their universal compatibility. These documents are opened through a standard internet web browser, although any media format, including movies or sound recordings, could be incorporated in the development of the help facility using the same procedures.

#### **8.6.2.3 Hazard Identification**

SAFEVR™ was initially developed as a *hazard spotting* application. Consequently, it includes features that may be used to specifically define objects or configurations as particular hazards. The hazard itself is an



operator available for use as part of the IECS networks controlling the application. Given the presence of one or more objects or certain combinations of objects, a hazard can be switched on or off. The user can identify the hazard within the scene by selecting the associated object using the *hazard spotting* mode.

#### **8.6.2.4 Extension to Initial CFD data Library**

The range of the CFD simulation data library previously developed by Hargreaves et al (2000) had been used to develop and evaluate the first phase of the construction of the integrated application. Since the range of scenarios present in this data library had not been specifically designed to demonstrate the consequences of good and bad practice within auxiliary ventilated drivages, it was concluded that a further series of CFD model simulations were required.

For example, during the progression of the cut cycle, the maintenance of a fixed forcing duct orientation did not serve to highlight the detrimental effects of installing this duct such that the forcing jet was not parallel to the adjacent wall.

It was therefore decided to construct a number of other CFD models based upon the physical geometry of the original drivage, to extend the number of ventilation scenarios available. In particular, simulation models were constructed that would depict a number of scenarios that both demonstrate examples of bad mining or ventilation practice, and illustrate the beneficial effects that may be produced by the enactment of an appropriate remedial measure. To this end a number of CFD solutions were obtained demonstrating examples of poor practice in terms of installation, operation and maintenance. Installation factors included, the alteration of the orientation of the duct centre line such that the force ventilation jet moved away from the wall of the drivage, reducing its scouring effect across the face. Maintenance and operational factors included, a reduction in the fresh air delivered by the force duct due to a puncturing of the duct, the

deterioration or deliberate interference with a duct joint outbye of the face. Operational factors include the failure to advance the force with advance of the cut to maintain the distance of the force duct outlet to the face and hence maintain the fresh airflow delivered to the face cut.

As many UK collieries employ continuous miner systems ventilated by conventional force and exhaust overlap auxiliary ventilation systems, it was decided to widen the scope of the CFD models to simulate the ventilation and gas dilution characteristics experienced within such headings.

The additions specified in this section for the CFD data library were selected based upon the need to incorporate more cause and effect demonstrations regarding good and bad practice, to widen the range of scenarios covered and to incorporate the functionality of hazard spotting to the application.

A more detailed discussion of the construction of the additional CFD model and their associated simulation data is included in section 8.6.3.

#### **8.6.2.5 The Development of the Final Application Hazard Map**

The data library map specified for the final second phase application is detailed in figure 8.23 depicting all included CFD data sets and associated hazards. The scenario number scheme was modified to reflect the changes made to this application.

The section classified as *other* in the far right column of the library map, represents the additional CFD simulation models constructed to specifically demonstrate additional examples of good and bad ventilation practice. Should the *OK* flag be chosen this reverts the simulation model to the original scenario upon which the modified models were based. A description of each simulation scenario, (numbered 1-21) is also given:

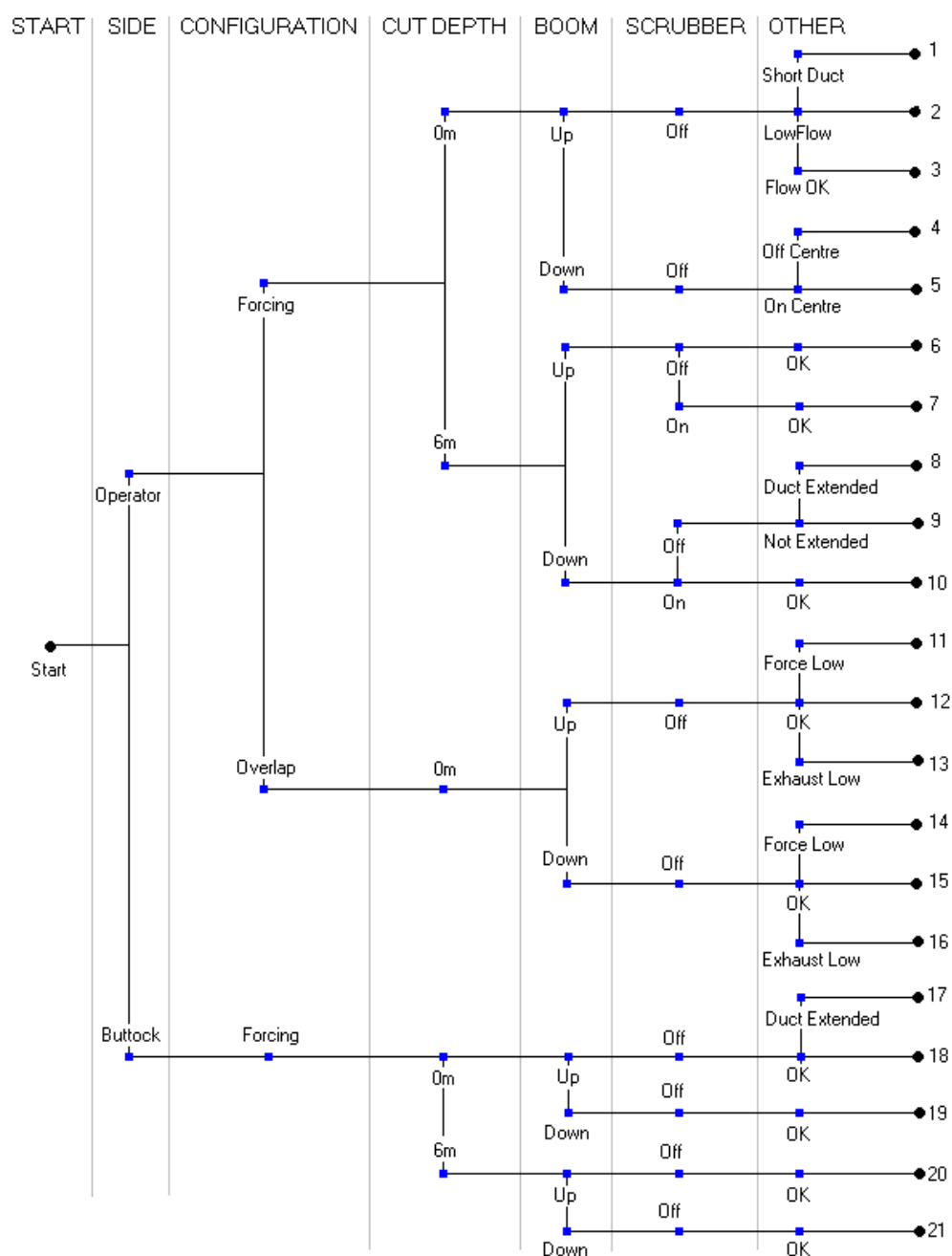


Figure 8.23 Final application data library map

**Scenario 1:** The outlet to the force duct is moved back a further 5m from back from the face of the drivage. Duct outlet to face distance in excess of 10m reduced the momentum and hence penetration of the force jet, reducing its ability to scour the face cut. This may result in an increase in the methane concentration levels experienced within the vicinity of the face of the heading.

**Scenario 2:** A reduction in the fresh air quantity delivered by the force duct is modelled to represent the effects that may be produced due to damage to the duct line outbye of the face or the force fan. The reduction in fresh airflow delivered will result in an increase in the methane concentration levels experienced within the vicinity of the face of the heading.

**Scenario 3:** As scenario 2 with adequate fresh flow. This scenario represents the ideal ventilation configuration with the forcing duct placed 5m from the cutting face. When the cutting boom is raised it obstructs the fresh air jet, highlighted by the separation of airflow around the boom.

**Scenario 4:** As scenarios 2 & 3 with the boom lowered and the force duct alignment offset, such that the outlet to the force duct points from right to left across the face of the drivage. This represents a poor standard of installation. The consequence is that the force jet is unable to effectively scour the methane liberated on the right hand side of the face, resulting in an increase in the methane concentration experienced on the right hand side of the face.

**Scenario 5:** As scenario 4 with the ducting installed correctly. Can be compared to scenario 3 to visualise difference in ventilation characteristics caused by cutting boom orientation.

**Scenario 6:** Cut depth increased to 6m. The outlet to the force duct is not advanced to follow the cut. The resultant reduced penetration of the fresh air jet creates an increase in the methane concentration experienced in the vicinity of the cutting face.

**Scenario 7:** As scenario 6 but with an operation of exhaust scrubber fan mounted on the left hand side of the CM machine. The methane concentration levels experienced at the face are observed to reduce when the scrubber fan is switched on. The changes in the effectiveness of the face ventilation characteristics initiated on the activation of the exhaust fan are clearly visible.

**Scenario 8:** As scenario 6, but with an advance of the force duct to follow the cut when the cutting boom is in the lowered position. The methane concentration levels are reduced as the airflow penetrates further into the cut and more effectively scours the face.

**Scenario 9:** As scenario 8 with no extension of the forcing duct to follow the cut. The methane concentration levels are observed to rise as duct is not extended into cut.

**Scenario 10:** The activation of the exhaust scrubber fan causes reduction in methane concentration due to an improvement in face fresh airflow and scouring. Similar to scenario 7 with cutting boom in lowered position.

**Scenario 11:** CM Cutting boom up, use of force/exhaust overlap auxiliary ventilation configuration. A reduction in the fresh air quantity delivered by the force duct is modelled to represent the effects that may be produced due to damage to the duct line outbye of the face or the force fan. The reduction in fresh airflow delivered will result in an increase in the methane concentration levels experienced within the vicinity of the face of the heading.

**Scenario 12:** Optimum force/exhaust overlap auxiliary ventilation configuration. The combination of both the force and exhaust ventilation systems providing adequate face ventilation and methane dilution.

**Scenario 13:** Cutting boom up, with force/exhaust overlap auxiliary ventilation configuration. Reduction in airflow drawn by the exhaust fan modelled to simulate either damage to the overlap duct or deterioration in the performance of the exhaust fan. An increase in the methane concentration is observed, which reflects a deterioration in the quantity of fresh air scouring the face.

**Scenarios 14-16:** As scenarios 11-13 with cutting boom in lowered position demonstrating different ventilation characteristics.

**Scenario 17:** As Scenario 18 with duct extended as per operator side.

**Scenario 18/19:** Buttock cut side boom in lowered and raised positions. Can be compared to scenarios 3 & 5.

**Scenario 20/21:** Buttock cut side boom in lowered and raised positions at increased cut depth of 6m. Outlet to force duct retained at original distance from face. The increase in methane concentration at the cutting face can be clearly visualised owing to the poor penetration of the forcing airflow.

### **8.6.3 The Creation of the Additional CFD Simulation Models**

#### **8.6.3.1 General Parameters**

The additional CFD models and simulation data sets specified in the new data library map above, were constructed and solved. These additional models were based upon the original CFD model configurations employed by Hargreaves et al (2000). As these original models had employed a detailed validation process, it was therefore imperative that the additional models constructed matched the calibration parameters of the original models. To this end the original build files used to construct the original CFD models were used as blueprints for the construction of the new simulation models. All parameters were preserved in order to maintain the original calibration and level of confidence in the results. This was of particular importance in respect of the mesh controls employed, as these had been determined through a series of exhaustive mesh sensitivity studies.

To create the new models, small changes were made to the appropriate geometrical boundaries and flow conditions. In the case of the overlap system the mesh controls used in the original forcing duct were transferred to the additional overlap exhaust duct. The new models were therefore identical to the original models in terms of calibrated parameters. The major parameters used for the CFD models were detailed in section 8.3.2. The models were constructed and solved using CFX5 v5™ with the results being

processed as all prior models. The following section details each new model in terms of the new boundaries imposed.

### 8.6.3.2 Application of CFD to Extended Scenarios

For the purposes of this thesis this section provides a detailed account of the development and results of the additional CFD scenarios discussed in general terms in previous sections. As an example, scenario 4 is considered. Scenario 4 was based upon scenario 3 the geometry layout of which is depicted in figure 8.24.

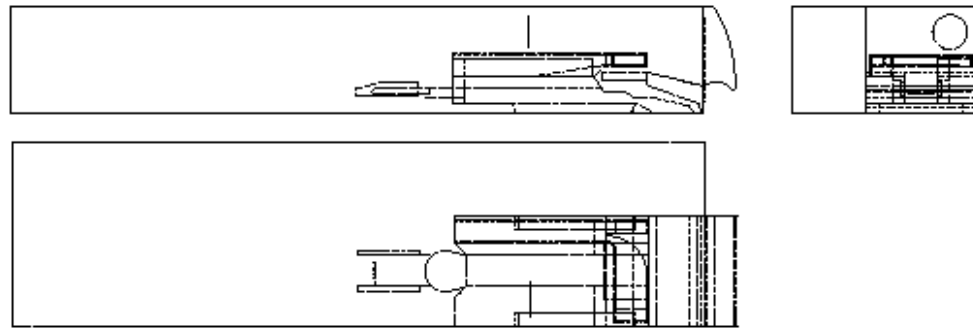


Figure 8.24 General geometric layout of Scenario 3

Scenario 3 represented the operator side cut at an early stage with a minimal cut depth with the boom lowered. As such the characteristics of the ventilation to the face area were good, leading to a prediction of a relatively low methane concentration in the face area. Scenario 4 was therefore designed to provide a ‘comparator’ to scenario 3 whereby an aspect of the model was altered to represent an example of poor ventilation practice. The aspect of the model chosen to represent an example of poor practice was the orientation of the forcing duct in the region of the forcing outlet. This factor is critical to the efficient operation of the ventilation system since the jet of air emanating from the duct must ‘cling’ to the adjacent wall before scouring the face region. Any misalignment caused by either poor installation in the first instance or lack of maintenance following damage, therefore has a significant influence upon the ability of the jet to scour the face effectively.

The geometry of the scenario 4 model was specified such that the outlet of the forcing duct would be skewed 1m to the left of the original outlet as per scenario 3. Using CFX™ Build V5 the geometry of the original scenario 3 model was modified by deleting the original ducting and redefining the new misaligned duct with a 1m offset rotated on the Y axis only with the necessary angle positioned 5m from the outlet of the duct. Figure 8.25 illustrates the alteration made to the geometry.

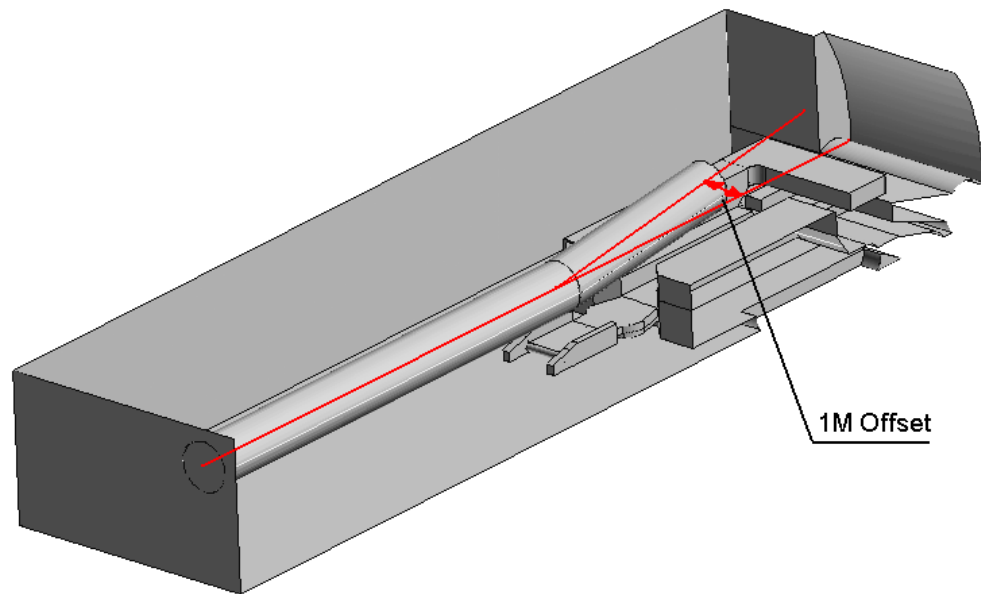


Figure 8.25 Offset duct detail from Scenario 4

The new surfaces were then used to reconstruct the volume fluid domain topology leaving a single volume ready for meshing. Since the original model (scenario 3) had used a mesh defined through mesh sensitivity testing (Hargreaves et al 2000) it was critical that the new mesh for the modified model employed identical mesh concentrations. This was achieved by simply transferring the appropriate mesh control criteria as used on the original model to the new model on the appropriate surfaces. Since the ducting geometry had changed the mesh control criteria had to be modified to accommodate for the new geometry. Hargreaves used a default mesh control for the ducting whereby two points were specified central to the inlet and outlet planes of the ducting, the mesh control operated by an inverse expansion away from the line created between these two points ensuring that higher mesh densities were constructed at the walls of the duct. To modify



this mesh control to accommodate for the skewed ducting required the simple addition of a third point coincident with the plane at which the ducting moved away from its true line. The mesh control was therefore split into two segments using the same inverse expansion criteria.

The remaining boundary conditions were set as per the original model. These are detailed as follows.

- Turbulence Model
  - The standard k-e turbulence model was employed
- Carrier Fluid
  - Air was employed as the carrier fluid
  - The viscosity of the air was set at  $1.725 \times 10^{-5}$  kg/m/s
  - The density of the air was set at 1.284 kg/m<sup>3</sup>
- Wall Roughness
  - The depth of the wall roughness function was set at 0.05m
- **Inlet Condition**
  - Inlet mass flow rate defined as 6m<sup>3</sup>/s
- Outbye Condition
  - Outbye velocity set as free boundary.
  - Static reference pressure set to 0 Pa

The CFX™ V5 Solver was run according and the solution returned when a state of convergence was achieved.

The results of the solution were plotted using the default vector, contouring and streamline schemes available from within the CFX™ V5 post-processing environment. Although the results were intended for processing using the specially developed interface utility the default visualisations produced illustrate the flow characteristics well for the purposes of this thesis.

To demonstrate the flow characteristics of the scenario 4 data set identical visualisations were produced for the scenario 3 data set to provide a comparison. Figure 8.26 illustrates the streamlines for both scenarios

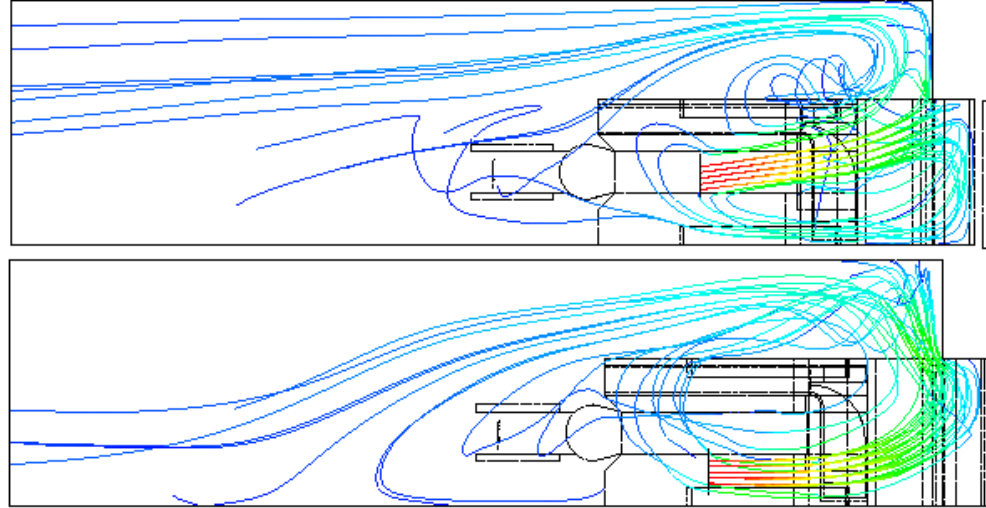


Figure 8.26 Streamline visualisation for Scenario 3 (below) and Scenario 4 (above)

**The streamline visualisations clearly demonstrate the splitting of the jet for scenario 4 whereby the bulk flow divides across the face. This effect can be illustrated in more detail by consideration of the velocity vectors displayed in the region of the face, (figure 8.27). Here, the vectors for scenario 4 can be clearly seen to sweep to the right as opposed to the uniform scouring to the left as per the scenario 3 data set.**

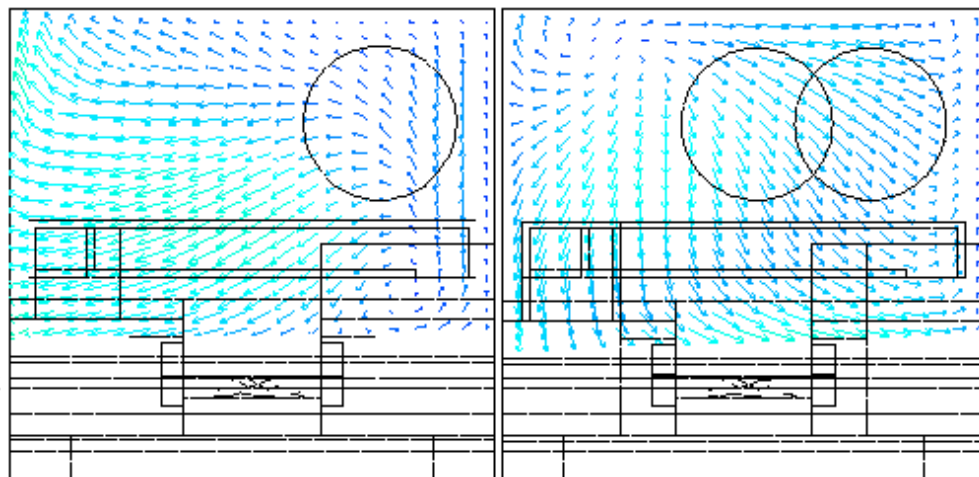


Figure 8.27 Face velocity vectors, Scenario 3 (left) and Scenario 4 (right)

Figure 8.28 illustrates the same type of vector plot detailing the flow characteristics from a plane coincident with the centre line of the forcing duct.

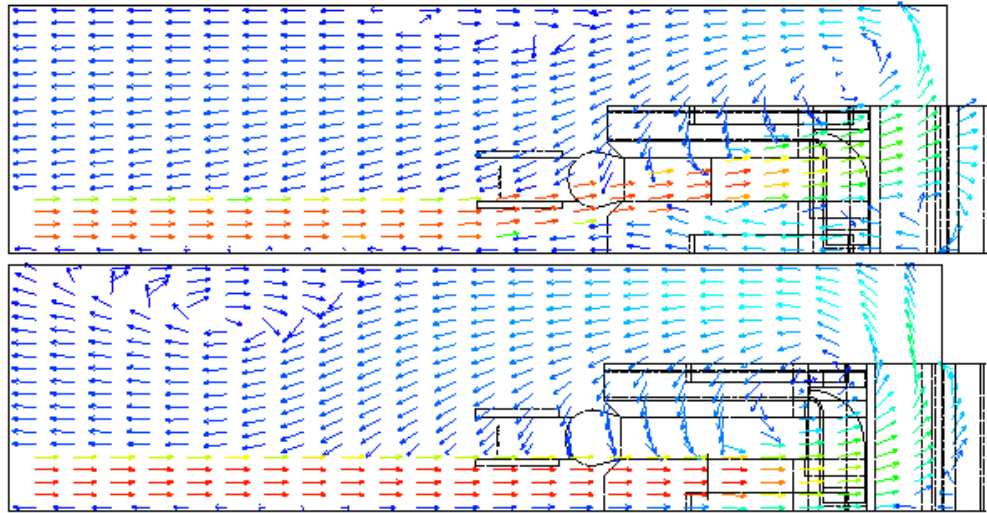


Figure 8.28 Vector plot of Scenario 3 (above) and Scenario 4 (below)

Figure 8.29 illustrates the methane contour plot displayed at the face region demonstrating the consequences of the misaligned duct from scenario 4 as a higher concentration of methane around the far right region where the jets penetration is reduced.

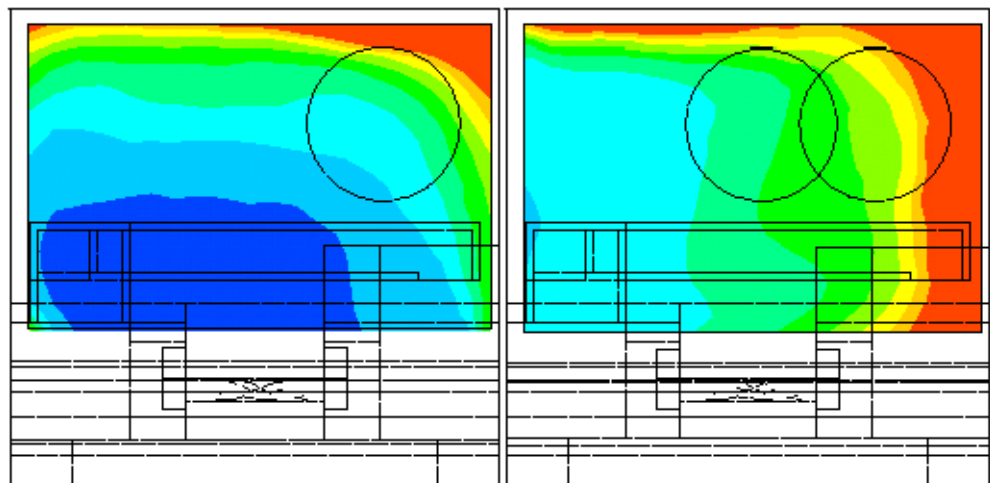


Figure 8.29 Methane contour plot Scenario 3 (left) Scenario 4 (right), 0-1%

Each of the remaining 11 additional CFD models were constructed upon the same principle, each demonstrating a different example of poor practice. The results of the 11 additional models are included for reference in appendix IV.

### 8.6.3.3 Classification of Additional Models

Each new CFD model was created as either a modification of geometry, boundary flow condition or a combination of both applied to a single original model. Eleven additional models, scenarios 1,3,4,8,11-17, were constructed for the second phase of the application development. The general details of each are illustrated in figures 8.30-8.36. The details of any modified boundary conditions are given on the illustration.

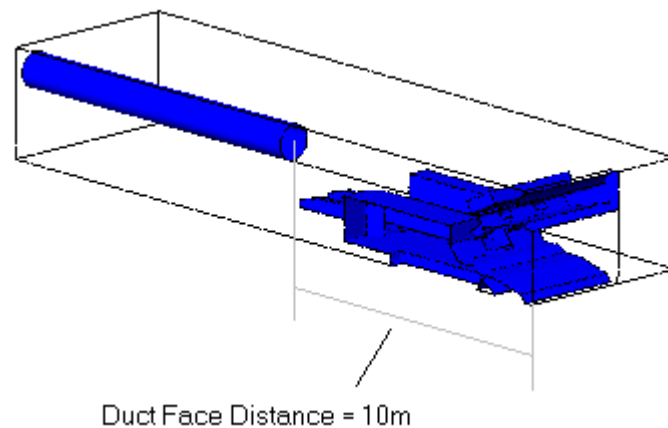


Figure 8.30 Short duct CFD model

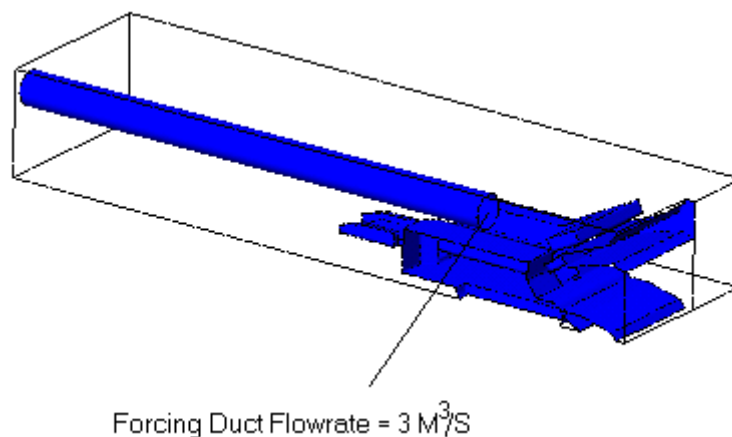


Figure 8.31 Reduced flowrate CFD model

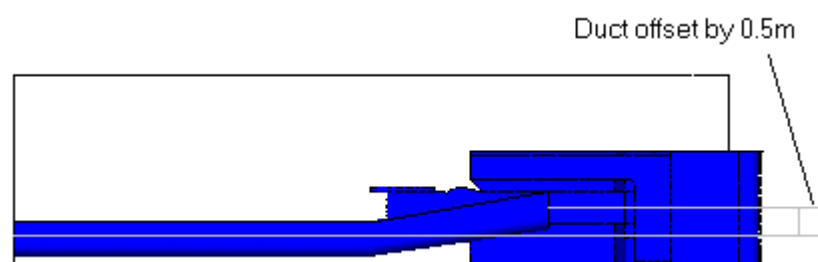


Figure 8.32 Off-centre duct installation CFD model

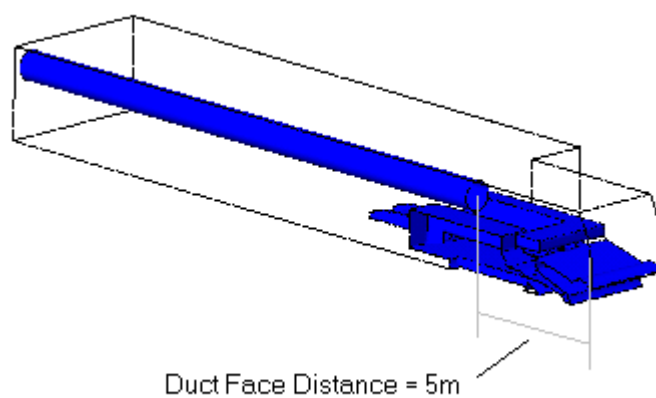


Figure 8.33 Extended duct CFD model (operator side)

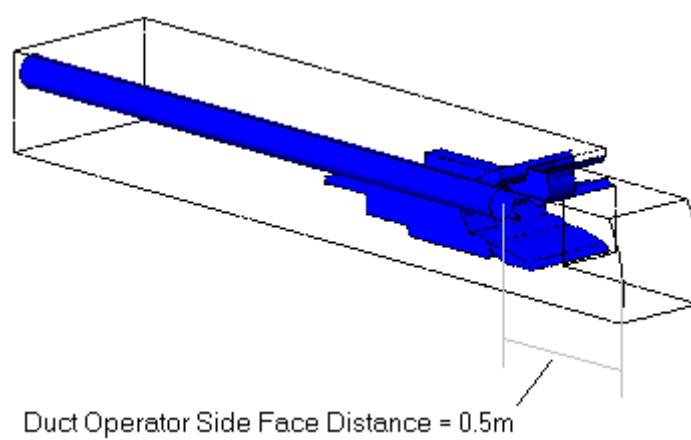


Figure 8.34 Extended duct CFD model (buttock side)

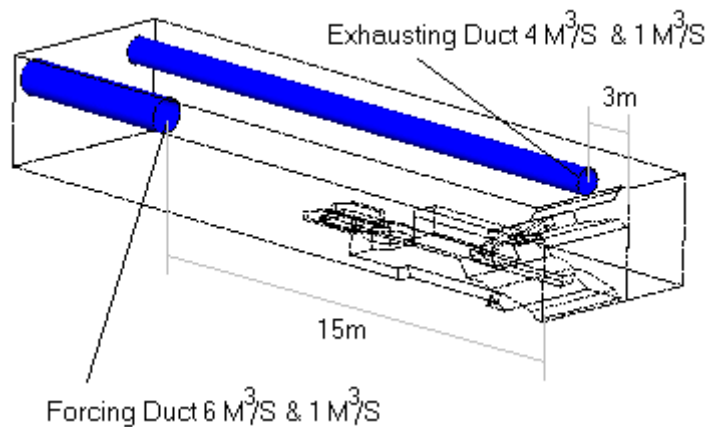


Figure 8.35 Overlap CFD model, boom raised

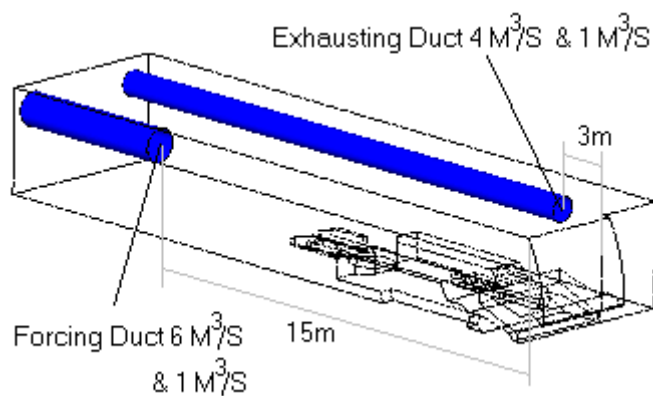


Figure 8.36 Overlap CFD model, boom lowered

#### 8.6.4 IECS Map

The second phase of the application development focussed largely upon widening the scope of the application by increasing the available simulation scenarios, in addition to the provision of active online documentation.

In the evaluation of the first phase application there were no operational problems associated with the design and implementation of the IECS, using the visual operator based language of the SAFEVR™ builder application. There were therefore no structural changes made in order to produce the IECS for the second phase of the application. The changes to the IECS were

mainly associated with changing the object/operator associations to allow for different or new objects, the layout was not altered in this respect.

One major addition to the IECS was the inclusion of the operator networks used to control the HTML based online assistance. These were simple operator networks based upon a user request for a specific type of document (levels 1-3), the identification of the current scenario and visualisations present, and the display of the correct document.

### 8.6.5 Application Screen Shots

The application was executed according to all the specifications detailed within this section. The following pages contain some representative screen shots of the application detailing a range of scenarios and application functions, figures 8.37-8.45. For a full description of each scenario depicted the reader is referred to section 8.6.2.5.

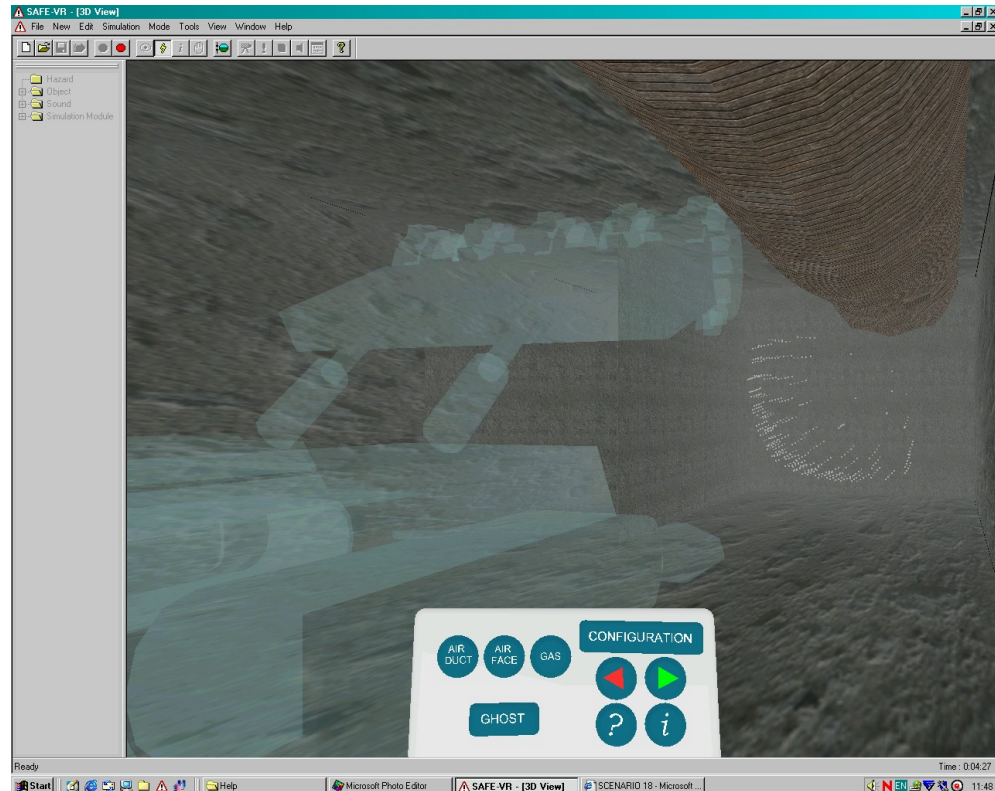


Figure 8.37 Scenario 18, CM ghost with duct airflow visualisation active.



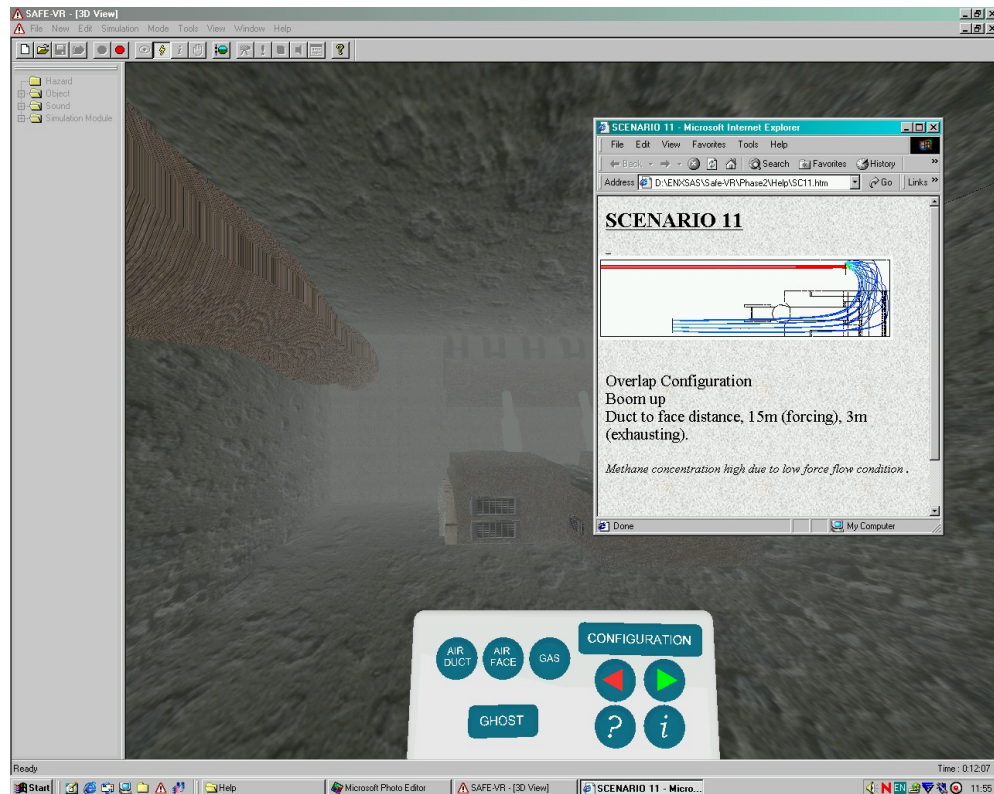


Figure 8.38 Scenario 11, Level 3 HTML documentation active

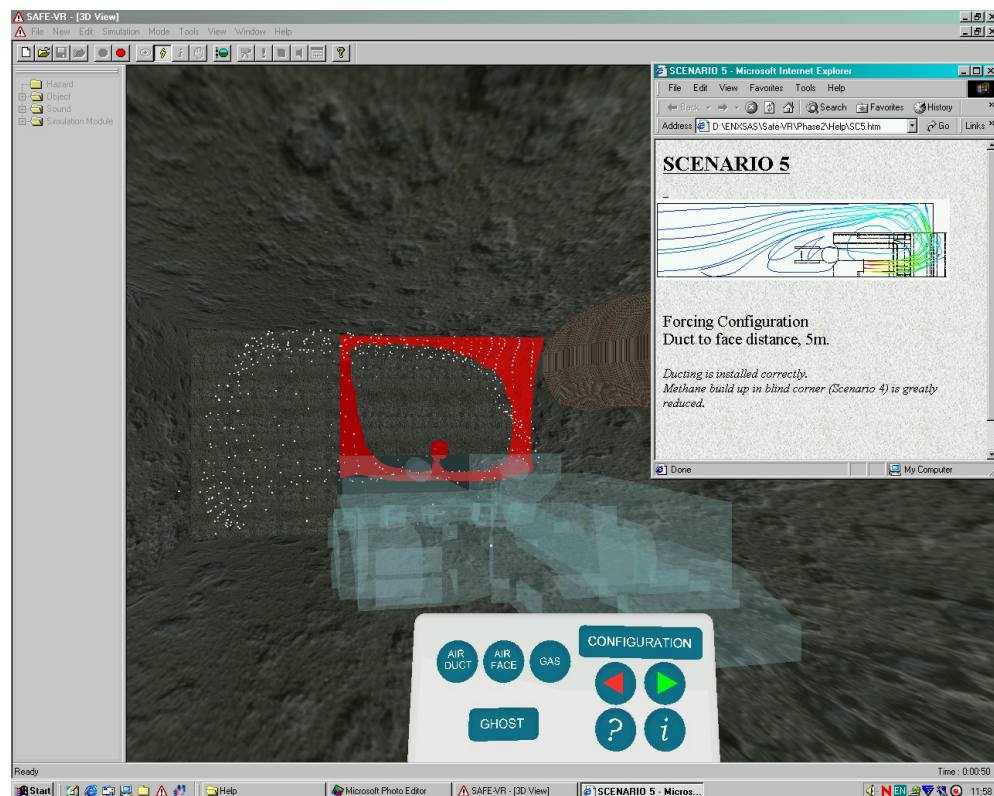


Figure 8.39 Scenario 5, CM ghost with methane and face ventilation visualisations



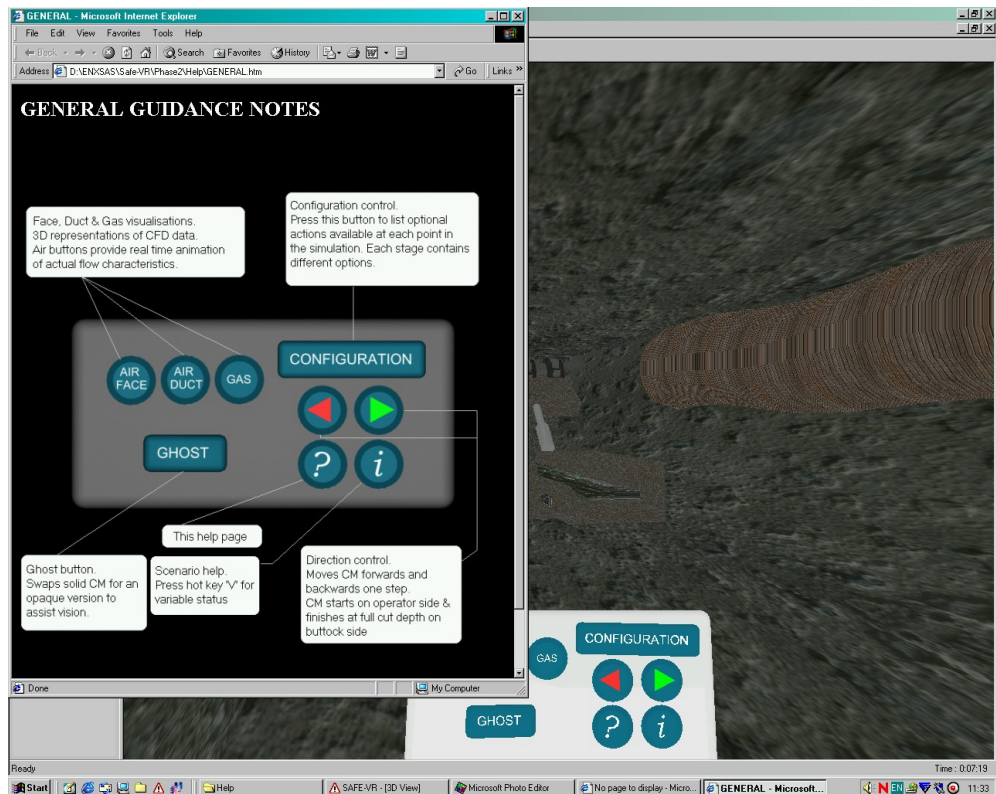


Figure 8.40 Scenario 3, Level 2 HTML documentation (general help) active

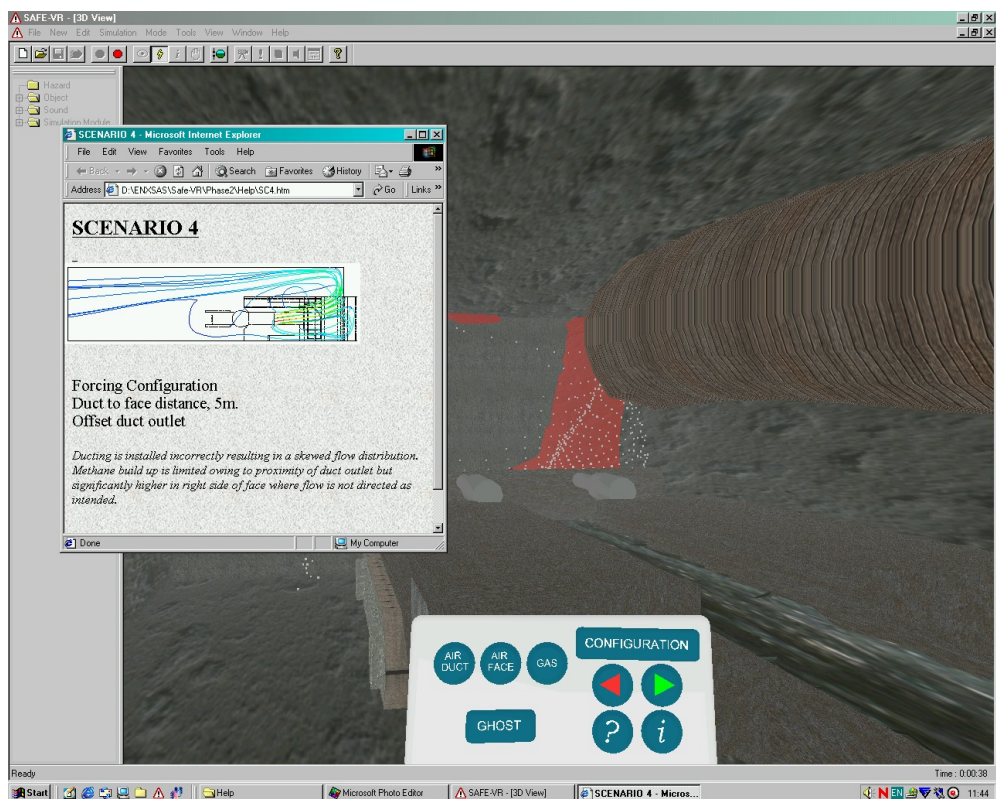


Figure 8.41 Scenario 4, Level 3 HTML documentation, methane and face airflow visualisation

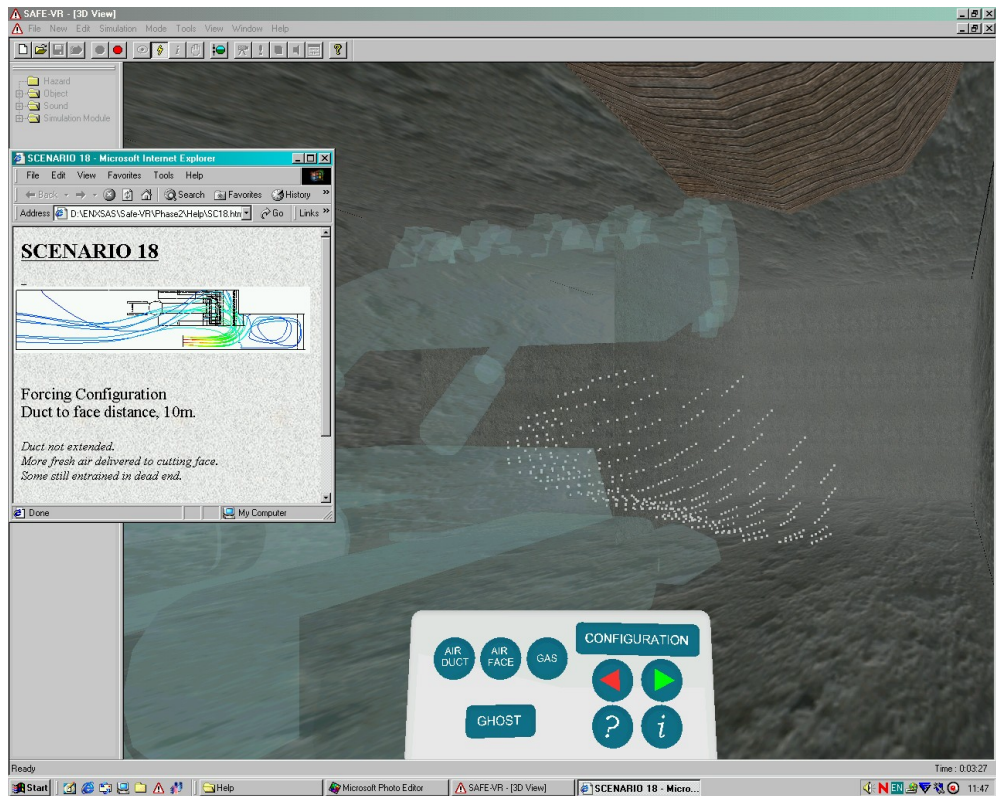


Figure 8.42 Scenario 18, Level 3 HTML documentation, duct airflow visualisation

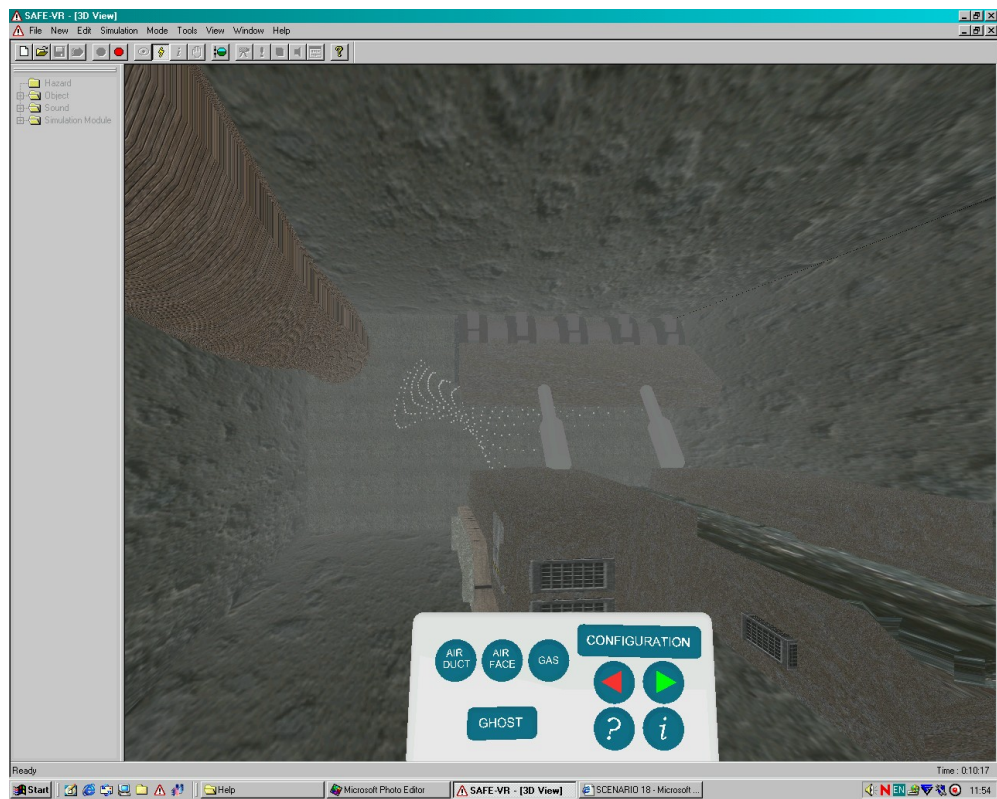


Figure 8.43 Scenario 12, Face airflow visualisation



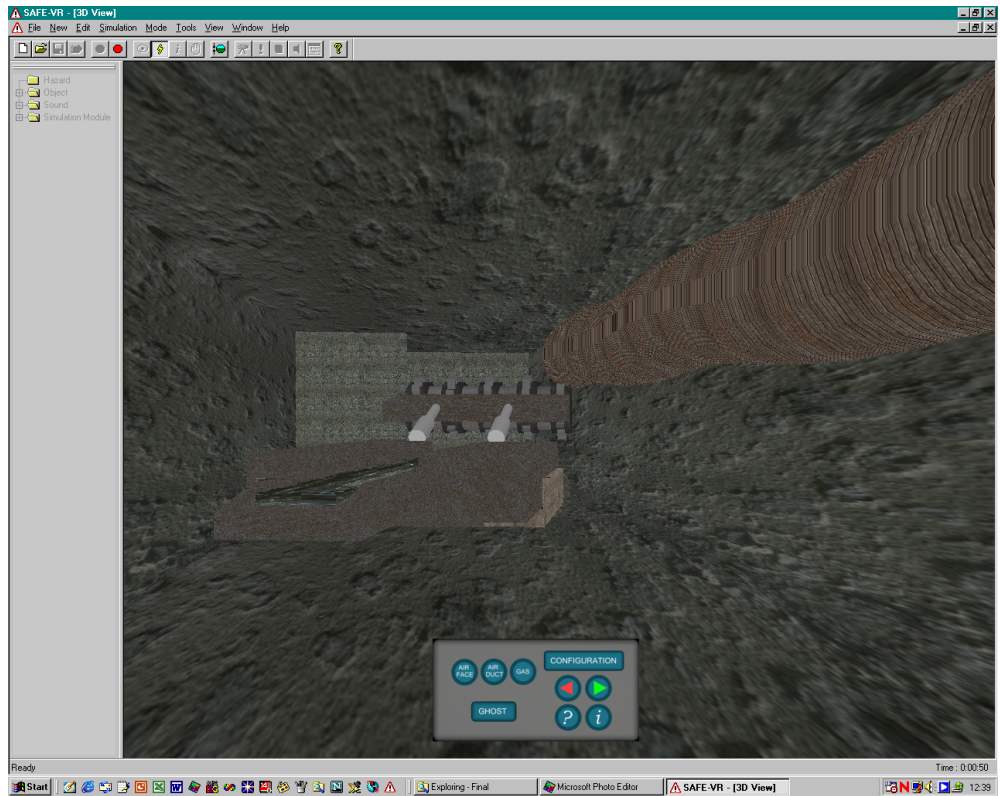


Figure 8.44 Miner reversing into buttock side cut position

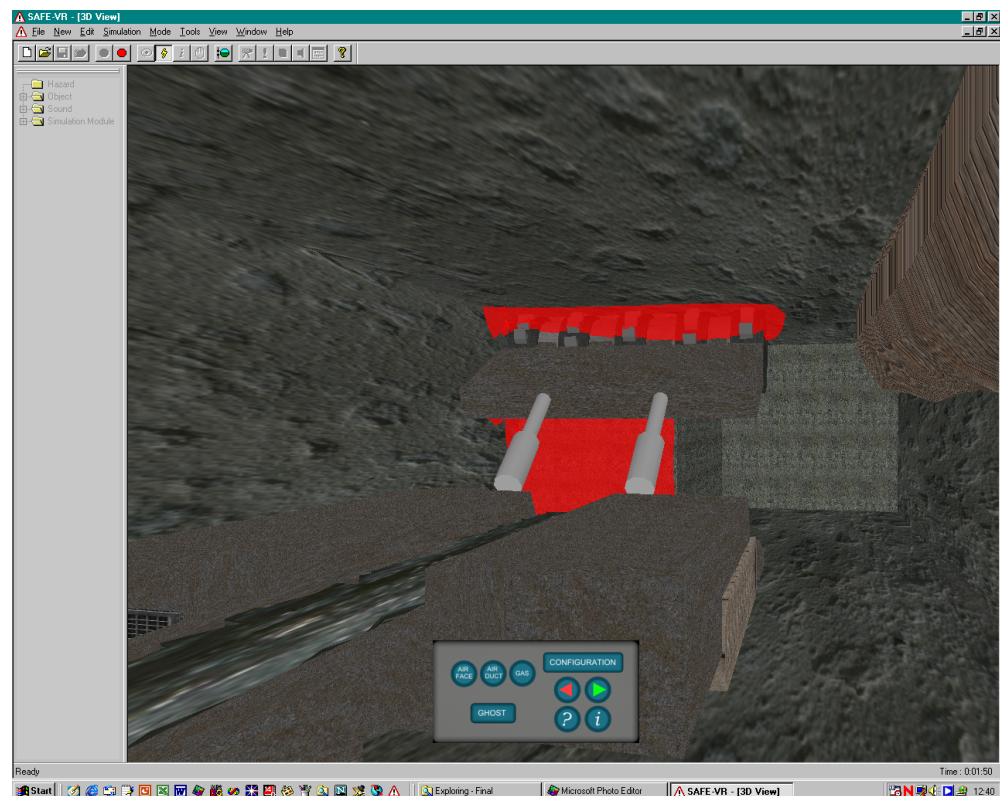


Figure 8.45 Scenario 18, methane gas dispersion

## **8.7 Application Assessments**

### **8.7.1 Extent of Hardware Capabilities**

Throughout the development of the VR application the limits imposed by the processing power and memory storage capacity of the available hardware have imposed strict boundaries upon the extent to which the application could deliver its final objectives. The application as specified and tested during the second phase of development was representative of the limits of the available desktop architecture hardware used for the construction and evaluation of the application.

The boundaries imposed by the available hardware were considered reached at the point where either the system latency or instability became apparent. This was shown to be clearly problematic during the first phase of development whereby the hardware was unable to support a large enough number of scenarios within the application, necessary to realise an effective training tool. The upgraded hardware used for the second phase did not exhibit the same limitations. The main limiting factor was found to be the number of objects required to be stored rather than the scene polygon count, which is more often associated with the limits of a VR application. The environment itself was constructed using a relatively small number of polygons in the region of 7,000. Each visualisation object was likewise small rarely exceeding 10,000 polygons. Assuming a maximum number of three visualisations exhibited within the scene at any one time, the maximum polygon count displayed and requiring interactive rendering was never more than 37,000. This represents a relatively low count within the VR application field, where the use of a polygon counts of over 100,000 is common. The limitation is therefore primarily focussed upon the requirement of the application to store all required visualisation objects in RAM, to be accessed as required. Since the effectiveness of the application is proportional to the number of alternative scenarios presented to the user, this defines the critical boundary. The second phase of the application development demonstrated

that the capabilities of desktop hardware as a foundation for such an application had only just aligned themselves with the objectives of the project.

### **8.7.2 Performance of Scientific Data Visualisations**

The inclusion of scientific data within the application was intended to serve as an explanation and demonstration of why certain procedures are carried out in order to maintain adequate face ventilation. The technical performance has been covered in the previous section detailing hardware limits.

The visualisation characteristics were chosen such that the primary characteristics of each particular scenario could be demonstrated visually to the potential user. Since the incorporation of numerous scenarios was fundamental to the design of the application it was important that the visualisations for each scenario were created using the same parameters to allow direct comparison and consequent appreciation of the change in ventilation characteristic for each scenario. In this respect, the visualisations performed well. Changes made to the configuration leading to a new scenario led to visible changes in each visualisation. This was particularly effective with regard to the seeded particle animations viewed in the region of the cutting face where even small changes could be easily observed as a change in face flow characteristic.

The airflow animations seeded from the forcing duct outlet performed less well, differences were evident though it was difficult to make direct quantifiable comparisons. This may be due to the extended life and scattering of the particles in comparison to the face region animation. Under these conditions it was difficult to recall the precise characteristics of the duct airflow of the previous scenario, hence an appreciation of the change was difficult.

The methane dispersion isosurfaces were much more accommodating in terms of making direct comparisons based upon the recollection of the visualisation of the previous scenario. Differences were easily observed owing to the static nature of the visualisation, there was a minimal amount of information on display. The display of methane isosurfaces also worked well with the face region flow animations since the two are directly related. Concentrations of methane were seen to collect in regions of dead air exhibited by the face flow animation.

### 8.7.3 Comparison of Application with Project Objective

The original project objective was defined in Chapter 1, in general terms as *the creation of a software based educational aid to be used in the training of ventilation supervisory officials and heading teams*. The following key contributory factors were used as a reference upon which the application in its final form could be compared.

- *This training package will enable the visualisation of the consequences of potentially hazardous events associated with the ventilation of rapid development drivages.*
  - The ultimate consequences associated with poor ventilation practice such as localised ignitions or explosions are not displayed within the VR application. The application works upon the principle of demonstrating cause and effect relationships, i.e. a change to the installation of the ventilation system leading to the effects manifested in terms of the general body concentration of the mixed methane gas emissions.
- *The project will involve the structured integration of computational fluid dynamics (CFD) data into a virtual reality (VR) environment with the aim of allowing trainees much greater appreciation of the*

*reasoning behind current regulations regarding ventilation procedures.*

- The CFD visualisations incorporated within the application were designed to demonstrate visually the link between a change in physical environment, the consequent change in air movement and the final effect upon methane dispersion.
- *The project will address this concern by effectively increasing the perceptual ability of the trainee and allowing the exposure to hazardous situations not obtainable through traditional training techniques.*
  - Cause and effect in terms of ventilation characteristic cannot be observed in the real world. However, the application uses graphical visualisations in a static and dynamic manner such that ventilation characteristics can be observed intuitively requiring no detailed explanation. The application therefore extends the users perception to those environmental characteristics that cannot be observed in reality. The user is therefore able to modify their behaviour according to a greater number of influences.

#### **8.7.4 Conclusions**

The following conclusions were drawn based upon the work carried out during the second phase of application development.

*By widening the range of CFD data made available to the application development process the educational potential of the application had increased.*

*The limits imposed by the upgraded hardware used for testing during phase 2 represented the minimum required to adequately satisfy the global project objectives.*

*By using additional HTML based documentation it was possible to incorporate active instruction into the application.*

## **8.8 Summary**

This chapter has detailed the work carried out during the development of the application and implementation of the interface utility developed in Chapter 8 along with the application of 3D modelling methods and the use of the VR simulation building application, SAFEVR™.

The CFD simulation data library upon which the application was developed around was described in terms of the variables contained within SAFEVR™. These variables formed the basis upon which the scenarios could be controlled from within the first phase of the application. The scenarios were based upon the orientation of the CM cutting boom, the depth of cut, the location of the cut and the activation of the exhaust scrubber fan. This represented a potential 24 possible scenarios for which CFD data was provided. Due to anticipated limitations imposed by available computer hardware the initial application development was concerned with the simulation data representing the ventilation of the machine operator side cut only.

The development of the final application was split into two primary phases. The first phase detailed the VR world building, the animation and CFD data post processing required to generate the object library for the application. In addition, the control of the application was implemented using the built in visual logic based programming language within SAFEVR™. This was described as the IECS and details of the major control networks were provided. Also introduced within the first phase was the user control methodology. The control panel and available options were described appropriately. The section detailing the first phase development concluded with the illustration of a number of computer screen image captures detailing the application running at various stages. A discussion and series of



conclusions were drawn based upon the identified weakness of the first phase application.

Phase 2 of the development of the application addressed those weaknesses identified during the first phase. This was primarily concerned with the creation of an additional series of CFD models to exhibit further scenarios depicting examples of good and bad practice and the initiation of remedial measures to recover potential hazardous situations. Details of the construction and solution of the additional CFD models were provided. The development and use of an HTML based online assistance aid to improve the self-learning and training experience of the user was also detailed. The Chapter concluded with an overall subjective evaluation of the performance of the applications in satisfying the original objectives of the project.

## CHAPTER 9

### SUMMARY, CONCLUSIONS AND FURTHER WORK

The following sections present and summarise the main findings of the proceeding investigations. General conclusions are given and discussed and areas of potential future investigation are highlighted.

#### 9.1 Summary of Thesis Investigations

The first six chapters presented necessary technical background to the subject area under investigation. The remainder of the thesis introduced and demonstrated the methodologies and techniques developed to provide an integrated VR world model within which to view the simulation of ventilation and methane gas dispersion models produced by CFD models.

During the development of the application leading up to and as presented in Chapter 8 a number of conclusions were drawn regarding the methods and procedures necessary for the completion of the project in addition to the performance of the application itself. These are summarised in the following conclusions.

**Chapter 6** presented a preliminary evaluation of the visual effectiveness of directly importing standard CFD data visualisations representing a flow domain reflecting those characteristics present within an auxiliary ventilated driveway into a VR environment. It was shown that the standard representations of flow data performed badly within the VR context in two respects. Firstly, the visualisations were not optimised in terms of their construction exhibiting relatively high polygon usage irrelevant within a CFD post processing environment but critical within the VR context. Secondly, the visualisations were shown to lack clarity when viewed from the internal perspective of the VR context.

CFD representations of geometry exhibit only those characteristics relevant to fluid flow. VR representations incorporate a much higher level of detail. When displaying CFD data within a VR world primary boundaries must match the CFD data domain precisely thus limiting the realism of the VR representation to that of the CFD model. The reduction in detail can be balanced through the use of detailed textures.

The main limiting factor in respect of the ability of the application to incorporate a wide range of scenarios is the requirement that the visualisation objects be pre-processed and stored in memory.

The application demonstrated that CFD data primarily used as a basis of scientific evaluation could be incorporated into a VR training style environment in a manner such that common ventilation characteristics could be demonstrated visually within a recognisable context thus offering the potential upon which to build an educational tool.

**Chapter 7** detailed an evaluation of some current visualisation algorithms. In scientific terms absolute accuracy is a primary objective at the cost of computationally intensive algorithms. It was shown that in the case of the display of visualisation data to an immersed observer the level of accuracy can be reduced to that of 'visible error' thus allowing the utilisation of coarse algorithms such as Hill Climbing.

The analysis presented Chapter 7 demonstrated that coarse algorithms could be applied to static data where the number of glyphs was sufficient to demonstrate a generalised characteristic.

It was shown that for the purposes of particle tracing coarse algorithms such as the HC scheme were not sufficiently accurate since the inherent error was demonstrated to present a visible error upon consideration of the cumulative effect over the particle trace lifespan. It was also shown that trace termination was a particular problem inherent within this approach.

A variable time step VSI based algorithm using an Eulerian approach incorporating a linear error tolerance of 0.025m was the minimum required to produce negligible visible trace divergence over a lifespan of 10 seconds for a trace passing through a representative range of flow conditions.

**Chapter 8** detailed the work undertaken to complete the final application and satisfy the original project objective. The project achieved its primary objective in that a complete VR based application incorporating CFD data in the form of static and dynamic visualisations was created using a combination of commercially available 3D modelling software and through the application of known flow visualisation algorithms to raw text based CFD data. It was shown that in order for an application such as this to be constructed it was necessary to bridge the gap between CFD output and VR visualisation through the application of an interface utility designed specifically for the task.

## **9.2 Original Contributions to Knowledge**

*This study has involved the performance of a number of evaluation exercises the results of which have guided the development of the final application. In particular, the results and conclusions of the following series of studies were employed:*

- *The quantitative and qualitative assessment of the ability of current CFD and VR methods and technologies to integrate into one environment and the identification of deficiencies existing with those current methods.*
- *The evaluation of existing CFD data visualisation algorithms applied to scalar and vector data originating from a CFD*

*representation of the type of flows present in a typical rapid development driveage.*

- The definition and visualisation of numerical accuracy of two interpolation schemes (HC and VSI) applied to scalar data and vector data using a range of fixed time steps and variable time step with linear error tolerance control.
- The construction of graphical visualisations based upon the above algorithmic approaches using computationally efficient methods allowing real time rendering within a VR environment.
- The construction of a representative VR based rapid development driveage environment for the purposes of viewing CFD based data visualisations relating to airflow and pollutant dispersion in response to a users actions using a logic based control system.
- The visualisation of cause and effect relationships governing the development of hazardous scenarios within the rapid development driveage environment.

### **9.3 Further Work**

From the summaries and conclusions detailed within this thesis a number of recommendations were made regarding the potential development of this research:

The use of a purpose designed VR simulation building application, SAFEVR™, fulfilled a critical role in offering a stable foundation upon which the application could be built. In addition, this application offered a visual operator based programming language that facilitated the control of user interaction. However, the major limitation to the adoption of this approach was the high level of computer memory storage required to store the large number of objects associated with each visualisation scenario. Consequently, it would be an advantage if SAFEVR™ and other simulation building applications were able to offer real time post-processing of finite based data visualisations sets. The CFD simulation data sets, required for the

visualisation of each scenario, are relatively small. Thus, given that further developments in the data optimisation procedures detailed in Chapter 5 are forthcoming, and the use of the next generation of computer processors, the real time processing of the simulation data may soon be realised. This advance will reduce the need to pre-process and store all of the visualisation objects required for each ventilation scenario. However, this advancement will still be limited by the amount of computer storage available to store the original CFD simulation data in place of the visualisation objects.

The use of HTML based documentation greatly increased the educational support for the use of the application. This aspect of the project could be further developed to incorporate existing training media, including extracts from books, digital images stills and videos. This would reinforce the context and realism of the scenarios displayed and thus greatly improve the educational and training value of the application.

The success of the application is greatly influenced by the ability of the CFD simulation models to accurately replicate and clearly communicate the flow processes that dictate the cause and effect of potential environmental hazards. It is therefore essential that further field validated CFD simulation models be developed, such that both improvements to current models are made and further additional scenario simulations added, within future developments of the application.

## REFERENCES

**Aeschliman, D.P., Oberkamp, W.L., Blottner, F.G. (1995)** *A Proposed Methodology for Computational Fluid Dynamics Code Verification, Calibration and Validation*. IEEE.

**Alexandrou, A. (1999)** *Fundamentals of Fluid Dynamics*. US Imports & PHIPES.

**Bakke, P., Leach, S.J. (1962)** *Principles of Formulation and Dispersion of Methane Roof Layers and some Remedial Measures*. Mineral Engineering, 22, pp645-658.

**Bardorfer, A., Munih, M., Zupan, A., Primožic, A. (2001)** *Upper Limb Motion Analysis Using Haptic Interface*. IEEE/ASME Transactions on Mechatronics, Vol. 6, No. 3, September.

**Bartsch, M., Clemens, M., Hippler, T., Weiland, T. (2001)** *Advanced Electromagnetic Field Visualisation Using the Virtual Reality Modelling Language Standard*. IEEE Transactions on Magnetics, Vol. 37, No. 5, September.

**Batchelor, G.K. (1967)** *An Introduction to Fluid Dynamics*. Cambridge University Press.

**Boud, A.C., Haniff, D.J., Baber, C., Steiner, S.J. (1999)** *Virtual Reality and Augmented Reality as a Training Tool for Assembly Tasks*. IEEE. pp32-36.

**Bradley, R.G. (1988)** *CFD Validation Philosophy*. AGARD Symposium on Validation of Computational Fluid Dynamics, Paper 1, Portugal.

**Brooks, F.P. (1999)** *Whats Real About Virtual Reality?*. IEEE.

**Buning, P. (1989)** *Numerical Algorithms in CFD Post Processing, Computer Graphics and Flow Visualization in Computational Fluid Dynamics*. Von Karmen Institute for Fluid Dynamics Lecture Series, July.

**Buning, P. (1988)** *Sources of Error in the Graphical Analysis of CFD Results*. Journal of Scientific Computing, No. 2, Vol. 3.

**Brodlie, K.W., Gallop, J.R., Grant, A.L., Haswell, J. (1999)** *Review of Visualization Systems*. Advisory Group on Computer Graphics Technical Report. 24<sup>th</sup> February.

**Calizaya, F., Mousset-Jones, P., (1997)** *A Method of Designing Auxiliary Ventilation Systems for Long Single Underground Openings*. Proceedings of the 6<sup>th</sup> US Mine Ventilation Symposium, pp245-250.

**Cashdollar, K.L., (1996)** *Coal Dust Explosibility*. Journal of Loss Prevention in the Process Industry. Vol. 9, No. 1, pp65-76.

**Chambers, J.M., Cleveland, W.S., Turkey, P.A. (1983)** *Graphical Methods for Data Analysis*. Wadsworth.

**Chang, S.K. (1989)** *Principles of Pictorial Information Systems Design*. Prentice Hall.

**Chasse, P. (1993)** *Sensitivity Study of Different Modelling Techniques for the Computer Simulation of Tunnel Fires Comparison with Experimental Measurements*. The CFDS International Users Conference.

**Chen, Q., Xu, W. (1998)** *A Zero Equation Turbulence Model for Indoor Airflow Simulation*. Energy and Buildings, 28, pp137-144.



**Chiyotani, K., Hosoda, Y., Aizawa, Y. (1998)** *The Measurement of IL-1 IL8, TNF for the Diagnosis of Pneumoconiosis. Advances in the Prevention of Occupational Respiratory Diseases.* Elsevier, Amsterdam, pp845-848.

**Chung, T (1977)** *Finite Element Analysis in Fluid Dynamics.* McGraw Hill, pp 60-90.

**Cignoni, P., Costanza, D., Montani, C., Rochini, C., Scopigno, R. (1996)** *Simplification of Tetrahedral Meshes with Accurate Error Evaluation.* IEEE.

**Clark, J. (1976)** *Heirarchical Geometric Models for Visible Surface Display.* COMM, ACM 19, No. 10.

**COSHH HSE (1999)** *Health & Safety Executive 1999a.* COSHH Regulations, HSE Books.

**Cosman, M., Schumacker, R. (1981)** *System Strategies to optimise CIG Image Content.* Proceedings IMAGE II Conference, Arizona.

**D'Cruz, M., Eastgate, R., Wilson, J.R. (1997)** *A Study into the Issues Involved when Applying Virtual Reality Technology to Training Applications.* VIRART. VIRART (Virtual Reality Applications Research Team), Department of Manufacturing Engineering & Operations Management, University of Nottingham.

**Darmofal, D. & Haimes, R. (1994)** *An Analysis of 3D Particle Path Integration Algorithms.* Journal of Computational Physics, 123, pp182-195.

**Darmofal, D. & Haimes, R. (1992)** *Visualisation of 3D Vector Fields: Variations on a Stream.* AIAA.

**DeLeon, V., Berry, R. (2000)** *Bringing VR to the Desktop: Are You Game?.* Interpretive Environments, IEEE Multimedia, IEEE.

**Denby, B., Schofield, D., McClarenon, D., Williams, M., Walsha, T. (1998)** *Hazard Awareness Training for Mining Situations using Virtual Reality*, Proceedings of APCOM XXVII Symposium, London, UK, 19<sup>th</sup>-23<sup>rd</sup> April.

**Dhatt, G., Touzot, G. (1984)** *The Finite Element Method Displayed*. J.Wiley, pp110.

**Duffy, V.G. (1999)** *Impact of an Intelligent Tutor on Risk and Sound Perception in CNC Machining*. IEEE.

**Durst, F., Melling, A., Whitelaw, J.H. (1981)** *Principles and Practice of Laser Doppler Anemometry*. AC. Press, London.

**Ebert, D.S., Yagel, R., Scott, J., Kurzion, Y., (1994)** *Volume Rendering Methods for Computational Fluid Dynamics Visualization*. IEEE.

**Feiner, S., Thalmann, D. (2000)** *Virtual Reality*. IEEE.

**Foley, J. (2000)** *Getting There; The Top Ten Problems Left*. Vision 2000. IEEE, January/February.

**Fuchs, H., Kedem, Z.M., Uselton, S.P. (1977)** *Optimal Surface Reconstruction Using Planar Contours*. Comm of the ACM 20, 10, pp693-702, October.

**Gadomski, R.R., Atchison, D.J., Jero, A.J., Haney, R.A. (1985)** *Evaluation of a Portable Hand Held Respirable Dust Monitor*. 2<sup>nd</sup> US Mine Ventilation Symposium, Reno, NV.

**Gallagher, R.S. (1991)** *Span Filtering: An Optimization Scheme for Volume Visualization of Large Finite Element Models*. IEEE Proceedings Visualization '91. pp68-74.

**Garcke, H., Preusser, T., Rumpf, M., Telea, A., Weikard, U., Van Wijk, K. (2001).** *A Phase Field Model for Continuous Clustering on Vector Fields*. IEEE Transactions on Visualization and Computer Graphics, Vol. 7, No. 3, July-September.

**Giles, M., Haines, R. (1990)** *Advanced Interactive Visualization for CFD*. Computer Systems in Engineering, Vol. 1, No. 1, pp51-62.

**Gilham, S., Deaves, D.M., Woodburn, P. (2000)** *Mitigation of Dense Gas Releases within Buildings: Validation of CFD Modelling*. Journal of Hazardous Materials, 71, pp193-218.

**Globus, A (1994)** *Principles of Information Display for Visualization Practitioners*. Report NAS 94 002. NASA Contract NAS 2-12961. November.

**Goebel, M., Hirose, M., Rosenblum, L. (2001)** *Today's VR*. IEEE, November/December.

**Groves, J., Cain, J.R. (2000)** *A Survey of Exposure to Diesel Engine Exhaust Emissions in the Workplace*. Annals of Occupational Hygiene, Vol. 44, No. 6, pp435-447.

**Hall, C.R., Stiles, R.J., Horwitz, C.D. (1998)** *Virtual Reality for Training: Evaluating Knowledge Retention*. IEEE. pp184-189.

**Hargreaves, D.M, Lowndes, I.S. (2001)** *An Assessment of the Future use of Computational Fluid Dynamics for Network Modelling*. Proceedings of the 7<sup>th</sup> International Mine Ventilation Congress. Krakow, Poland, June 2001.

**Hargreaves D.M., Lowndes, I.S (2000)** *The Evaluation of the Design and Operation of Alternative Auxiliary Ventilation Layouts for use with*

*Continuous Miner Systems in Rapid Development Drivages*. ECSC Project No. 7220-AC-857, Final Report, December.

**Hargreaves D.M., Moloney, K.W., Lowndes, I.S (1998)** *Preliminary Computational Fluid Dynamics Simulations of Methane Dispersion in a Heading*. 2<sup>nd</sup> International Symposium on Mine Environmental Engineering, Brunel University, UK, pp204-213, July.

**Hoppe, H. (1996)** *Progressive Meshes*. Computer Graphics, Vol. 30..

**Huang, J., Menq, C. (2001)** *Automatic Data Segmentation for Geometric Feature Extraction from Unorganized 3D Co-ordinate Points*. IEEE Transactions on Robotics and Automation, Vol. 17, No. 3, June.

**Hultquist, J.P.M (1994)** *Constructing Stream Surfaces in Steady 3D Vector Fields*. NASA AMES Research Centre.

**Hultquist, J.P.M (1995)** *Interactive Numerical Flow Visualization using Stream Surfaces*. PhD Dissertation. University North Carolina, Chapel Hill, May.

**Hunt, R.W.G (1998)** *Measuring Colour*. Fountain Press, UK, p23.

**IARC, (1989)** *IARC Monographs on the Evaluation of Carcinogenic Risks to Humans. Diesel and Gasoline Engine Exhausts and some Nitroarenes*. Vol. 46.

**Isoh, T., Yamaguchi, Y., Koyamada, K. (2001)** *Fast Isosurface Generation using the Volume Thinning Algorithm*. IEEE Transactions on Visualization and Computer Graphics, Vol. 7, No. 1, January-March.

**Jazbec, M., Fletcher, D.F., Hayes, B.S. (2000)** *Simulation of the Ignition of Lean Methane Mixtures using CFD Modelling and a Reduced Chemistry Mechanism*. Applied Mathematical Modelling, 24, pp689-696.

**Jin, L., Wen, Z. (2001)** *Adorning VRML Worlds with Environmental Aspects*. IEEE Computer Graphics & Applications, January/February.

**Johnson, A., Moher, T., Cho, Yong Joo., Lin La Ju. (2002)** *Augmenting Elementary School Education with VR*. IEEE Computer Graphics & Applications. March/April.

**Kenwright, D (1997)** *Visualization Algorithms for Gigabyte Datasets*. Report, NASA AMES Research Centre.

**Kenwright, D., Lane, D. (1996)** *Interactive Time-Dependent Particle Tracing using Unstructured Grids*. . IEEE Transactions on Visualization and Computer Graphics, Vol. 2, No. 2, June.

**Kenwright, D., Lane, D. (1995)** *Optimization of Time-Dependent Particle Tracing using Tetrahedral Decomposition*. Proceedings Visualisation 1995, IEEE CS Press, pp321-328, Atlanta, October.

**Kenwright, D., Mallinson, G, D., (1992)** *A 3D Streamline Tracking Algorithm Using Dual Stream Functions*. IEEE.

**Keppel, E. (1975)** *Approximating Complex Surfaces by Traingulation of Contour Lines*. IBM. J. Res. Develop. 19,1, pp2-11, January.

**Kniss, J., McCormick, P., Hansen, C., (2001)** *Interactive Texture Based Volume Rendering for Large Data Sets*. IEEE, 2001, July/August.

**Konduri, I.M., McPherson, M.J., Topuz, E. (1997)** *Experimental and Numerical Modelling of Jet Fans for Auxiliary Ventilation in Mines*.

Proceedings 6<sup>th</sup> International Mine Ventilation Congress. May 17<sup>th</sup>-22<sup>nd</sup>, Pittsburgh, Pennsylvania.

**Kosslyn, S. (1994)** *Image & Brain: The Resolution of the Imagery Debate*. MIT Press, Cambridge, Mas, USA.

**Kuhner, S., Rank, E., Crafczyk, M. (2001)** *Efficient Reduction of 3D Simulation Results Based on Spacetree Data Structures for Data Analysis in Virtual Reality Environments*. AVR II & CONVR 2001, Chalmers, Gothenburg, Sweden, October 4<sup>th</sup>-5<sup>th</sup>.

**Lam, C.K.G., Bremhorst, K.** *A Modified Form of the k e Model for Predicting Wall Turbulence*. ASME, Journal of Fluid Engineering, 103, pp456-460.

**Larsson, P., Vastfjall, D., Kleiner, M. (2001)** *Do We Really Live in a Silent World? The (Mis)use of Audio in Virtual Envinronments*. AVR II & CONVR 2001, Chalmers, Gothenburg, Sweden, October 4<sup>th</sup>-5<sup>th</sup>.

**Lawton, M. 1999** *Advancing 3d Through VRML on the WEB*. IEEE Computer Graphics & Applications.

**Lohner, R., Ambrosiano, J. (1990)** *A Vectorized Particle Tracer for Unstructured Grids*. Journal of Computational Physics, Vol. 91, pp22-31.

**Lombard, M., Ditton, T. (1997)** *At the Heart of It All, The Concept of Presence*. Journal of Computer Mediated Communication. (Internet), 3, 2, Internet Address. [Http://www.ascusc.org/jcmc/vol3/issue2/lombard.html](http://www.ascusc.org/jcmc/vol3/issue2/lombard.html), Accessed 5<sup>th</sup> October.

**Lorenson, W.E (1987)** *Marching Cubes: A High Resolution 3D Surface Construction Algorithm*. Computer Graphics, Volume 21, No. 4, July.

**Lowndes, I.S., Roberts, B.H., Moloney, K.W. (1994)** *Environmental Monitoring and Control in Headings*. ECSC Research Project 7220-AC/847, October.

**Luebke, D. (1997)** *A Survey of Polygonal Simplification Algorithms*. UNC Technical Report TR97-045.

**Luebke, D. (2001)** *A Developers Survey of Polygonal Simplification Algorithms*. IEEE, May/June.

**Madrzykowski, D., Vettori, R.L. (2000)** *Simulation of the Dynamics of the Fire at 3146 Cherry Tree Road NE Washington DC May 30<sup>th</sup> 1999*. National Institute of Standards and Technology, Report NISTIR 6510.

**Mathew, M.D., Wilkes, N.S., (1986)** *Particle Tracking for 3 Dimensional Fluid Flow Predictions*. Harwell (AERA) Report 12153, June.

**Mc Donald, L (1999)** *Using Colour Effectively in Computer Graphics*. IEEE, July/August.

**McPherson, M.J. (1992)** *Subsurface Ventilation and Environmental Engineering*. Chapman & Hall.

**Meetz, E.J., Meyer, C.F. (1993)** *Some Applications of Ductless Fans in Board and Pillar Headings in South African Coal Mines*. Proceedings of the 6<sup>th</sup> US Mine Ventilation Symposium, pp475-481.

**Mehta, U.B (1988)** *Flight Performance Estimation Utilizing Computational Fluid Dynamics*. Proceedings of the 5<sup>th</sup> National Aerospace Plane Technology Symposium, Vol. 1, October.

**Meyer, C.F. (1994)** *Evaluation of the Suitability of Using Jet Fans to Ventilate Continuous Miner Headings in Collieries*. SIMRAC Final Report, Project No. Col 116, September.

**Moloney, K. (1997)** *An Analysis of Airflow Patterns in Auxiliary Ventilated Drivages*. Phd Thesis, University of Nottingham.

**Moloney K W, Hargreaves, D.M, Lowndes I S (1998)** *Assessment concerning the accuracy of computational fluid dynamic (CFD) simulations in underground auxiliary ventilated headings*, Proceedings of APCOM XXVI, London, May.

**Moloney, K., Hargrave, G.K., and Lowndes, I.S. (1999)** *An analysis of flow patterns in auxiliary ventilated drivages*. Transactions of the Institution of Mining and Metallurgy (Section A: Mining industry), 108, pp 17-26

**Montani, C., Scatini, R., Scopigno, R. (2000)** *Decreasing Isosurface Complexity Via Discrete Fitting*. Computer Aided Geometric Design, Vol.17, pp207-232.

**Mowafy, L., Russo, T., Millar, L. (1993)** *Is Presence a Training Issue?*. IEEE. pp124-125.

**Mutama, K.R. (1996)** *The Experimental Investigation of Jet Fan Aerodynamics Using Wind Tunnel Modelling*. ASME, Journal of Fluids Engineering, Vol. 118, pp322-328, June.

**Nadeau, D.R. (1999)** *Building Virtual Worlds with VRML*. IEEE, March/April.

**Noack, K. (1996)** *Control of Gas Emissions in Underground Coal Mines*. International Journal of Coal Geology, 35, pp57-82.

**Noor, A.K., Wasfy, T.M. (2001)** *Simulation of Physical Experiments in Immersive Virtual Environments*. Engineering Computations, Vol. 18, No. 3/4, pp515-538.



**Oxford (1992)** *Concise Oxford Dictionary*. Oxford University Press.

**Philbin, D.A., Ribarsky, W., Walker, N., Hubbard, C.E. (1998)** *Training in Virtual Environments: An Evaluation of Task Appropriateness*. IEEE, pp210.

**Praja, R.J. (2000)** *Real Reality*. Vision 2000. IEEE. January/February.

**Ren, T.X., Edwards, J.S., Jozefowicz, R.R. (1997)** *CFD Modelling of Methane Flow Around Longwall Faces*. Proceedings of the 6<sup>th</sup> International Mine Ventilation Congress, pp247-251.

**Renze, K.J., Oliver J.H. (1996)** *Generalized Unstructured Decimation*. IEEE, C,G &A, Vol. 16, No. 6, pp24-32.

**Ribarsky, W., Bolter, J., Bosch, A., Teylingen, R. (1994)** *Visualisation and Analysis using VR*. IEEE Computer Graphics & Applications.

**Robinson, J., Webster, J. (2001)** *Virtual Reality; A Developers Perspective*. AVR II & CONVR 2001. Conference at Chlamers, Gothenburg, Sweden, October 4<sup>th</sup>-5<sup>th</sup>.

**Rosenblum, L.J (1994)** *Research Issues in Scientific Visualization*. March 1994. IEEE.

**RosenBlum, L., Burdea, G., Tachi, S. (1998)** *VR Reborn* IEEE Computer Graphics and Applications.

**Rosenblum, L., Macedonia, M. (2000)** *Wake Up VR: Virtual Reality Beyond Projection Screens*. IEEE, Computer Graphics & Applications.

**Rosenblum, L.J (2000)** *Virtual & Augmented Reality 2020*. Vision 2000, IEEE, January/February.

**Russ, K., Wetherelt, A. (1999)** *Large Scale Mine Visualisation Using VRML*. IEEE Computer Graphics & Applications. 1999.

**Sabin, M.A., (1986)** *A Survey of Contouring Methods*. Computer Graphics Forum, Vol. 5, pp325-339.

**Sadarjoen, A., Walsum, T. Hin, A.J.S, Post, F.H. (1994)** *Particle Tracing Algorithms for Curvilinear Grids*. Proceedings fifth Eurographics Workshop Visualization in Scientific Computing. Rostock, Germany, May.

**Samtaney, R., Silver, D., Zabusky, N., Cao, J. (1994)** *Visualising Features and Tracking their Evolution*. IEEE Computer, July.

**Sapko, M.J., Weiss, E.S., Cashdollar, K.L., Zlochower, I.A. (2000)** *Experimental Mine and Laboratory Dust Explosion Research at NIOSH*. Journal of Loss Prevention in the Process Industries, pp229-242.

**Sarathay, S., Shujace, K., Cannon, K. (2000)** *Visualisation of Large Complex Datasets Using Virtual Reality*. IEEE.

**Shen, Han-Wei., Johnson, C.R. (1994)** *Differential Volume Rendering: A Fast Volume Visualization Technique for Flow Animation*. IEEE.

**Shiratubin, M.F., Thabet, W. (2001)** *Making the Transition Toward an Alternative VR*. AVR II & CONVR 2001. Conference at Chalmers, Gothenburg, Sweden, October 4<sup>th</sup>-5<sup>th</sup>.

**Shuttleworth, S. (1963)** *Ventilation at the Face of a Heading, Studies in the Laboratory and Underground*. Journal of Rock Mechanics, 1, pp79-92.

**Shultz, M., Reuding, T., Ertl, T. (1998)** *Analysing Engineering Simulations in a Virtual Environment*. IEEE, November/December.

**Sikorski, K., Ueng, S.K., Ma, Kwan-Lui. (1995)** *Fast Algorithms for Visualising Fluid Motion in Steady Flow on Unstructured Grids*. IEEE.

**Squelch, A.P. (1998)** *Application of Virtual Reality for Hazard Awareness Training in South African Gold Mines*. PhD Thesis, University of Nottingham.

**Star Wu, X., Topuz E. (1998)** *Analysis of Mine Ventilation Systems using Operations Research Methods*. Int. Trans. Opl. Res., Vol. 5, No. 4, pp245-254.

**Stone, L., Erickson, T., Bederson, B., Rothman, P. (1994)** *Visualising Data; Is VR the Key?* IEEE.

**Stytz, M.R., Frieder, G., Frieder, O. (1991)** *Three Dimensional Medical Imaging: Algorithms and Computer Systems*. ACM Computing Survey, 23 (4), pp421-499.

**Sutherland, I.E. (1965)** *The Uitimate Display*. Invited lecture, IFIP Congress 1965, also published as "Computer Displays" Scientific American, Vol. 222, No.6, pp57-81, June.

**Sutherland, I.E. (1966)** *Computer Graphics; Ten Unsolved Problems*. Datamation, Vol. 12, No. 5, pp22-27.

**Svidt, K., Bjerg, B., Nielson, T. (2001)** *Initial Studies on Virtual Reality Visualisation of 3D Airflow in Ventilated Livestock Buildings*. AVR II & CONVR 2001. Conference at Chlamers, Gothenburg, Sweden, October 4<sup>th</sup>-5<sup>th</sup>.

**Tam, E.K., Maurel, C., Desbiens, P., Marceau, R.J. (1998)** *A Low Cost PC Orientated Virtual Environment for Operator Training*. IEEE Transactions on Power Systems, Vol. 13, No. 3, August.

**Tam, E.K., Badra, S., Marceau, R.J., Marin, M.A. (1999)** *A Web Based Virtual Environment for Operator Training*. IEEE Transactions on Power Systems, Vol. 14, No. 3, August.

**Tamura, Y., Yamamoto, H., Katayama, H. (2001)** *Mixed Reality: Future Dreams Seen at the Border Between Real and Virtual Worlds*. IEEE, November/December.

**Thimons, E.D., Brechtel, C.E., Adam, M.E., Agapito, J.F.T. (1986)** *Face Ventilation for Oil Shale Mining*. Information Circular No. 9118, US Bureau of Mines.

**Trotts, I.J., Hanmann, B., Joy, K.I., Wiley, D.F. (1998)** *Simplification of Tetrahedral Meshes*. IEEE Visualization 1998 Conf. pp287-295.

**Ueng, Shyh-Kuang., Sikorski, C., Ma, Kwan-Lui. (1996)** *Efficient Streamline, Streamribbon and Streamtube Construction on Unstructured Grids*. IEEE Transactions on Visualization and Computer Graphics, Vol. 2, No. 2, June.

**Ueng, Shyh-Kuang., Sikorski, C., Ma, Kwan-Lui. (1996)** *Out of Core Streamline Visualization on Large Unstructured Meshes*. IEEE Transactions on Visualization and Computer Graphics, Vol. 3, No. 4, October-December.

**Versteeg, H.K., Malalasekera, W. (1995)** *An Introduction to Computational Fluid Dynamics: The Finite Volume Method*. Longman Press.

**Volpe, G. (1987)** *Streamlines and Streamribbons in Aerodynamics*. AIAA Paper, June.

**Walsha, T., Denby, B., Schofield, D. (1998)** *Virtual Realist Based Computer Simulation Program Modelling Underground Fires and*

*Explosions*. 10<sup>th</sup> European Simulation Symposium, Simulation Technology, Science & Art, October 26<sup>th</sup>-28<sup>th</sup>.

**Walsha, T. (1999)** *The Application of Virtual Reality to the Simulation of Mine Fires and Explosions*. Phd Thesis. The University of Nottingham.

**Walsum, T., Post, F., Silver, D., Post, F.J. (1996)** *Feature Extraction and Iconic Visualisation*. IEEE Transactions on Visualization and Computer Graphics, Vol. 2, No. 2, June.

**Wernecke, J (1996)** *The VRML2 Handbook*, Addison-Wesley, Reading.

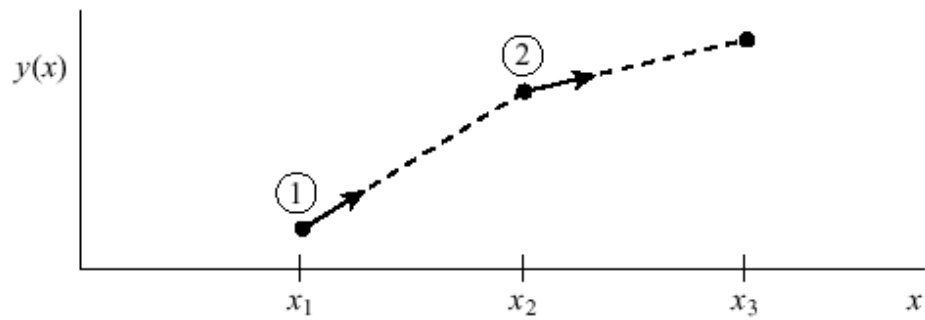
**Westermann, R., Johnson, C., Ertl, T. (2001)** *Topology Preserving Smoothing of Vector Fields*. IEEE Transactions on Visualization and Computer Graphics, Vol. 7, No. 3, July-September.

**Williams, P.L., Max, N.L., Stein, C.M. (1998)** *A High Accuracy Volume Renderer for Unstructured Data*. IEEE Transactions on Visualization and Computer Graphics, Vol. 3, No. 4, October-December.

**Wittenburg, G. (1995)** *Training With Virtual Reality*. Assembly Automation, Vol. 15, No. 3, pp12-14.

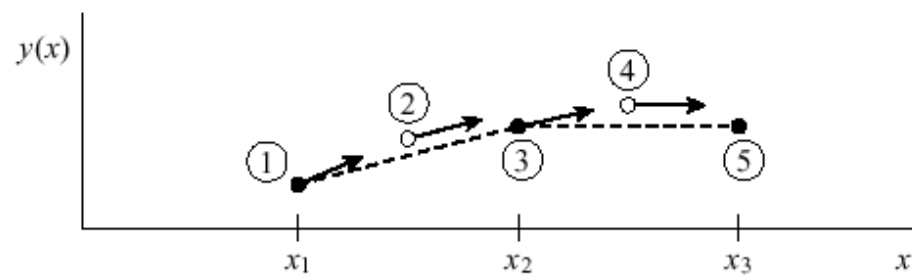
**Woodburn, P.J., Britter, R.E. (1996)** *CFD Simulations of a Tunnel Fire: Part 1*. Journal of Fire Safety, 26, pp35-62.

## APPENDIX I     Runge-Kutta 2<sup>nd</sup> and 4<sup>th</sup> Order



Euler's Method

$$y_{n+1} = y_n + hf(x_n, y_n)$$

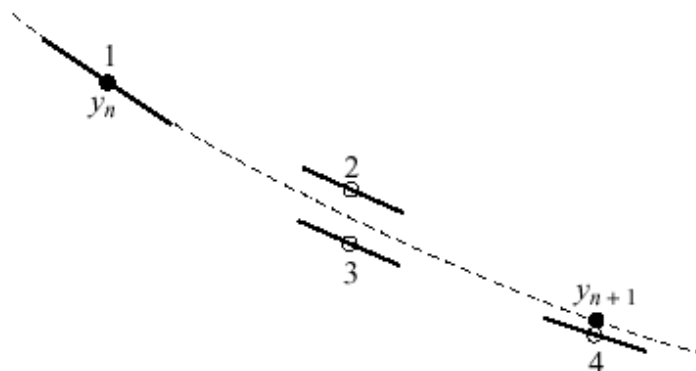


Runge-Kutta 2nd Order

$$k_1 = hf(x_n, y_n)$$

$$k_2 = hf\left(x_n + \frac{1}{2}h, y_n + \frac{1}{2}k_1\right)$$

$$y_{n+1} = y_n + k_2 + O(h^3)$$



Runge-Kutta 4th Order

$$k_1 = hf(x_n, y_n)$$

$$k_2 = hf\left(x_n + \frac{h}{2}, y_n + \frac{k_1}{2}\right)$$

$$k_3 = hf\left(x_n + \frac{h}{2}, y_n + \frac{k_2}{2}\right)$$

$$k_4 = hf(x_n + h, y_n + k_3)$$

$$y_{n+1} = y_n + \frac{k_1}{6} + \frac{k_2}{3} + \frac{k_3}{3} + \frac{k_4}{6} + O(h^5)$$

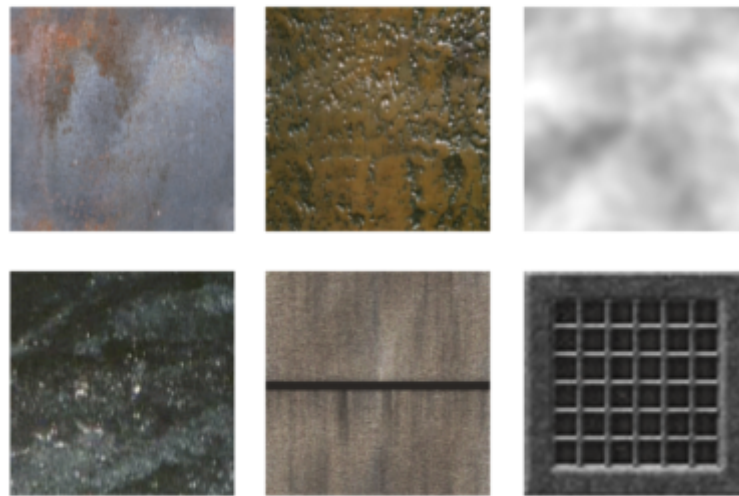
## APPENDIX II    VRML'97 Nodes

Anchor  
Appearance  
AudioClip  
Background  
Billboard  
Box  
Collision  
Color  
ColorInterpolator  
Cone  
Coordinate  
CoordinateInterpolator  
Cylinder  
CylinderSensor  
DirectionalLight  
ElevationGrid  
Extrusion  
Fog  
FontStyle  
Group  
ImageTexture  
IndexedFaceSet  
IndexedLineSet  
Inline  
LOD  
Material  
MovieTexture  
NavigationInfo  
Normal  
NormalInterpolator  
OrientationInterpolator  
PixelTexture  
PlaneSensor  
PointLight  
PointSet  
PositionInterpolator  
ProximitySensor  
ScalarInterpolator  
Script  
Shape  
Sound  
Sphere  
SphereSensor  
SpotLight  
Switch  
Text  
TextureCoordinate  
TextureTransform  
TimeSensor  
TouchSensor  
Transform  
Viewpoint  
VisibilitySensor  
WorldInfo

## APPENDIX III    Model Textures



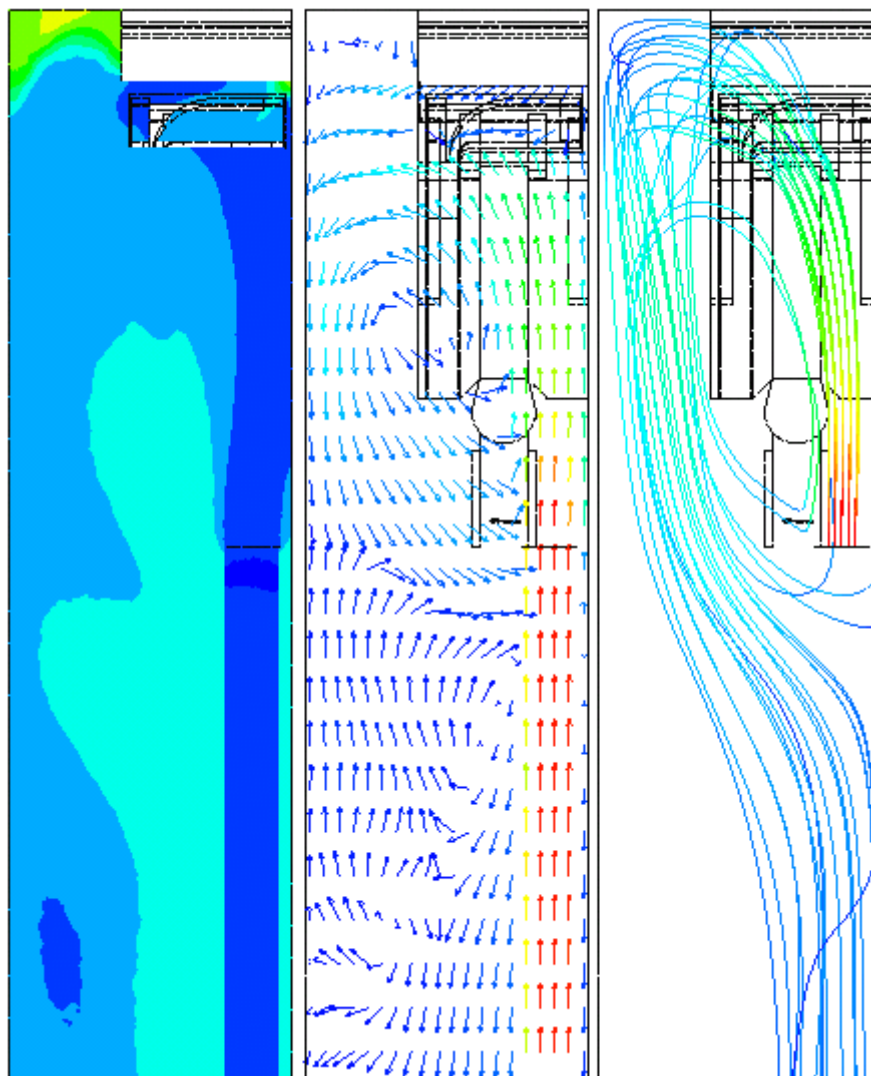
Environment Texture Bitmaps



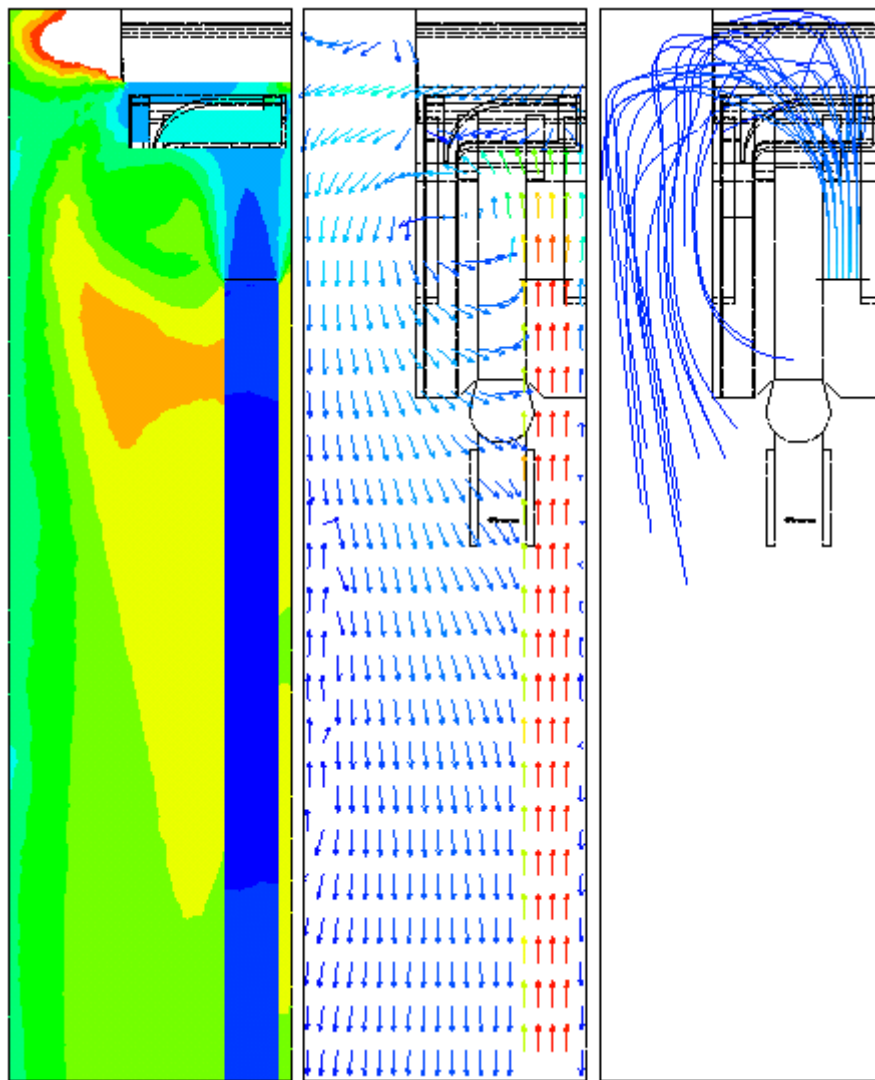
CM Equipment Texture Bitmaps



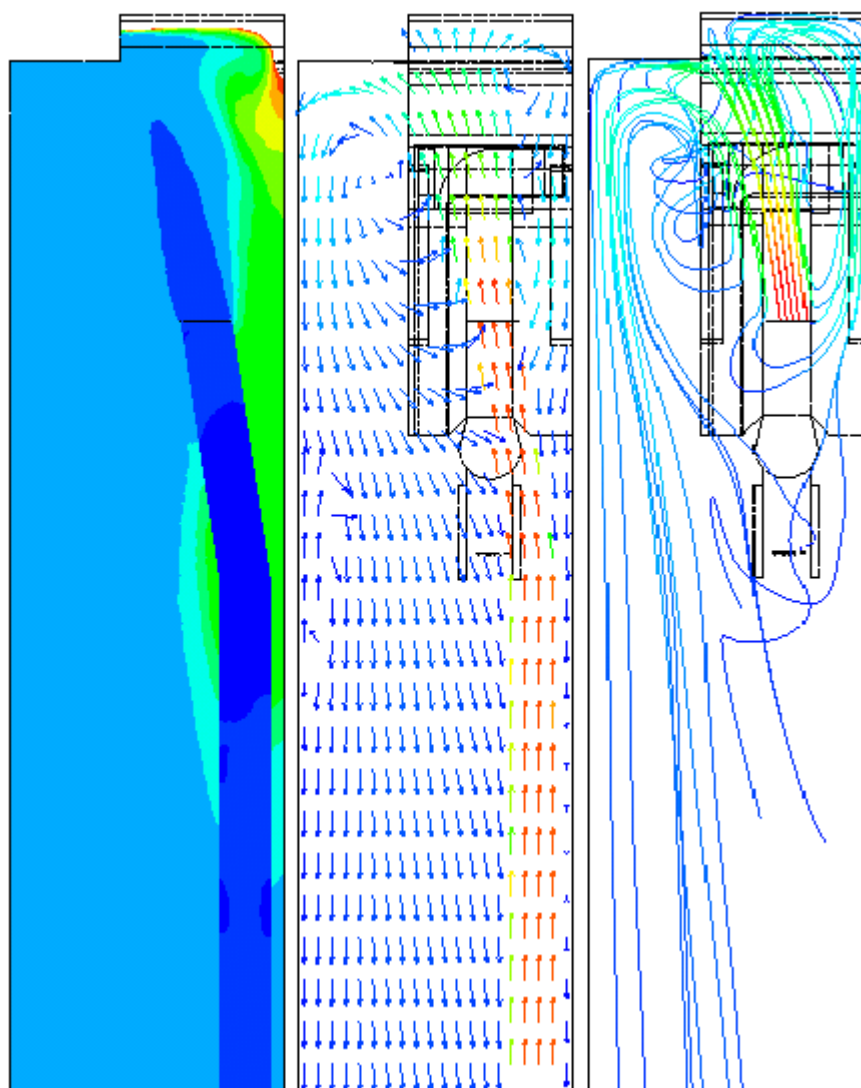
**APPENDIX IV    CFD RESULTS DATA**  
**METHANE 0-1%, VELOCITY VECTORS, STREAMLINES**



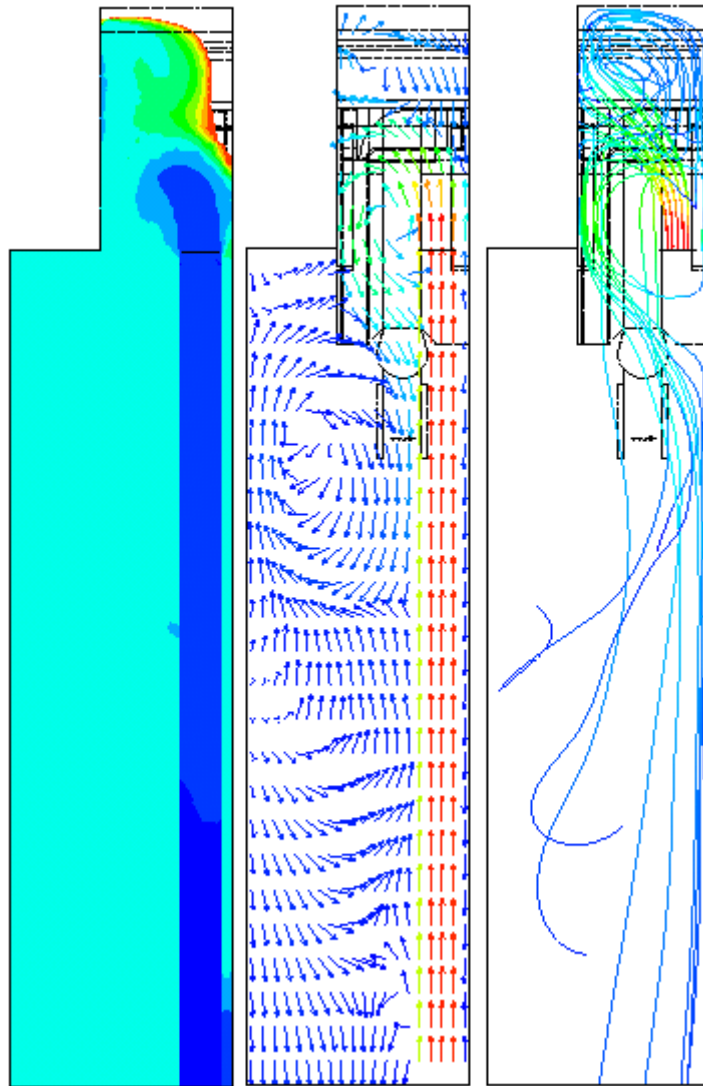
**SCENARIO 1**



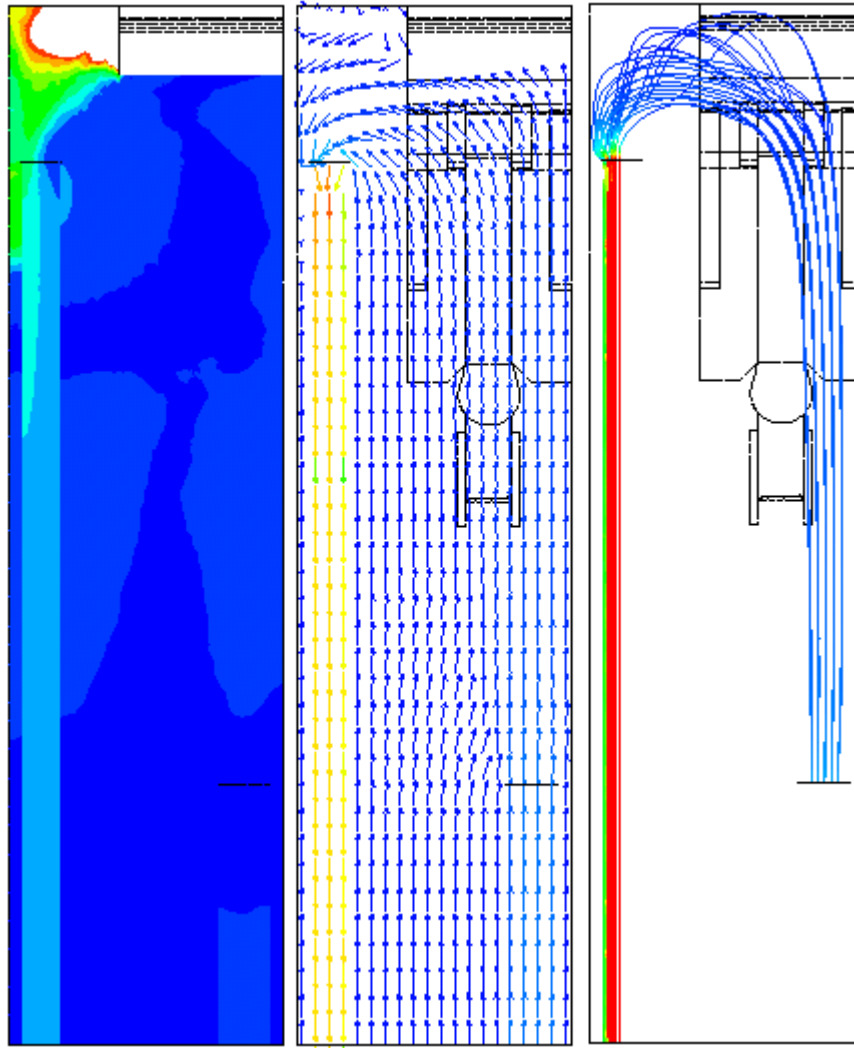
**SCENARIO 2**



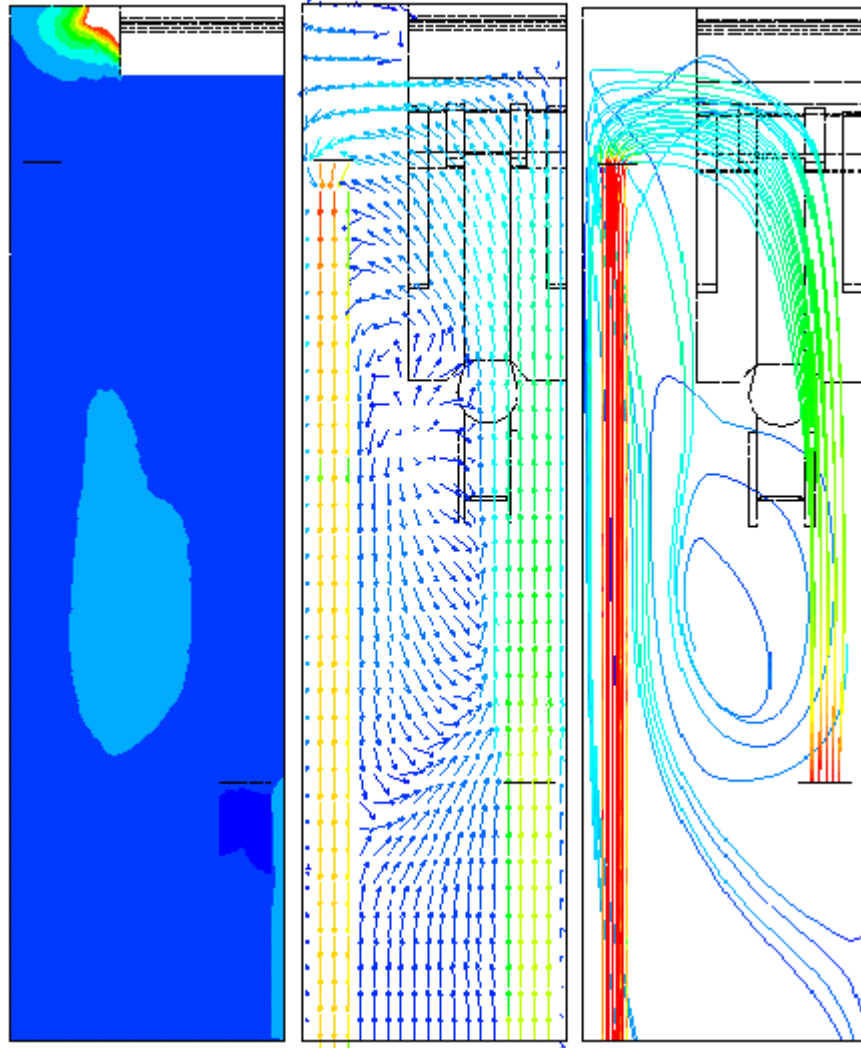
**SCENARIO 4**



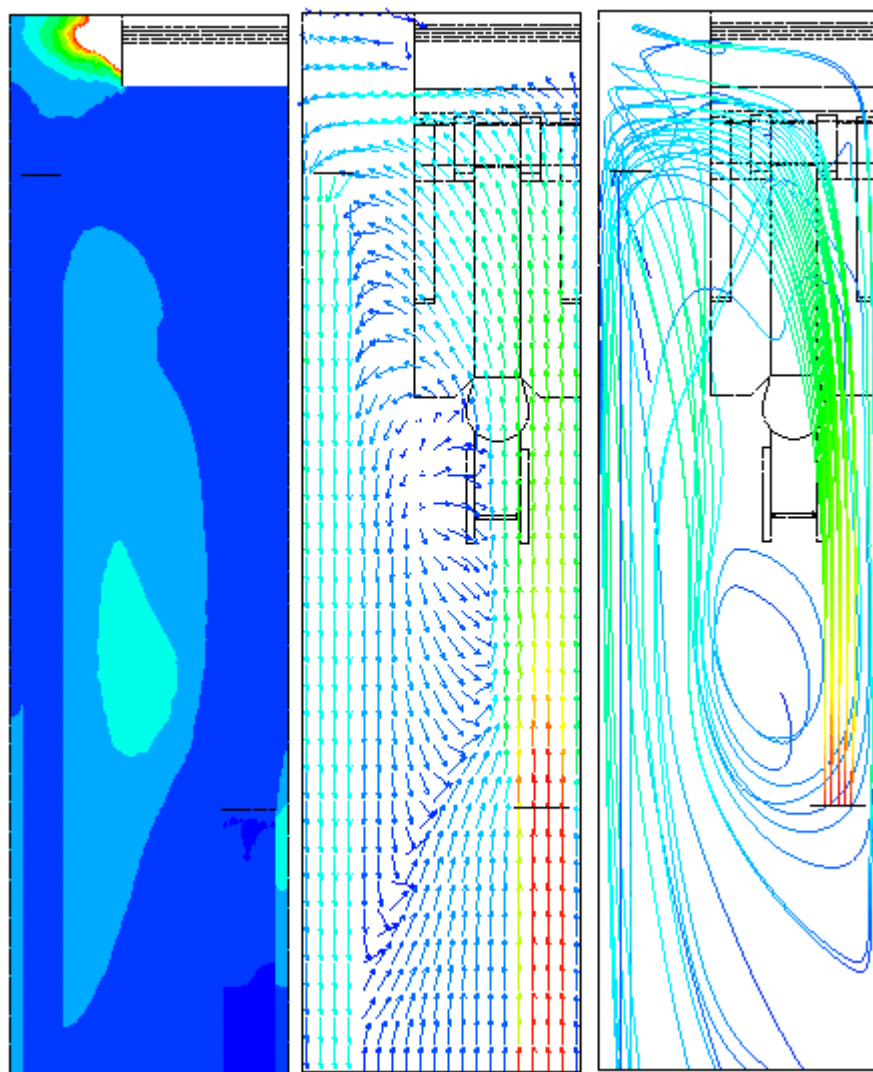
**SCENARIO 8**



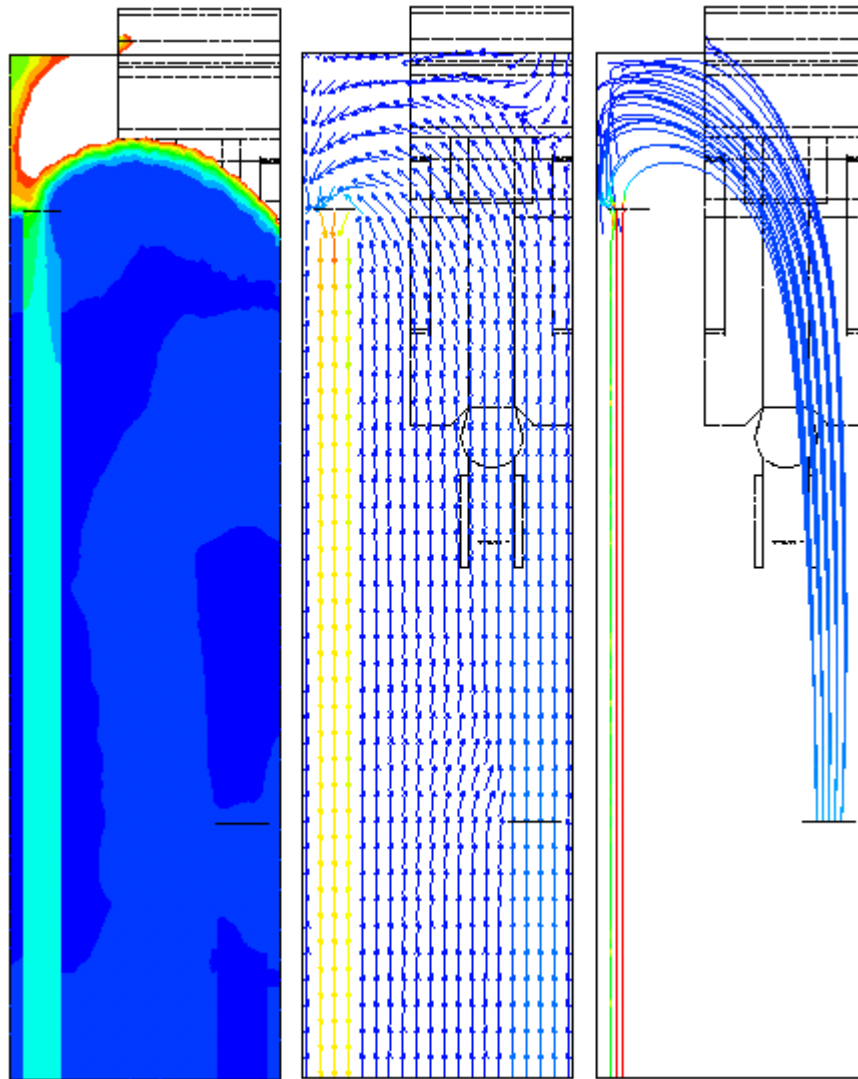
**SCENARIO 11**



**SCENARIO 12**

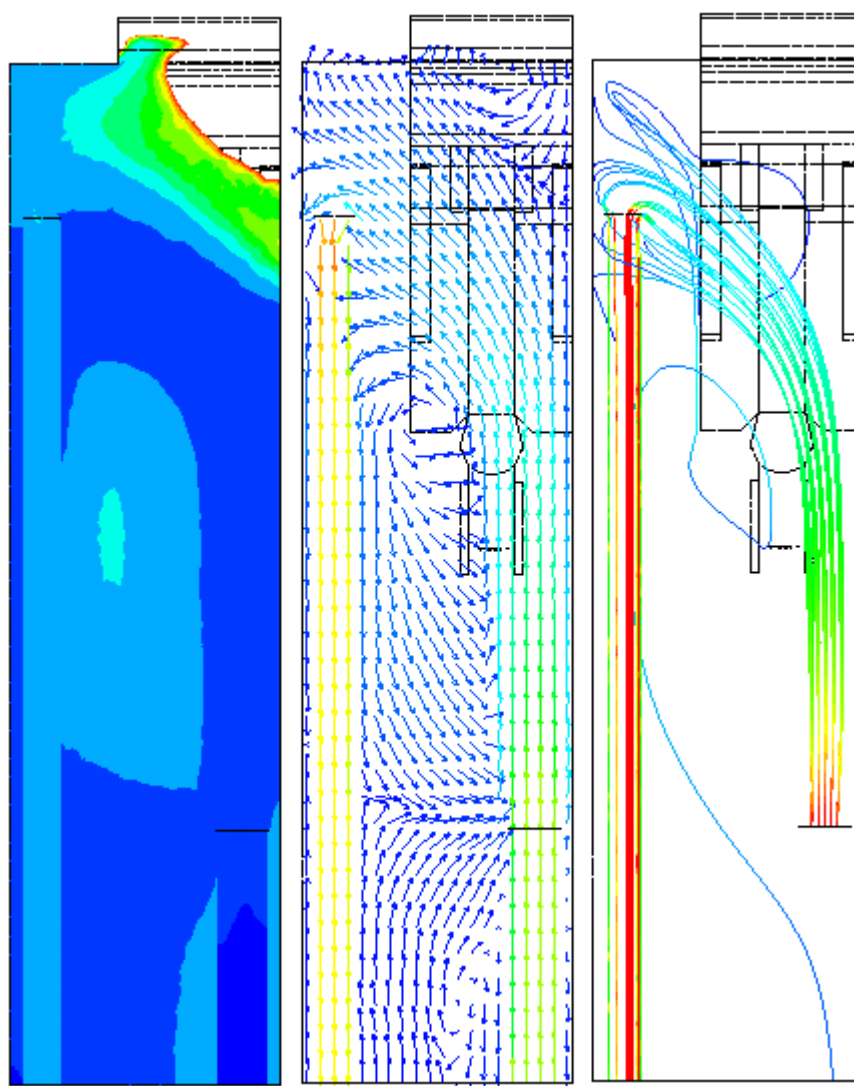


**SCENARIO 13**

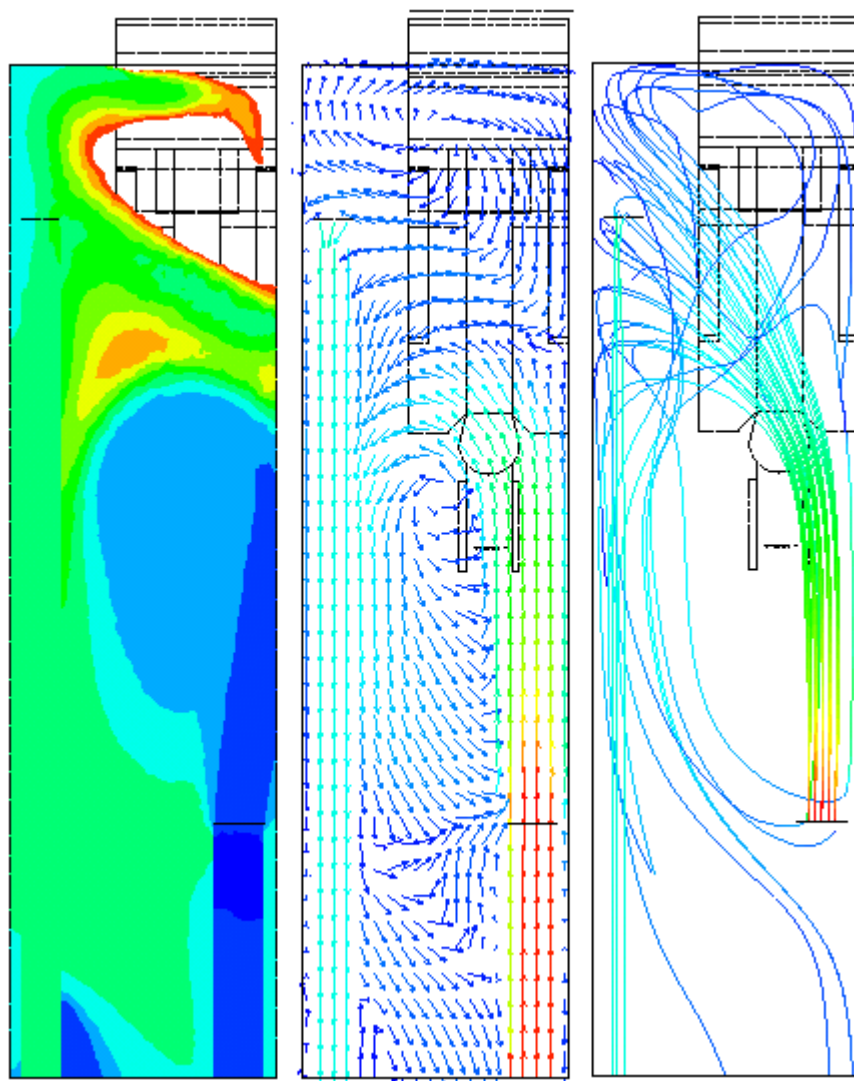


**SCENARIO 14**

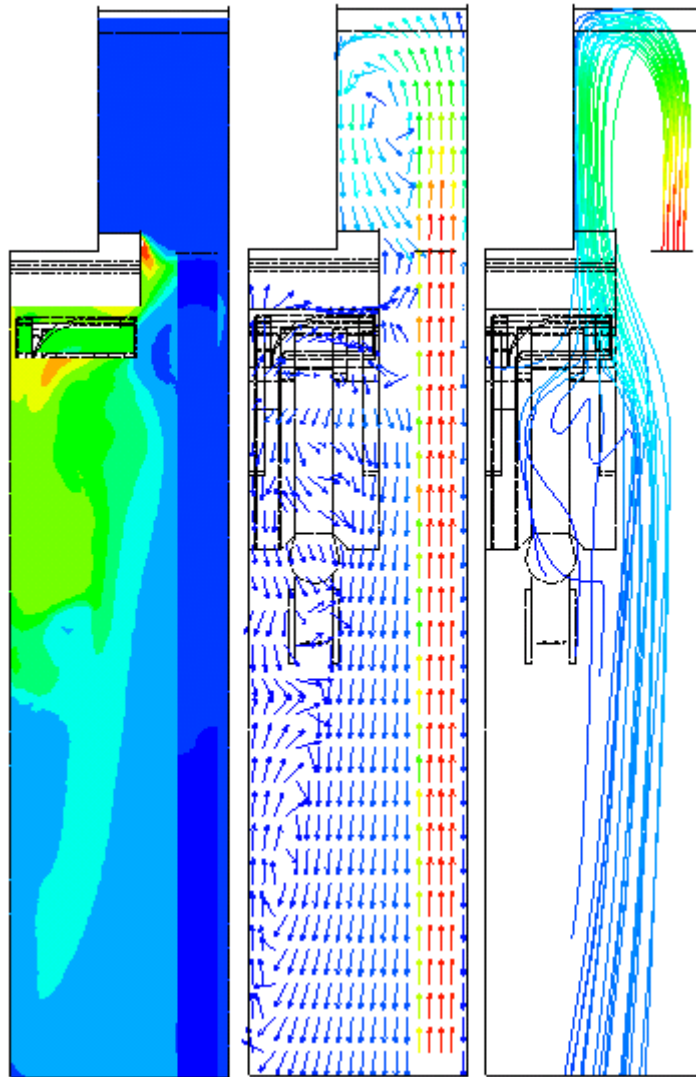




**SCENARIO 15**



**SCENARIO 16**



**SCENARIO 17**